DISSERTATION | DOCTORAL THESIS

Titel | Title

Towards Functional Nanopapers and Hybrids

verfasst von | submitted by

Florian Mayer BSc MSc

angestrebter akademischer Grad | in partial fulfilment of the requirements for the degree of

Doktor der Naturwissenschaften (Dr.rer.nat.)

Wien | Vienna, 2025

Studienkennzahl lt. Studienblatt | Degree programme code as it appears on the student record sheet:	UA 796 605 419
Dissertationsgebiet lt. Studienblatt | Field of study as it appears on the student record sheet:	Chemie
Betreut von | Supervisor:	Univ.-Prof. Dr. Alexander Bismarck
Mitbetreut von | Co-Supervisor:	Dipl.-Ing. Dr.techn. Andreas Mautner Privatdoz.

„Was lange währt wird endlich gut“

Abstract

In the search for sustainable and renewable engineering materials, free standing films formed from nanocellulose fibres – often termed cellulose nanopapers (CNPs) due to the similarities of their production to traditional papermaking processes – are often treated as candidates to replace fossil-based polymers in a variety of applications. Despite their potential, several key drawbacks in the use and production of CNPs can be identified such as their inherent brittleness, their time-consuming production procedures and the fact that the introduction of charged surface moieties, which would allow for an even wider application, in some cases exasperates these problems even further. In my thesis, I aim to address these challenges through the development and investigation of post treatments and production processes, as well as the development of a hybridisation approach combining nanocellulose membranes with highly functionalised polymers.

Targeting the inherent brittleness of CNPs, I demonstrated, that mercerisation, i.e. treatment of the fully formed nanopapers with strong alkaline solutions, allowed for the partial transformation of the strong yet brittle cellulose I polymorph into the more ductile cellulose II. This simple and fast post-treatment tripled the strain to failure and drastically increased (up to 590% of the original value) the modulus of toughness of the resulting CNPs while maintaining tensile strengths of over 100 MPa.

While this treatment improved the mechanical properties of CNPs prepared via filtration without adding significantly time-consuming steps to the process, the filtration times remained a major concern. Thus, I investigated the use of ethanol/water mixtures instead of pure water as suspension medium during CNP preparation and found, that this reduced the filtration times by over 70 %. While ethanolic suspensions proved to result in more porous and thus weaker nanopapers, a simple rewetting and drying protocol was developed to yield CNPs with the same density as those produced from aqueous suspensions. These rewetted nanopapers were shown to possess almost three times higher strain to failure and superior optical properties (high luminous transmittance and lower haze) than CNPs prepared directly from aqueous suspensions.

Building on this processing platform, I extended the use of ethanolic suspension media, to enable the fabrication of hybrid membranes for water purification combining nanocellulose and sulfonated hypercrosslinked polymers (SHCPs). By entrapping SHCP particles within the cellulose network during filtration from ethanolic suspensions, I created a hybrid material that combines the ultrafiltration capability of nanocellulose membranes with the high charge density and surface area of SHCPs. This approach maintains the previously established fast filtration times and comparably higher porosity – and thus permeance – of CNPs prepared from non-aqueous suspensions and comprised of uncharged cellulose nanofibres while simultaneously eliminating the need for time intensive purification steps during nanocellulose modification. These hybrid membranes exhibit synergistic effects by both enhancing the water permeance through the membrane and increasing the Cu^{2+} ion adsorption capacity of the polymer entrapped within them (≈100 mg g^{-1}) allowing them to outperform the pure polymer (71 mg g^{-1}) and commercially available ion exchange resins. The membranes also proved capable of removing traces of toxic heavy metal such as Sr^{2+} and Ba^{2+}, from solutions with excess concentrations of common water hardness elements, demonstrating high ion-exchange capability.

Overall, the work of this thesis contributes towards the use of CNPs, with tailored mechanical properties, efficient production methods and enhanced functionality for specialised applications, as replacements for fossil based high performance materials. The strategies developed herein provide a roadmap for targeting current limitations and for expanding the utilisation of nanocellulose-based papers and hybrids.

Zusammenfassung

Auf der Suche nach nachhaltigen und erneuerbaren technischen Materialien werden freistehende Filme aus Nanocellulosefasern, welche oft, aufgrund der Ähnlichkeit ihrer Herstellung mit klassischen Papierherstellungsverfahren, als Cellulose-Nanopapiere (CNP) bezeichnet werden, als vielversprechende Kandidaten betrachtet, um fossile Kunststoffe zu ersetzen. Trotz ihres Potentials lassen sich auch mehrere zentrale Nachteile bei der Produktion und Verwendung von CNP identifizieren, wie zum Beispiel ihre inhärente Sprödigkeit sowie die zeitaufwändigen Verfahren, die für ihre Herstellung nötig sind. Des Weiteren führt die Modifizierung der Cellulose Oberfläche mit geladenen Gruppen – welche weitere Anwendungsgebiete erschließen würden – in vielen Fällen zu noch höherer Sprödigkeit und längeren Produktionszeiten. Das Ziel meiner Dissertation war daher, diese Herausforderungen durch die Modifikation von Produktionsbedingungen und der Entwicklung von Nachbehandlungsstrategien und einer Hybridisierungsstrategie, welche CNPs mit dicht funktionalisierten, hochvernetzten Polymeren kombiniert, zu adressieren.

In meiner Dissertation konnte ich zeigen, dass die Behandlung von Nanopapieren mit stark alkalischen Lösungen – Merzerisierung genannt – eine partielle Umwandlung des mechanisch starken, aber spröden Cellulose I Allomorphs in das duktilere Cellulose II Allomorph ermöglichte. Mit dieser einfachen und schnellen Nachbehandlung konnte die Bruchdehnung der CNP verdreifacht werden und die Brucharbeit (bis zu 590 % des ursprungswertes), und damit die Zähigkeit der CNP, bei gleichzeitigem Erhalt von Zugfestigkeiten von über 100 MPa, signifikant erhöht werden.

Während Merzerisierung die mechanischen Eigenschaften von CNP, welche durch Filtration hergestellt wurden, deutlich verbessern konnte, ohne den Prozess wesentlich zu verlangsamen, blieben dennoch die langen Filtrationszeiten ein wesentliches Problem bei der CNP-Produktion. Daher untersuchte ich die Verwendung von Ethanol/Wasser Gemischen anstelle von nur Wasser als Suspensionsmedium für die CNP-Herstellung und fand, dass so die Filtrationszeiten um über 70 % reduziert werden konnten. Die Verwendung ethanolischer Suspensionsmittel führte zwar zu poröseren, und infolgedessen

mechanisch schwächeren CNP, jedoch konnte dies durch ein einfaches und schnelles Wiederbefeuchtungs- und Trocknungsprotokoll, welches im Zuge dieser Dissertation entwickelt wurde – kompensiert werden, sodass die resultierenden Nanopapiere ähnliche Dichten wie jene, welche aus wässrigen Suspensionen hergestellt wurden, erreichten. Die so nachbehandelten Nanopapiere wiesen eine fast dreimal höhere Bruchdehnung und bessere optischen Eigenschaften (höhere Transparenz und niedrigere Trübung) auf als die direkt aus wässrigen Suspensionen hergestellten Referenzpapiere.

Aufbauend auf dieser Prozessplattform konnte die Verwendung eines ethanolischen Suspensionsmediums zur Herstellung von Hybridmaterialien erweitert werden, welche Nanocellulose mit sulfonierten und hochvernetzten Polymeren (SHCP) kombinieren. Durch die Immobilisierung von SHCP-Partikeln innerhalb eines Nanocellulose Netzwerks konnte ein Hybridmaterial geschaffen werden, das die Ultrafiltrationsfähigkeit von CNP und die hohe Ladungsdichte und große Oberfläche von SHCP vereint. So konnte die bereits etablierte erhöhte Filtrationsgeschwindigkeit und höhere Porosität – und damit auch Permeabilität – von CNP aus ethanolischen Suspensionen beibehalten werden, während die Zeit aufwändigen Reaktions- und Reinigungsschritte der Nanocellulose-Modifizierung entfielen. Die so hergestellten Hybridmembranen zeigten synergistische Effekte da sowohl die Permeabilität der Membranen stieg als auch die Cu^{2+} Ionen-Adsorptionskapazität des eingebetteten Polymers (≈100 mg g^{-1}) die des reinen Polymers (71 mg g^{-1}) und jene einiger kommerzieller Cu^{2+} Ionenaustauscher übertraf. Weiters erwiesen sich die Membranen als geeignet für die Adsorption von Spuren toxischer Schwermetalle wie Sr^{2+} und Ba^{2+} aus Lösungen mit starkem Überschuss an Wasserhärtebildnern wie Mg^{2+} und Ca^{2+}, was ihre Eignung zur Wasserreinigung weiter unterstreicht.

Insgesamt tragen die Ergebnisse dieser Dissertation dazu bei, CNP mit maßgeschneiderten mechanischen und optischen Eigenschaften und mit erweiterter Funktionalität durch effiziente Methoden herzustellen und so als Ersatz für fossile Hochleistungsmaterialien nutzbar zu machen. Die entwickelten Prozesse und Strategien bieten einen Leitfaden, um die aktuellen Grenzen in der Produktion von Nanocellulose basierten Papieren und Hybridmaterialien zu überwinden und so deren Einsatzgebiete zu erweitern.

Acknowledgements

First and foremost, I would like to express my deepest gratitude to my supervisor Prof. Alexander Bismarck, who has not only forever shaped me as a scientist with his exemplary standards and demands for scientific excellence, critical and creative thinking and integrity, but who is also one of the most supportive and kind supervisors I could have ever wished for. The working group he has cultivated at the university of Vienna has and will forever feel like a second family to me. For all this, and more: Thank you Alex, it was an amazing time!

Deep gratitude also goes to my Co-Supervisor, Prof. Andreas Mautner, whose supervision since the beginning of my master's thesis has led me to choose nanocellulose as my field of research, and who was always available when it came to bouncing ideas back and forth, and who spent countless hours reading and helping me improve my manuscripts. Thanks Andreas, without you, this thesis would not have been possible.

A heartfelt thanks also goes to Prof. Robert Woodward, who came to my office right after our lab had burned down and I was as close to quitting as I would ever be, and suggested to "look into this interesting research paper about 5-HMF generation from cellulose via SHCPs" together, which turned into 3 publications and a significant part of my dissertation, and who was always up for a fun chat when things were looking down. Thanks Herr Förster!

Further thanks go to all my colleagues and friends at PaCE for their invaluable input into my research and more importantly for making the time it took to finish this dissertation an interesting, fun and educational one, every single lunch, every game night, and the countless hours spent joking in the office are truly cherished memories. I'd also like to thank all the students I had the pleasure of supervising and working with during my time at UniVie – Alexander, Amanda, Josef, Klaus, Manon, Marion, Paul, San J., and Sarah – whose lab work has contributed greatly to some of my publications, and whom in some cases have gone on to become colleagues and good friends (looking at you Paul).

Special thanks also to the people that co-authored the publications comprising the core of this dissertation: Alexander Prado-Roller, Paul Schweng, Simone Bräuer, Sebastian Hummer, Gunda Koellensperger, Bill Sampson and Daniela Wloch and all the other people with whom I had the pleasure on working on a variety of publications together. Also, thanks to all the people that helped behind the scenes by either providing support with measurements, or support with wrangling the administrative Behemoth: Johannes Theiner, Stefan Puchegger, Angela Eberhart, Claudia Weber, Angelika Menner, Qixiang (John) Jiang, Claudia Mitterer, and all the people working at the SSC Chemie.

A huge thank you also to all the supervisors, teachers and the “first generation students” of the ABC&M doctoral school, for welcoming me so warmly at BoKU and for making every retreat and excursion an amazing time, I hold all of these memories dear and look forward to seeing you guys at conferences and other occasions in the future. Special thanks in this regard go to Antje and Rosi, for always being available when it comes to questions about cellulose chemistry and analytics, and who graciously have supported me on many occasions with measurements and advice.

The people who set me on the path to pursue a Doctorate in materials chemistry, like Prof. Stefan Hochstöger who was the best chemistry teacher one could wish for in my time at the Gymnasium WT, as well as Prof. Dr. Gerhard Zifferer who suggested I might be interested in pursuing a bachelor thesis with this – at the time – newly arrived Professor from London and who will be dearly missed also deserve my deepest gratitude.

To my family, my parents, my brother Philipp, and his girlfriend Verena, I would like to say: Danke für all die Unterstützung die ich von euch erhalten habe. Danke dafür, dass ich immer heimkommen konnte, wenn’s mal wo gedrückt hat, und dafür, dass ihr mich immer dazu ermutigt und mich dabei unterstützt habt meinem Traumstudium nachzugehen. Und auch wenn sie leider nicht mehr erleben konnten, auch danke an meine Opas und Omas, ich hätte mir keine bessere Familie wünschen können. Danke für Alles.

Last but not least, I’d like to thank all the people that made my time outside of Uni a very special one: Thanks to my best friend Philipp & his wife Clara and their little ones and to my university-and-beyond-gang that have been with for what feels forever – Alice & Felix, Stefan & Evi, Kathi & Markus, Alex & Co, Tobi & Delphine, Elli, Lukas and Sarah – I truly believe that the DnD nights, the Monday game sessions and all our other get togethers, parties and holidays were majorly responsible for keeping my sanity intact during this part of my life.

To everyone whom I have forgotten in this short and definitely incomplete list: I am truly sorry, but rest assured, that you and all the other people will forever have a special place in my heart. Thank you all once again, you are a major reason for why I am where I am today, and I will always be grateful for that.

Helsinki, Finland, August 2025

Florian Mayer

List of Publications

This doctoral dissertation is based on the following publications, which are referred in the text by their Roman numerals

> **Publication I:** Mayer, F., Prado-Roller, A., Mautner, A., & Bismarck, A. (2024). Retain strength, gain ductility: tough and transparent nanopapers by mercerisation. Cellulose, 31(3), 1533-1544. DOI: 10.1007/s10570-023-05714-7
>
> **Publication II:** Mayer, F., Sampson, W. W., Wloch, D., Mautner, A., & Bismarck, A. (in Submission as of July 2025) Towards the Efficient Preparation of Tough Cellulose Nanopapers.
>
> **Publication III:** Mayer, F., Schweng, P., Braeuer, S., Hummer, S., Koellensperger, G., Mautner, A., Woodward, R., & Bismarck, A. (2024). Best of Both Worlds: Adsorptive Ultrafiltration Nanocellulose-Hypercrosslinked Polymer Hybrid Membranes for Metal Ion Removal. Small Science, 4(10) e2400182 DOI: 10.1002/smsc.202400182

The contributions of FM to the relevant publications were as follows:

> **Publication I, II and III:** FM designed the experimental procedure and manufactured the studied nanopaper and hybrid membranes, supervised and performed data gathering and evaluation, conceptualised and wrote the manuscript, and designed the figures and plots.

Furthermore, FM contributed to the following publications during his time working on this dissertation

> **Publication A1:** Blocher, A.*, Mayer, F.*, Schweng, P., Tikovits, T. M., Yousefi, N., & Woodward, R. T. (2022). One-pot route to fine-tuned hypercrosslinked polymer solid acid catalysts. Mater. Adv., 3(15), 6335-6342. DOI: 10.1039/D2MA00379A
>
> **Publication A2:** Schweng, P., Mayer, F., Galehdari, D., Weiland, K., & Woodward, R. T. (2023). A Robust and Low-Cost Sulfonated Hypercrosslinked Polymer for Atmospheric Water Harvesting. Small, 19(50), e2304562. DOI: 10.1002/smll.202304562
>
> **Publication A3:** Mautner, A., Kobkeatthawin, T., Mayer, F., Plessl, C., Gorgieva, S., Kokol, V., & Bismarck, A. (2019). Rapid Water Softening with TEMPO-Oxidized/Phosphorylated Nanopapers. Nanomaterials (Basel), 9(2).
>
> **Publication A4:** Marino, S. G., Mayer, F., Bismarck, A., & Czel, G. (2020). Effect of Plasma-Treatment of Interleaved Thermoplastic Films on Delamination in Interlayer Fibre Hybrid Composite Laminates. Polymers (Basel), 12(12).

* Both Authors contributed equally to this publication

Publication A5: Richstein, R., Eisen, C., Ge, L., Chalermnon, M., Mayer, F., Keppler, B. K., Chin, J. M., & Reithofer, M. R. (2023). NHC stabilized copper nanoparticles via reduction of a copper NHC complex. Chem Commun (Camb), 59(64), 9738-9741.

Publication A6: Ge, L., Trinh, T.K.H., Li, C., Mayer, F., Chin, J.M., Chen, C.L. & Reithofer, M.R. (2025). Directed Synthesis of Gold Nanoparticle Superstructures Using Self-Assembling Peptoids Containing Metal-Bonding N-Heterocyclic Carbenes. *Nano Lett. 25, 31, 12049–12058*

Table of Contents

List of abbreviations & symbols

Symbols and Variables

Symbol	Description	Unit
θ	diffraction angle	°
Γ	nanopaper grammage	g m^{-1}
Φ	porosity	%
A	area	m^2
ε_f	strain to failure	%
ε	tensile strain	%
ρ	density	kg m^{-1}
σ	tensile strength	MPa
b	shear bond strength	N m^{-2}
b_1/b_2	rel. diff. in shear bond strength	dimensionless
CAGR	compounded annual growth	%
d	linear nanofibril density	kg m^{-1}
d	nanopaper thickness	µm
E	Young's modulus	GPa
E_a	Activation energy	kJ mol^{-1}
g	gravitational constant	6.674 10^{-11} m^{-3} kg^{-1} s^{-2}
h	height	m
h_o	initial sorption rate	mg g^{-1} min^{-1}
k_1	1st order rate constant	min^{-1}
k_2	2nd order rate constant	g mg^{-1} min^{-1}
K_f	Modulus of toughness	MPa or MJ m^{-3}
L	length	m
m	mass	g
M	specific Modulus	MN m kg^{-1}
m_{ads}	adsorbed mass	mg
m_{pol}	mass of polymer tested	g
P	nanofibril diameter	m
p	pressure	bar or barg
q	adsorption capacity	mg g^{-1}
q_a	adsorption capacity per area	g m^{-2}
q_e	equilibrium adsorption capacity	mg g^{-1}
R	universal gas constant	8.3145 J K^{-1} mol^{-1}
RBA	relative bonded area	dimensionless
T (Arrhenius plot)	temperature	K or °C
T (Page eq.)	specific strength / tensile index	kN m kg^{-1}
t	time	min
WoF	work of fracture	see K_f
Z	zero span tensile index	kN m kg^{-1}

Abbreviations

CNC..... cellulose nanocrystals
CNF..... cellulose nanofibres
CNP..... cellulose nanopaper
CSC..... cellulose synthetase complex
DI water ..... deionised water
DMAc ..... N,N-dimethyl acetamide
ICP-MS ..... inductively coupled plasma-mass spectroscopy
MOF..... metal-organic framework
PMMA..... polymethyl methacrylate
PXRD ..... wide angle powder X-ray diffraction
SEM ..... scanning electron microscopy
SHCP..... sulfonated hypercrosslinked polymer
TEMPO ..... (2,2,6,6-Tetramethylpiperidin-1-yl)oxyl
XPS ..... X-ray induced photoelectron spectroscopy

List of Figures

List of Tables

1. Introduction

It is the almost unanimous scientific consensus (97-99.9 % of peer-reviewed literature), that he widespread dependency on fossil resources such as oil and gas, for the production of consumer goods and engineering materials, has severe impacts on the ecosystems of our planet.[1] Alongside the contamination and destruction of natural habitats with plastic waste and its degradation products – microplastics – the production of polymer materials also introduces more carbon based greenhouse gases into the atmosphere, thus greatly contributing to global warming.[2-5] The dangers of anthropogenic climate change are multivariant and range from longer, more frequent, and more severe weather events, heat waves and an increase in the sea level, which endangers coastal communities, to severe disruptions in global agriculture and food production, due to water scarcity.[6-8] It is thus imperative to develop engineering materials based on renewable and potentially carbon neutral resources, to replace fossil-based fuels and materials. The most promising resource for such materials can be found in cellulose, which is well known and often quoted to be the most abundant biopolymer on our planet.[9] Cellulose, associated in a complex with lignin and hemicelluloses, forms the structural component in all green plants, is also synthesised by a variety of bacteria, animals (*tunicata*) and, if harvested correctly, fulfils the requirements to be deemed sustainable and renewable.[10] Aside from its historical uses for the production of textiles, as a writing material (paper), building material and fuel (wood), cellulose has been investigated for a variety of high value applications by utilising its nano-scale or monomer building blocks.[11, 12]

Native cellulose can be broken down via comminution into a variety of nanomaterials, such as cellulose nanocrystals (CNC) or cellulose nanofibres (CNF), which in turn can be utilized for the production of hydrogels, as reinforcement for polymers or for the manufacture of films and membranes, often termed cellulose nanopapers (CNPs).[13-15]

Cellulose nanopapers in particular have garnered considerable research interest in recent years as they offer excellent physical, optical, and chemical properties at low densities.[16, 17] The abundance of hydroxyl groups on the surfaces of cellulose nanomaterials can be used for several modification reactions, such as oxidation,

phosphorylation or click-type reactions to impart various chemical functionalities onto the resulting CNPs allowing to further customise and improve their utilisation.[18-20] The potential applications for CNPs are manyfold and include – among others – their use for composite production, energy storage and production, water treatment, packaging, and the fabrication of substrates and conductive membranes in (printable) electronics.[21-24]

Nevertheless, the high-volume application of CNPs faces a number of challenges which need to be addressed in order to increase their viability among which are long dewatering times during their production or modification, which they owe to a combination of large surface area and their hygroscopic nature. In contrast to conventional paper, nanopapers possess excellent tensile moduli and strengths but are extremely brittle. Several strategies attempting to improve the ductility and toughness of CNPs have been disclosed; these include the formation of hierarchical structures,[25] surface modification,[26, 27] and further refinement of the CNF feedstock.[28] Unfortunately, most techniques used to improve the ductility of CNPs as well as those used to introduce high densities of functional (charged) moieties to CNF surfaces extend the already prohibitively long dewatering times during CNP production: Most modifications require washing, purification, and subsequent up-concentration steps, which increase the time and energy spent on filtration and centrifugation of the nanocellulose exponentially.[29-31] Some strategies to reduce the preparation times of CNPs have been reported in literature, amongst which the use of specific counter ions or the control of the pH of the suspension medium to facilitate faster filtration of carboxylated CNFs,[30, 32-34] and the use of solvent exchange with various organic solvents to improve the drying speed and control the porosity of CNPs post filtration are the most prevalent.[35, 36] The use of non-aqueous, low-surface tension suspension media for nanopaper preparation was found to yield nanopapers with significantly higher porosity, an effect which can be positive for some applications, e.g. nano-filterpapers or 2D reinforcement for polymers, yet also drastically reduces the mechanical properties of the resulting CNPs.[37, 38] Furthermore, Mautner et al.[39] found that, when preparing nanocellulose membranes from modified CNFs, a significant portion of the functional groups are not utilised, as only those groups exposed on the CNPs surfaces can interact with adsorbents, while most functional moieties are inaccessible within the bulk of the nanocellulose network.

1.1. Aim and objectives of the thesis

In my thesis, I aim to provide solutions for the tightly intertwined set of challenges opposing efficient CNP production identified in the previous section: their long

preparation times, their brittle nature, and the low accessibility of functional groups within nanopapers. The following objectives have been identified and will be addressed in my thesis to achieve the specific aim.

- Objective I: To develop a methodology allowing to reduce the brittleness of nanopapers without compromising tensile modulus and strength, nor increasing the filtration times during paper production.
- Objective II: To increase the filtration speed of nanopapers during production, by exploring the use of a low surface tension suspension medium.
- Objective III: To counterbalance the negative effects of using low surface tension suspension media during paper production, such as lower porosity and fibre bond strength, resulting in CNPs with lower tensile strength and lower optical transparency via an easy and time efficient procedure.
- Objective IV: To increase the functional group loading of CNPs, without incurring the long and labour intense preparation and filtration times inherent to both the production of charged CNF as well as the preparation of CNPs thereof.

Publication I explores the possibility of using an alkaline treatment, also known as "mercerisation", after CNP production to increase the ductility of nanopapers without increasing dewatering times. **Publication II** investigates the use of a non-aqueous solvent, ethanol, as suspension medium during CNP preparation, and the possibility to utilise the lower surface tension and increased filter cake porosity, to increase the filtration speed. Furthermore, **publication II** also focuses on the development of simple post treatment routes to improve the mechanical properties of CNPs prepared from ethanolic suspension, which previously have been shown to possess higher porosity and lower tensile strength than CNPs produced from water. **Publication III** investigates the possibility to mitigate the need to use modified CNFs for preparation of functionalised CNPs for use as adsorptive or catalytic membranes by exploring the generation of hybrid CNP membranes comprising nanocellulose and highly functionalised high surface area polymers.

Overall, the publications included in this thesis disclosed novel approaches to potentially improve the efficiency and viability of nanopapers produced via filtration, a method often identified as among the most promising for scale up,[40] and thus potentially allowing to replace a range of fossil fuel based materials with cellulose based ones.

2. Literature Review

2.1. Cellulose

Since prehistoric times, cellulose-based materials has been of vital importance for the proliferation of the human race, be it in the form of fuel, building material for shelter or tools, as textile for clothing or as writing material.[9, 41] Although used for millennia before, the actual substance was first described and termed “cellulose” by Payen in 1838,[42] when he discovered a fibrous residue after treating plant materials with acids and ammonia. Over 80 years later, cellulose was used as one of the main examples by Staudinger to describe the concept of polymers, who recognised that cellulose was a covalently linked chain of repeating D-glucose (Figure 1) units, thus founding the field of macromolecular chemistry.[43, 44]

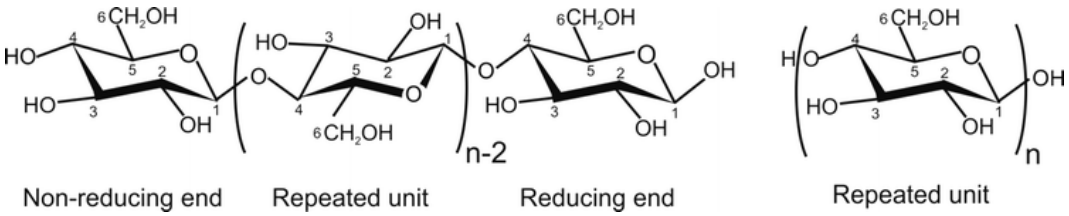

Figure 1: Structure of a cellulose molecule (left) and the repeating glucose unit (left). (French, 2017)[44] Reprinted with permission from Springer Nature.

Since its discovery, cellulose has been extensively studied and was found to consists of polymeric chains of a few hundred to up to 20.000 repeating units of length.[9, 45] In nature, cellulose is mainly synthesised in the cell wall of green plants, as their main structural component, in combination with other polymers such as hemicellulose and lignin but can also be synthesised by certain bacteria or animals.[17] The polymer chains of naturally occurring celluloses are clustered together in a specific crystal structure, which will be discussed in more detail in a subsequent chapter, to form structures termed “elementary fibrils”, with lengths strongly depending on the cellulose source, spanning from a few hundred nanometres up to several micrometres.[46, 47] The exact number of cellulose chains forming the cross-section of each elementary fibril varies from source to source, but is usually reported as between 18 and 36 in discreet multiples of 6.[45, 48, 49] The reason for elementary fibrils comprising cellulose molecules in multiples of six is hypothesized to be based in the structure of the cellulose synthase complex (CSC)

of plants, which consists of six subunits called *rosette*s, which each in turn are formed from a hexagonal arrangement of six cellulose synthetase proteins (CesA) each producing one cellulose molecule. Some of the CesA protein rosettes however are deactivated. However, a comprehensive model of the CSC is still under debate in the scientific community.[45, 49-52]

Industrially, cellulosic materials are of great importance for almost all aspects of modern life: cellulose pulp is both used for the production of (tissue) papers and cardboard, [53, 54] as well as feedstock for the production of regenerated cellulose fibres and yarns, such as viscose and rayon. Cellulose is also commonly used as a valuable platform chemical, for the production of food and pharmaceutical additives.[55-57] Furthermore, lignocellulosic materials can be hydrolysed and broken down into glucose and its oligomers, which in turn serve as platform chemicals for the synthesis of wide variety of other chemicals offering renewable and green production routes towards various polymer materials and fuels.[58]

2.2. Nanocellulose

More recently, a significant amount of research focussed on the production of cellulose based nanomaterials, termed cellulose nanofibres (CNF) and cellulose nanocrystals (CNC)[46]: CNF are obtained by defibrillating native cellulose fibres down to their elementary fibrils, yielding a nanomaterial with a high aspect ratio and exceptional mechanical and chemical properties[11, 17] whereas CNCs are produced by controlled hydrolysis of cellulosic materials to yield highly crystalline, stiff cellulose rods.[59] The specific processes employed for nanocellulose production are manifold and include mechanical defibrillation via grinding,[60] high pressure homogenisation[15] or twin screw extrusion.[61] Additional chemical and enzymatic processes, which are often employed to decrease the energy consumption of the defibrillation processes and to introduce additional functionalities to the CNFs, include TEMPO mediated oxidation,[18, 62] phosphorylation[63, 64], periodate oxidation,[65] a variety of enzymatic processes,[66] or even the use of the digestive system of gramini- and folivores.[67]

Among the first proposed applications for nanocellulose, was its use as an emulsifier and stabilising agent in the food industry disclosed in a patent by Turbak et al. already in the 1980s[68] and since then, it has been employed in a wide variety of industries. In 2024, the global nanocellulose market valued at US$ 635.0 million and is projected to reach US$ 3.6 billion in 2032 representing a CAGR of 23.7 %

according to an analysis performed by markets and markets[†]. The pulp and paper industry holds the largest share of this market and uses nanocellulose as an additive or coating to increase the paper's mechanical and barrier properties as well as their printing behaviour.[69-72] In the conservation of historical artifacts, nanocellulose coatings have been used with great success to stabilise damaged and burnt book pages.[73] The hygroscopic nature and large surface area of nanocellulose have been greatly explored in the production of hydrogels, which are utilised as functional and antimicrobial wound dressings, as scaffolds for bone and tissue regeneration and as 3D printing inks.[74-76]

2.3. Cellulose nanopapers

One of the most prominent fields of nanocellulose research are free standing films with structures and production routes similar to traditional paper, thus termed cellulose nanopaper (CNP). Nanopapers have been first disclosed by Revol et al. in 1992[77] – using CNCs – and later by Dufresne et al. in 1997[78] who fabricated CNPs from CNF extracted from sugar beets. Owing to the outstanding properties of CNF, CNPs combine high mechanical strengths and elastic moduli at a low density rivalling or outperforming the properties of a wide variety of other engineering materials, such as polymers, composites and ceramics (Figure 2), with high chemical resistance, optical transparency and low thermal expansion coefficients.[16, 17, 36, 79]

Since their first realisation, nanopapers have been investigated for a broad range of applications spanning both high-value niche, as well as high volume applications[21-23]: CNPs have been reported as promising candidates for renewable, strong and transparent carrier materials as substrate for flexible electronic devices, such as antennas,[80] electroluminescent films and displays,[81, 82] electrodes,[83, 84] and transistors,[85] in which electronic conductivity is usually imparted to the CNPs by coating or impregnation with conductive inks, based on Ag nanowires, carbon nanotubes, or conductive polymers. For energy storage, the porous, thin and robust nature of CNPs lends itself to the production of separator membranes as well as electrode materials for batteries, supercapacitors, and fuel cells.[23, 86-88]

[†] Markets and Markets: Nanocellulose Market by Type (MFC & NCF, CNC/NCC), Raw Material (Wood, Non-wood) Application (Paper & Pulp, Composites, Paints & Coatings, Biomedical & Pharmaceuticals, Electronics and Sensors), and Region – Global Forecast to 2032, Link in (accessed 22.10.2024): https://www.marketsandmarkets.com/Market-Reports/nano-cellulose-market-56392090.html

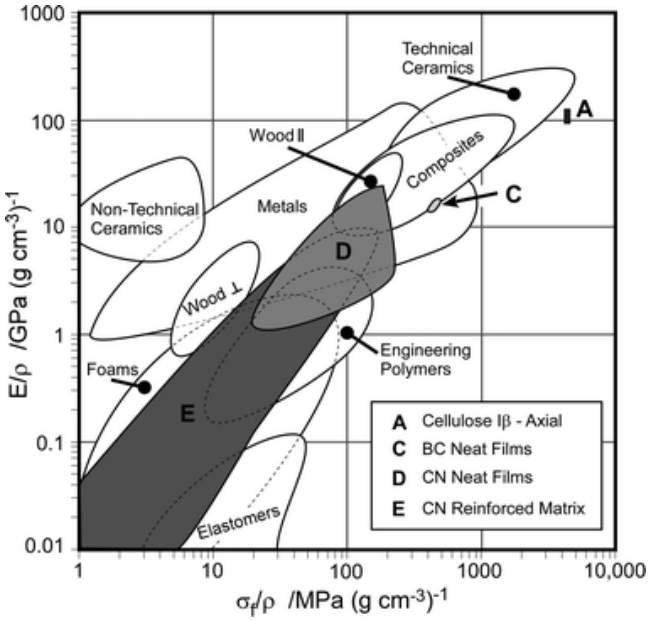

Figure 2: Ashby plot juxtaposing specific moduli (E/ρ) and specific tensile strengths (σ/ρ) of A: nanocellulose fibres, C: freestanding films of bacterial cellulose, D: freestanding films of cellulose nanoparticles (here CN) – i.e. CNPs – and E: composites containing a CN reinforcement (≤ 30 %) with typical values of other engineering materials. (Moon et al. 2011)[17] Reproduced with permission from Royal Society of Chemistry.

Zhang et al.[89] reported the use of carbonised nanocellulose aerogel electrodes in combination with a CNP separator layer, enabling the formation of "all-nanocellulose" based supercapacitors. CNPs were also investigated for energy harvesting applications, for instance in solar cells, where they are used as a carrier and coating material, with high optical transmittance and low reflectiveness,[90, 91] or in tribo- or piezoelectric nanogenerators for energy production and sensing applications.[92, 93] Another promising field of application for nanocellulose based films is the development of renewable and biodegradable packaging, especially food packaging, solutions.[22, 94, 95] Especially the optical transparency of thin nanocellulose films[96] and their non-toxic, even edible, nature[97] alongside their good oxygen and grease barrier properties[98] make CNPs promising candidates to replace fossil-based films and coatings in the food packing industry. A major drawback for the implementation of CNPs in packaging currently is the inherent hydrophilicity of cellulose, leading to high water vapour transmission rates and generally decreased mechanical properties when wet or in high humidity conditions.[99, 100] Several procedures to reduce the water vapour transmission rate and overall water resistance of CNPs have been proposed ranging from chemical modification of nanocellulose surfaces,[101] crosslinking[102] to low pressure-plasma fluorination,[103] and are an extensive topic of current research. Due to their inherent microporosity, surface area and abundant availability of surface hydroxyl groups, cellulose nanopapers are investigated extensively for the use in gas

separation and liquid purification applications. [104-107] The small fibril diameters of CNFs results in pores of the same order of magnitude in produced CNPs and thus, CNPs have been extensively studied for the preparation of ultrafiltration membranes (i.e. the removal of nanometre sized particles) from water.[107-109] The main drawback of using CNPs as ultrafiltration membranes however, is their low permeance when compared to synthetic polymer membranes, which has to be counteracted by carefully tailoring their properties by adapting the production processes to include freeze drying[110] or controlling their porosity via solvent exchange.[64] Besides their use size exclusion membranes, the use of CNPs in affinity membranes for targeted adsorption or as ion exchangers has also been studied. Nanopapers made from phosphorylated, carboxylated or sulfated CNFs have been explored for the selective removal of heavy metal ions from waste or to facilitate water softening, while CNFs with cationic moieties have proven efficient for the removal of problematic anions, such as phosphates, nitrates and sulfates.[39, 63, 64, 111-113] Finally, CNPs are also widely studied as reinforcement in laminated composite materials; it was reported that the properties of the resulting composites are directly dependent on the mechanical properties and the porosity of the nanopaper itself, and thus, efficient ways to produce mechanically strong nanopapers are in great demand.[114, 115]

2.4. Cellulose nanopaper production routes

Among the currently employed production techniques for CNPs, three main ones – casting, coating, and filtration – along with advantages and disadvantages can be identified.[40, 116]

Casting aqueous suspensions of CNF and/or CNC to produce CNPs (Figure 3 A) – the earliest reported fabrication method[77, 78] – usually involves pouring the nanocellulose suspensions into either flat moulds, or following a more recent development, depositing nanocellulose suspensions continuously on rollers or conveyors,[117] before drying at elevated temperatures or under vacuum. This method allows for control over the structure and properties of the resulting nanopapers by tailoring the evaporation rate and the addition of different solutes to the suspension.[118]

Producing CNPs via coating (Figure 3B) is usually accomplished similar to the casting method, but the CNF suspension is deposited – in batch or continuous processes – on top of a porous carrier material, which in turn creates a CNP top layer usually bonded to the carrier.[72, 118, 119] It has to be noted, that this method usually yields CNP coatings or laminates rather than freestanding films.

The filtration method (Figure 3 C) is similar to traditional papermaking processes: a dilute CNF suspension is dewatered by either vacuum or positive pressure filtration, forming a filter cake, which is subsequently consolidated via heat and pressure to obtain uniform CNPs.[120] While this method offers a comparatively fast method (in relation to evaporation based ones) to prepare CNPs, its efficiency is greatly impacted by the desired grammage and thus thickness of the resulting nanopaper as well as the diameter of the CNF used for paper production, as the formation of a filter cake with nanometre sized pores gradually reduces the filtration efficiency, creating a greater and greater resistance in the filtration system.

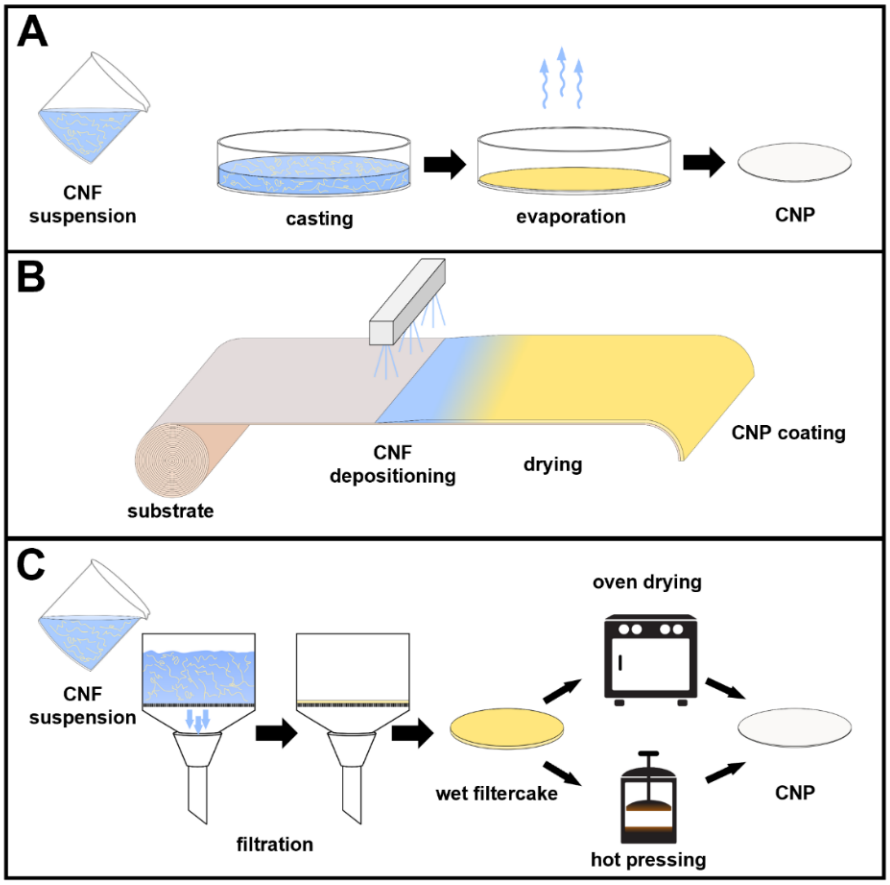

Figure 3: Schematic representation of the three most common methods to produce cellulose nanopapers: casting (A), coating (B), and filtration (C)

2.5. Challenges of CNP production and application

Despite their great potential, CNPs also suffer from drawbacks such as brittleness,[121] low wet strength,[99, 122] long production times,[116, 120, 123, 124] which are further increased by undesirable effects when modified CNFs or CNCs with high surface charge are used[33, 125].

2.5.1. CNPs are strong with high stiffness, yet poor ductility

Cellulose nanopapers, offering exceptional tensile strength and stiffness, at comparatively low densities are impacted by a trade-off affecting many synthetic materials, as high stiffness and strength often entail low ductility and toughness, and vice versa.[126] The overall ductility of cellulose nanopapers is quite low, with a majority of CNPs prepared from unmodified CNFs of lignocellulosic origin possessing strains to failure ε of 5 % or less.[121, 127] Several reports have been published, which address the challenge of creating more ductile CNPs while maintaining high elastic moduli and tensile strengths in a multitude of ways. The careful choice and refinement of the CNF stock to consist of cellulose molecules with higher degree of polymerisation, i.e. longer fibres, has generally resulted in the production of tougher CNPs, and was explained by a mechanism of network slippage, combined with the breakage and reformation of interfibrillar hydrogen bonds, which can happen more often in networks with longer fibres prior to disentanglement of the network.[28, 36] The combination of different types of nanocellulose, for example TEMPO-oxidised CNFs with bacterial cellulose has also been shown to have a favourable effect on the mechanical properties.[25] Sehaqui et al.[26] fabricated highly ductile CNPs by first forming cellulose hydrogels and then using supercritical CO_2 drying to dewater them. Other reports use chemical modification of CNFs to increase toughness of CNPs: Guzman-Puyol et al.[128, 129] reported two methods to increase the toughness of nanopapers by either preparing nanopapers from C6 fluorinated nanocellulose esters, or casting them from mixtures of CNFs, trifluoroacetic acid and naringin (a compound found in citrus fruits), which also imparts them with UV-blocking capabilities. Kriechbaum and Bergström grafted CNF fibres with gelatin moieties and impregnated the resulting films with gelatin and tannin solutions, to prepare CNPs with high toughness and wet strength, albeit at the cost of a reduction of the mechanical properties in the dry state. Another route for the production of more ductile CNPs is the formation of all-cellulose composites by partially dissolving and then regenerating the cellulose present in the CNP network: Both Gindl and Keckes,[130] as well as Abbot and Bismarck[131] have reported procedures on this, which involve solvent exchanging the nanocellulose suspensions to dimethylacetamide (DMAc) followed by partial dissolution of the cellulose by LiCl/DMAc – a known cellulose solvent – followed by regeneration of the cellulose yielding CNPs with high tensile strength, ductility and transparency. Chen et al.[132] have utilised a similar approach by adding ionic liquids – also well-known cellulose solvents – to the CNF suspension during filtration, resulting in CNF-gel filter-cakes which were then processed into highly ductile and mechanically strong nanopapers. All these methods however

add significant cost to the CNP production process, as they either entail additional modification and/or processing steps, require specific high-grade (i.e. low hemicellulose content, low polydispersity, and high crystallinity) CNF feedstock, employ expensive and/or dangerous reagents, or negatively impact the already lengthy dewatering times during CNP preparation.

2.5.2. Dewatering of nanocellulose suspensions

The combination of the high surface area, the hydrophilic nature of cellulose and the need to use highly diluted stock solutions to avoid uneven deposition, clogging of machinery or entrapment of air bubbles in the filter cake – resulting in voids in the finished CNPs – make the dewatering and drying of nanocellulose a topic of great scientific and industrial interest and are the reason for it being identified as one of the main barriers for the commercialisation of nanocellulose based products.[31, 133] In case of the casting and coating methods this means, that large amounts of energy and time are required to allow for the evaporation of the water spanning several hours to days.[116, 120, 124, 134] The filtration method has commonly been reported as a faster route to prepare CNPs, compared to the other two routes,[116, 120] however, filtration times of multiple hours are still common.[29] The main reason for the long filtration times of nanocellulose suspensions can be found in the formation of a nanocellulose gel filter cake with nanometre sized pores and high surface area, which causes a significant increase in the filtration resistance of the system, as described by the Kozeny-Carman equation describing fluid flow through granular beds.[135] This also explains the drastic increase in filtration times, when using TEMPO-oxidised CNFs as feedstock for CNP production, as these are, due to their surface charge, even more hydrophilic and repel each other in aqueous suspensions. Moreover, they generally have a smaller diameter and thus higher surface area than their non-charged counterparts.[25] Several studies have reported the addition of different salts to the suspension medium or controlling the pH of the suspension medium to reduce electrostatic attraction of individual fibres to improve the dewatering speed.[30, 32-34] Reports by Wetterling et al.[136] and Karna et al.[137] describe the combination of pressure filtration with electric fields to facilitate “electro-assisted“ filtration which increases the dewatering speed significantly. Two methods to increase the dewatering speed of CNFs suspensions reported by Sethi et al.[29, 138] are the combination of grafting lactone moieties to the CNFs before filtration with ultrasonication, or the combination of CNFs with non-delignified wood nanofibrils, to introduce hydrophobic domains and channels into the developing filter cake. The formed channels allow water to pass without significantly interacting with the cellulose surface. All strategies discussed to dewater nanocellulose suspensions more efficiently have their merits, yet it is still

of vital importance to expand the portfolio of dewatering strategies available to be able to fit a wide variety of use cases.

2.5.3. Production of CNPs from functionalised CNFs

While cellulose fibres and their nanoscale derivatives already offer a wide variety of benefits, the introduction of surface moieties, such as charged or functional groups, binding sites or modifications facilitating easier dissolution of the cellulose molecules allows for new avenues for the utilisation of cellulosic materials as discussed previously. Historically but also still industrially important modifications for the preparation of cellulose films and fibrils are the derivatisation of cellulose via xanthogenation,[139, 140] carbamation,[141] and nitration[142] to facilitate efficient dissolution and reprecipitation of cellulose molecules. More recently, the (2,2,6,6-tetramethylpiperidin-1-yl)oxyl (TEMPO) mediated oxidation of the C6 hydroxyl group of cellulose,[18, 62, 143] has been widely explored as pretreatment of wood pulp to facilitate easier disintegration to nanocellulose, as well as a method to prepare CNFs bearing carboxylic groups for the production of functionalised CNPs. Other important routes to introduce charge to CNF surfaces include phosphorylation[19, 39, 63, 64] and sulfation.[144-146] Many other techniques are also used to introduce a variety of other functionalities to the fibril surface by grafting polymers to or from cellulose.[20] The use of modified CNFs for the fabrication of functionalised CNPs however comes with some severe drawbacks as it oftentimes greatly reduces the process efficiency and overall feasibility of CNP production: The presence of charged groups on the fibril surface negatively impact the dewatering speed as discussed above, often leading to drastically increased dewatering times compared to the already long dewatering times of unmodified CNF.[30, 31, 33] Additionally, a fact often ignored in literature, is that most modifications require washing and further purification steps, thus adding additional filtration or centrifugation steps to the process, exponentially increasing the time and water consumption.[62] Furthermore, experiments by Mautner et al.[39] have shown, that a large portion of the functional groups of CNFs in CNPs are not accessible as they are located in the bulk of the material, covered by other fibrils. Thus, if one wants to implement functionalised CNPs on larger scale as is proposed for example in water treatment applications, strategies for the introduction of these functionalities without negatively impacting the overall production times and not wasting precious work effort to introduce functional groups later lost in the bulk of the material, need to be developed.

2.6. The cellulose I and II allomorphs and mercerisation

Auspiciously, cellulose already offers solutions for some of its inherent flaws, as can be seen in the case of its brittle nature as several cellulose allomorphs with different crystal structure, and different physical, chemical, and mechanical properties have been discovered: Native cellulose and thus CNFs are highly oriented structures with short amorphous regions separating the crystalline regions along the elementary fibrils.[17] The crystal structure of native cellulose, termed "cellulose I", consists of layers of long, parallel cellulose molecules (i.e. having the same directionality, as defined by the reducing – the side of the chain containing a free aldehyde, which can be oxidised – and non-reducing end – the side of the chain without said aldehyde – of the sugars, as denoted in Figure 1) arranged in layers held together by hydrogen bonds stacked on top of each other by hydrophobic interactions.[147, 148] Through a variety of chemical processes, cellulose I can be transformed into other allomorphs[149] most importantly cellulose II.[150] Thermodynamically, cellulose II is the more stable allomorph and the crystal structure cellulose recrystallizes after dissolution – regeneration – and thus often termed "synthetic cellulose".[130, 150] Contrary to the layered and stacked structure of cellulose I, cellulose II consists of a three-dimensional network of hydrogen bonded cellulose molecules with an antiparallel chain orientation (Figure 4 left).[151-153] Compared to cellulose I, cellulose II is more ductile yet mechanically weaker.[130, 154, 155]

The partial transformation of cellulose I to cellulose II using LiCl/DMAc or ionic liquids – as discussed in section 2.5.1 – has been explored for the generation of ductile CNPs thus increasing their overall ductility. However, this transformation can also be facilitated via a much simpler, yet effective alkaline treatment which is termed "mercerisation" after the British scientist John Mercer, who invented the process in 1844. Mercerisation is widely used in the textile industry to improve the haptics of cotton.[156] The exact mechanism of this process is still up for discussion but it is hypothesized to be caused by swelling of individual elementary fibrils of a macroscopic cellulose fibre followed by either interdigitation of neighbouring fibres running in opposite directions (proposed by Kolpak and Blackwell in 1978[153, 157]) or by "back folding" of cellulose molecules withing the same fibril (proposed by Buleon, Chanzy & Roche in 1977[158]) thus transforming the parallel cellulose I allomorph into the antiparallel cellulose II allomorph upon deswelling and recrystallization (Figure 4 right).[159-162]

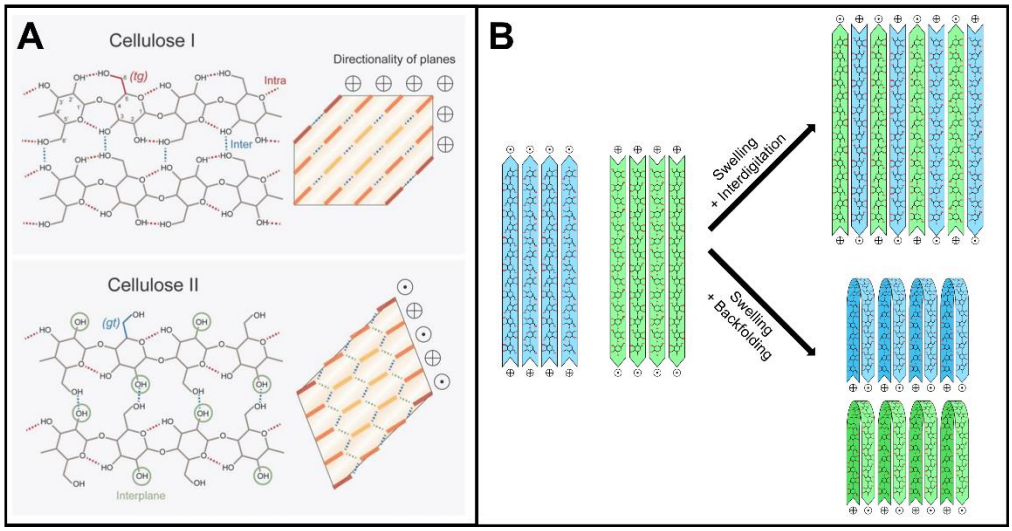

Figure 4: A) Differences in the intra and inter chain and interplane bonding structure of Cellulose I and II alongside the directionality of the chains (Wohlert et al. 2021)[163], reproduced from Springer Nature under CC BY 4.0 and B) a schematic depiction of the two proposed mechanisms of mercerisation.

Contrary to mercerisation of macroscopic cellulose fibres such as cotton or flax, the influence of alkaline treatments on nanocellulose structures is significantly less explored. To date, alkaline treatments were mainly used as a purification step for suspensions of bacterial nanocellulose (i.e. cellulose nanofibrils synthesized by various strains of bacteria, such as *Komatagaeibacter*) or from certain lignocellulosic sources, to remove bacteria, cells and proteins and to dissolve hemicelluloses.[67, 123] Some studies have reported the use of alkaline treatments to improve the mechanical properties of nanocellulose structures, such as Wang et al.[164] who used mercerisation and sodium chlorite treatment to facilitate the production of cellulose II nanofibres which yielded nanopapers of higher toughness (1.5 times that of CNPs prepared from cellulose I nanofibres) yet ~30 % lower tensile strength. The impact of mercerisation of as-grown bacterial cellulose pellicles was studied by Faria-Tischer et al.[165] who found that the transformation to cellulose II yielded pellicles with a smoother and more transparent surface. Hu et. al.[166] investigated the use of mercerised, never-dried, as-grown tubes of bacterial cellulose pellicles/hydrogels for vascular grafts reporting that the treatment was beneficial for the mechanical properties drastically increasing the burst pressure and tensile strength. Mercerisation of never-dried, as-grown bacterial cellulose sheets was also studied by Wloch et al.[167] for the fabrication of optically transparent, low-cellulose-loading laminated PMMA composites; They found that while the strain to failure and toughness of the pellicles increased significantly after alkaline treatment, they also lost up to 40 % of their tensile strength. The use of mercerisation of nanopapers prepared from relatively low-grade lignocellulosic sources has, aside from the work to be presented in this thesis,

to the best of my knowledge not been explored, but could offer a simple, relatively low-cost and tuneable procedure for the preparation of nanopapers with tailormade mechanical and optical properties.

2.7. Non-aqueous suspension media for nanopaper production

The use of non-aqueous solvents for the suspension of CNFs has been reported to aid composite production as the increased paper porosity permits better impregnation with the resin system as compared to conventional nanopapers. [115] Furthermore, the use of lower surface tension suspension media, enables for water-sensitive modifications of CNFs or to serve as pretreatment for more elaborate drying methods such as supercritical CO_2 drying.[31, 168, 169] Various groups reported the use of solvent exchange of filter cakes after filtration from water to a range of organic solvents to control the optical and mechanical properties of the resulting CNPs.[36, 37, 170, 171] Solvent exchange to non-aqueous solvents has been of particular interest in search for drying techniques that produce re-dispersible CNFs avoiding hornification between fibrils.[35, 172-174] Onyianta et al.[35] reported, that the filtration speed of CNF suspensions increased after each solvent exchange step to isopropyl alcohol, which could indicate the potential of using non-aqueous solvents as suspension media for CNP production via filtration. Previous reports – while not reporting on the influence of the suspension medium on the CNP preparation speed – described substantial influence of the suspension medium on the porosity, transparency, and the haze of the resulting nanopapers. [37, 38, 115, 170, 175] Ferguson et al. [175] investigated the influence of the surface tension of the suspension medium on the CNP porosity, and observed that the use of higher surface tension suspension media yielded CNPs with lower porosity. Hsieh et al. [37] reported the use of ethanol as suspension medium during filtration, yielding high-haze, high-transparency CNPs. The increase in porosity accompanying the use of low surface tension liquids for CNP production however comes at a detriment to their mechanical properties,[38] as a reduction in the envelope density inherently reduces the amount of load bearing material present leading to fewer fibre-fibre contacts throughout the network, resulting in overall weaker papers. This effect was predicted by Campbell in a seminal contribution, in which he postulated, that the surface tension of the suspension liquid during paper production (and by extension nanopaper production), greatly impacts the interfibrillar capillary forces (often termed Campbell forces) arising during drying: higher surface tension liquids enact higher Campbell forces on the network that pull neighbouring fibrils of the network in close enough contact for hornification [47, 176, 177] to occur, resulting in a denser network. A decrease in porosity not only impacts the mechanical properties

of the CNPs due to simply more load bearing material being present but also by generating an increased fibre-fibre bonding area which contributes directly to the tensile index of the resulting cellulose network, as predicted by the theory of Page, which can be stated as (Eq. 1):

$$\frac{1}{T} = \frac{9}{8\,Z} + \frac{12\,\delta}{b\,P\,L\,RBA} \qquad (1)$$

where T [kN m kg^{-1}] is the specific strength or 'tensile index' of a (nano)paper, Z [kN m kg^{-1}] the zero span tensile index, δ [kg m^{-1}] the linear density of nanofibrils of perimeter P [m] and mean length L [m]; the relative bonded area and the shear bond strength per unit area are represented by RBA and b [N m^{-2}], respectively. Therefore, if one wants to utilise low-surface tension, organic solvents for the efficient production of CNPs, strategies to combat the losses of mechanical properties must be devised.

2.8. Functionalisation of CNPs through hybridisation

Since the introduction of charged and functional groups to the surface of CNPs leads – as discussed in section 2.5.3 – to drastically increased production times and costs, other strategies for the introduction of functionality during CNP preparation are needed. One such route could be the use of hybridisation – i.e. the combination of two or more nano- or microscale materials yielding a material with properties in between its constituents or wholly new properties.[178] Hybridisation has been widely explored to impart electrical conductivity to nanopapers by incorporating Ag nanowires into the network[179] or to form CNP hybrids with electrostatic shielding properties by hybridising CNFs with graphene.[180] Hybrids of CNFs and ZnO nanoparticles have been investigated for use in anti-counterfeiting applications to include hidden information on the surfaces of banknotes and documents,[181] while hybrids of CNFs and Ag nanoparticles were shown to useful for the detection of pesticides in fruits and vegetables.[182] Hybrids of CNFs and nano-clays were demonstrated to possess excellent barrier properties and flame retardancy.[183, 184] In the field of water treatment and metal ion removal, a hybrid structure of pulp fines (i.e. the finest fraction of cellulose pulp used for paper production) and a metal-organic framework (MOF) has been used for the selective adsorption of Au ions from dissolved e-waste.[185]

2.8.1. Sulfonated Hypercrosslinked Polymers for CNF-Hybrids

Metal-organic frameworks used for the production and functionalisation of cellulose hybrids come with certain drawbacks in the context of using them for some applications, such as water purification, which include their tendency to be moisture sensitive and degrade when exposed to water and their high synthesis

costs, requiring expensive metal salts, linkers and solvents.[186] As alternative to MOFs, different classes of highly functionalised polymeric materials have been developed addressing said flaws.

During my thesis, I collaborated on the synthesis and application of sulfonated hypercrosslinked polymers (SHCPs), a class of polymeric materials that can be easily synthesised using Friedel-Crafts chemistry (Figure 5).[187]

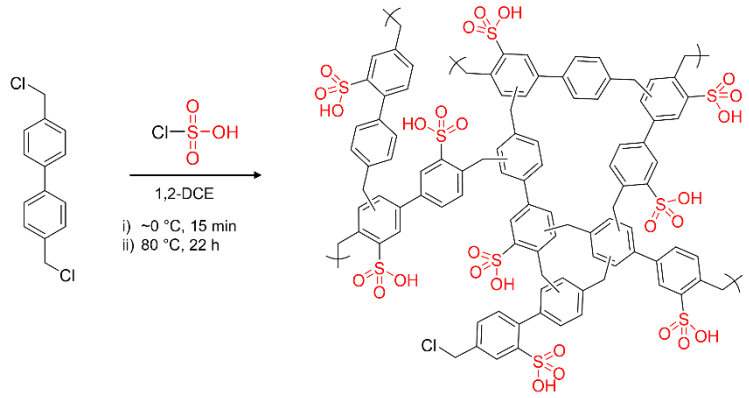

Figure 5: Reaction scheme of the synthesis of SHCPs as developed in publication A1. Publication A1, ©2024, the authors. Reproduced from the Royal Society of Chemistry under CC BY 3.0.

In publication A1, A. Blocher and I reported a one-pot approach for the synthesis of SHCP using chlorosulfonic acid as a simultaneous crosslinking and sulfonation agent, drastically reducing the synthesis time while increasing the surface area and functionalisation density compared to previously established routes. SHCPs and other porous organic polymers show great potential for use as catalysts or as high-capacity ion exchange materials, for applications like water softening and adsorbents for a variety of contaminants.[188-191] SHCPs are also typically not solution processable and often can only be synthesised in the form of powders, which in turn prohibits the direct manufacture of membranes.

2.8.2. CNF/SHCP hybrid structures for water treatment

Considering the shortcomings of SHCPs such as their low mechanical strength due to the fact that they are powders, their lack of solution processability, different strategies for their implementation in water treatment have to be developed such as their incorporation in matrices of polydimethylsiloxane,[192] poly[1-trimethylsilyl)-1-propyne],[193] or polymers with intrinsic microporosity.[194] Another possible way could be, to form CNF/SHCP hybrids, similar to the previously mentioned hybrids of pulp fines and MOFs. Such structures would lend themselves for the efficient production of highly functionalised hybrids, overcoming the low mechanical properties of SHCPs. Additionally, CNPs have

been shown to be capable of ultrafiltration,[38, 195] i.e. the removal of particles larger than 2 nm.[196] This can potentially yield a method to efficiently produce nanocellulose based films with a high amount of accessible functional groups, capable of ultrafiltration.

3. Experimental

This section will give a condensed overview of the relevant experimental procedures used to generate the data presented in this thesis. Important, novel and unusual methods will be presented in more detail, for more common analytical methods the reader is referred to the respective sections of the individual publications. Information about the used materials and chemicals, can be found in the materials sections of the respective publications.

3.1. Production and characterisation of starting materials

3.1.1. Nanocellulose Production (publication I, II & III)

Never dried cellulose pulp sheets (*Picea abies* and *Pinus spp.*) provided by Stendal (Berlin, Germany) were cut into small pieces (roughly 1 × 1 cm^2) and submerged in water at a consistency of 10 wt.-% for 18 h prior to an initial blending step in a conventional kitchen blender (Kult pro, WMF, Germany) at 1200 W for 1 min. The resulting suspension was passed ten times through a high-speed disc mill (Granomat JP 150, Fuchs, Switzerland) while gradually reducing the gap size between the grindstones and adding water as needed after each pass to ensure a suitable consistency grinding. The resulting nanocellulose suspension was up-concentrated to a cellulose dry mass content of ~4 wt.-% by gravity filtration through a cotton cloth bag and stored at 4°C until further use.

3.1.2. SHCP-Synthesis and Characterisation (publication III & A1)

Sulfonated hypercrosslinked polymers were synthesised according to a procedure developed in an additional publication (A1). In a beaker, 10 mmol (2.51 g) of 4,4'-bis(chloromethyl)-1,1'-biphenyl were dissolved in 1,2-dichloroethane (25 mL) at RT (25°C) before adding 40 mmol (4.66 g) of chlorosulfonic acid suspended in 1,2-dichloroethane (5 mL), followed by heating to 80°C and keeping the reaction at that temperature for 22 h. The resulting polymer was filtered and washed with ~100 mL methanol and subsequently Soxhlet extracted using methanol, which was followed by drying under vacuum at 80°C overnight to obtain a fine, brittle powder. The brown polymeric powder was termed SHCP-10 and stored in an airtight free-standing polypropylene (PP) tube at room temperature. The elemental composition of SHCP-10 was determined using X-ray induced photoelectron spectroscopy (XPS) and elemental analysis.

3.1.2.1. Kinetic investigation of Cu^{2+} ion adsorption onto SHCP-10

A suspension of 100 mg SHCP-10 powder in 25 mL of a 10 mmol L^{-1} $CuCl_2$ solution was used for the kinetic studies for the adsorption of Cu^{2+} onto SHPC-10. The studies were carried out in triplicate and at 30, 40, and 50°C, respectively. Samples of 100 µL were taken after 0.5, 1, 1.5, 2, 3, 5, 10, 60 and 1440 min, and purified by passing through a syringe filter, to remove residual polymer. Their Cu^{2+} content was determined via inductively coupled plasma-mass spectroscopy (ICP-MS, Agilent 7800 Agilent Technologies, Santa Clara, USA). The measured adsorption capacities, were plotted against the residence time, and fitted using pseudo first-order and pseudo second-order models:

$$q_t = q_e\,(1 - e^{-k_1 t}) \tag{2}$$

$$q_t = \frac{k_2 {q_e}^2 t}{1 + k_2 q_e t} \tag{3}$$

where q_t is the uptake of Cu^{2+} (mg g^{-1}) at any given time t (min), q_e the equilibrium adsorption capacity (mg g^{-1}), and k_1 and k_2 the first and second order rate constant, respectively. Iterative, non-linear regression was used as a fitting method to reduce biases introduced by the uneven temporal spacing of the datapoints, and the fitting range was adjusted from t = 0 to the plateau region of the curve, which indicated equilibrium (t = 1440 min for 30°C, t = 60 min for 40°C, and t = 10 min for 50°C). The experimental equilibrium adsorption capacity $q_{e,exp}$ was determined as the adsorption capacity at t = 1440 min. The kinetic parameters determined via the pseudo second-order model were further used to calculate the initial sorption rate h_o according to (Eq. 4):

$$h_0 = k_2 {q_e}^2 \tag{4}$$

The activation energy E_a of the reaction was determined by plotting them as an Arrhenius plot ($\ln(k_2)$ vs. T^{-1}) according to (Eq. 5):

$$\ln(k_2) = \frac{-E_a}{RT} + \ln(A) \tag{5}$$

3.2. Production of nanopapers (publication I & II)

Nanopapers and hybrids were prepared following a procedure similar to traditional paper-making. In brief, a desired amount of nanocellulose was suspended in the chosen suspension medium (ethanol/water mixtures or pure water), and homogenized by blending in a commercial kitchen blender (BL-4473, Tristar) at 2000 W for 30 s. The suspension was then transferred to a Büchner funnel with a 125 mm fritted glass disk, lined with a filter paper (VWR 413, VWR Leuven, Belgium) and filtered using vacuum produced by a water-jet pump. The

filtration was considered finished after a dense, yet still wet filter cake had formed, and droplets sucked into the filter flask were more than 15 s apart. The wet filter cake was subsequently removed from the filter paper and sandwiched between two stainless steel sheets lined with two layers of blotting paper (3MM Chr VWR, Lutterworth, UK) and pressed at room temperature under 1.5 to 2 ton-force for 10-30 s to remove excess suspension medium before replacing the blotting papers with one blotting paper and one release paper and hot-pressing the filter cake at 120°C under 1.5 to 2 ton-force for 15 min to consolidate the network and form the nanopaper. Information about the CNF dry mass, suspension medium composition and eventual post processing procedures of all CNPs of publications I & II can be found in Table 1 and Table 2.

3.3. Mercerisation of aqueous CNPs (publication I)

Nanopapers were affixed in a custom-built PMMA frame (Figure 6) and submerged into NaOH solutions of various concentrations for defined time intervals (Table 1). After mercerisation, the nanopapers were taken out of the NaOH bath, rinsed with tap water (approximately 10 L) until neutral pH and removed from the PMMA frame, before they were placed between stainless steel plates, each lined with 2 layers of blotting papers, and dried at 110°C for 24 h under 10 kg-force.

3.4. Consolidation of Et-CNPs (publication II)

CNPs produced from ethanolic suspensions were consolidated by soaking in deionised water for 5 min. The wet papers were subsequently placed between two sheets of blotting paper to remove excess moisture, before being placed between steel sheets lined with blotting paper and release paper followed by drying in an oven at the designated temperature (Table 2).

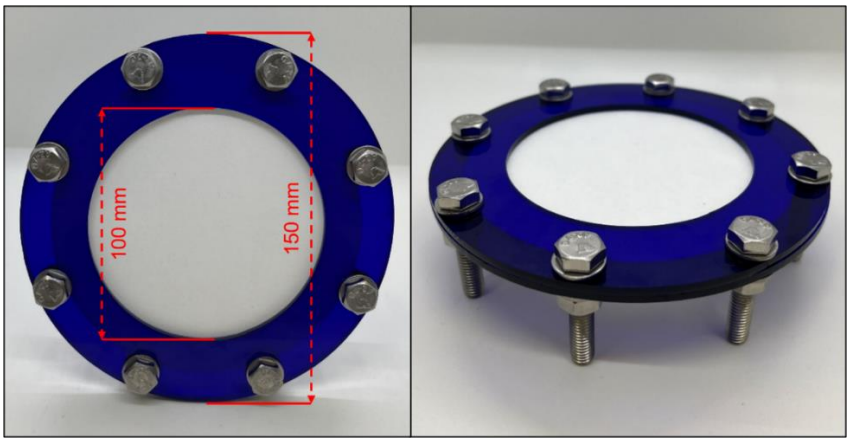

Figure 6: PMMA Frame used to affix CNPs during mercerisation. Publication I, © 2024 the authors. Reproduced from Springer Nature under CC BY 4.0.

Table 1: Sample codes and preparation and mercerisation parameters of all samples investigated in publication I. Samples were prepared in duplicates.

Sample name	Preparation Parameters		NaOH Concentration		Treatment Time
	Suspension Medium	CNF dry mass [g]	wt.-%	[mol L^{-1}]	[min]
Ref	Water	0.63	0	0	0
20% 2min			20	6.1	2
20% 10min			20	6.1	10
20% 60min			20	6.1	60
20% 24h			20	6.1	1440
40% 2min			40	14.3	2
40% 10min			40	14.3	10
40% 60min			40	14.3	60

Table 2: Sample codes, preparation parameters and eventual Post treatment steps of nanopapers prepared for rewetting and porosity studies of publication II.

Sample	Preparation Parameters		Notes	Post treatment
	Suspension Medium	CNF dry mass [g]		
H_2O-CNP	Water	1.2	-	-
Et-CNP-Ref	85 wt.-% EtOH	1.2	-	-
reEt-CNP-35	85 wt.-% EtOH	1.2	-	Rewetting and drying at 35 °C
reEt-CNP-70	85 wt.-% EtOH	1.2	-	Rewetting and drying at 70 °C
reEt-CNP-110	85 wt.-% EtOH	1.2	-	Rewetting and drying at 110 °C
Et-CNP-d	85 wt.-% EtOH	1.2	Dipped in H_2O before pressing	-
Por-0	Water	1.2	Test samples for influence of EtOH concentration on porosity	-
Por-10	10 wt.-% EtOH	1.2		-
Por-20	20 wt.-% EtOH	1.2		-
Por-30	30 wt.-% EtOH	1.2		-
Por-40	40 wt.-% EtOH	1.2		-
Por-50	50 wt.-% EtOH	1.2		-
Por-60	60 wt.-% EtOH	1.2		-
Por-70	70 wt.-% EtOH	1.2		-
Por-80	80 wt.-% EtOH	1.2		-
Por-90	90 wt.-% EtOH	1.2		-

3.5. Characterisation of CNPs (publication I & II)

Multiple test specimens shaped according to EN ISO 527-2, Type 1BB were punched out from each CNP and used to determine thickness d and weight to calculate the nanopaper grammage Γ and porosity Φ.

The specimen used to determine the physical properties were further used for measuring the tensile properties such as tensile strength σ, ultimate tensile strain ε_f, as well as the Young's modulus E, determined from the linear region of the resulting stress-strain curve as the secant between two strength values separated by a strain of 0.2 %. The modulus of toughness K_f – i.e. the energy a material can absorb during elastic and plastic deformation before failing – was determined by numerical integration of the area under the σ vs ε plots using the dimensionless strain ε from 0 to ε_f (Eq. 6):

$$K_f = \int_0^{\varepsilon_f} \sigma \mathrm{d}\varepsilon \qquad (5)$$

For the purpose of comparison it is important to point out, that K_f is often referred to as "work of fracture", *WoF* in literature (including in publication I).[26, 36, 132, 197] Per definition however, the work of fracture is the energy per unit area of new surface generated during fracture (J m^{-2}) while K_f is the energy per unit volume (Pa or J m^{-3}), which is the quantity reported as *WoF* in these papers. The modulus of toughness essentially is *WoF* normalised over the gauge length.

The paper tensile index (*cf.* specific strength) T was calculated from the load per unit width and grammage of the samples, and the specific modulus M obtained in the same way as the Young's modulus from the T vs ε plots.

The surface morphology of the prepared CNPs and hybrids was investigated by scanning electron microscopy (SEM) (Supra55VP, Zeiss, Austria) after sputtering them with an 8 nm layer of Au (80 %) and Pt (20 %) (Leica SCD 2020/EM QSG 100). The surface composition of the CNPs before and after mercerisation (publication I) was determined via X-ray photoelectron spectroscopy (XPS) (Nexsa, Thermo Scientific, UK).

The crystallinity of CNPs before and after mercerisation was determined by wide angle powder X-ray diffraction (PXRD) (Malvern PANalytical, Amelo, The Netherlands). The degree of crystallinity and ratio of the individual cellulose allomorphs of the cellulose samples were determined by Rietveld refinement using the ideal diffraction patterns of cellulose I_α and II as reported by Nishiyama et

al.[147] and French[198] using the software package High Score Plus, Version 4.9a (4.9.1.29739) (PANanalytical).

Haze and total luminous transmittance of recompacted CNPs were determined via UV-Vis spectroscopy (Lambda 356, PerkinElmer LAS Ltd., UK).

3.6. Preparation of CNF/SHCP hybrids (publication III)

The fabrication of three-layered hybrid structures entrapping the SHCP-10 powder particles (with the majority of the particles sized between 20 and 40 µm, as reported in the supplementary information of publication III) within the CNF network followed a modified version of the general CNP preparation procedure described in section 3.2:

Ethanolic suspensions containing a 1:1 weight ratio of CNF and SHCP-10 (0.2 wt.-% in total) were filtered onto a Büchner funnel (125 mm diameter) lined with a commercially available filter-paper (5–13 µm pore size, VWR 413) which also served as the bottom layer. After a dense, yet still slightly moist filter cake formed, the Büchner funnel was filled with an ethanolic suspension of pure CNF (0.2 wt.-%), which was filtered through the previously established filter cake to form a layer of pure CNF on top.

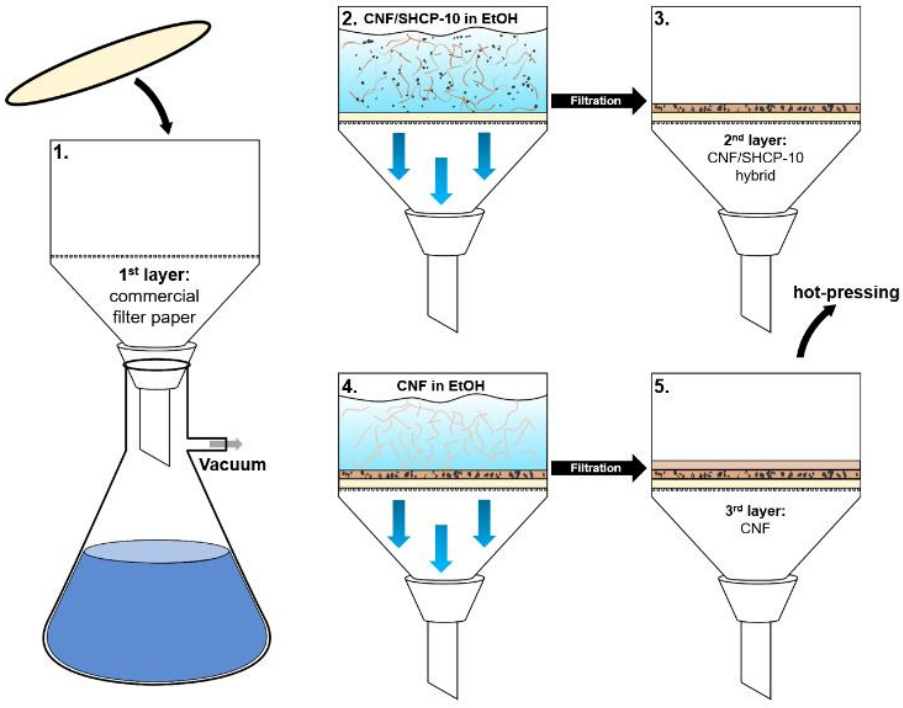

Figure 7: Schematic depiction of the individual filtration steps in the manufacture of CN/SHCP hybrids. Publication III © 2024, the authors. Reprinted from Wiley-VCH GmbH under CC BY 4.0.

The resulting three-layer hybrid sandwich structure was then taken out of the funnel and cold- and hot-pressed as described in section 3.2, with the exception, that the filter paper was not removed from the filter paper serving as the bottom layer. The composition of each hybrid and their sample code is summarised in Table 3.

Table 3: Sample code and layer grammages of hybrids prepared for publication III. Note: The middle layer grammage is the combined grammage of both constituents.

Sample Name	CNF/SHCP-10 middle layer [g m^{-1}]	Pure CNF top layer [g m^{-1}]
SHCP/CNF 20-5	20	5
SHCP/CNF 20-10	20	10
SHCP/CNF 20-25	20	25
SHCP/CNF 50-5	50	5
SHCP/CNF 50-10	50	10
SHCP/CNF 50-25	50	25
SHCP/CNF 100-5	100	5
SHCP/CNF 100-10	100	10
SHCP/CNF 100-25	100	25

3.7. Characterisation of CNF-SHCP hybrid membranes (publication III)

The water permeance of the manufactured hybrid membranes was tested in a dead-end flow cell (HP4750, Sterlitech). Permeate fractions were collected until the permeate volume per unit time, pressure and filter area changed by less than 2 % over the course of one hour, to ensure equilibrium was reached.

The same dead-end flow cell was used to test the heavy metal adsorption capacity of the manufactured CNF-SHCP-10 hybrids under dynamic conditions by forcing 200 mL of a 2.5 mmol L^{-1} $CuCl_2$ solution through the hybrid at a pressure which facilitated a flow rate of approx. 1 drop per second. The permeate was collected in 35 fractions of 5 mL each and their Cu^{2+} as well as the Cu^{2+} concentration in the remaining supernatant was determined. The total mass of adsorbed Cu^{2+} m_{ads}, was calculated as the sum of the removed Cu^{2+} of all fractions and was used in conjunction with the mass of SHCP-10 m_{pol} contained within each tested specimen (determined from the polymer loading and the active filtration area of the dead end flow cell used) to calculate the heavy metal adsorption capacity q (Eq. 7):

$$q = \frac{m_{ads}}{m_{pol}} \tag{7}$$

The adsorption capacity per unit area q_A of each hybrid was calculated from the total mass removed m_{ads} and the active filtration area A as shown in Eq. 8:

$$q_A = \frac{m_{ads}}{A} \tag{8}$$

To test the regenerateability of the hybrid membranes one of the membranes (SHCP/CNF 50-10) was flushed with 10 mL fractions of HCl (0.1 M, 120 mL total) while affixed in the dead-end flow cell. The fractions were collected, their copper content determined, and the dynamic heavy metal adsorption of the membrane was retested as described above until 3 adsorption cycles were finished.

To test the capability of the hybrids to remove traces of possibly harmful alkaline earth metal ions, such as Sr^{2+} and Ba^{2+}, in the presence of excess concentration of water hardness elements and to investigate possible selectivity towards one, dynamic adsorption tests using commercially available mineral water were performed using SHCP/CNF 100-5, following the same procedure as described above for the dynamic Cu^{2+} adsorption: 170 mL of a 1:1 mixture of commercial mineral water and ultrapure water (because of instrumental restrictions related to ICP-MS) were passed through SHCP/CNF 100-5 and collected in eleven fractions of 5 mL followed by 11 fractions of 10 mL. The ion concentration in the fractions was determined by ICP-MS.

The ultrafiltration capability of SHCP/CNF hybrids was investigated by forcing 10 mL of a gold nanoparticle suspension (10 nm diameter, 6×10^{11} particles per mL), through a 25 mm diameter disc of SHCP/CNF 20-5 at a pressure of 2 barg. The gold nanoparticle concentration before and after filtration was determined by UV-Vis spectroscopy (Agilent 8543 UV-vis Spectroscopy system, Agilent Technologies, Santa Clara, USA).

4. Results and Discussion

4.1. Influence of mercerisation on the properties of CNPs (publication I)

To target the first major issue identified in the literature review – the brittle nature of CNPs – without negatively impacting the already long filtration times during CNP production, I investigated the use of a simple post-processing method called mercerisation. Mercerisation is a procedure well established in the textile industry to increase lustre, tenacity and dyability of cotton fibres.[105] The goal of publication I therefore was the efficient production of ductile nanopapers with high strength produced from relatively low grade nanocellulose sources using this post-processing procedure.

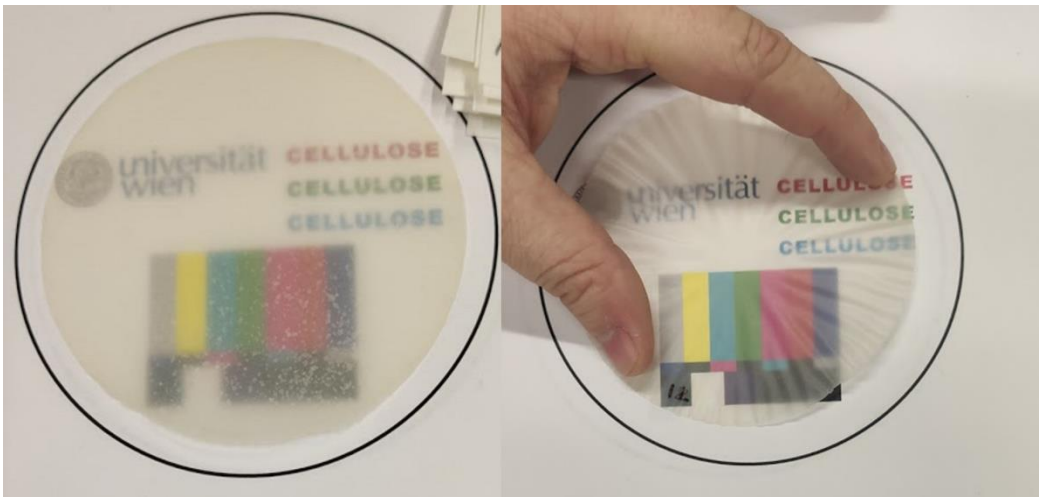

Figure 8: comparative photographs of a CNP mercerised without clamping in 40 wt.-% NaOH before (left) and after (right) treatment. The CNP exhibited significant shrinkage, and cockling during mercerisation, yet became significantly more transparent. Publication I, © 2024 the authors. Reproduced from Springer Nature under CC BY 4.0.

Preliminary tests however, showed a significant amount of shrinkage, cockling, and wrinkling of CNPs during subsequent drying, after being submerged in strongly alkaline solutions (Figure 8), which informed the experimental setup used in publication I; the use of a custom built fixation ring (Figure 6). The alkaline concentrations used were chosen to represent those commonly used in literature (20 wt.-% NaOH) and an excessively high concentration (40 wt.-% NaOH) to investigate eventual beneficial or detrimental effects of harsher conditions on the CNPs properties.

4.1.1. Changes of physical properties of CNPs during mercerisation

Constraining nanopapers during mercerisation proved to be effective to prevent lateral shrinkage and cockling of CNPs during mercerisation and led to an average increase of 8 % of the envelope density of the nanopaper density after mercerisation while t-tests revealed no significant difference of the nanopaper thickness before and after mercerisation of constrained nanopapers (Supplementary information of publication I). Mercerisation of an unrestrained nanopaper however, resulted in a drastic increase in thickness accompanied by lateral shrinking yielding a thickness increase of ~20 %.

4.1.2. Nano-structuring and fibril welding during mercerisation

SEM images of nanopaper surfaces (Figure 9) showed a gradual change of the fibrillar structure of unmercerised CNPs towards a surface covered by amorphous looking domains, termed “fibre welding” by Wloch at al.,[167] who observed similar effects when mercerising as-grown bacterial cellulose pellicles, indicating that cellulose I fibres are being encased by non-fibrillar cellulose II, which corresponds well with the postulated mechanism of mercerisation of fibre swelling followed by interdigitation and recrystallisation upon drying.[157] The micrographs also showed the formation of bulbous structures on the CNPs surface after mercerisation, which increased in amount and size when increasing the treatment times and/or the NaOH concentration.

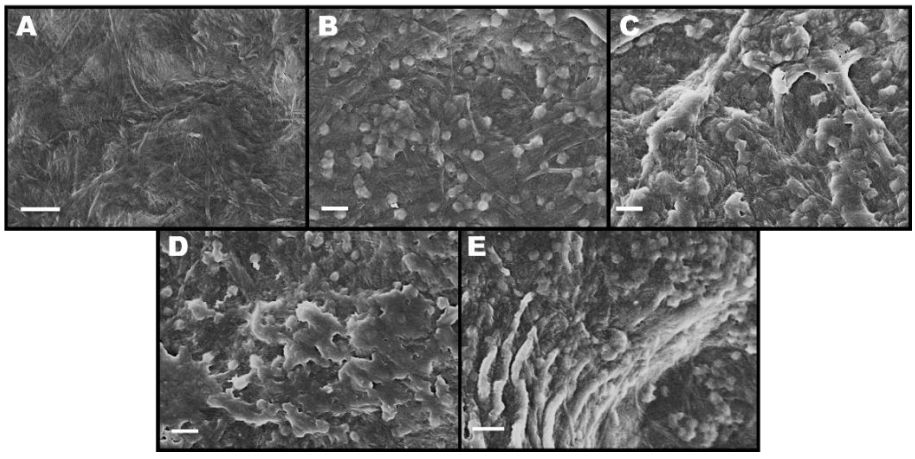

Figure 9: SEM images of the surfaces of samples treated in 20 wt.-% NaOH solutions. A) 0 min - Reference, B) 2 min, C) 10 min, D) 1 h, E) 24 h. The scale bar size corresponds to 1 µm. Publication I, © 2024 the authors. Reproduced from Springer Nature under CC BY 4.0.

XPS showed no significant difference in the elemental composition of the nanopapers before and after mercerisation, thus these bulbous structures likely formed during mercerisation, as the swelling cellulose II surrounding cellulose I fibrous cores is “squeezed” through the pores of the 2.5D randomly oriented

network recrystallising in the observed protrusions on the CNP's surface. With increasing treatment times, these cellulose II expulsions coalesce into the larger domains found on the surfaces of nanopapers mercerised for 1h and beyond (Figure 9 D and E).

4.1.3. Influence of mercerisation on the cellulose crystal structure in CNPs

Wide angle powder X-ray diffraction measurements followed by Rietveld refinement were used to assess the transformation of cellulose I_β to cellulose II (Figure 10). Initially the CNPs only showed the typical diffraction peaks of cellulose I_β with the peak at $2\theta \approx 22.5°$ corresponding to the (2 0 0) diffraction plane of cellulose I_β, and the diffraction peak centred around $2\theta \approx 15.7°$ corresponding to the compound peak of the I_β (1 -1 0) and the I_β (1 1 0) diffraction plane at 15° and ~16.5°, respectively slightly deviating from peak positions of $2\theta = 14.5°$ and 16.5° found in ideal cellulose I diffraction patterns.[198] The intensity of cellulose I_β diffraction peaks decreased after mercerisation and the characteristic peaks of cellulose II appeared, with peaks at $2\theta \approx 12.2°$, ~20.1° and ~21.7° corresponding to the (1 -1 0), (1 1 0) and (0 2 0) diffraction planes of cellulose II, respectively.[198] A sharper diffraction peak at $2\theta \approx 28.5$ was present in all mercerised nanopapers and could – with the help of XPS – be attributed to silica containing crystalline residues of the grindstones used for defibrillation during nanocellulose fabrication.

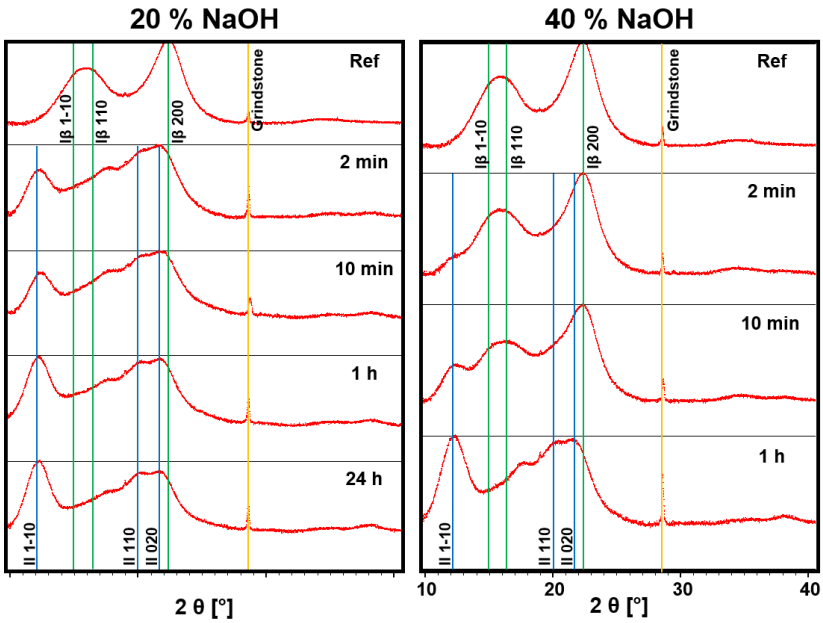

Figure 10: Wide angle PXRD diffractograms of untreated reference papers (Ref) and nanopapers mercerised for various times in 20 wt.-% (left) and 40 wt.-% (right) NaOH concentration. Publication I, © 2024 the authors. Reproduced from Springer Nature under CC BY 4.0.

The degree of crystallinity was determined using Rietveld refinement to separate the crystalline and amorphous phases of the PXRD diffractograms and was 69 % for the wood-based nanocellulose used in this thesis, which agreed well with literature.[199, 200] While mercerisation caused a gradual transformation of the cellulose I_β allomorph to the cellulose II allomorph, no change of the overall degree of crystallinity, which remained at ~70 %, was observed (Figure 11).

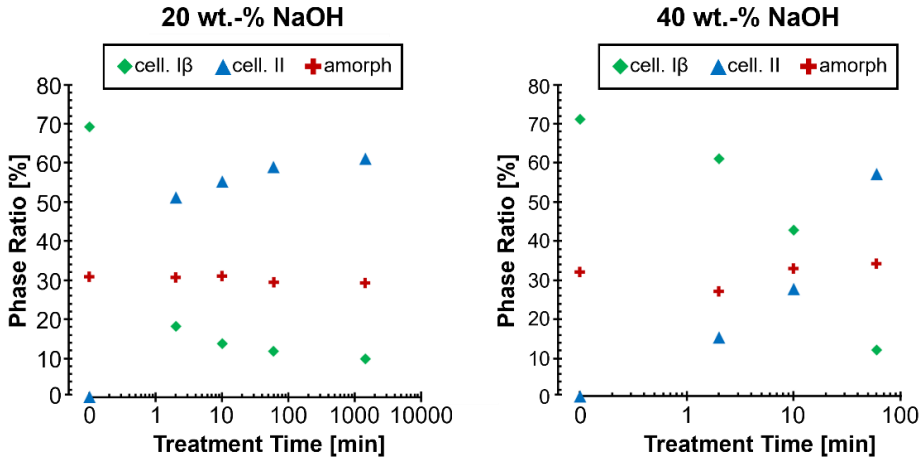

Figure 11: Degree of crystallinity of cellulose I_β and II, as well as amorphous phase content of untreated reference papers (ref) and nanopapers mercerised for various times at 20 wt.-% (left) and 40 wt.-% (right) NaOH concentration. Publication I, © 2024 the authors. Reproduced from Springer Nature under CC BY 4.0.

The transformation of cellulose I to cellulose II during mercerisation showed a strong dependence on the alkaline concentration, with nanopapers treated in 20 wt.-% NaOH solutions exhibiting rapid transformation speeds, reaching a cellulose II phase ratio of over 50 % within the first 2 min, which rose to 59 % after one hour and only marginally increased to 61 % after 24 h. Nanopapers treated in the much more concentrated 40 wt.-% NaOH solutions exhibited much lower transformation speeds, which was hypothesised to stem from a form of "passivation", in which the highly alkaline solution swells the outer layers of the nanofibril much faster, prohibiting further penetration of the NaOH solution into the fibrils, and thus slowing down the overall transformation rate.

4.1.4. Influence of mercerisation on mechanical properties of CNPs

In comparison to an unmercerised reference nanopaper, all mercerised CNPs possess significantly increased strains to failure ε_f, with those being mercerised in 20 wt.-% NaOH exceeding those mercerised in 40 wt.-% solutions (Figure 12 and Table 4). CNPs mercerised in 20 wt.% NaOH solutions reached their maximum ε_f values after 2 min of treatment whereas CNPs mercerised in 40 wt.-% NaOH solutions reached theirs after 10 min of treatment in accordance with the cellulose I to II transformation rates found by PXRD. The initial increase and subsequent

decrease of ε_f with increasing treatment times was attributed to the CNPs first reaching a cellulose I to II ratio resulting in a ductile yet strong network, followed by a gradual hydrolysis of the cellulose chains (as can be seen by the molecular weights reported in the supplementary information publication I), thus breaking up the continuity of the reinforcing cellulose I core network, resulting in a weaker network more prone to failure.

Table 4: Tensile properties of mercerised nanocellulose samples containing tensile strength (σ), strain to failure (ε_f), Young's Modulus (E) and Modulus of toughness (K_f)

Sample name	σ [MPa]	ε_f [%]	E [GPa]	K_f [MPa]
Ref	114.9 ± 2.1	1.7 ± 0.1	12.7 ± 0.9	1.2 ± 0.1
20% 2 min	102.0 ± 11.1	9.1 ± 1.3	7.2 ± 0.6	6.9 ± 1.0
20% 10 min	110.0 ± 3.2	6.0 ± 0.5	7.8 ± 0.7	5.0 ± 0.6
20% 60 min	105.4 ± 4.2	6.1 ± 1.1	7.3 ± 0.7	4.8 ± 1.1
20% 24 h	109.8 ± 6.5	5.1 ± 1.1	8.4 ± 1.2	4.1 ± 1.0
40% 2 min	118.0 ± 7.1	4.1 ± 0.7	10.6 ± 0.9	3.6 ± 0.8
40% 10 min	119.2 ± 3.3	4.6 ± 0.6	10.3 ± 0.9	4.1 ± 0.7
40% 60 min	111.7 ± 5.0	3.9 ± 0.5	9.4 ± 0.5	3.2 ± 0.5

CNPs mercerised in 40 wt.-% NaOH solutions had lower ε_f compared to their 20 wt.-% counterparts but retained their tensile strength, while reaching ε_f values of at least 230 % of the unmercerised reference nanopapers, with nanopapers treated for 2 min once more outperforming those treated longer. The retention of the tensile strength of CNPs treated with 40 wt.-% NaOH solutions alongside their lower ductility when compared to CNPs mercerised in 20 wt.-% NaOH solutions can be attributed to multiple factors: The retention of an intact cellulose I network due to the passivating effect of the harsher treatment yielding a network containing more of the stronger and less ductile cellulose I_β allomorph, which was supported by the results of the PXRD crystallinity studies. Furthermore, the swelling and recrystallisation during mercerisation leads to the formation of a denser network with less defects that can act as stress accumulation points compared to the untreated reference nanopaper. Mercerised CNPs had Young's moduli, which followed the inverse trend of their ε_f showing a trade-off between ductility and stiffness. The modulus of toughness K_f (termed work of fracture, *WoF*, in publication I) increased significantly over that of unmercerised reference CNPs (Table 4). The modulus of toughness followed the trend of ε_f for all mercerised nanopapers with an increase of at least 175 % ranging up to 590 % of K_f of the reference CNP.

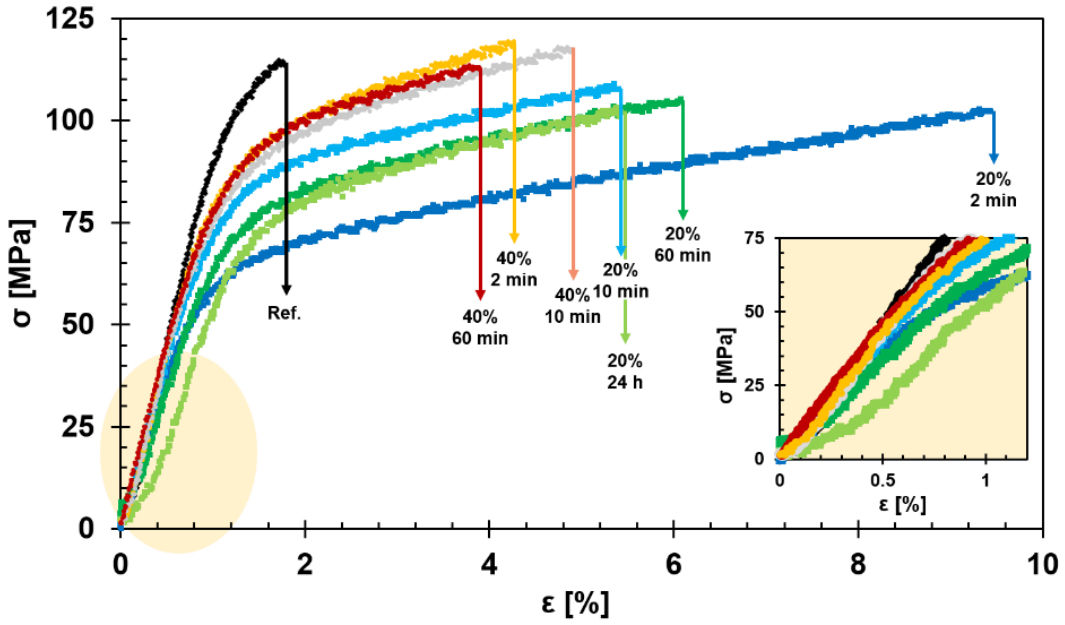

Figure 12: Representative stress strain curves of (mercerised) nanopapers. The inset diagram shows a magnification of the linear region used to calculate E. Publication I, © 2024 the authors. Reproduced from Springer Nature under CC BY 4.0.

Based on the results of the tensile tests two optimal treatment protocols can be identified:

- Mercerisation for short periods of times (i.e. 2 min) in 20 wt.-% NaOH yielded a significant improvement of the ductility and tensile toughness of CNPs of 535 % and 590 %, respectively, while retaining over 80 % of the CNP's Young's modulus and almost 90 % of its tensile strength.
- Mercerisation for 2 – 10 min in 40 wt.-% NaOH solutions yielded CNPs with both increased tensile strength, modulus of toughness and ductility.

4.2. Influence of the suspension medium on nanopaper production (publication II)

While publication I aimed to produce more ductile nanopapers, without negatively impacting the filtration times, publication II aimed to specifically target the improvement of the filtration speed during CNP preparation without compromising the mechanical properties of the nanopapers.

4.2.1. Impact of suspension medium on CNP filtration times

To compare the impact of the suspension medium on the filtration performance during nanopaper production, first a baseline had to be established: The filtration setup was filled with the respective suspension medium (DI water and 85 wt.-% ethanol, respectively) without nanocellulose present, which revealed no difference in the flow rates (4.4 ± 0.3 L min^{-1}) of both media through the filter membrane,

indicating that all eventual differences are caused by the presence of nanocellulose and the nascent filter cake. In the presence of nanocellulose, a drastic difference in the filtration speeds was observed, with CNF in water suspensions exhibiting a flow rate of 0.85 L h^{-1} and 85 wt.-% ethanol/CNF suspensions one of 3.16 L h^{-1} resulting in a reduction of the filtration time from 71 ± 3 min to 19 ± 1 min (a 73 % reduction). Initially, one might assume these results to be counterintuitive, as the viscosity of an 85 wt.-% ethanol in water mixture is significantly higher than that of pure water – 1.7 mPa s versus 1 mPa s, respectively – and, according to Darcy's law, should thus lead to longer filtration times. However, as a CNF filter cake forms during filtration, several other factors have to be taken into account; for example, the pressure drop over the forming filter cake, which is the sum of the vacuum applied from below (Δp) and the hydrostatic pressure ($\rho\, g\, h$) of the suspension medium. The hydrostatic pressure acting upon the two forming filter cakes ($P = \Delta p + \rho g h$)) is greater for pure water than for the water/ethanol mixture given the higher density of the former (0.998 g mL^{-1} and 0.831 g mL^{-1} at 20°C for water and 85 wt.-% ethanol/water mixtures respectively [201]). The lower initial hydrostatic pressure combined with the dipole moment of ethanol compared to water (1.69 D and 1.86 D, respectively)[201] would reduce the interactions between the CNF and the ethanolic suspension medium compared to the aqueous suspension medium. The lower pressure drop and the altered CNF/suspension medium interaction leads to the formation of a more porous initial CNF skin layer on top of the filter paper, analogous to the findings of Mattsson et al.[32] who observed similar effects when varying the pH of aqueous suspension media used during the filtration of microcrystalline cellulose. The greater porosity of the filter cake forming from an ethanolic suspension in turn led to a lower resistance to flow, as described by Kozeny and Carman,[135] thus leading to a faster flow through the nascent filter cake. Furthermore, the change to an ethanolic suspension medium reduces the thickness of the hydration shell around the hydrophilic cellulose fibres in the nascent filter cake, thus virtually increasing pore size and porosity and consequently decreasing the filtration resistance even further.

4.2.2. Impact of suspension medium composition on CNP porosity

I investigated the influence of the composition of the suspension medium on the porosity of the resulting nanopapers by gradually increasing the EtOH content in the suspension medium used during nanopaper production from 0 to 90 wt.-% in 10 wt.-% increments (Figure 13 A).

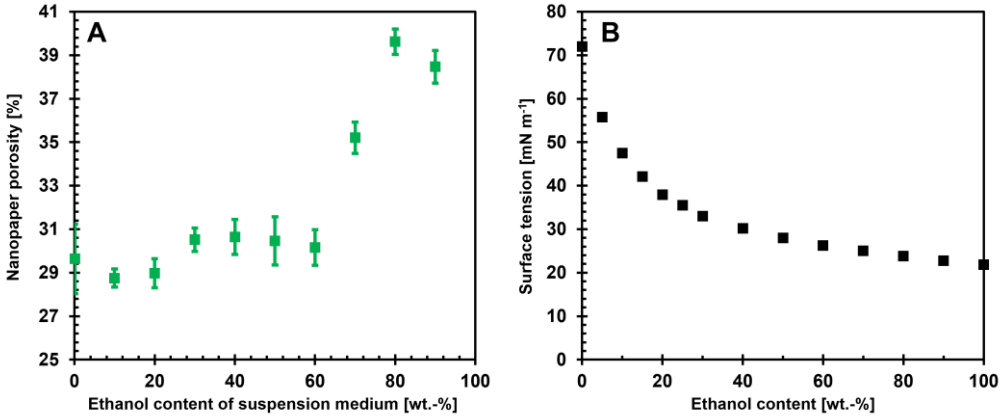

Figure 13: A) Dependency of nanopaper porosity on the suspension medium composition. Error bars are depicting the 95 % t-distributed confidence interval. Publication II © 2025, the authors, currently under submission. B) Surface tension of ethanol & water mixtures, generated using literature values (Vazquez 1995)[202]

Most noticeably, no change in the porosity of the resulting nanopapers can be observed up until the suspension medium contained 60 wt.-% ethanol, which is followed by a rapid porosity increase until 80 wt.-% after which it plateaued. The sudden change in nanopaper porosity between 60 and 80 wt.-% was attributed to Campbell forces, i.e. capillary forces exerted on the fibril network by the evaporating suspension medium during drying; The increase of the ethanol content leads to a gradual decrease of the mixture's surface tension (Figure 13B), and thus the capillary forces, and after reaching an ethanol content of over 60 wt.-% (i.e. surface tensions lower than 26.23 mN m^{-1}) these Campbell forces are no longer able to overcome the tension forces of the fibril network and are thus unable to pull the fibrils into close enough proximity for hornification to occur resulting in significantly less network compaction and thus, a more porous nanopaper. It should be noted that the 20 CNPs used to obtain the data of Figure 13 A were produced using CNF stock disintegrated with a lower powered disk mill (1.5 kW vs. 3.7 kW) and thus their porosities should not be directly compared to others in this thesis.

4.3. Impact of reconsolidation on the properties of EtOH-CNPs (publication II)

In publication II, I also investigated the influence of a reconsolidation step, i.e. submerging fully formed nanopapers prepared from ethanolic suspensions in water and re-drying them, on the CNPs properties. Considering the simplicity of the treatment, the effects are significantly improving the Et-CNP's properties in all tests, some even beyond those of CNPs produced from aqueous suspensions.

4.3.1. Changes in physical properties after recompaction of CNPs

The impact of the consolidation treatment after Et-CNP formation on the physical properties such as thickness and porosity compared to the reference nanopapers is shown in Table 5.

Table 5: Grammage Γ, thickness d, density ρ, and porosity ϕ with standard deviation of the different types of CNPs. Note: the grammage was determined by weighing at ambient conditions, thus including moisture entrapped at the fibril surface (~7 %)

Sample	Γ [g m^{-2}]	d [µm]	ρ [kg m^{-3}]	ϕ [%]
Et-CNP-ref	103.7 ± 2.0	98.9 ± 2.3	1049 ± 25	30.1 ± 1.7
reEt-CNP-35	113.7 ± 2.2	91.2 ± 2.1	1247 ± 25	16.8 ± 1.7
reEt-CNP-70	111.9 ± 1.4	89.1 ± 1.8	1256 ± 32	16.3 ± 2.1
reEt-CNP-110	113.2 ± 2.0	90.8 ± 2.3	1247 ± 33	16.9 ± 2.2
Et-CNP-d	108.2 ± 2.0	90.4 ± 2.6	1198 ± 32	20.1 ± 2.1
H_2O-CNP	106.0 ± 3.1	84.9 ± 2.5	1248 ± 29	16.8 ± 1.9

Statistical analysis (t-tests) revealed that density and porosity of reEt-CNPs and of H_2O-CNPs show no significant difference between one another, while the porosity of Et-CNPs is almost twofold that of all other samples, indicating network compaction driven by Campbell forces and hornification, yielding a denser, more consolidated network than would be possible with 85 wt.-% EtOH in water. The results show, that the changes in porosity during secondary drying are not temperature dependent, indicating that the sole driving factor is the higher surface tension of water compared to 85 wt.-% EtOH in water (72.8 mN m^{-1} and ~24mN m^{-1}, respectively)[202] resulting in higher capillary/Campbell forces during drying pulling more fibrils in close enough proximity for hornification to occur. Nanopapers produced from ethanolic suspensions and dipped in water while still ethanol wet prior to hot pressing possessed porosities in between those of Et-CNP-ref and H_2O-CNP, indicating that some ethanol remained in the structure, resulting in insufficiently high Campbell forces to fully compact the filter cake during hot-pressing.

Scanning electron micrographs of the nanopapers' cross-sections reveal a laminar structure in nanopapers (Figure 14) with large interlayer pore spaces for Et-CNP-ref (Figure 14 A). Nanopapers produced from aqueous suspensions (Figure 14 C) and reEt-CNPs (B) possess a denser structure with less interlaminar pore spaces, further indicating that the increased Campbell forces during recompaction "pull" the individual layers in CNPs together. SE micrographs of surface of Et-CNP-ref (Figure 14 D) reveal a looser network structure with more defects present, which

are not present in H_2O-CNPs (F) or recompacted CNPs (E), further substantiating the proposed mechanism of network compaction through capillary forces and hornification.

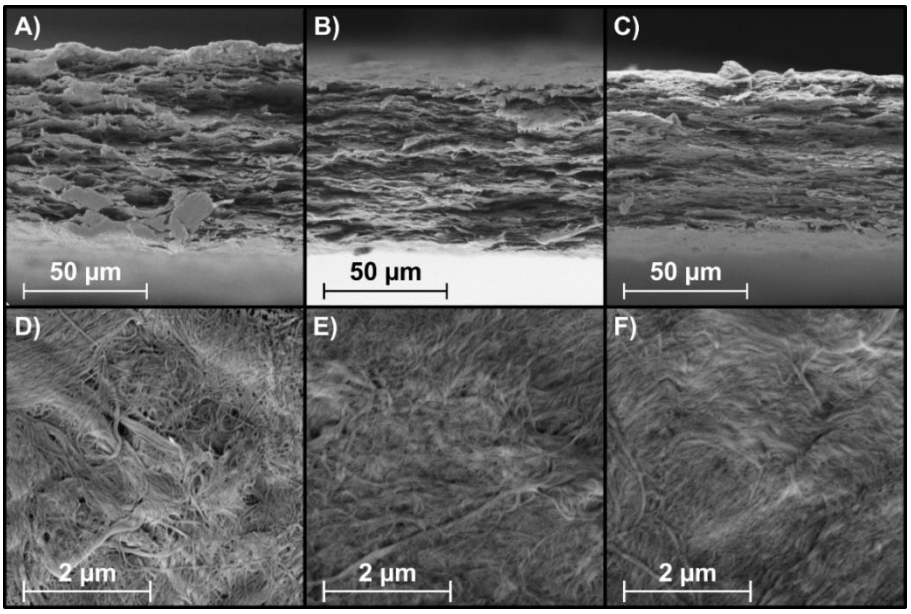

Figure 14: Representative SEM micrographs of nanopaper fracture surfaces after tensile testing (top row) and the nanopapers surface of Et-CNP-ref (A & D), reEt-CNP-70 (B & E) and H_2O-CNP (C & F). Publication II © 2025, the authors, currently under submission.

4.3.2. Changes in optical properties after recompaction

To evaluate the effect of recompaction on the optical properties, the total luminous transmittance of CNPs at 572 nm wavelength (analogous to the TAPPI T425 standard for paper opacity) were compared. When plotting the total luminous transmittance against the nanopaper porosity ϕ (Figure 15), one can see that nanopapers which were not recompacted, exhibit an inverse relation between porosity and transmittance. Recompacted Et-CNPs however, exhibited a significantly higher transmittance than H_2O-CNP at the same porosity.

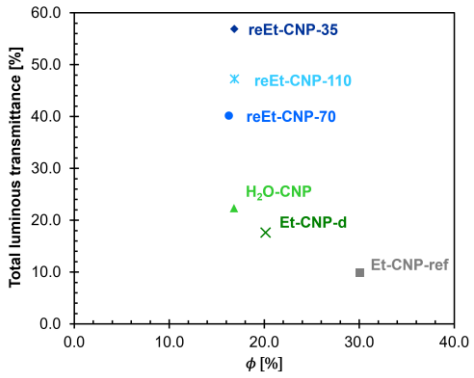

Figure 15: Total luminous transmittance of nanopapers in relation to their porosity ϕ. Publication II © 2025, the authors, currently under submission.

As transmittance is determined by reflection and absorption of light, and changes in adsorption between the different CNPs are negligible, differences in the reflective properties can be identified as being responsible for the differences in transmittance. Reflection occurs at interfaces within the network, such as interlaminar pore spaces and other defects, which indicates, that alongside the reduction of the interlaminar pore-spaces, a "relaxation" and reduction of voids and reflection points throughout the network occurred during the wetting and re-drying procedure, yielding CNPs with less scattering sites throughout.

4.3.3. Influence of recompaction on the mechanical properties of CNPs

Representative stress-strain curves (Figure 16) and the collected tensile data (Table 6) of as-produced and recompacted CNPs, reveal relatively low strains to failure of 2.5-3.4 % for Et-CNP-ref, Et-CNP-d and H_2O-CNP alike, whereas recompacted Et-CNPs were much more ductile, reaching values of up to 7.5 %. Conversely, (recompacted) Et-CNPs had lower tensile strength than those filtered from water indicating a trade-off between ductility and tensile strength.

Table 6: Tensile index T, ultimate tensile strain ε_f, (grammage corrected) specific modulus M, and Modulus of toughness K_f of all tested nanopapers.

Sample Name	T [kN m kg^{-1}]	ε_f [%]	M [MN m kg^{-1}]	K_f [MJ m^{-3}]
Et-CNP-ref	82.5 ± 3.4	2.8 ± 0.4	8.4 ± 0.6	1.7 ± 0.4
reEt-CNP-35	85.5 ± 3.0	7.5 ± 0.4	8.0 ± 0.4	6.4 ± 0.6
reEt-CNP-70	93.8 ± 3.4	5.6 ± 0.4	9.0 ± 0.4	5.2 ± 0.6
reEt-CNP-110	96.4 ± 4.0	5.1 ± 0.6	8.4 ± 0.6	4.7 ± 0.6
Et-CNP-d	104.1 ± 4.7	2.5 ± 0.3	9.8 ± 0.7	2.2 ± 0.3
H_2O-CNP	121.1 ± 7.1	3.3 ± 0.5	10.4 ± 0.6	3.6 ± 0.8

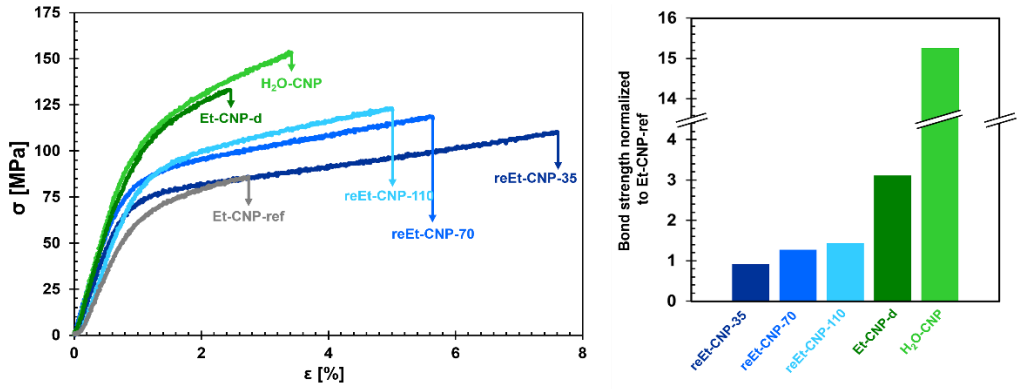

Figure 16: Representative stress-strain curves of all (recompacted) CNPs (A) and the relative bonding contributions to the tensile index normalized to that of Et-CNP-ref (B). Publication II © 2025, the authors, currently under submission.

A simple manipulation of Page's equation (as demonstrated in the supplementary information to publication II) can be used to show the relative differences in shear bond strength of two specimens (Eq. 9) using their tensile index T and porosity ϕ using the assumption that $Z_c = 8Z/9$ (with Z being the Zero span tensile strength of the CNFs used) is unaffected by the different suspension media used.

$$\frac{b_1}{b_2} = \frac{T_1}{T_2}\frac{(Z_c - T_2)}{(Z_c - T_1)}\frac{RBA_1}{RBA_2} \tag{9}$$

The relative bonded area RBA was calculated from the respective nanopaper porosities according to Eq. 10

$$RBA = 1 - \frac{\phi(1-\phi)(2-\phi)}{\ln(1/\phi)} \tag{10}$$

The relative difference in shear bond strength (b_1/b_2) compared to sample Et-CNP-ref is reported in the righthand side of Figure 16 and was calculated by assuming Z = 140 kN m kg^{-1} – the most likely value of Z. The results show a slight increase in the shear bond strength after the compaction treatments with increasing drying temperature, which also explains the increased tensile index of recompacted samples compared to EtOH-CNP-ref. The drastic increase of the strain to failure after water wetting and drying of Et-CNPs can – in light of the relative shear bond strengths – be attributed to a densification of the network while maintaining similar interfibrillar bond strengths as Et-CNP-ref, which allows for fibrils to slide over each other under tension until eventually failing yielding an overall more ductile network than is possible for the more hornified H_2O-CNPs. The greatly increased ductility of reEt-CNPs while maintaining most (~80 %) of the tensile strength of H_2O-CNPs results in a greatly increased (up to 178 % that of Et-CNP-ref) energy of deformation E_d and, therefore, tensile toughness.

4.4. Efficient introduction of functional groups to CNPs via hybridisation (publication III)

To target the third major issue of CNP production identified in the literature review, the difficulty of introducing functional groups to the CNPs without negatively impacting the production times, as the introduction of charged groups to the CNFs surface inevitably leads to lower permeance and thus also filtration times,[203] I used one of the key findings of publication II, i.e. the possibility to use ethanolic suspension media to speed up filtration during production. Rather than fabricating CNPs from modified CNFs, I used sulfonated hypercrosslinked polymers (SHCPs) for which a more efficient synthesis procedure was developed in publication A1 by A. Blocher and myself, to efficiently fabricate multi-layered

CNF hybrids which entrap SHCPs in their network structure. In preliminary experiments, I found, that using ethanol as a suspension medium – as shown in publication II – does not only substantially speed up the hybrid production but also facilitates a more even dispersion of the SHCP particles within the network, as it prevents their flocculation and agglomeration as observed in aqueous media. The strategy presented in publication III can be seen as a model system and could be expanded to a variety of hypercrosslinked polymers with different functional groups.

4.4.1. SHCP-CNF hybrid morphology and layer structure

A heuristic optimisation of the membrane production process to overcome initial issues such as cracking, delamination, poor filtration performance and uneven polymer deposition finally yielded a three-layered structure consisting of a commercial filter paper carrier-layer, onto which a SHCP/CNF hybrid layer, followed by a pure CNF capping layer was deposited from ethanolic suspensions. Figure 17 shows an exploded view of the three-layered structure, with a tight, uniform CNF top layer, a layer consisting of SHCP particles embedded in a CNF matrix, which were in turn deposited on the bottom layer, formed by a commercial filter paper comprising significantly larger fibres than the middle and top layer, acting as a structural support.

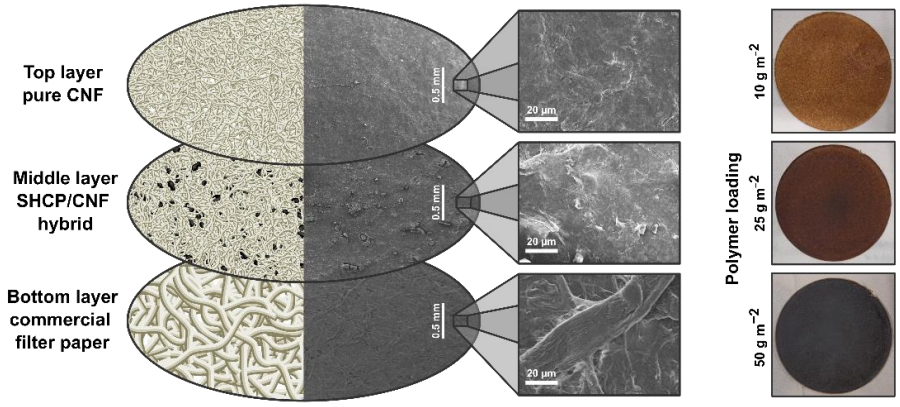

Figure 17: Composition of three-layer SHCP/CNF hybrid membranes with accompanying scanning electron micrographs (left) and photographs of wet hybrid membrane filter cake precursors (membrane diameters are 125 mm) with varying middle layer polymer loading (right). Publication III © 2024, the authors. Reprinted from Wiley-VCH GmbH under CC BY 4.0.

4.4.2. Water permeance through SHCP/CNF hybrid membranes

Figure 18 shows the equilibrium water permeance (A) as well as a schematic depiction of the dead-end cell setup used for permeance measurements (B). The equilibrium permanence was determined as the permeance measured after a change of less than 2 % in permeance was detected for two data points separated

by at least 1 h, which was necessary, as the measured permanence initially dropped gradually for all hybrid membranes due to fibre swelling and network compaction, which in turn increased the filtration resistance of the system. A reduction of the top layer grammage always lead to an increase in the permeance of hybrids, indicating that the top layer grammage is one of the main controlling factors of the nanopaper permeance. An increase of the grammage of the middle layer, lead to an increase in permeance for hybrid membranes with top layers of 10 and 25 g m^{-2}, which was ascribed to the SHCP-10 particles which aided channel formation due to an increased pore volume and by potentially preventing network compression. This trend was not present in SHCP/CNF hybrids with 5 g m^{-2} top layers, which already exhibited much higher permeances. SHCP/CNF 20-5 could not be tested, as the drop in pressure when opening the dead-end flow cell during the refill steps necessary after 200 mL had passed the cell, led to some expansion of compacted membranes, which in turn caused cracking of the ultrathin top and middle layer.

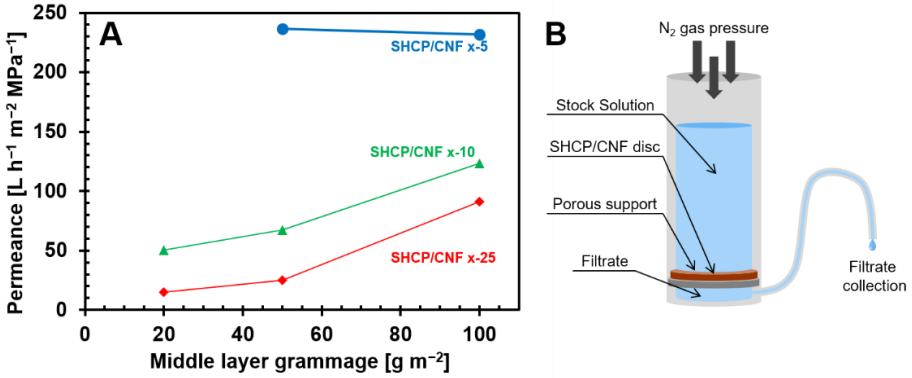

Figure 18: Equilibrium permeance of SHCP/CNF hybrid membranes as a function of middle and top layer grammage (A) and a schematic depiction of the dead-end cell test setup (B). Note: the errors are too small to be shown. Lines are provided to guide the eye and do not represent additional data points. Publication III © 2024, the authors. Reprinted from Wiley-VCH GmbH under CC BY 4.0.

4.4.3. Metal ion adsorption by SHCP-10 and SHCP/CNF hybrids

4.4.3.1. Cu^{2+} adsorption kinetics on SHCP-10

To investigate the suitability of SHCP-10 for heavy metal ion removal from aqueous solutions and to elucidate the adsorption mechanism, kinetic studies were performed at different temperatures using Cu^{2+} as a model ion (Figure 19 and Table 7). The Cu^{2+} adsorption curves on SHCP-10 suggest that a pseudo-second order kinetic model was the most accurate representation of the adsorption mechanism, which agreed with the findings of James et al.[190] who studied the adsorption of Cs^{1+} and Sr^{2+} on another SHCP. The Arrhenius plot of the results yielded a relatively high activation energy of 128 kJ mol^{-1} for the adsorption of copper onto SHCP-10, which alongside its pseudo second-order nature implies a chemisorption-based

process, i.e. the interaction of the adsorbate with specific binding sites – the sulfonate groups of SHCP-10 – on the adsorbents surface.

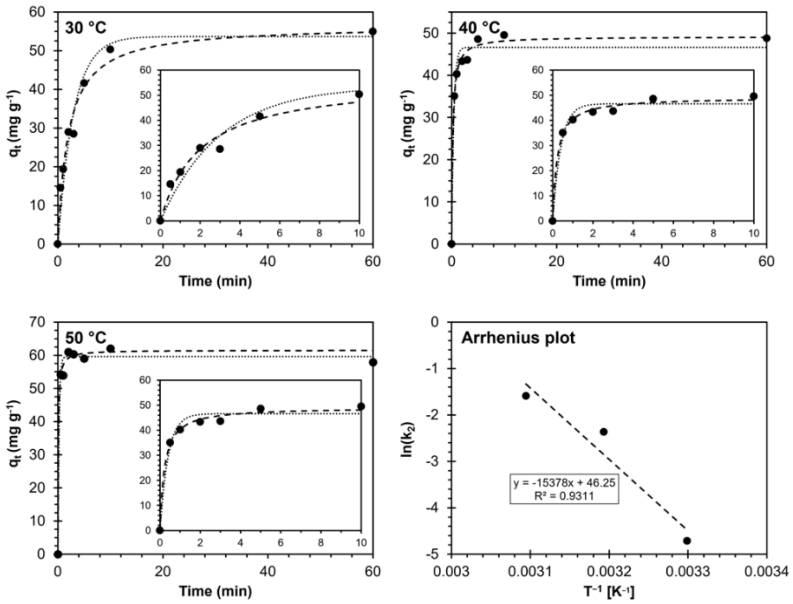

Figure 19: Adsorption studies at different temperatures T. The experimental data is depicted as solid dots, the pseudo first-order and the pseudo second-order model are represented by dotted and dashed lines, respectively. The bottom right graph presents the Arrhenius plot including the fitting function. Publication III © 2024, the authors. Reprinted from Wiley-VCH GmbH under CC BY 4.0.

SHCP-10 has equilibrium adsorption capacities q_e (Table 7), which outperform modified CNFs, such as phosphorylated nanocellulose, and are in the same range as the commercial Cu^{2+}-ion exchange resin AmberSep™‡ and other adsorptive ultrafiltration membranes derived from polyvinyltetrazole-co-polyacrylonitrile[204] or other sulfonated hypercrosslinked polymers[190] used for the adsorption of Cs^{1+} and Sr^{2+} when normalized to the respective ions negative charge.

Table 7: Parameters obtained by data fitting the experimental data of the adsorption of Cu^{2+} on SHCP-10 to pseudo first- and second-order models

		Pseudo first order kinetic model			Pseudo second order kinetic model			
T [°C]	$q_{e,exp}$ [mg g^{-1}]	$q_{e,cal}$ [mg g^{-1}]	k_1 [min^{-1}]	R^2	$q_{e,cal}$ [mg g^{-1}]	k_2 [g mg^{-1} min^{-1}]	h_0 [mg g^{-1} min^{-1}]	R^2
30	55 ± 5	54	0.34	0.9459	57	0.0090	29	0.9724
40	55 ± 4	47	2.5	0.8845	49	0.094	230	0.9720
50	59 ± 9	60	4.4	0.9276	62	0.20	770	0.9634

‡ Product data sheet AmberSepTM M4195 and AmberSepTM M4195 UPS Chelating Resins. Link in: https://www.dupont.com/content/dam/water/amer/us/en/water/public/documents/en/IER-AmberSep-M4195-and-M4195-UPS-PDS-45-D00810-en.pdf accessed on 25.03.2025

4.4.3.2. Dynamic Cu^{2+} adsorption and regeneration of hybrid membranes

The Cu^{2+} adsorption capacity of SHCP/CNF hybrids was determined by dynamic adsorption experiments performed in a dead end flow cell (Figure 20), and indicate, that higher SHCP-10 loading lead to a slight decrease in the relative adsorption capacity (i.e. the amount of Cu^{2+} adsorbed per gram of polymer) (Figure 20 left) yet an increased absolute adsorption capacity per unit area of the membranes (Figure 20 right). The reduction of the relative adsorption capacity was attributed to the formation of SHCP-10 agglomerates, rendering some particles inaccessible. However, the relative adsorption capacity of SHCP-10 embedded in CNF matrices tested in dynamic tests, significantly outperformed that of SHCP-10 tested under static conditions (Section 4.4.3.1), which was hypothesised to be facilitated by the continuous replacement of depleted Cu^{2+} solution, as well as improved availability of SHCP-10 surface, due to spatial distribution in the CNF network.

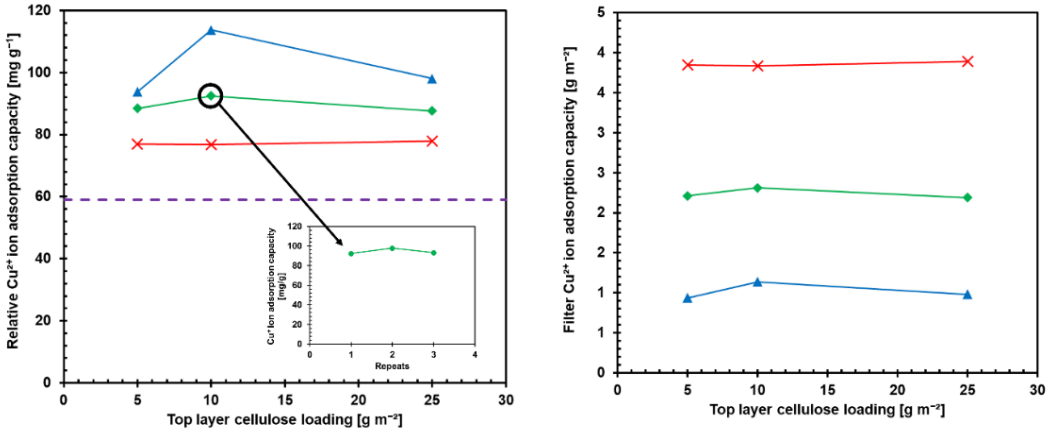

Figure 20: Relative Cu^{2+} adsorption capacity per gram of SHCP-10 as a function of middle and top layer grammages of SHCP/CNF hybrid membranes (left) and its performance after two regeneration cycles (inset). The purple dashed line corresponds to the highest batch sorption capacity of SHCP-10. The absolute copper adsorption capacity per m² of hybrid membrane is shown in (right). Note: Lines are provided as a guide to the eye and do not represent additional data points Publication III © 2024, the authors. Reprinted from Wiley-VCH GmbH under CC BY 4.0.

The regeneratability of SHCP/CNF hybrids was tested by flushing SHCP/CNF 50-10 – which represented the median top and middle layer thickness – with 120 mL of a 0.1 M aqueous HCl after adsorption (Figure 20 left inset). The membrane exhibited excellent recyclability and did not lose adsorption capacity after regeneration.

4.4.3.3. SHCP retention in SHCP/CNF hybrids

To investigate the possibility of SHCP particles leaching during use of the hybrid membranes, the sulfur content of DI water passed through a membrane water was measured using ICP-MS and compared to that of a blank (Figure 21). Asides from a marginal increase in the first fraction, no increase in the sulfur content was observed indicating full entrapment of SHCP-10 in the hybrid membranes.

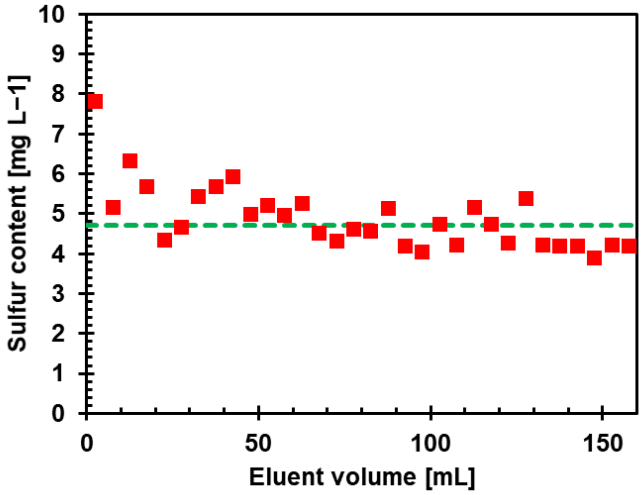

Figure 21: Sulfur content of water passed through a hybrid (red squares) vs the sulfur content of a blank water sample (green dashes). Note: Data was obtained from single measurement) Publication III © 2024, the authors. Reprinted from Wiley-VCH GmbH under CC BY 4.0.

4.4.3.4. Competitive metal ion adsorption on hybrids

SHCP/CNF 100-5 was used to study the adsorption of commercial mineral water, as this hybrid membrane combined both high permeance and high total adsorption capacity. Mineral water was chosen as a model for real world application as it contains a complex combination of the most important water hardness elements, Ca and Mg, and traces of other, potentially problematic alkaline earth metals such as Sr, and Ba. While naturally occurring Strontium, and thus the contents of the mineral water, does not pose a health concern, its artificial radioisotope ^{89}Sr is commonly used for radiopharmaceutical[205] applications and can be found in nuclear waste.[206] Barium is a common weighing agent in oil and gas drilling fluids, and high concentrations of dissolved barium – far exceeding those found in the commercial mineral water used – are considered neurotoxic, making the efficient removal of both Ba and Sr ions from solution a desirable goal for water treatment materials. Additionally, the adsorption of Cu^{2+} in the presence of Mg^{2+} and Ca^{2+} ions was investigated in a simulated mineral water solution containing 1 mmol L^{-1} of each ion simulating medium to high hardness water with high copper

contamination, as can be found in the effluent wastewater of mirror making factories.[63] The use of simulated mineral water for the investigation of Cu^{2+} adsorption was necessitated by the fact, that copper ions would precipitate as water insoluble copper carbonate when in contact with the carbonate ions present in sparkling mineral water. Figure 22 shows the relative breakthrough curves of each ion, in relation to its stock concentration, for both the investigation of commercial mineral water (A) and copper contaminated simulated mineral water (B).

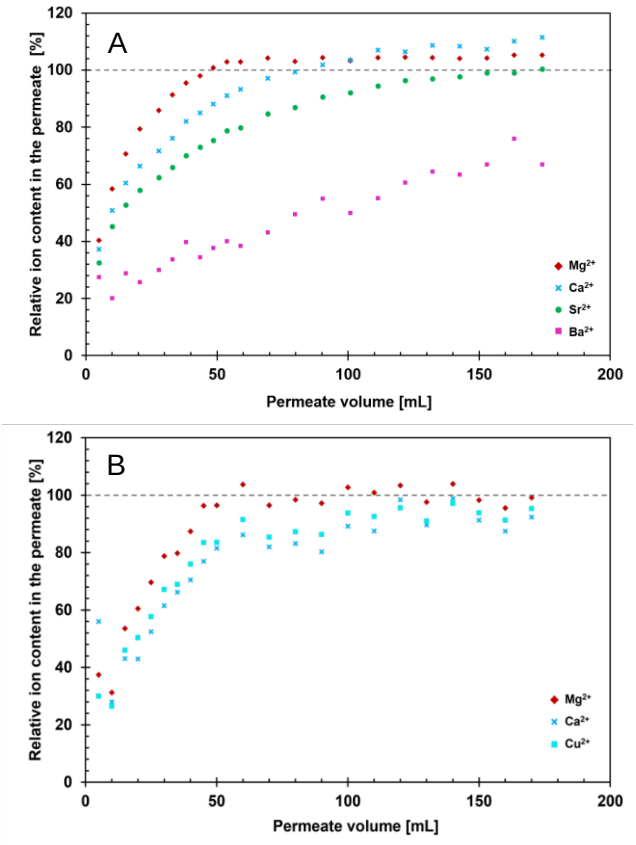

Figure 22: Relative breakthrough curves of ions found in **(A)** commercial mineral water upon treatment with hybrid membrane SHCP/CNF 100-5 with absolute concentrations of the relevant metal ions in the stock solution before passing through SHCP/CNF 100-5 of Mg^{2+} = 82 mg L^{-1}, Ca^{2+} = 109 mg L^{-1}, Sr^{2+} = 3.2 mg L^{-1}, and Ba^{2+} = 0.42 mg L^{-1}, and **(B)** of an artificial wastewater sample containing Mg^{2+}, Ca^{2+} and Cu^{2+} ions upon treatment with hybrid membrane SHCP/CNF 100-5 with absolute concentrations of the metal ions in the solution before passing through SHCP/CNF 100-5 of 1 mmol L^{-1}, corresponding to Ca^{2+} = 40 mg L^{-1}, Mg^{2+} = 24 mg L^{-1}, and Cu^{2+} = 63.5 mg L^{-1}. Typical relative standard deviations of the measurement are 2-3 % and are not shown in the graph for legibility. Publication III © 2024, the authors. Reprinted from Wiley-VCH GmbH under CC BY 4.0.

SHCP/CNF hybrid membranes were able to effectively remove a wide variety of ions from solution (Figure 22). Even with common hardness water hardness elements present in excess compared to other contaminants like alkaline earth metals (Figure 22A) and heavy metal ions (Figure 22B), the hybrids were able to adsorb the latter groups at a significant rate. At first, 60-70 % of all ions were removed from solution, which decreased in subsequent fractions, as the sulfonate

sites in the hybrid membranes were saturated. In the tests using commercial mineral water, the adsorption of Sr^{2+} and Ba^{2+} continued for the full duration of the experiment, while Cu^{2+} followed an adsorption behaviour much more akin to that of Mg^{2+} and Ca^{2+}. When viewing both graphs of Figure 22 in conjuncture, the adsorption efficiency of the individual ions appears to follow the solubility of the sulfate salts of each individual ion: $MgSO_4$ (pK_{sp} = -0.981) > $CuSO_4$ (pK_{sp} = 1.72) > $CaSO_4$ (pK_{sp} = 3.64) > $SrSO_4$ (pK_{sp} = 6.46) > $BaSO_4$ (pK_{sp} = 9.97). The results of testing commercial mineral water suggested, that, after saturation with Mg^{2+} and Ca^{2+}, chemical equilibrium ensured there were always a number of unoccupied adsorption sites present, which can be populated with the trace fractions of the less soluble Ba^{2+} and Sr^{2+}, leading to an increase in the relative concentration of Ca^{2+} and Mg^{2+} in later fractions, a phaenomenon which was not observed when testing copper contaminated simulated mineral water, as the solubilities and concentrations of all three ions were similar. These results suggest that the combination of SHCP-10 and CNFs yields hybrid materials that can adsorb significant amounts of potentially toxic alkaline earth metal and heavy metal ions, even in the presence of the most common water hardness elements. The suspected selectivity according to the sulfate solubility offers a potential method to predict the adsorption behaviour of other ion combinations and warrants future investigation.

4.4.4. Ultrafiltration performance of SHCP/CNF hybrids

SHCP/CNF 20-5, the hybrid with the lowest amount of nanocellulose deposited both in the middle and top layer was chosen as substrate to test the ultrafiltration of 10 nm Au nanoparticles, as it can be assumed, that hybrid membranes with thicker middle or top layers would exhibit improved or at the least equal particle rejection performance.

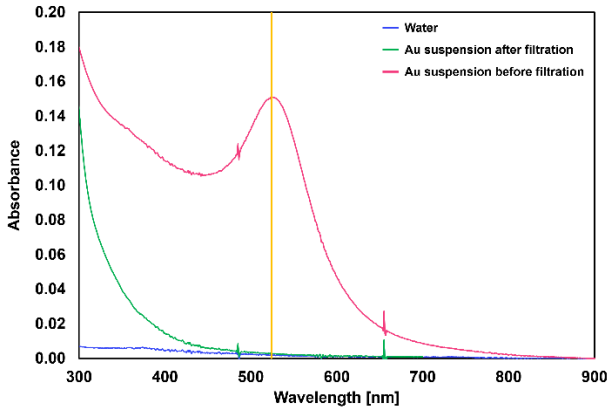

Figure 23: UV-Vis spectra comparing Au NP stock solution before (red) and after (green) passing through SHCP/CNF 20-5. The spectrum of water is included as reference. The yellow line denotes the peak maximum at 524 nm. Publication III © 2024, the authors. Reprinted from Wiley-VCH GmbH under CC BY 4.0.

UV-vis spectra of the Au nanoparticle suspension before and after filtration through SHCP/CNF 20-5 (Figure 23) showed full rejection of the 10 nm particles, with the characteristic Au nanoparticle adsorption peak at 524 nm vanishing while the adsorption peak-shoulder of the dissolved citric acid stabilizer in the solution remained. The ultrafiltration performance of SHCP/CNF 20-5 suggests that SHCP/CNF hybrids are capable of fully removing microplastics (smallest currently reported size ~1 μm),[207] bacteria and even viruses (>20 nm size)[208, 209] rendering them suitable for a wide variety of water treatment and ion exchange applications.

5. Conclusions

The aim of my dissertation work was to investigate the production and properties of cellulose nanopapers, and to improve upon established procedures to facilitate efficient manufacture and functionalisation of cellulose based nanopapers with favourable mechanical and optical properties. A nanocellulose stock material prepared by a simple defibrillation procedure without any subsequent purification or sorting steps was chosen as starting material for all experiments to show that the herein devised methods are not limited to nanocellulose materials produced with lengthy and expensive procedures.

First, an easy, yet underexplored method for the improvement of the mechanical properties of nanopapers, in the form of mercerisation of CNPs under tension, was investigated. By controlling the gradual transformation of the cellulose I allomorph to cellulose II, – as confirmed by XRD – by varying the treatment times and alkaline concentrations during mercerisation, I was able to establish two procedures that either yield an overall improvement of the CNPs mechanical properties or facilitate the trade-off of a small percentage of tensile strength for a drastic increase in ductility and tensile toughness. Most auspiciously, both treatment strategies were found to require short treatment times of 2-10 min and also improved the optical properties of the treated CNPs and, as this is a post-treatment step, they do not negatively impact the filtration times during CNP production.

Going on from these findings, I developed a method to drastically reduce the filtration times during CNP production, by means of using ethanol/water mixtures instead of water as suspension medium. While the filtration of CNPs from ethanolic instead of aqueous suspensions was explored in previous publications to control the porosity of CNPs, none of these works – to the best of my knowledge – explored and/or documented the potential for the reduction of filtration times required to produce nanopapers. The reduction of the filtration times was then combined with a simple post-treatment step (rewetting and drying) to fabricate CNPs with significantly higher ductility, optical transmission, and toughness, than nanopapers prepared by the slower filtration from aqueous media.

Thirdly, a method for the functionalisation of CNPs was investigated, which omits the sometimes-difficult direct modification of nanocellulose fibres and rather explores the possibility of using nanocellulose as an in situ formed matrix, entrapping particles of hypercrosslinked polymers with a high density of functional groups. This hybridisation approach allowed for the simultaneous alleviation of the HCPs drawback of poor solution processability and low mechanical strength, as well as the use of a fully bio-based, carrier material which could be easily digested after use, to reclaim the more expensive SHCP particles for use in the production of new hybrids. Once again using ethanol as a suspension medium during the preparation of SHCP/CNF hybrids allowed for fast and efficient preparation of hybrid materials for simultaneous filtration and ion exchange applications. The SHCP/CNF hybrids exhibited the ability to adsorb several potentially toxic metal ions, even in the presence of excess concentrations of common water hardness elements, such as Mg and Ca, and proved capable of fully rejecting Au nanoparticles with 10 nm diameter proving their ultrafiltration capability.

Overall, the findings of this thesis offer a portfolio of novel production methods and post-processing strategies, to alleviate some of the most significant problems when aiming to use CNPs to replace other engineering materials.

6. Outlook

The methods to improve the production of cellulose nanopapers, their properties, and the development of functional hybrid materials, could lay the foundation for a variety of future works, as optimisation of the treatment parameters and the scale up of the treatment methods should be investigated.

Expanding the concept of non-aqueous suspension media to other classes of nanocellulose, such as TEMPO-oxidised,[18, 62] phosphorylated[39, 63, 64] or sulfonated nanocelluloses[210] could greatly increase the impact of the technique, as these materials are notoriously difficult to dewater,[203] yet offer exceptional mechanical and optical properties.[25] The opportunity to increase/control the porosity while also increasing production speeds, offers potential for a variety of industrial applications, such as the fabrication of separator papers for capacitors or batteries or the fabrication of high transmission, high haze substrate for paper based electronics.[37]

The mercerisation procedure could be optimized by investigating a more expansive matrix of treatment times and conditions. Especially the investigation of even shorter treatment times in the case of 20 wt.-% NaOH treatments could yield beneficial results. Furthermore, the influence of the CNFs origin on the mercerisation treatment warrants further research, as the presence or absence of hemicellulose would most likely influence the overall procedure.

The concept of hybridising CNFs with porous organic polymers lays the foundation of a significant amount of future investigation, as it can be expanded to encompass a wide variety of polymers with an even broader range of functional groups, potentially allowing for the incorporation of functionalities that would not be possible with cellulose alone. The application of nanocellulose hybrids with ultrafiltration capability, and high density of functional groups is not limited to water treatment but can be expanded to encompass reactive filtration membranes, which combine catalytic conversion of the components of a potential permeate while also acting as filtration membranes.

This work reflects how the preparation of CNPs in the future can be optimised from a variety of angles, to not yield “the strongest” nanopapers possible but to produce materials that can be customised to fit the specific needs of a potential application.

7. References

[1] Veckalov, B.; Geiger, S. J.; Bartos, F.; White, M. P.; Rutjens, B. T.; van Harreveld, F.; Stablum, F.; Akin, B.; Aldoh, A.; Bai, J.; Berglund, F.; Bratina Zimic, A.; Broyles, M.; Catania, A.; Chen, A.; Chorzepa, M.; Farahat, E.; Gotz, J.; Hoter-Ishay, B.; Jordan, G.; Joustra, S.; Klingebiel, J.; Krajnc, Z.; Krug, A.; Andersen, T. L.; Loloff, J.; Natarajan, D.; Newman-Oktan, S.; Niehoff, E.; Paerels, C.; Papirmeister, R.; Peregrina, S.; Pohl, F.; Remso, A.; Roh, A.; Rusyidi, B.; Schmidt, J.; Shavgulidze, M.; Vellinho Nardin, V.; Wang, R.; Warner, K.; Wattier, M.; Wong, C. Y.; Younssi, M.; Ruggeri, K.; van der Linden, S., *Nat Hum Behav* **2024**. DOI 10.1038/s41562-024-01928-2.

[2] Thompson, R. C.; Swan, S. H.; Moore, C. J.; vom Saal, F. S., *Philos Trans R Soc Lond B Biol Sci* **2009,** *364* (1526), 1973-6. DOI 10.1098/rstb.2009.0054.

[3] Thompson, R. C.; Courtene-Jones, W.; Boucher, J.; Pahl, S.; Raubenheimer, K.; Koelmans, A. A., *Science* **2024,** *386* (6720), eadl2746. DOI 10.1126/science.adl2746.

[4] Ford, H. V.; Jones, N. H.; Davies, A. J.; Godley, B. J.; Jambeck, J. R.; Napper, I. E.; Suckling, C. C.; Williams, G. J.; Woodall, L. C.; Koldewey, H. J., *Sci. Total Environ.* **2022,** *806* (Pt 1), 150392. DOI 10.1016/j.scitotenv.2021.150392.

[5] Shen, M.; Huang, W.; Chen, M.; Song, B.; Zeng, G.; Zhang, Y., *J. Cleaner Prod.* **2020,** *254*. DOI 10.1016/j.jclepro.2020.120138.

[6] Mimura, N., *Proc Jpn Acad Ser B Phys Biol Sci* **2013,** *89* (7), 281-301. DOI 10.2183/pjab.89.281.

[7] Sato, H.; Mizoi, J.; Shinozaki, K.; Yamaguchi-Shinozaki, K., *Plant J* **2024,** *117* (6), 1873-1892. DOI 10.1111/tpj.16612.

[8] Zandalinas, S. I.; Fritschi, F. B.; Mittler, R., *Trends Plant Sci* **2021,** *26* (6), 588-599. DOI 10.1016/j.tplants.2021.02.011.

[9] Klemm, D.; Heublein, B.; Fink, H. P.; Bohn, A., *Angew. Chem. Int. Ed. Engl.* **2005,** *44* (22), 3358-93. DOI 10.1002/anie.200460587.

[10] Li, T.; Chen, C.; Brozena, A. H.; Zhu, J. Y.; Xu, L.; Driemeier, C.; Dai, J.; Rojas, O. J.; Isogai, A.; Wagberg, L.; Hu, L., *Nature* **2021,** *590* (7844), 47-56. DOI 10.1038/s41586-020-03167-7.

[11] Klemm, D.; Kramer, F.; Moritz, S.; Lindstrom, T.; Ankerfors, M.; Gray, D.; Dorris, A., *Angew. Chem. Int. Ed. Engl.* **2011,** *50* (24), 5438-66. DOI 10.1002/anie.201001273.

[12] Shaghaleh, H.; Xu, X.; Wang, S., *RSC Adv.* **2018,** *8* (2), 825-842. DOI 10.1039/c7ra11157f.

[13] Rånby, B. G.; Ribi, E., *Experientia* **1950,** *6* (1), 12-4. DOI 10.1007/BF02154044.

[14] Rånby, B. G., *Discussions of the Faraday Society* **1951,** *11*, 158-164. DOI https://doi.org/10.1039/DF9511100158.

[15] Turbak, A. F.; Snyder, F. W.; Sandberg, K. R. In *Microfibrillated cellulose, a new cellulose product: properties, uses, and commercial potential*, 9. cellulose conference, Syracuse, NY, USA, 1983-01-01; Syracuse, NY, USA, **1982**.

[16] Syverud, K.; Stenius, P., *Cellulose* **2008,** *16* (1), 75-85. DOI 10.1007/s10570-008-9244-2.

[17] Moon, R. J.; Martini, A.; Nairn, J.; Simonsen, J.; Youngblood, J., *Chem. Soc. Rev.* **2011,** *40* (7), 3941-94. DOI 10.1039/c0cs00108b.

[18] Saito, T.; Nishiyama, Y.; Putaux, J. L.; Vignon, M.; Isogai, A., *Biomacromolecules* **2006,** *7* (6), 1687-91. DOI 10.1021/bm060154s.

[19] Kröger, M.; Badara, O.; Pääkkönen, T.; Schlapp-Hackl, I.; Hietala, S.; Kontturi, E., *Biomacromolecules* **2023,** *24* (3), 1318-1328. DOI 10.1021/acs.biomac.2c01363.
[20] Thakur, V.; Guleria, A.; Kumar, S.; Sharma, S.; Singh, K., *Mater. Adv.* **2021,** *2* (6), 1872-1895. DOI 10.1039/d1ma00049g.
[21] Dufresne, A., *Current Forestry Reports* **2019,** *5* (2), 76-89. DOI 10.1007/s40725-019-00088-1.
[22] Ahankari, S. S.; Subhedar, A. R.; Bhadauria, S. S.; Dufresne, A., *Carbohydr. Polym.* **2021,** *255*, 117479. DOI 10.1016/j.carbpol.2020.117479.
[23] Shen, H.; Peng, S.; Luo, Q.; Zhou, J.; He, J. H.; Zhou, G.; Xu, X., *Advanced Functional Materials* **2023,** *33* (23). DOI 10.1002/adfm.202213820.
[24] Etale, A.; Onyianta, A. J.; Turner, S. R.; Eichhorn, S. J., *Chem. Rev.* **2023,** *123* (5), 2016-2048. DOI 10.1021/acs.chemrev.2c00477.
[25] Mautner, A.; Mayer, F.; Hervy, M.; Lee, K. Y.; Bismarck, A., *Philos. Trans. R. Soc., A* **2018,** *376* (2112). DOI 10.1098/rsta.2017.0043.
[26] Sehaqui, H.; Zhou, Q.; Ikkala, O.; Berglund, L. A., *Biomacromolecules* **2011,** *12* (10), 3638-44. DOI 10.1021/bm2008907.
[27] Zhang, D.; Jin, K.; Lim, K. H.; Jie, S.; Wang, W.-J.; Yang, X., *Green Chemistry* **2023,** *25* (12), 4696-4704. DOI 10.1039/d3gc00632h.
[28] Zhu, H.; Zhu, S.; Jia, Z.; Parvinian, S.; Li, Y.; Vaaland, O.; Hu, L.; Li, T., *Proc Natl Acad Sci U S A* **2015,** *112* (29), 8971-6. DOI 10.1073/pnas.1502870112.
[29] Sethi, J.; Visanko, M.; Osterberg, M.; Sirvio, J. A., *Carbohydr. Polym.* **2019,** *203*, 148-156. DOI 10.1016/j.carbpol.2018.09.037.
[30] Reid, M. S.; Suganda, W.; Östmark, E.; Brolin, A.; Wågberg, L., *ACS Sustainable Chem. Eng.* **2023,** *11* (46), 16428-16441. DOI 10.1021/acssuschemeng.3c02871.
[31] Sinquefield, S.; Ciesielski, P. N.; Li, K.; Gardner, D. J.; Ozcan, S., *ACS Sustainable Chem. Eng.* **2020,** *8* (26), 9601-9615. DOI 10.1021/acssuschemeng.0c01797.
[32] Mattsson, T.; Sedin, M.; Theliander, H., *Separation and Purification Technology* **2012,** *96*, 139-146. DOI 10.1016/j.seppur.2012.05.029.
[33] Fall, A.; Henriksson, M.; Karppinen, A.; Opstad, A.; Heggset, E. B.; Syverud, K., *Cellulose* **2022,** *29* (14), 7649-7662. DOI 10.1007/s10570-022-04719-y.
[34] Sim, K.; Lee, J.; Lee, H.; Youn, H. J., *Cellulose* **2015,** *22* (6), 3689-3700. DOI 10.1007/s10570-015-0784-y.
[35] Onyianta, A. J.; Xu, G.; Etale, A.; Eloi, J. C.; Eichhorn, S. J., *Carbohydr. Polym.* **2023,** *314*, 120943. DOI 10.1016/j.carbpol.2023.120943.
[36] Henriksson, M.; Berglund, L. A.; Isaksson, P.; Lindstrom, T.; Nishino, T., *Biomacromolecules* **2008,** *9* (6), 1579-85. DOI 10.1021/bm800038n.
[37] Hsieh, M. C.; Koga, H.; Suganuma, K.; Nogi, M., *Sci. Rep.* **2017,** *7*, 41590. DOI 10.1038/srep41590.
[38] Mautner, A.; Bismarck, A., *Carbohydr. Polym.* **2021,** *251*, 117130. DOI 10.1016/j.carbpol.2020.117130.
[39] Mautner, A.; Maples, H. A.; Kobkeatthawin, T.; Kokol, V.; Karim, Z.; Li, K.; Bismarck, A., *International Journal of Environmental Science and Technology* **2016,** *13* (8), 1861-1872. DOI 10.1007/s13762-016-1026-z.
[40] Liu, W.; Liu, K.; Du, H.; Zheng, T.; Zhang, N.; Xu, T.; Pang, B.; Zhang, X.; Si, C.; Zhang, K., *Nano-Micro Lett.* **2022,** *14* (1), 104. DOI 10.1007/s40820-022-00849-x.
[41] Hon, D. N. S., *Cellulose* **1994,** *1* (1), 1-25. DOI 10.1007/bf00818796.
[42] Payen, A., *C. R. Acad. Sci.* **1838,** *7* (lu 17 décembre 1838), 1052-1056.
[43] Staudinger, H., *Berichte der deutschen chemischen Gesellschaft (A and B Series)* **1920,** *53* (6), 1073-1085. DOI https://doi.org/10.1002/cber.19200530627.
[44] French, A. D., *Cellulose* **2017,** *24* (11), 4605-4609. DOI 10.1007/s10570-017-1450-3.

[45] Habibi, Y.; Lucia, L. A.; Rojas, O. J., *Chem. Rev.* **2010,** *110* (6), 3479-500. DOI 10.1021/cr900339w.
[46] Klemm, D.; Cranston, E. D.; Fischer, D.; Gama, M.; Kedzior, S. A.; Kralisch, D.; Kramer, F.; Kondo, T.; Lindström, T.; Nietzsche, S.; Petzold-Welcke, K.; Rauchfuß, F., *Mater. Today* **2018,** *21* (7), 720-748. DOI 10.1016/j.mattod.2018.02.001.
[47] Jayme, G.; Hunger, G., *Monatsh. Chem.* **1956,** *87* (1), 8-23. DOI 10.1007/bf00903586.
[48] Vincent, J. F. V., *Mater. Today* **2002,** *5* (12), 28-41. DOI 10.1016/s1369-7021(02)01237-3.
[49] McFarlane, H. E.; Doring, A.; Persson, S., *Annu Rev Plant Biol* **2014,** *65*, 69-94. DOI 10.1146/annurev-arplant-050213-040240.
[50] Hill, J. L., Jr.; Hammudi, M. B.; Tien, M., *Plant Cell* **2014,** *26* (12), 4834-42. DOI 10.1105/tpc.114.131193.
[51] Polko, J. K.; Kieber, J. J., *Plant Cell* **2019,** *31* (2), 282-296. DOI 10.1105/tpc.18.00760.
[52] Lampugnani, E. R.; Flores-Sandoval, E.; Tan, Q. W.; Mutwil, M.; Bowman, J. L.; Persson, S., *Trends Plant Sci* **2019,** *24* (5), 402-412. DOI 10.1016/j.tplants.2019.02.011.
[53] Kapun, T.; Zule, J.; Fabjan, E.; Hočevar, B.; Grilc, M.; Likozar, B., *European Journal of Wood and Wood Products* **2022,** *80* (2), 501-514. DOI 10.1007/s00107-021-01779-y.
[54] Lev, R.; Tanninen, P.; Lyytikäinen, J.; Leminen, V., *BioResources* **2023,** *18* (4). DOI 10.15376/biores.18.4.Lev.
[55] Kamel, R.; El-Wakil, N. A.; Dufresne, A.; Elkasabgy, N. A., *Int. J. Biol. Macromol.* **2020,** *163*, 1579-1590. DOI 10.1016/j.ijbiomac.2020.07.242.
[56] El Allaoui, B.; Benzeid, H.; Zari, N.; Qaiss, A. e. k.; Bouhfid, R., *Journal of Drug Delivery Science and Technology* **2023,** *88*. DOI 10.1016/j.jddst.2023.104899.
[57] Chandel, N.; Jain, K.; Jain, A.; Raj, T.; Patel, A. K.; Yang, Y.-H.; Bhatia, S. K., *Ind. Crops Prod.* **2023,** *201*. DOI 10.1016/j.indcrop.2023.116929.
[58] Kilpinen, A. T.; Paakkonen, T.; Nieminen, K.; Kontturi, E., *Ind. Eng. Chem. Res.* **2023,** *62* (41), 16922-16930. DOI 10.1021/acs.iecr.3c01894.
[59] Kontturi, E.; Meriluoto, A.; Penttila, P. A.; Baccile, N.; Malho, J. M.; Potthast, A.; Rosenau, T.; Ruokolainen, J.; Serimaa, R.; Laine, J.; Sixta, H., *Angew. Chem. Int. Ed. Engl.* **2016,** *55* (46), 14455-14458. DOI 10.1002/anie.201606626.
[60] Iwamoto, S.; Nakagaito, A. N.; Yano, H.; Nogi, M., *Appl. Phys. A* **2005,** *81* (6), 1109-1112. DOI 10.1007/s00339-005-3316-z.
[61] Ho, T. T. T.; Abe, K.; Zimmermann, T.; Yano, H., *Cellulose* **2014,** *22* (1), 421-433. DOI 10.1007/s10570-014-0518-6.
[62] Saito, T.; Kimura, S.; Nishiyama, Y.; Isogai, A., *Biomacromolecules* **2007,** *8* (8), 2485-91. DOI 10.1021/bm0703970.
[63] Liu, P.; Borrell, P. F.; Bozic, M.; Kokol, V.; Oksman, K.; Mathew, A. P., *J. Hazard. Mater.* **2015,** *294*, 177-85. DOI 10.1016/j.jhazmat.2015.04.001.
[64] Mautner, A.; Kobkeatthawin, T.; Mayer, F.; Plessl, C.; Gorgieva, S.; Kokol, V.; Bismarck, A., *Nanomaterials (Basel)* **2019,** *9* (2). DOI 10.3390/nano9020136.
[65] Liimatainen, H.; Visanko, M.; Sirvio, J. A.; Hormi, O. E.; Niinimaki, J., *Biomacromolecules* **2012,** *13* (5), 1592-7. DOI 10.1021/bm300319m.
[66] Ribeiro, R. S. A.; Pohlmann, B. C.; Calado, V.; Bojorge, N.; Pereira, N., Jr., *Eng Life Sci* **2019,** *19* (4), 279-291. DOI 10.1002/elsc.201800158.
[67] Weiland, K.; Wlcek, B.; Krexner, T.; Kral, I.; Kontturi, E.; Mautner, A.; Bauer, A.; Bismarck, A., *ACS Sustainable Chem. Eng.* **2021,** *9* (46), 15506-15513. DOI 10.1021/acssuschemeng.1c05175.
[68] Gómez H, C.; Serpa, A.; Velásquez-Cock, J.; Gañán, P.; Castro, C.; Vélez, L.; Zuluaga, R., *Food Hydrocolloids* **2016,** *57*, 178-186. DOI 10.1016/j.foodhyd.2016.01.023.

[69] Taipale, T.; Österberg, M.; Nykänen, A.; Ruokolainen, J.; Laine, J., *Cellulose* **2010,** *17* (5), 1005-1020. DOI 10.1007/s10570-010-9431-9.
[70] Sehaqui, H.; Allais, M.; Zhou, Q.; Berglund, L. A., *Composites Science and Technology* **2011,** *71* (3), 382-387. DOI 10.1016/j.compscitech.2010.12.007.
[71] Das, A. K.; Islam, M. N.; Ashaduzzaman, M.; Nazhad, M. M., *Journal of Packaging Technology and Research* **2020,** *4* (3), 253-260. DOI 10.1007/s41783-020-00097-7.
[72] Spagnuolo, L.; D'Orsi, R.; Operamolla, A., *Chempluschem* **2022,** *87* (8), e202200204. DOI w.
[73] Völkel, L.; Ahn, K.; Hähner, U.; Gindl-Altmutter, W.; Potthast, A., *Heritage Science* **2017,** *5* (1). DOI 10.1186/s40494-017-0134-5.
[74] Baniasadi, H.; Abidnejad, R.; Fazeli, M.; Lipponen, J.; Niskanen, J.; Kontturi, E.; Seppala, J.; Rojas, O. J., *Adv. Colloid Interface Sci.* **2024,** *324*, 103095. DOI 10.1016/j.cis.2024.103095.
[75] Curvello, R.; Raghuwanshi, V. S.; Garnier, G., *Adv. Colloid Interface Sci.* **2019,** *267*, 47-61. DOI 10.1016/j.cis.2019.03.002.
[76] Jiao, H.; Lu, X.; Li, Y.; Zhang, H.; Fu, Y.; Zhong, C.; Wang, Q.; Ullah, M. W.; Liu, H.; Yong, Y. C.; Liu, J., *Int. J. Biol. Macromol.* **2024,** *274* (Pt 2), 133515. DOI 10.1016/j.ijbiomac.2024.133515.
[77] Revol, J. F.; Bradford, H.; Giasson, J.; Marchessault, R. H.; Gray, D. G., *Int. J. Biol. Macromol.* **1992,** *14* (3), 170-2. DOI 10.1016/s0141-8130(05)80008-x.
[78] Dufresne, A.; Cavaillé, J.-Y.; Vignon, M. R., *J. Appl. Polym. Sci.* **1997,** *64* (6), 1185-1194. DOI 10.1002/(sici)1097-4628(19970509)64:6<1185::Aid-app19>3.0.Co;2-v.
[79] Miao, C.; Du, H.; Parit, M.; Jiang, Z.; Tippur, H. V.; Zhang, X.; Liu, Z.; Li, J.; Wang, R., *Cellulose* **2020,** *27* (6), 3181-3195. DOI 10.1007/s10570-020-03015-x.
[80] Nogi, M.; Komoda, N.; Otsuka, K.; Suganuma, K., *Nanoscale* **2013,** *5* (10), 4395-9. DOI 10.1039/c3nr00231d.
[81] Ji, S.; Jang, J.; Cho, E.; Kim, S. H.; Kang, E. S.; Kim, J.; Kim, H. K.; Kong, H.; Kim, S. K.; Kim, J. Y.; Park, J. U., *Adv. Mater.* **2017,** *29* (24). DOI 10.1002/adma.201700538.
[82] Zhang, K.; Chen, G.; Li, R. a.; Zhao, K.; Shen, J.; Tian, J.; He, M., *ACS Sustainable Chem. Eng.* **2020,** *8* (13), 5132-5139. DOI 10.1021/acssuschemeng.9b07266.
[83] Rao, J.; Lv, Z.; Ding, Q.; Chen, G.; Hao, X.; Bian, J.; Guan, Y.; Peng, F., *ACS Sustainable Chem. Eng.* **2021,** *9* (8), 3337-3346. DOI 10.1021/acssuschemeng.0c09408.
[84] Wang, Z.; Zhang, X.; Zhou, S.; Edström, K.; Strømme, M.; Nyholm, L., *Advanced Functional Materials* **2018,** *28* (48). DOI 10.1002/adfm.201804038.
[85] Dai, S.; Chu, Y.; Liu, D.; Cao, F.; Wu, X.; Zhou, J.; Zhou, B.; Chen, Y.; Huang, J., *Nat. Commun.* **2018,** *9* (1), 2737. DOI 10.1038/s41467-018-05155-y.
[86] Kim, H.; Guccini, V.; Lu, H.; Salazar-Alvarez, G.; Lindbergh, G.; Cornell, A., *ACS Applied Energy Materials* **2018,** *2* (2), 1241-1250. DOI 10.1021/acsaem.8b01797.
[87] Zheng, W.; Fan, L.; Zhou, J.; Meng, Z.; Ye, D.; Xu, J., *Int. J. Biol. Macromol.* **2024,** *256* (Pt 2), 128497. DOI 10.1016/j.ijbiomac.2023.128497.
[88] Guo, R.; Zhang, L.; Lu, Y.; Zhang, X.; Yang, D., *Journal of Energy Chemistry* **2020,** *51*, 342-361. DOI 10.1016/j.jechem.2020.04.029.
[89] Zhang, Q.; Chen, C.; Chen, W.; Pastel, G.; Guo, X.; Liu, S.; Wang, Q.; Liu, Y.; Li, J.; Yu, H.; Hu, L., *ACS Appl. Mater. Interfaces* **2019,** *11* (6), 5919-5927. DOI 10.1021/acsami.8b17414.
[90] Gao, L.; Chao, L.; Hou, M.; Liang, J.; Chen, Y.; Yu, H.-D.; Huang, W., *npj Flexible Electronics* **2019,** *3* (1). DOI 10.1038/s41528-019-0048-2.
[91] Wu, J.; Che, X.; Hu, H.-C.; Xu, H.; Li, B.; Liu, Y.; Li, J.; Ni, Y.; Zhang, X.; Ouyang, X., *J. Mater. Chem. A* **2020,** *8* (11), 5442-5448. DOI 10.1039/c9ta14039e.

[92] Kim, H.-J.; Yim, E.-C.; Kim, J.-H.; Kim, S.-J.; Park, J.-Y.; Oh, I.-K., *Nano Energy* **2017,** *33*, 130-137. DOI 10.1016/j.nanoen.2017.01.035.
[93] Yao, C.; Hernandez, A.; Yu, Y.; Cai, Z.; Wang, X., *Nano Energy* **2016,** *30*, 103-108. DOI 10.1016/j.nanoen.2016.09.036.
[94] Li, F.; Mascheroni, E.; Piergiovanni, L., *Packaging Technology and Science* **2015,** *28* (6), 475-508. DOI 10.1002/pts.2121.
[95] Chen, G.; Koon-Yang, L.; Bismarck, A.; Li, R., Cellulose materials and methods of making and using same. Google Patents: **2021**.
[96] Nogi, M.; Iwamoto, S.; Nakagaito, A. N.; Yano, H., *Adv. Mater.* **2009,** *21* (16), 1595-1598. DOI 10.1002/adma.200803174.
[97] Zhang, X.; Jian, J.; Luo, Z.; Li, G.; Huang, Y.; Wu, Y.; Li, D.; Li, L., *Carbohydr. Polym.* **2024,** *346*, 122632. DOI 10.1016/j.carbpol.2024.122632.
[98] Aulin, C.; Gällstedt, M.; Lindström, T., *Cellulose* **2010,** *17* (3), 559-574. DOI 10.1007/s10570-009-9393-y.
[99] Walther, A.; Lossada, F.; Benselfelt, T.; Kriechbaum, K.; Berglund, L.; Ikkala, O.; Saito, T.; Wagberg, L.; Bergstrom, L., *Biomacromolecules* **2020,** *21* (6), 2536-2540. DOI 10.1021/acs.biomac.0c00330.
[100] Spence, K. L.; Venditti, R. A.; Rojas, O. J.; Habibi, Y.; Pawlak, J. J., *Cellulose* **2010,** *17* (4), 835-848. DOI 10.1007/s10570-010-9424-8.
[101] Sehaqui, H.; Zimmermann, T.; Tingaut, P., *Cellulose* **2013,** *21* (1), 367-382. DOI 10.1007/s10570-013-0110-5.
[102] Toivonen, M. S.; Kurki-Suonio, S.; Schacher, F. H.; Hietala, S.; Rojas, O. J.; Ikkala, O., *Biomacromolecules* **2015,** *16* (3), 1062-71. DOI 10.1021/acs.biomac.5b00145.
[103] Oberlintner, A.; Shvalya, V.; Vasudevan, A.; Vengust, D.; Likozar, B.; Cvelbar, U.; Novak, U., *Appl. Surf. Sci.* **2022,** *581*. DOI 10.1016/j.apsusc.2021.152276.
[104] Hokkanen, S.; Repo, E.; Bhatnagar, A.; Tang, W. Z.; Sillanpaa, M., *Environ. Technol.* **2014,** *35* (17-20), 2334-46. DOI 10.1080/09593330.2014.903300.
[105] Roy Choudhury, A. K., 5 - Acid–alkali finish. In *Principles of Textile Finishing*, Roy Choudhury, A. K., Ed. Woodhead Publishing: 2017; pp 79-108.
[106] Torstensen, J. Ø.; Helberg, R. M. L.; Deng, L.; Gregersen, Ø. W.; Syverud, K., *International Journal of Greenhouse Gas Control* **2019,** *81*, 93-102. DOI 10.1016/j.ijggc.2018.10.007.
[107] Shibazaki, H.; Kuga, S.; Onabe, F.; Usuda, M., *J. Appl. Polym. Sci.* **1993,** *50* (6), 965-969.
[108] Mautner, A.; Lee, K.-Y.; Tammelin, T.; Mathew, A. P.; Nedoma, A. J.; Li, K.; Bismarck, A., *React. Funct. Polym.* **2015,** *86*, 209-214. DOI 10.1016/j.reactfunctpolym.2014.09.014.
[109] Metreveli, G.; Wagberg, L.; Emmoth, E.; Belak, S.; Stromme, M.; Mihranyan, A., *Adv Healthc Mater* **2014,** *3* (10), 1546-50, 1524. DOI 10.1002/adhm.201300641.
[110] Karim, Z.; Svedberg, A.; Lee, K. Y.; Khan, M. J., *Sci. Rep.* **2019,** *9* (1), 10277. DOI 10.1038/s41598-019-46812-6.
[111] Mautner, A.; Kobkeatthawin, T.; Bismarck, A., *Resource-Efficient Technologies* **2017,** *3* (1), 22-28. DOI 10.1016/j.reffit.2017.01.005.
[112] Mautner, A.; Maples, H. A.; Sehaqui, H.; Zimmermann, T.; Perez de Larraya, U.; Mathew, A. P.; Lai, C. Y.; Li, K.; Bismarck, A., *Environmental Science: Water Research & Technology* **2016,** *2* (1), 117-124. DOI 10.1039/c5ew00139k.
[113] Sehaqui, H.; Mautner, A.; Perez de Larraya, U.; Pfenninger, N.; Tingaut, P.; Zimmermann, T., *Carbohydr. Polym.* **2016,** *135*, 334-40. DOI 10.1016/j.carbpol.2015.08.091.
[114] Mautner, A.; Lucenius, J.; Österberg, M.; Bismarck, A., *Cellulose* **2017,** *24* (4), 1759-1773. DOI 10.1007/s10570-017-1220-2.
[115] Mautner, A.; Nawawi, W. M. F. W.; Lee, K.-Y.; Bismarck, A., *Composites Part A* **2020,** *131*. DOI 10.1016/j.compositesa.2020.105779.

[116] Österberg, M.; Vartiainen, J.; Lucenius, J.; Hippi, U.; Seppala, J.; Serimaa, R.; Laine, J., *ACS Appl. Mater. Interfaces* **2013,** *5* (11), 4640-7. DOI 10.1021/am401046x.
[117] Vartiainen, J.; Kaljunen, T.; Kunnari, V.; Lahtinen, P.; Tammelin, T., Large-scale production of CNF films. In *Production and Applications of Cellulose Nanomaterials*, Postek, M. T.; Moon, R. J.; Rudie, A. W.; Bilodeau, M. A., Eds. TAPPI Press: 2013; pp 239-240.
[118] Hubbe, M. A.; Ferrer, A.; Tyagi, P.; Yin, Y.; Salas, C.; Pal, L.; Rojas, O. J., *BioResources* **2017,** *12* (1), 2143-2233. DOI 10.15376/biores.12.1.2143-2233.
[119] Cherian, R. M.; Tharayil, A.; Varghese, R. T.; Antony, T.; Kargarzadeh, H.; Chirayil, C. J.; Thomas, S., *Carbohydr. Polym.* **2022,** *282*, 119123. DOI 10.1016/j.carbpol.2022.119123.
[120] Sehaqui, H.; Liu, A.; Zhou, Q.; Berglund, L. A., *Biomacromolecules* **2010,** *11* (9), 2195-8. DOI 10.1021/bm100490s.
[121] Hervy, M.; Santmarti, A.; Lahtinen, P.; Tammelin, T.; Lee, K.-Y., *Materials & Design* **2017,** *121*, 421-429. DOI 10.1016/j.matdes.2017.02.081.
[122] Kriechbaum, K.; Bergstrom, L., *Biomacromolecules* **2020,** *21* (5), 1720-1728. DOI 10.1021/acs.biomac.9b01655.
[123] Hervy, M.; Bock, F.; Lee, K.-Y., *Composites Science and Technology* **2018,** *167*, 126-133. DOI 10.1016/j.compscitech.2018.07.027.
[124] Nadeem, H.; Dehghani, M.; Garnier, G.; Batchelor, W., *J. Cleaner Prod.* **2022,** *342*. DOI 10.1016/j.jclepro.2022.130890.
[125] Mendoza, L.; Gunawardhana, T.; Batchelor, W.; Garnier, G., *J. Colloid Interface Sci.* **2018,** *525*, 119-125. DOI 10.1016/j.jcis.2018.04.077.
[126] Ritchie, R. O., *Nat Mater* **2011,** *10* (11), 817-22. DOI 10.1038/nmat3115.
[127] Mokhena, T. C.; Sadiku, E. R.; Mochane, M. J.; Ray, S. S.; John, M. J.; Mtibe, A., *Carbohydr. Polym.* **2021,** *273*, 118507. DOI 10.1016/j.carbpol.2021.118507.
[128] Guzman-Puyol, S.; Tedeschi, G.; Goldoni, L.; Benítez, J. J.; Ceseracciu, L.; Koschella, A.; Heinze, T.; Athanassiou, A.; Heredia-Guerrero, J. A., *Food Hydrocolloids* **2022,** *128*. DOI 10.1016/j.foodhyd.2022.107562.
[129] Guzman-Puyol, S.; Hierrezuelo, J.; Benitez, J. J.; Tedeschi, G.; Porras-Vazquez, J. M.; Heredia, A.; Athanassiou, A.; Romero, D.; Heredia-Guerrero, J. A., *Int. J. Biol. Macromol.* **2022,** *209* (Pt B), 1985-1994. DOI 10.1016/j.ijbiomac.2022.04.177.
[130] Gindl, W.; Keckes, J., *Polymer* **2005,** *46* (23), 10221-10225. DOI 10.1016/j.polymer.2005.08.040.
[131] Abbott, A.; Bismarck, A., *Cellulose* **2010,** *17* (4), 779-791. DOI 10.1007/s10570-010-9427-5.
[132] Chen, F.; Xiang, W.; Sawada, D.; Bai, L.; Hummel, M.; Sixta, H.; Budtova, T., *ACS Nano* **2020,** *14* (9), 11150-11159. DOI 10.1021/acsnano.0c02302.
[133] Solhi, L.; Guccini, V.; Heise, K.; Solala, I.; Niinivaara, E.; Xu, W.; Mihhels, K.; Kroger, M.; Meng, Z.; Wohlert, J.; Tao, H.; Cranston, E. D.; Kontturi, E., *Chem. Rev.* **2023,** *123* (5), 1925-2015. DOI 10.1021/acs.chemrev.2c00611.
[134] Lindström, T.; Aulin, C., *Scand. J. For. Res.* **2014,** *29* (4), 345-351. DOI 10.1080/02827581.2014.928365.
[135] Carman, P. C., *Chem. Eng. Res. Des.* **1997,** *75*, S32-S48. DOI 10.1016/s0263-8762(97)80003-2.
[136] Wetterling, J.; Jonsson, S.; Mattsson, T.; Theliander, H., *Industrial & Engineering Chemistry Research* **2017,** *56* (44), 12789-12798. DOI 10.1021/acs.iecr.7b03575.
[137] Karna, N. K.; Lidén, A.; Wohlert, J.; Theliander, H., *Industrial & Engineering Chemistry Research* **2021,** *60* (48), 17663-17676. DOI 10.1021/acs.iecr.1c03749.
[138] Sethi, J.; Oksman, K.; Illikainen, M.; Sirvio, J. A., *Carbohydr. Polym.* **2018,** *197*, 92-99. DOI 10.1016/j.carbpol.2018.05.072.

[139] Gondhalekar, S. C.; Pawar, P. J.; Dhumal, S. S.; Thakre, S. S., *Cellulose* **2019,** *26* (3), 1595-1604. DOI 10.1007/s10570-018-2213-5.
[140] Wilkes, A. G., The viscose process. In *Regenerated cellulose fibres*, 1st ed.; Woodings, C., Ed. Woodhead publishing Ltd and CRC Press LLC: Cambridge, 2001; pp 37-61.
[141] Segal, L.; Eggerton, F. V., *Textile Research Journal* **1961,** *31* (5), 460-471. DOI 10.1177/004051756103100510.
[142] Saunders, C. W.; Taylor, L. T., *Journal of Energetic Materials* **1990,** *8* (3), 149-203. DOI 10.1080/07370659008012572.
[143] Isogai, A.; Saito, T.; Fukuzumi, H., *Nanoscale* **2011,** *3* (1), 71-85. DOI 10.1039/c0nr00583e.
[144] Carvajal-Barriga, E. J.; Fitzgerald, W.; Dimitriadis, E. K.; Margolis, L.; Fields, R. D., *Sci. Rep.* **2023,** *13* (1), 6959. DOI 10.1038/s41598-023-33686-y.
[145] Pingrey, B.; Hsieh, Y. L., *Biomacromolecules* **2022,** *23* (3), 1269-1277. DOI 10.1021/acs.biomac.1c01505.
[146] Sirviö, J. A.; Ukkola, J.; Liimatainen, H., *Cellulose* **2019,** *26* (4), 2303-2316. DOI 10.1007/s10570-019-02257-8.
[147] Nishiyama, Y.; Langan, P.; Chanzy, H., *J. Am. Chem. Soc.* **2002,** *124* (31), 9074-82. DOI 10.1021/ja0257319.
[148] Nishiyama, Y.; Sugiyama, J.; Chanzy, H.; Langan, P., *J. Am. Chem. Soc.* **2003,** *125* (47), 14300-6. DOI 10.1021/ja037055w.
[149] Ishikawa, A.; Okano, T.; Sugiyama, J., *Polymer* **1997,** *38* (2), 463-468. DOI 10.1016/s0032-3861(96)00516-2.
[150] Wang, J.; Wang, L.; Gardner, D. J.; Shaler, S. M.; Cai, Z., *Cellulose* **2021,** *28* (8), 4511-4543. DOI 10.1007/s10570-021-03771-4.
[151] Kroon-Batenburg, L. M.; Kroon, J., *Glycoconj J* **1997,** *14* (5), 677-90. DOI 10.1023/a:1018509231331.
[152] Langan, P.; Nishiyama, Y.; Chanzy, H., *Biomacromolecules* **2001,** *2* (2), 410-6. DOI 10.1021/bm005612q.
[153] Kolpak, F. J.; Weih, M.; Blackwell, J., *Polymer* **1978,** *19* (2), 123-131. DOI 10.1016/0032-3861(78)90027-7.
[154] Djahedi, C.; Berglund, L. A.; Wohlert, J., *Carbohydr. Polym.* **2015,** *130*, 175-82. DOI 10.1016/j.carbpol.2015.04.073.
[155] Nishino, T.; Takano, K.; Nakamae, K., *J. Polym. Sci., Part B: Polym. Phys.* **2003,** *33* (11), 1647-1651. DOI 10.1002/polb.1995.090331110.
[156] Binz, A., *Angew. Chem.* **2006,** *11* (26), 595-600. DOI 10.1002/ange.18980112602.
[157] Kolpak, F. J.; Blackwell, J., *Polymer* **1978,** *19* (2), 132-135. DOI 10.1016/0032-3861(78)90028-9.
[158] Buleon, A.; Chanzy, H.; Roche, E., *Journal of Polymer Science: Polymer Letters Edition* **1977,** *15* (5), 265-270. DOI 10.1002/pol.1977.130150502.
[159] Kim, N. H.; Imai, T.; Wada, M.; Sugiyama, J., *Biomacromolecules* **2006,** *7* (1), 274-80. DOI 10.1021/bm0506391.
[160] Okano, T.; Sarko, A., *J. Appl. Polym. Sci.* **1984,** *29* (12), 4175-4182. DOI 10.1002/app.1984.070291247.
[161] Okano, T.; Sarko, A., *J. Appl. Polym. Sci.* **1985,** *30* (1), 325-332. DOI 10.1002/app.1985.070300128.
[162] Sawada, D.; Nishiyama, Y.; Shah, R.; Forsyth, V. T.; Mossou, E.; O'Neill, H. M.; Wada, M.; Langan, P., *Nat. Commun.* **2022,** *13* (1), 6189. DOI 10.1038/s41467-022-33812-w.
[163] Wohlert, M.; Benselfelt, T.; Wågberg, L.; Furó, I.; Berglund, L. A.; Wohlert, J., *Cellulose* **2021,** *29* (1), 1-23. DOI 10.1007/s10570-021-04325-4.
[164] Wang, H.; Li, D.; Yano, H.; Abe, K., *Cellulose* **2014,** *21* (3), 1505-1515. DOI 10.1007/s10570-014-0222-6.
[165] Faria-Tischer, P. C.; Tischer, C. A.; Heux, L.; Le Denmat, S.; Picart, C.; Sierakowski, M. R.; Putaux, J. L., *Mater Sci Eng C Mater Biol Appl* **2015,** *51*, 167-73. DOI 10.1016/j.msec.2015.02.025.

[166] Hu, G.; Chen, L.; Zhao, S.; Hong, F. F., *Chem. Eng. J.* **2022,** *428*. DOI 10.1016/j.cej.2021.131104.
[167] Wloch, D.; Herrera, N.; Lee, K.-Y., *Composites Part A* **2023,** *172*. DOI 10.1016/j.compositesa.2023.107583.
[168] Peng, Y.; Gardner, D. J.; Han, Y.; Kiziltas, A.; Cai, Z.; Tshabalala, M. A., *Cellulose* **2013,** *20* (5), 2379-2392. DOI 10.1007/s10570-013-0019-z.
[169] Siqueira, G.; Bras, J.; Dufresne, A., *Biomacromolecules* **2009,** *10* (2), 425-32. DOI 10.1021/bm801193d.
[170] Huang, Y.; Kasuga, T.; Nogi, M.; Koga, H., *RSC Adv.* **2023,** *13* (31), 21494-21501. DOI 10.1039/d3ra03840h.
[171] Sim, K.; Ryu, J.; Youn, H. J., *Fibers and Polymers* **2015,** *16* (2), 294-301. DOI 10.1007/s12221-015-0294-4.
[172] Araki, J.; Arita, T., *Chem. Lett.* **2017,** *46* (9), 1438-1441. DOI 10.1246/cl.170588.
[173] Huang, D.; Wu, M.; Wang, C.; Kuga, S.; Huang, Y., *ACS Sustainable Chem. Eng.* **2020,** *8* (30), 11389-11395. DOI 10.1021/acssuschemeng.0c03688.
[174] Hanif, Z.; Jeon, H.; Tran, T. H.; Jegal, J.; Park, S.-A.; Kim, S.-M.; Park, J.; Hwang, S. Y.; Oh, D. X., *Journal of Polymer Research* **2017,** *25* (3). DOI 10.1007/s10965-017-1343-z.
[175] Ferguson, A.; Khan, U.; Walsh, M.; Lee, K. Y.; Bismarck, A.; Shaffer, M. S.; Coleman, J. N.; Bergin, S. D., *Biomacromolecules* **2016,** *17* (5), 1845-53. DOI 10.1021/acs.biomac.6b00278.
[176] Jayme, G., *Wochenbl. Papierfabr.* **1944,** *6*, 187-194.
[177] Minor, J. L., *Prog. Pap. Recycl.* **1994,** *3* (2), 93-95.
[178] Gu, H.; Liu, C.; Zhu, J.; Gu, J.; Wujcik, E. K.; Shao, L.; Wang, N.; Wei, H.; Scaffaro, R.; Zhang, J.; Guo, Z., *Advanced Composites and Hybrid Materials* **2017,** *1* (1), 1-5. DOI 10.1007/s42114-017-0017-y.
[179] Liu, K.; Liu, W.; Li, W.; Duan, Y.; Zhou, K.; Zhang, S.; Ni, S.; Xu, T.; Du, H.; Si, C., *Advanced Composites and Hybrid Materials* **2022,** *5* (2), 1078-1089. DOI 10.1007/s42114-022-00425-2.
[180] Trache, D.; Tarchoun, A. F.; Abdelaziz, A.; Bessa, W.; Hussin, M. H.; Brosse, N.; Thakur, V. K., *Nanoscale* **2022,** *14* (35), 12515-12546. DOI 10.1039/d2nr01967a.
[181] Ngoensawat, U.; Parnsubsakul, A.; Kaitphaiboonwet, S.; Wutikhun, T.; Sapcharoenkun, C.; Pienpinijtham, P.; Ekgasit, S., *Carbohydr. Polym.* **2021,** *262*, 117864. DOI 10.1016/j.carbpol.2021.117864.
[182] Parnsubsakul, A.; Ngoensawat, U.; Wutikhun, T.; Sukmanee, T.; Sapcharoenkun, C.; Pienpinijtham, P.; Ekgasit, S., *Carbohydr. Polym.* **2020,** *235*, 115956. DOI 10.1016/j.carbpol.2020.115956.
[183] Carosio, F.; Medina, L.; Kochumalayil, J.; Berglund, L. A., *Advanced Materials Interfaces* **2021,** *8* (18). DOI 10.1002/admi.202101111.
[184] Gorur, Y. C.; Francon, H. S.; Sethi, J.; Maddalena, L.; Montanari, C.; Reid, M. S.; Erlandsson, J.; Carosio, F.; Larsson, P. A.; Wågberg, L., *ACS Applied Nano Materials* **2022,** *5* (7), 9188-9200. DOI 10.1021/acsanm.2c01530.
[185] Xu, Q.; Du, X.-H.; Luo, D.; Strømme, M.; Zhang, Q.-F.; Xu, C., *Chem. Eng. J.* **2023,** *458*. DOI 10.1016/j.cej.2023.141498.
[186] Schweng, P.; Mayer, F.; Galehdari, D.; Weiland, K.; Woodward, R. T., *Small* **2023,** *19* (50), e2304562. DOI 10.1002/smll.202304562.
[187] Tan, L.; Tan, B., *Chem. Soc. Rev.* **2017,** *46* (11), 3322-3356. DOI 10.1039/c6cs00851h.
[188] Gu, J.; Zhang, J.; Li, D.; Yuan, H.; Chen, Y., *Journal of Chemical Technology & Biotechnology* **2019,** *94* (10), 3073-3083. DOI 10.1002/jctb.6107.
[189] Bhunia, S.; Banerjee, B.; Bhaumik, A., *ChemComm* **2015,** *51* (24), 5020-3. DOI 10.1039/c4cc09872b.
[190] James, A. M.; Harding, S.; Robshaw, T.; Bramall, N.; Ogden, M. D.; Dawson, R., *ACS Appl. Mater. Interfaces* **2019,** *11* (25), 22464-22473. DOI 10.1021/acsami.9b06295.

[191] Xiong, G.; Zhang, Q.; Ren, B.; You, L.; Ding, F.; He, Y.; Fan, X.; Wang, N.; Sun, Y., *ChemistrySelect* **2020,** *5* (22), 6541-6548. DOI 10.1002/slct.202000927.
[192] Zhou, H.; Akram, A.; Semiao, A. J. C.; Malpass-Evans, R.; Lau, C. H.; McKeown, N. B.; Zhang, W., *J. Membr. Sci.* **2022,** *644*. DOI 10.1016/j.memsci.2021.120172.
[193] Lau, C. H.; Mulet, X.; Konstas, K.; Doherty, C. M.; Sani, M. A.; Separovic, F.; Hill, M. R.; Wood, C. D., *Angew. Chem. Int. Ed. Engl.* **2016,** *55* (6), 1998-2001. DOI 10.1002/anie.201508070.
[194] Bhavsar, R. S.; Mitra, T.; Adams, D. J.; Cooper, A. I.; Budd, P. M., *J. Membr. Sci.* **2018,** *564*, 878-886. DOI 10.1016/j.memsci.2018.07.089.
[195] Barhoum, A.; Deshmukh, K.; Garcia-Betancourt, M. L.; Alibakhshi, S.; Mousavi, S. M.; Meftahi, A.; Sabery, M. S. K.; Samyn, P., *Carbohydr. Polym.* **2023,** *317*, 121057. DOI 10.1016/j.carbpol.2023.121057.
[196] Koros, W. J.; Ma, Y. H.; Shimidzu, T., *Pure Appl. Chem.* **1996,** *68* (7), 1479-1489. DOI 10.1351/pac199668071479.
[197] Svagan, A. J.; Samir, M. A.; Berglund, L. A., *Biomacromolecules* **2007,** *8* (8), 2556-63. DOI 10.1021/bm0703160.
[198] French, A. D., *Cellulose* **2013,** *21* (2), 885-896. DOI 10.1007/s10570-013-0030-4.
[199] Ahvenainen, P.; Kontro, I.; Svedström, K., *Cellulose* **2016,** *23* (2), 1073-1086. DOI 10.1007/s10570-016-0881-6.
[200] Daicho, K.; Saito, T.; Fujisawa, S.; Isogai, A., *ACS Applied Nano Materials* **2018,** *1* (10), 5774-5785. DOI 10.1021/acsanm.8b01438.
[201] Lide, D. R., *CRC Handbook of Chemistry and Physics*. 84 ed.; CRC Press: **2003**.
[202] Vazquez, G.; Alvarez, E.; Navaza, J. M., *Journal of Chemical & Engineering Data* **1995,** *40* (3), 611-614. DOI 10.1021/je00019a016.
[203] Mautner, A.; Lee, K. Y.; Lahtinen, P.; Hakalahti, M.; Tammelin, T.; Li, K.; Bismarck, A., *ChemComm* **2014,** *50* (43), 5778-81. DOI 10.1039/c4cc00467a.
[204] Kumar, M.; Shevate, R.; Hilke, R.; Peinemann, K.-V., *Chem. Eng. J.* **2016,** *301*, 306-314. DOI 10.1016/j.cej.2016.05.006.
[205] Robinson, R. G., *JAMA, J. Am. Med. Assoc.* **1995,** *274* (5). DOI 10.1001/jama.1995.03530050068035.
[206] Reynolds, J. G.; Cooke, G. A.; Herting, D. L., *J. Radioanal. Nucl. Chem.* **2020,** *326* (1), 435-443. DOI 10.1007/s10967-020-07296-1.
[207] Kooi, M.; Koelmans, A. A., *Environ. Sci. Technol. Lett.* **2019,** *6* (9), 551-557. DOI 10.1021/acs.estlett.9b00379.
[208] Baker, T. S.; Olson, N. H.; Fuller, S. D., *Microbiol. Mol. Biol. Rev.* **1999,** *63* (4), 862-922, table of contents. DOI 10.1128/MMBR.63.4.862-922.1999.
[209] Louten, J., Virus Structure and Classification. In *Essential Human Virology*, Elsevier: 2016; pp 19-29.
[210] Bayer, T.; Cunning, B. V.; Šmíd, B.; Selyanchyn, R.; Fujikawa, S.; Sasaki, K.; Lyth, S. M., *Cellulose* **2021,** *28* (3), 1355-1367. DOI 10.1007/s10570-020-03593-w.

Publication I

Mayer, F., Prado-Roller, A., Mautner, A., & Bismarck, A. (2024). Retain strength, gain ductility: tough and transparent nanopapers by mercerisation. *Cellulose*, 31(3), 1533-1544.
DOI: 10.1007/s10570-023-05714-7

Cellulose (2024) 31:1533–1544
https://doi.org/10.1007/s10570-023-05714-7

ORIGINAL RESEARCH

Retain strength, gain ductility: tough and transparent nanopapers by mercerisation

Florian Mayer · Alexander Prado-Roller · Andreas Mautner · Alexander Bismarck

Received: 30 June 2023 / Accepted: 22 December 2023 / Published online: 4 January 2024

Abstract Nanocellulose papers offer high tensile strength and modulus but suffer from drawbacks such as their brittle nature. We show that mercerisation of cellulose nanopapers in strong alkaline media for 2 min to 24 h results in the (partial) transformation of native cellulose I into the more ductile cellulose II allomorph. The strain to failure of mercerised nanopapers tripled compared to the original nanopapers while retaining their tensile strength in excess of 100 MPa at the expense of a slight drop in modulus resulting in a significant increase in toughness (total work of fracture). An additional advantage of mercerisation is a reduction in porosity of the nanopapers and increased transparency.

Keywords Nanocellulose · Mercerisation · Nanopapers · All cellulose composites · Toughness

Introduction

Thin nanocellulose films, also called nanopapers, show great potential in a myriad of possible applications such as substrates for printable electronics (Koga et al. 2013, 2014; Fujisaki et al. 2014; Zhu et al. 2014), water treatment membranes (Mautner et al. 2015, 2016, 2019; Mautner 2020; Fijoł et al. 2023), and as 2 dimensional reinforcement for

Supplementary Information The online version contains supplementary material available at https://doi.org/10.1007/s10570-023-05714-7.

F. Mayer · A. Mautner · A. Bismarck
Institute of Materials Chemistry and Research, Polymer and Composite Engineering (PaCE) Group, Faculty of Chemistry, University of Vienna, Währinger Straße 42, 1090 Vienna, Austria

A. Prado-Roller
Institute of Inorganic Chemistry - Functional Materials, Faculty of Chemistry, University of Vienna, Währinger Straße 42, 1090 Vienna, Austria

A. Mautner (✉)
Institute of Environmental Biotechnology, IFA-Tulln, University of Natural Resources and Life Sciences, Vienna, Konrad-Lorenz-Straße 20, 3430 Tulln an der Donau, Austria
e-mail: andreas.mautner@boku.ac.at

A. Bismarck
Department of Chemical Engineering, Imperial College London, South Kensington Campus, London SW7 2AZ, UK

A. Bismarck (✉)
Division of Materials Science, Department of Engineering Sciences and Mathematics, Luleå University of Technology, Luleå 971 87, Sweden
e-mail: alexander.bismarck@univie.ac.at

polymers (Mautner et al. 2017, 2020) amongst many others. These applications pose different requirements on nanopapers, rendering the tuneability of the mechanical, optical and morphological properties a necessity. Specifically, nanopapers prepared from cellulose nanofibrils (CNFs) by filtration and hot-pressing akin to traditional papermaking are promising for these applications. Such cellulose nanopapers are stiff and strong but brittle (Hervy et al. 2017), lack full transparency (Xu et al. 2016), and are sensitive to moisture resulting in low wet strength (Kriechbaum and Bergström 2020; Walther et al. 2020). A variety of methods to address this conundrum have been reported. For instance, we suggested a hybridisation approach to fashion nanopapers with improved tensile strength, strain to failure and toughness by hybridising different types of nanofibrils exhibiting various dimensions and exploiting their different chemical and mechanical properties (Mautner et al. 2018). Sehaqui et al. (2011) dried unmodified and TEMPO-oxidised nanocellulose using supercritical CO_2 to prepare nanopapers with high strain to failure while Guzman-Puyol et al. (2022b) prepared papers from C6 fluorinated nanocellulose esters to considerably increase the toughness of the resulting nanopapers. The same group (Guzman-Puyol et al. 2022a) also reported a method to combine nanocellulose and naringin in trifluoroacetic acid and cast films from these mixtures, which exhibited increased toughness and UV-blocking capabilities. Kriechbaum and Bergström (2020) produced optically transparent nanocellulose films with high wet strength and UV-blocking properties by grafting nanocellulose with gelatin moieties followed by impregnation of films prepared from this material with a gelatin and tannin solution, which resulted in films with greatly improved wet strength while sacrificing strain to failure and toughness in the dry state. Gindl and Keckes (2005) and Abbott and Bismarck (2010) prepared all-cellulose composites by first solvent exchanging nanocellulose to dimethylacetamide and subsequently partially dissolving the nanofibrils using LiCl/dimethylacetamide followed by regeneration to all-cellulose composites with high tensile strength and optical transparency. All the processes detailed above are either time-consuming and/or resource-intensive chemical procedures to modify the raw material or employ expensive reagents, additives or treatment methods. To tailor strength and stiffness without sacrificing toughness (or work of fracture) methods need to be developed that could be easily implemented into existing industrial processes adding little extra cost to be viable for broad industrial applications.

Auspiciously, cellulose itself offers a solution to this problem as it can be transformed into different allomorphs covering a broad array of mechanical properties. The naturally occurring cellulose allomorph (cellulose I) is synthesised by plants, bacteria and some animals. Cellulose II does not occur in nature and, thus, is often referred to as "synthetic cellulose". Cellulose I exhibits a more ordered structure, with its crystalline regions being formed by layers of parallel cellulose molecules formed via hydrogen bonds stacked on top of each other and held together through hydrophobic interactions (Nishiyama et al. 2002, 2003). Cellulose II on the other hand is composed of a tight 3D network of hydrogen bonded cellulose molecules with some disorder in the pattern (Kroon-Batenburg and Kroon 1997). The differences in structure between cellulose I and II also affect their mechanical properties: Cellulose I has a Young's modulus and ultimate tensile strength approximately 50% higher than that of cellulose II according to modelling reports (Nishino et al. 1995; Moon et al. 2011; Djahedi et al. 2015). Cellulose I can be transformed into cellulose II using a simple yet efficient alkaline treatment, commonly referred to as mercerisation named after John Mercer, a British scientist who invented the process in 1844 (Binz 1898). Mercerisation is widely used in the textile industry to improve the lustre and sheen of cotton fibres. This transformation is hypothesised to occur by swelling individual cellulose elementary fibrils, which constitute the macroscopic cotton fibres, causing neighbouring fibres to interdigitate and thus transforming cellulose I into cellulose II (Kim et al. 2006). The thermodynamically more stable cellulose II is more ductile compared to cellulose I (Gindl and Keckes 2005).

Alkaline treatment was already applied to nanocellulose, but to date, it was almost exclusively performed directly on nanocellulose suspensions, e.g. as a purification step to remove organic residues from bacterial cellulose cultures, i.e. nanocellulose synthesised by various strains of bacteria, such as *Komatagaeibacter*, or to degrade and solubilise hemicellulose residues from wood pulp derived nanocellulose. Mercerisation is hypothesised to require the interdigitation of two antiparallel

aligned nanocellulose (Kim et al. 2006) fibrils that are right next to each other, alkaline treatment of individualised fibrils in suspension usually does not result in the transformation of cellulose I fibrils into the cellulose II as they are well separated in suspension and thus the interdigitation step of the process is impeded. To produce cellulose II nanofibres with significantly higher toughness yet lower ultimate tensile strength in nanopaper form as compared with standard CNF nanopapers, Wang et al. (2014) combined mercerisation of wood pulp with extensive sodium chlorite treatment prior to defibrillation in a homogeniser. Faria-Tischer et al. (2015) used an alkaline treatment to fully convert as-grown bacterial cellulose pellicles into cellulose II and reported improved transparency and smoother surfaces of the resulting compacted mercerised pellicles. Hu et al. (2022) mercerised never dried, as-grown bacterial cellulose tubes to produce small-calibre vascular grafts with enhanced mechanical properties. Wloch et al. (2023) used alkaline treatment on never dried, as-grown bacterial cellulose pellicles and found that mercerized pellicles had significantly higher strains to failure but lost up to 40% in tensile strength. Mercerised BC pellicles were also used to fabricate low cellulose loading optically transparent composites. Mercerisation of ready-made, dried and 'hornified' CNF nanopapers to improve their tensile and optical properties has not been reported before but could be a simple, low-cost method to obtain nanopapers with tailored mechanical properties.

We propose that alkaline treatment of a randomly oriented and compacted network of nanocellulose fibrils will result in effective partial mercerisation of the whole nanopaper sheet. We hypothesise that the outer layers of individual nanofibrils in contact with other fibrils can be (partially) transformed into cellulose II resulting in an all-cellulose composite comprising a cellulose I core embedded in a matrix of weaker yet more ductile cellulose II. This process is anticipated to also increase the optical transparency of the nanopapers as both swelling and interdigitation should reduce the porosity and thus the haze of the nanopapers, increasing their suitability, e.g. for composites, packaging materials or surface coatings. Particular focus is placed on the use of nanocellulose produced in a simple and cost-effective way without prior enzymatic or chemical treatments or classification processes.

Experimental

Materials

Sodium hydroxide pellets were purchased from W. Neuber's Enkel (Vienna, Austria). We produced CNFs from never-dried elemental chlorine-free bleached softwood (*Picea abies and Pinus spp.*) pulp, obtained from Stendal (Berlin, Germany). The pulp comprised 81.3% cellulose, 12.6% hemicellulose and 0.3% ash (Josset et al. 2014). Unless specified otherwise, deionised water was used in all experiments.

Preparation of nanocellulose

Nanocellulose was prepared by cutting 100 g of pulp into small pieces (approx. 10×10 mm^2) and submerging them for 18 h in 1 L of water prior to blending (Kult Pro, WMF, Germany) at 1200 W for 1 min. The resulting homogeneous suspension was then passed 10 times through a high-speed disc mill (Granomat JP 150, Fuchs, Switzerland). The ten-step gap size indicator of the grinder was set to 10, marking the distance at which two grindstones just touched resulting in an audible sound. After the addition of the cellulose suspension the gap size was continuously reduced, starting at 9 during the first pass down to 5.5 during the tenth cycle. More water was added after each pass as required to ensure a consistency suitable for passing the dispersion through the mill. In lieu of specific measurements, and because of the constantly changing state of the suspension due to fibre defibrillation, and thus the gradual increase of the viscosity of the suspension, water was added to keep the viscosity somewhere between that of whole milk (2 mPa s) and Ketchup (2000 mPa s) (Koocheki et al. 2009). The resulting nanocellulose suspension was up-concentrated to 4 wt% by gravity filtration through a cotton cloth and then stored at 4 °C until use.

Preparation of nanocellulose papers

Papers with a grammage of 50 g m^{-2} were prepared by blending nanocellulose (0.613 g dry weight) with water in a kitchen blender (Kult Pro, WMF, Germany) at 1200 W for 30 s to obtain a homogeneous CNF suspension with a consistency of 0.2 wt%. This suspension was then vacuum filtered using a Büchner funnel with a 125 mm diameter fritted glass disc onto

a filter paper (VWR 413, VWR, Leuven, Belgium) to obtain a filter cake, which was subsequently sandwiched between 4 sheets of blotting paper (3MM Chr VWR, Lutterworth, UK) and pressed in a hydraulic press (type 25-12-2 H, Carver Inc., Wabash, USA) at 20 °C for 10 s under a weight of 1.5 ton-force to remove excess water. The pre-pressed filter cake was then sandwiched between steel plates, fresh blotting and release paper and hot pressed at 120 °C for 15 min under 1.5 ton-force to consolidate the nanopapers.

Mercerisation of nanocellulose papers

Nanopapers were framed in a custom-made PMMA frame (Fig. 1) consisting of two identical rings with an inner diameter of 100 mm and an outer diameter of 150 mm, which was laser-cut from 3 mm thick PMMA sheets and fixed with eight M8 stainless steel bolts each tightened with a torque wrench set to 5 Nm to apply even pressure across the outside of the nanopapers preventing shrinkage that commonly occurs during mercerisation (Goldthwait 1965). This frame system, holding a nanopaper, was subsequently immersed into NaOH solutions of various concentrations for defined time intervals (Table 1).

After treatment, the frame holding the mercerised paper was removed from the alkaline bath and rinsed with tap water (approx. 10 L) until pH 7 removing NaOH. Afterwards, the papers were removed from the PMMA frame, sandwiched between four sheets of blotting paper (two on top, two on bottom) and dried at 110 °C for 24 h between two stainless steel plates under 10 kg-force to avoid warpage.

Table 1 Preparation parameters and names of all samples. Samples were prepared in duplicates

Sample name	NaOH concentration		Treatment time
	wt%	[mol L^{-1}]	[min]
Ref	0	0	0
20% 2 min	20	6.1	2
20% 10 min	20	6.1	10
20% 60 min	20	6.1	60
20% 24 h	20	6.1	1440
40% 2 min	40	14.3	2
40% 10 min	40	14.3	10
40% 60 min	40	14.3	60

Chemical composition determined by X-ray photoelectron spectroscopy

The surface composition of nanopapers before and after mercerisation was analysed by X-ray photoelectron spectroscopy (XPS). For each sample, a survey spectrum with a step size of 1 eV and a pass energy of 200 eV was recorded. Element-specific high-resolution spectra for carbon (C1s 279–298 eV), nitrogen (N1s 392–410 eV), oxygen (O1s 525–545 eV), as well as sodium (Na1s 1062–1079 eV), calcium (Ca2p 340–360) and silicon (Si1p 95–110 eV) with step sizes of 0.1 eV and a pass energy of 50 eV, were acquired. All spectra were recorded using Al-K_α X-rays at 72 W at a spot size of 400 µm on a photoelectron spectrometer (Nexsa, Thermo Scientific, UK). After the initial measurement, the sample surfaces were ablated using a beam of Ar clusters of 1000 atoms and an energy of 6 keV. Peak fitting

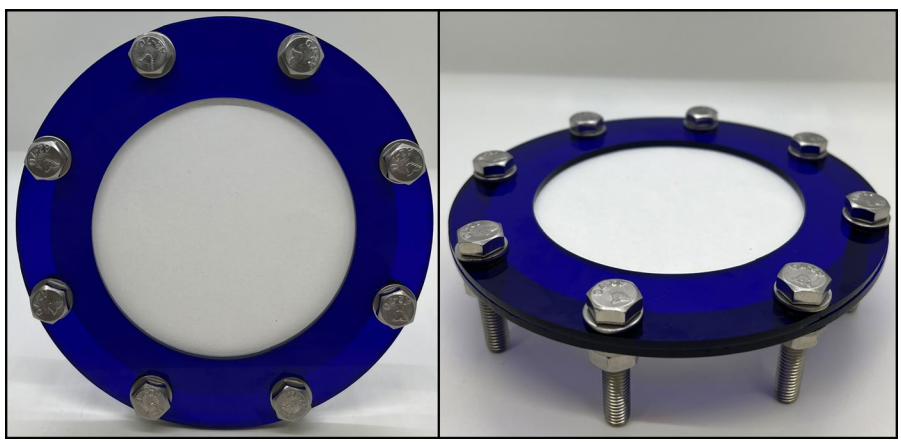

Fig. 1 Front and side view of the custom-made PMMA frame used during mercerisation to ensure the dimensional stability of nanopapers during treatment

was performed using the software package Avantage (v5.9931, Thermo Fisher Scientific, UK) and the atomic composition was calculated from the peak area using the integrated ALTHERMO1 scaling factor database.

Cellulose crystallinity determined wide-angle Powder X-ray diffraction

Wide angle powder X-ray diffraction (PXRD) was performed on cellulose films using an Empyrean Powder Diffractometer (Malvern PANalytical, Amelo, The Netherlands) using Cu-K_α X-ray source with a wavelength of 1.54 Å in θ/θ-mode. Specimens were fixed to a reflection-transmission spinner and recorded in reflection mode, using a Bragg-Brentano mirror. All measurements are continuous scans in the 2θ range of 6 to 45°, with a step size of 0.0131°, a counting time per step of 49.47 s and a spinning rotation time of 8 s. The degree of crystallinity and the crystalline composition of the cellulose samples was determined by Rietveld refinement using the ideal diffraction patterns of cellulose Iβ and II as reported by Nishiyama et al. (2002) and French (2014) using the software package High Score Plus, Version 4.9a (4.9.1.29739) (PANanalytical). A detailed description of the workflow, cif files used and Rietveld refined diffractograms can be found in SI Sect. 1.

Porosity, density and thickness of nanopapers

Eight test specimens radially distributed across one half of the paper (Fig. SI 2–1) were punched out from the mercerised and non-mercerised papers using a punch die (Zwick ZCP 020 Manual Cutting Press, Zwick, Ulm, Germany). The dogbone-shaped test specimens (EN ISO 527-2, Type 1BB) had an overall length of 30 mm with a 20 mm long and 2 mm wide middle section. The test specimens had an area A of 85.81 mm^2. The thickness d of each test specimen was measured at five points evenly distributed along their length (Fig. SI 2–1) using a digital micrometre (705-12229, RS Components, Corby, UK). The specimens were weighed using an microbalance (MSA 225P, Sartorius, Göttingen, Germany) and used to determine the average paper grammage Γ (Eq. 1), envelope density ρ_e (Eq. 2) and porosity Φ (Eq. 3) from the measured mass m, A and d of the specimens by approximating the skeletal density ρ_s of both cellulose I and II to be 1606 kg m^{-3} (Daicho et al. 2022).

$$\Gamma = \frac{m}{A} \tag{1}$$

$$\rho_e = \frac{\Gamma}{d} \tag{2}$$

$$\Phi = \frac{\rho_e}{\rho_s} \times 100 \tag{3}$$

Tensile properties of (mercerised) nanopapers

Tensile tests were performed on a minimum of at least eight specimens for each (mercerised) nanopaper sample at 25 °C and 35–40% RH using a dual column universal test frame (Instron Model 5969 Dual column Universal Testing System, Instron, Darmstadt, Germany) equipped with a 1 kN load cell. The tensile strain was recorded using a non-contact video extensometer (Gig ProE, iMETRIUM, Bristol UK). The sample thickness was approximately 50 µm. Tensile tests were performed at a gauge length of 15 mm and a crosshead displacement speed of 1 mm min^{-1}. The Young's modulus (elastic Modulus E) was determined in the linear elastic region of the stress-strain curves as a secant between two strength values separated by 0.2% strain according to a procedure previously established by us (Mautner et al. 2018). The absorbed energy during tensile fracture (J m^{-3}) was determined from the area under the stress-strain curves.

Scanning electron microscopy

To investigate the microstructure of the nanopapers before and after mercerisation, micrographs were taken using a scanning electron microscope (SEM, ZEISS Supra 55 VP, Carl Zeiss GmbH, Jena, Germany) operated at an accelerating voltage of 2 kV and a working distance of 7.2 mm. The specimens were mounted onto aluminium sample holders using carbon tape and gold coated (Leica SCD 050/EM QSG 100) at 60 mA for 60 s prior to SEM imaging.

Results and discussion

Mercerisation was primarily performed at a NaOH concentration of 20 wt% –the common concentration used for mercerisation of cellulose fibres– in accordance with previous reports (Kolpak et al. 1978; Wang et al. 2014; Faria-Tischer et al. 2015; Hu et al. 2022; Sawada et al. 2022). In addition, a concentration of 40 wt% NaOH was chosen to investigate whether harsher and more concentrated alkaline conditions would have a favourable effect on the treatment. Preliminary experiments showed that mercerisation and subsequent drying resulted in significant shrinkage and subsequent cockling of the nanopapers as the cellulose fibril network consolidated (Fig. SI 3–1). To counteract shrinkage we fixed nanopapers in a frame allowing to preserve the original dimensions of the papers as confirmed by the thickness and of the mercerised nanopapers (Table SI 3–1). All samples treated while being fixed in the frame exhibited thicknesses close to those of the samples before mercerisation with an average deviation of a mere 4%. Mercerisation of an unframed nanopaper caused swelling as the whole network contracted resulting in a thickness increase of ~20%. After mercerisation of constrained nanopapers, the envelope density of all networks increased on average by 8% corresponding to an average porosity of 32 ± 1% compared with 37 ± 2% for nanopapers prior to mercerisation.

Figure 2 juxtaposes a reference nanopaper (left) and a nanopaper mercerised in 40 wt% NaOH for 10 min (right) taken at different distances away from the original (picture of a flower). The comparative photographs show the effect of alkaline treatment on both transparency and haze, with the former increasing and the latter decreasing. These changes were primarily attributed to the reduction of porosity as well as a decrease in surface roughness of mercerised nanopapers reducing light scattering. Decreasing surface roughness after mercerisation of nanopapers was also found by Faria-Tischer et al. (2015) for mercerised bacterial cellulose nanopapers. On a macroscopic level, a smoother and more uniform surface was generated, which affected their haptic properties that changed drastically from a rough "papery" texture to a smooth, almost plastic film-like texture.

Scanning electron micrographs (Fig. 3) revealed a change of surface morphology accompanying the (partial) transformation of cellulose I to II. SEM

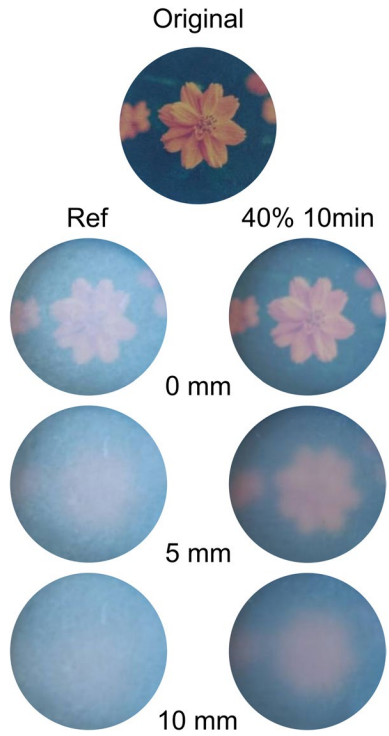

Fig. 2 Representative images of a picture of a flower (top) and of the same picture photographed through nanopapers (camera settings: shutter speed of 1/5, ISO of 80, white balance of 3200 K at fixed at a distance of 13.5 cm from reference image) before (left) and after mercerisation for 10 min in 40 wt% NaOH solution (right) directly on top of an image (0 mm) and gradually further away (5 & 10 mm, respectively)

images of the reference sample (Fig. 3A) show a fibrous network structure with distinctly visible fibrils whereas the mercerised samples showed a much less fibrillar structure on their surface (Fig. 3B–E) and fracture surfaces (Fig. SI 3–2). It appears that fibrils fused into larger fibrillar structures, which disappear with longer treatment times indicating that swelling and transformation occur gradually. Our observation is in good agreement with the postulated mechanism of mercerisation by fibre swelling and interdigitation (Kim et al. 2006).

SEM also revealed the appearance of bulbous structures on the surface of mercerised nanopapers. The amount and size of these structures increased with longer treatment times and in harsher alkaline treatment conditions. We hypothesise that the structures consist of cellulose II expulsed from the network and consequently "squeezed" through the pores

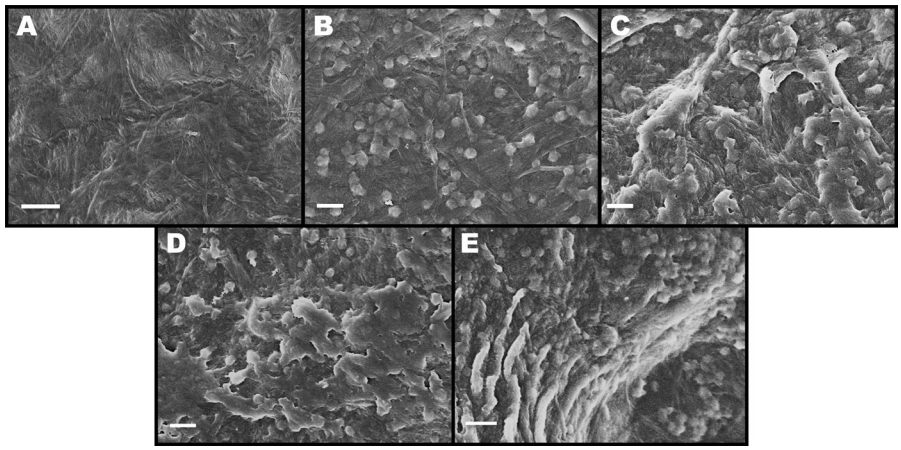

Fig. 3 SEM images of the surfaces of samples treated in 20 wt% NaOH solutions. **A** Reference, **B** 2 min, **C** 10 min, **D** 1 h, **E** 24 h. The scale bar size corresponds to 1 µm

in the surface of the network during the swelling step. A possible explanation for this rather unexpected texturing of the nanopaper surface will be attempted further below.

XPS showed that the chemical composition of the nanopapers did not change during mercerisation (Fig. SI 4–1). Un/mercerised nanopapers consisted of pure cellulose containing minute amounts of inorganic contaminants stemming from the processing of the pulp as well as from the grindstone (Fig. SI 4–2).

Wide-angle PXRD was used to monitor the transformation of cellulose I into cellulose II. Diffractograms of mercerised nanopapers (Fig. 4 and Fig. SI 1–1 to SI 1–8) show the typical diffraction peaks of cellulose I_β. We assigned the diffraction peak at $2\theta \approx 22.5°$ to the (2 0 0) diffraction plane of cellulose I_β, while the diffraction peak centred around $2\theta \approx 15.7°$ was assigned to be a compound peak of the I_β(1–1 0) and the I_β(1 1 0) diffraction plane at 15° and ~16.5°, respectively (French 2014). It should be noted, that the ideal X-ray diffraction pattern of native cellulose I should consist of two diffraction peaks with equal intensity at $2\theta = 14.5°$ and 16.5° (French 2014). The main diffraction peaks of cellulose II

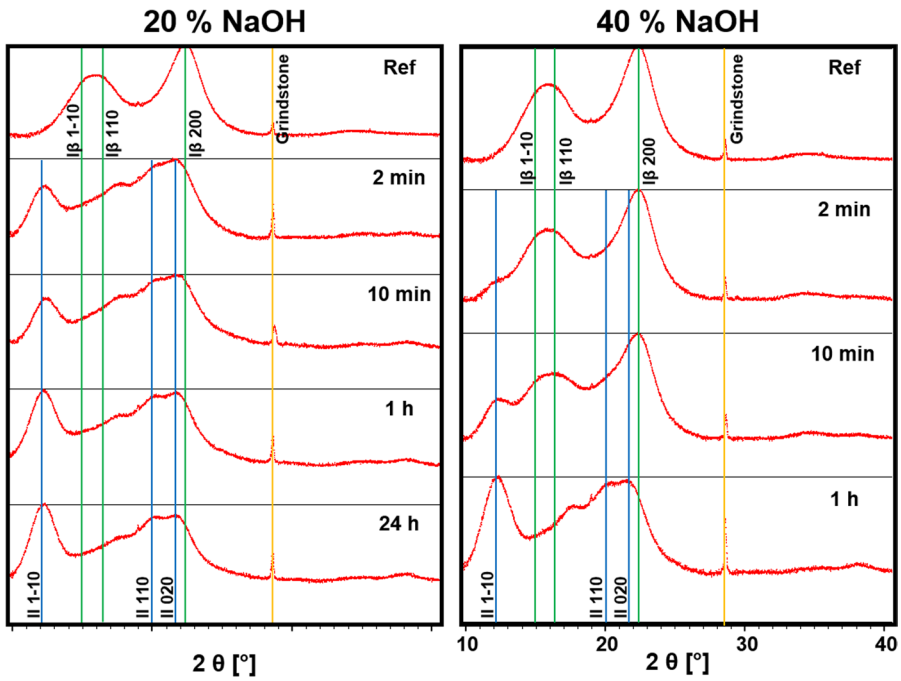

Fig. 4 Wide angle PXRD diffractograms of untreated reference papers (Ref) and nanopapers mercerised for various times in 20 wt% (left) and 40 wt% (right) NaOH concentration

occur at 2θ ≈ 12.2°, ~ 20.1° and ~ 21.7° corresponding to the (1–1 0), (1 1 0) and (0 2 0) diffraction planes of cellulose II, respectively (French 2014). The sharp diffraction peak at ~ 28.5° was attributed to presence of crystalline residue from the grindstone, which could be confirmed by the silicon found in XPS (Fig. SI 4–1 and Fig. SI 4–2).

Our starting wood-based nanocellulose possessed a degree of crystallinity of 69% in agreement with the literature (Hermans and Weidinger 1949; Ahvenainen et al. 2016; Daicho et al. 2018). During mercerisation, cellulose I_β is transformed into cellulose II as apparent in the diffractograms (Fig. 4). The overall degree of crystallinity of the cellulose did not change and remained constant at ~ 70% (Fig. 5). Samples treated with 20 wt% NaOH exhibited a rapid transformation from cellulose I to II already within the first 2 min. After a mercerisation time of 1 h, the cellulose II content increased only slightly from 59 to 61% over the course of the subsequent 23 h. The final material is still a composite comprising cellulose I crystallites embedded in a cellulose II matrix, connected by amorphous cellulose. When using 40 wt% NaOH solutions for mercerisation, the transformation from cellulose I to II occurs at a significantly lower rate resulting in a more gradual compositional change but the amorphous phase content remained constant at around 30%. We hypothesise the difference in transformation speed to be due to higher alkaline concentrations causing significantly faster swelling of the fibril surfaces, thus leading to a faster transformation of cellulose I to II slowing down access of the alkaline solution to the core regions of the fibrils—creating a "passivation" layer around a cellulose I core—resulting in an overall lower transformation rate. The XRD data thus suggest that the desired effect of obtaining a nanopaper with a core of cellulose I nanofibres fibres embedded in a matrix of cellulose II can be best achieved in 20 wt% NaOH solution at short treatment times. Treatment times in excess of 10 min result in only marginal gains of transformation to cellulose II. When using 40 wt% NaOH solutions the transition to cellulose II occurs over longer time intervals, allowing for better control of the crystalline composition.

Representative stress-strain curves of the mercerised and reference nanopapers are shown in Fig. 6. Compared to the reference sample, all mercerised samples show significantly increased strains to failure (ε_b). Nanopapers mercerised in 20 wt% NaOH solution exhibited the highest ε_b after 2 min treatment time and a subsequent decrease with increasing treatment times. Nanopapers mercerised in 40 wt%

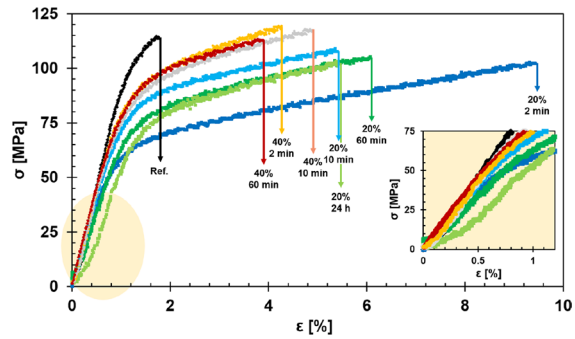

Fig. 6 Representative stress strain curves of (mercerised) nanopapers. The inset diagram shows a magnification of the linear region used to calculate E

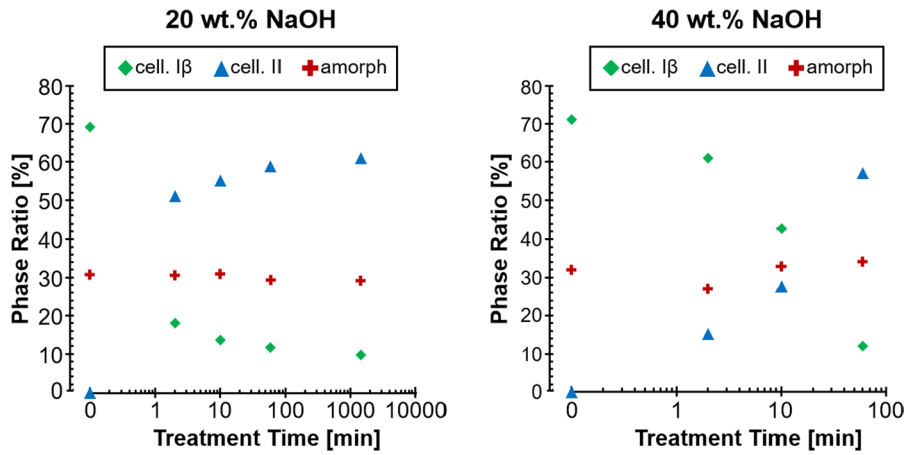

Fig. 5 Degree of crystallinity of cellulose I_β and II, as well as amorphous phase content of untreated reference papers (ref) and nanopapers mercerised for various times at 20 wt% (left) and 40 wt% (right) NaOH concentration

NaOH solutions also exhibited increased ε_b but to a lesser extent compared with the samples treated in 20 wt% alkaline solutions. The maximum ε_b of the sample subset mercerised in 40 wt% NaOH solutions was reached for a treatment time of 10 min, after which ε_b decreased again in concordance with the XRD results reported above. These suggest a slower progression of the cellulose I to II transformation in the samples mercerised in 40 wt% NaOH solution, which causes an optimal cellulose I/II ratio for the formation of an all-cellulose composite to be reached at a slower rate. The influence of the alkaline treatment on the ultimate tensile strength and strain to failure of the individual samples can be attributed to the cellulose I to II transformation occuring during mercerisation at room temperature. During alkaline pulping at elevated temperatures (e.g. at 170 ºC) cellulose molecules are hydrolysed. Longer treatment times led to cellulose with a lower degree of polymerisation (Berggren et al. 2002). However, in our case we did not observe a significant change in average molar mass between mercerised nanopaper irrespectively of mercerisation conditions (Fig. SI 5–1). The only observed change occurred in the lower molecular weight fractions, which decreased likely due to dissolution of those fractions with increasing treatment times.

Nanopapers mercerised with 20 wt% alkaline solutions had lower ultimate tensile strength compared to reference nanopapers and the values for all samples were, within their margin of error, at the same level (Table 2). Nanopapers treated in 40 wt% NaOH solution retained the ultimate tensile strength of the original nanopapers while ε_f increased. The trend found among the strain to failure, was attributed to multiple processes taking place simultaneously, however, primarily the conversion from cellulose I to the weaker and more ductile cellulose II allomorph was responsible for this effect. As the swelling and conversion process happened very fast for samples mercerised in 20 wt% solutions, no significant influence of the treatment time on their tensile strength could be detected, apart from the significantly larger margin of uncertainty for the nanopaper with 2 min treatment. The retained tensile strength of nanopapers treated for 2 and 10 min with 40 wt% NaOH was mainly attributed to the densification of the network, as observed for nanopapers that were mercerised for longer periods of time (Table SI 3−1).

Table 2 Tensile properties of mercerised nanocellulose samples containing tensile strength (σ), strain to failure (ε_f), Young's Modulus (E) and work of fracture (WoF)

Sample name	σ (MPa)	ε_f (%)	E (GPa)	WoF (MPa)
Ref	114.9 ± 2.1	1.7 ± 0.1	12.7 ± 0.9	1.2 ± 0.1
20% 2 min	102.0 ± 11.1	9.1 ± 1.3	7.2 ± 0.6	6.9 ± 1.0
20% 10 min	110.0 ± 3.2	6.0 ± 0.5	7.8 ± 0.7	5.0 ± 0.6
20% 60 min	105.4 ± 4.2	6.1 ± 1.1	7.3 ± 0.7	4.8 ± 1.1
20% 24 h	109.8 ± 6.5	5.1 ± 1.1	8.4 ± 1.2	4.1 ± 1.0
40% 2 min	118.0 ± 7.1	4.1 ± 0.7	10.6 ± 0.9	3.6 ± 0.8
40% 10 min	119.2 ± 3.3	4.6 ± 0.6	10.3 ± 0.9	4.1 ± 0.7
40% 60 min	111.7 ± 5.0	3.9 ± 0.5	9.4 ± 0.5	3.2 ± 0.5

The Young's moduli of nanopapers mercerised in 20 wt% NaOH solutions followed the inverse trend of ε_b (Table 2) and were significantly lower than those treated in 40 wt% NaOH solutions, which in turn exhibited Young's moduli lower than the reference, indicating a trade-off between stiffness and ductility. The Young's moduli and tensile strengths of mercerised nanopapers also compare well to those of cellulose II (Cellophane) films found in the literature (Fink et al. 2001; Leppänen et al. 2020). However, a direct comparison should be made with care, as those dense Cellophane membranes were prepared using different methods and starting materials were not nanofibrillated network structures and commercial cellophane films are often plasticised.

The work of fracture (WoF), i.e. the area under the stress-strain curve, which is a measure of the toughness of a material (Sehaqui et al. 2011) increases significantly for all mercerised nanopapers over that of the reference paper (1.2 MPa) following the trend for the strain to failure. A minimum increase of WoF of 175% and peak values of 6.9 MPa, corresponding to 590% of the original value, were obtained. The results of three of the nanopapers are particularly remarkable. Nanopapers mercerised for 2 min in 20 wt% NaOH exhibited the highest increase in both ε_b and WoF, while papers mercerised for 2 and 10 min in 40 wt% NaOH solution exhibited an increase both in tensile strength and strain to failure, thus significantly increasing WoF of these materials while retaining

over 80% of the Young's modulus of the original nanopaper. Our results show the beneficial effect of partial mercerisation of nanopapers forming all-cellulose composites by transformation of cellulose I to cellulose II both in terms of mechanical properties, resulting in increased toughness while retaining strength at the expense of a slight drop in modulus, and enhanced transparency. In particular, the short treatment times needed render this process suitable for a "drop-in" solution in processes where high throughput is necessary.

We investigated the mercerisation of nanopapers consisting of an in-plane randomly oriented, hornified nanocellulose I fibrillar network. We hypothesised that during mercerisation in caustic soda the fibrils in the network start swelling but in the constrained network, the swollen phase surrounding the cellulose I cores filled the pores (resulting in the reduced porosity, Table SI 3 –1) and excess near the surface was expelled through the pores (Fig. SI 6 −1). In the swollen state the transformation of celllose I to II could occur in two different places: (i) between neighbouring or intersecting fibrils thus "welding" (Wloch et al. 2023) those fibrils together and (ii) between cellulose molecules of the swollen phase extruded through the pores in the constrained fibrillar network. After regeneration this likely resulted in the bulbous structures observed on the surfaces of mercerised nanopapers (Fig. 3). The "welding" of neighbouring or intersecting fibrils possibly caused by interdigitating cellulose molecules originating from close cellulose fibrils with different cellulose I orientation created cellulose II sheaths surrounding cellulose I cores. Irrespectively of the exact mechanism of the cellulose I to II transformation during mercerisation, the results taken together with the observation that the fraction of amorphous cellulose remained unaffected by mercerisation point towards the existence of stiffer and stronger cellulose I cores embedded within the more ductile and less strong cellulose II matrix. The mechanical properties (Fig. 6) can be explained the hybridisation of cellulose I and cellulose II with a random orientation of cellulose I fibrils within the matrix. Upon loading, fibrils can reorient in the loading direction and stress is transferred through the matrix into the stiffer component. Subsequently, after raching the yield (knee) point, the stiffer cellulose I elements start failing and cellulose II takes over the stress distributing it through the material resulting in eventual final failure. The observed stress strain behaviour is in analogy to that of hybrid (Bunsell and Harris 1974) and/or angle-ply (Fuller and Wisnom 2015) composites.

Conclusion

We investigated the influence of mercerisation of pulp-derived cellulose nanopapers under pretension on their mechanical properties; two different NaOH concentrations and the effect of treatment time were investigated. Mercerisation of nanopapers causes the partial conversion of cellulose I into II resulting in significant increases of both strain to failure and toughness of the treated nanopapers as their tensile strength was retained. The transformation of cellulose I to II was confirmed by XRD. Mercerised nanopapers had a higher envelope density and thus lower porosity as compared to the original materials. We found that short mercerisation times yielded nanopapers that can be considered all cellulose composites comprising a blend of cellulose I and II offering high tensile strength, modulus and toughness. An additional benefit of mercerisation was the observed increase in transparency of the resulting nanopapers.

Acknowledgments We acknowledge funding provided by the University of Vienna through the Institute of Materials Chemistry. We are grateful to Klaus Ritter for the preliminary experiments, which in effect guided us to an improved experimental procedure. We greatly apprechiate Dr Irina Sulaeva and Prof. Antje Potthast (Department of Chemistry, Institute for Chemistry of Renewables, University of Natural Resources and Life Sciences (BOKU)) for their help in determining the cellulose molecular weight and the dicussions of the results.

Author contributions Conceptualisation of this study and experiment design by FM, AM and AB. Material preparation, data collection by FM and AP-R. Data analysis by FM, AP-R and AB. The first manuscript draft was written by FM and all authors contributed to editing the manuscript. All authors have read and approved of the final manuscript.

Funding Open access funding provided by University of Vienna. Partial financial support was received from the University of Vienna and the Institute of Materials Chemistry under Grant Number 371300.

Data Availability The corresponding author will provide raw data upon request.

Declarations

Conflict of interests The authors have no relevant financial or non-financial interests to disclose.

Ethical approval and consent to participate No ethics approval was required for this study.

Consent for publication All authors consent to the publication of this manuscript.

References

Abbott A, Bismarck A (2010) Self-reinforced cellulose nanocomposites. Cellulose 17:779–791. https://doi.org/10.1007/s10570-010-9427-5

Ahvenainen P, Kontro I, Svedström K (2016) Comparison of sample crystallinity determination methods by X-ray diffraction for challenging cellulose I materials. Cellulose 23:1073–1086. https://doi.org/10.1007/s10570-016-0881-6

Berggren R, Molin U, Berthold F et al (2002) Alkaline degradation of birch and spruce: influence of degradation conditions on molecular mass distributions and fibre strength. Carbohydr Polym 51:255–264. https://doi.org/10.1016/S0144-8617(02)00160-1

Binz A (1898) Die Mercerisation Der Baumwolle. Z für Angew Chemie 11:595–600. https://doi.org/10.1002/ange.18980112602

Bunsell AR, Harris B (1974) Hybrid carbon and glass fibre composites. Composites 5:157–164. https://doi.org/10.1016/0010-4361(74)90107-4

Daicho K, Saito T, Fujisawa S, Isogai A (2018) The crystallinity of nanocellulose: dispersion-induced disordering of the grain boundary in biologically structured cellulose. ACS Appl Nano Mater 1:5774–5785. https://doi.org/10.1021/acsanm.8b01438

Daicho K, Fujisawa S, Saito T (2022) Linear correlation between true density and crystallinity of regenerated and mercerized celluloses. Biomacromolecules. https://doi.org/10.1021/acs.biomac.2c01067

Djahedi C, Berglund LA, Wohlert J (2015) Molecular deformation mechanisms in cellulose allomorphs and the role of hydrogen bonds. Carbohydr Polym 130:175–182. https://doi.org/10.1016/j.carbpol.2015.04.073

Faria-Tischer PCS, Tischer CA, Heux L et al (2015) Preparation of cellulose II and IIII films by allomorphic conversion of bacterial cellulose I pellicles. Mater Sci Eng C 51:167–173. https://doi.org/10.1016/j.msec.2015.02.025

Fijoł N, Aguilar-Sánchez A, Ruiz-Caldas MX et al (2023) 3D printed polylactic acid (PLA) filters reinforced with polysaccharide nanofibers for metal ions capture and microplastics separation from water. Chem Eng J. https://doi.org/10.1016/j.cej.2022.141153

Fink HP, Weigel P, Purz HJ, Ganster J (2001) Structure formation of regenerated cellulose materials from NMMO-solutions. Prog Polym Sci 26:1473–1524. https://doi.org/10.1016/S0079-6700(01)00025-9

French AD (2014) Idealized powder diffraction patterns for cellulose polymorphs. Cellulose 21:885–896. https://doi.org/10.1007/s10570-013-0030-4

Fujisaki Y, Koga H, Nakajima Y et al (2014) Transparent nanopaper-based flexible organic thin-film transistor array. Adv Funct Mater 24:1657–1663. https://doi.org/10.1002/adfm.201303024

Fuller JD, Wisnom MR (2015) Pseudo-ductility and damage suppression in thin ply CFRP angle-ply laminates. Compos Part A Appl Sci Manuf 69:64–71. https://doi.org/10.1016/j.compositesa.2014.11.004

Gindl W, Keckes J (2005) All-cellulose nanocomposite. Polymer 46:10221–10225. https://doi.org/10.1016/j.polymer.2005.08.040

Goldthwait CF (1965) Shrinkage of cotton fibers in sodium hydroxide solutions and resulting elastic properties. Text Res J 35:986–992. https://doi.org/10.1177/004051756503501104

Guzman-Puyol S, Hierrezuelo J, Benítez JJ et al (2022) Transparent, UV-blocking, and high barrier cellulose-based bioplastics with naringin as active food packaging materials. Int J Biol Macromol 209:1985–1994. https://doi.org/10.1016/j.ijbiomac.2022.04.177

Guzman-Puyol S, Tedeschi G, Goldoni L et al (2022) Grease-proof, hydrophobic, and biodegradable food packaging bioplastics from C6-fluorinated cellulose esters. Food Hydrocoll. https://doi.org/10.1016/j.foodhyd.2022.107562

Hermans PH, Weidinger A (1949) X-ray studies on the crystallinity of cellulose. J Polym Sci 4:135–144. https://doi.org/10.1002/pol.1949.120040203

Hervy M, Santmarti A, Lahtinen P et al (2017) Sample geometry dependency on the measured tensile properties of cellulose nanopapers. Mater Des 121:421–429. https://doi.org/10.1016/j.matdes.2017.02.081

Hu G, Chen L, Zhao S, Hong FF (2022) Mercerization of tubular bacterial nanocellulose for control of the size and performance of small-caliber vascular grafts. Chem Eng J 428:131104. https://doi.org/10.1016/j.cej.2021.131104

Josset S, Orsolini P, Siqueira G et al (2014) Energy consumption of the nanofibrillation of bleached pulp, wheat straw and recycled newspaper through a grinding process. Nord Pulp Pap Res J 29:167–175. https://doi.org/10.3183/NPPRJ-2014-29-01-p167-175

Kim NH, Imai T, Wada M, Sugiyama J (2006) Molecular directionality in cellulose polymorphs. Biomacromol 7:274–280. https://doi.org/10.1021/bm0506391

Koga H, Saito T, Kitaoka T et al (2013) Transparent, conductive, and printable composites consisting of TEMPO-oxidized nanocellulose and carbon nanotube. Biomacromol 14:1160–1165. https://doi.org/10.1021/bm400075f

Koga H, Nogi M, Komoda N et al (2014) Uniformly connected conductive networks on cellulose nanofiber paper for transparent paper electronics. NPG Asia Mater 6:1–8. https://doi.org/10.1038/am.2014.9

Kolpak FJ, Weih M, Blackwell J (1978) Mercerization of cellulose: 1. Determination of the structure of Mercerized cotton. Polymer 19:123–131. https://doi.org/10.1016/0032-3861(78)90027-7

Koocheki A, Ghandi A, Razavi SMA et al (2009) The rheological properties of ketchup as a function of different hydrocolloids and temperature. Int J Food Sci Technol 44:596–602. https://doi.org/10.1111/j.1365-2621.2008.01868.x

Kriechbaum K, Bergström L (2020) Antioxidant and UV-Blocking leather-inspired nanocellulose-based films with High Wet Strength. Biomacromol 21:1720–1728. https://doi.org/10.1021/acs.biomac.9b01655

Kroon-Batenburg LMJ, Kroon J (1997) The crystal and molecular structures of cellulose I and II. Glycoconj J 14:677–690. https://doi.org/10.1023/A:1018509231331

Leppänen I, Vikman M, Harlin A, Orelma H (2020) Enzymatic degradation and pilot-scale composting of cellulose-based films with different Chemical structures. J Polym Environ 28:458–470. https://doi.org/10.1007/s10924-019-01621-w

Mautner A (2020) Nanocellulose water treatment membranes and filters: a review. Polym Int 69:741–751. https://doi.org/10.1002/pi.5993

Mautner A, Lee K-Y, Tammelin T et al (2015) Cellulose nanopapers as tight aqueous ultra-filtration membranes. React Funct Polym 86:209–214. https://doi.org/10.1016/j.reactfunctpolym.2014.09.014

Mautner A, Maples HA, Sehaqui H et al (2016) Nitrate removal from water using a nanopaper ion-exchanger. Environ Sci Water Res Technol 2:117–124. https://doi.org/10.1039/c5ew00139k

Mautner A, Lucenius J, Österberg M, Bismarck A (2017) Multilayer nanopaper based composites. Cellulose 24:1759–1773. https://doi.org/10.1007/s10570-017-1220-2

Mautner A, Mayer F, Hervy M et al (2018) Better together: synergy in nanocellulose blends. Philos Trans R Soc A Math Phys Eng Sci 376:20170043. https://doi.org/10.1098/rsta.2017.0043

Mautner A, Kobkeatthawin T, Mayer F et al (2019) Rapid water softening with TEMPO-oxidized/phosphorylated nanopapers. Nanomaterials 9:1–18. https://doi.org/10.3390/nano9020136

Mautner A, Nawawi WMFW, Lee KY, Bismarck A (2020) High porosity cellulose nanopapers as reinforcement in multi-layer epoxy laminates. Compos Part A Appl Sci Manuf 131:105779. https://doi.org/10.1016/j.compositesa.2020.105779

Moon RJ, Martini A, Nairn J et al (2011) Cellulose nanomaterials review: structure, properties and nanocomposites. Chem Soc Rev 40:3941. https://doi.org/10.1039/c0cs00108b

Nishino T, Takano K, Nakamae K (1995) Elastic modulus of the crystalline regions of cellulose polymorphs. J Polym Sci Part B Polym Phys 33:1647–1651. https://doi.org/10.1002/polb.1995.090331110

Nishiyama Y, Langan P, Chanzy H (2002) Crystal structure and hydrogen-bonding system in cellulose I_β from synchrotron X-ray and neutron fiber diffraction. J Am Chem Soc 124:9074–9082. https://doi.org/10.1021/ja0257319

Nishiyama Y, Sugiyama J, Chanzy H, Langan P (2003) Crystal structure and hydrogen bonding system in cellulose I α from synchrotron x-ray and neutron fiber diffraction. J Am Chem Soc 125:14300–14306. https://doi.org/10.1021/ja037055w

Sawada D, Nishiyama Y, Shah R et al (2022) Untangling the threads of cellulose mercerization. Nat Commun 13:1–6. https://doi.org/10.1038/s41467-022-33812-w

Sehaqui H, Zhou Q, Ikkala O, Berglund LA (2011) Strong and tough cellulose nanopaper with high specific surface area and porosity. Biomacromol 12:3638–3644. https://doi.org/10.1021/bm2008907

Walther A, Lossada F, Benselfelt T et al (2020) Best practice for reporting wet mechanical properties of nanocellulose-based materials. Biomacromol 21:2536–2540. https://doi.org/10.1021/acs.biomac.0c00330

Wang H, Li D, Yano H, Abe K (2014) Preparation of tough cellulose II nanofibers with high thermal stability from wood. Cellulose 21:1505–1515. https://doi.org/10.1007/s10570-014-0222-6

Wloch D, Herrera N, Lee KY (2023) Optically transparent laminated acrylic composites reinforced with mercerised bacterial cellulose nanopaper. Compos Part A Appl Sci Manuf 172:107583. https://doi.org/10.1016/j.compositesa.2023.107583

Xu X, Zhou J, Jiang L et al (2016) Highly transparent, low-haze, hybrid cellulose nanopaper as electrodes for flexible electronics. Nanoscale 8:12294–12306. https://doi.org/10.1039/c6nr02245f

Zhu H, Fang Z, Preston C et al (2014) Transparent paper: fabrications, properties, and device applications. Energy Environ Sci 7:269–287. https://doi.org/10.1039/C3EE43024C

Supplementary Information

Retain strength, gain ductility: tough and transparent nanopapers by mercerisation

SI Section 1: Workflow used for Riedveld refinement of wide angle PXRD diffractograms of un/mercerised nanopapers

Conditions and workflow

The Rietveld fitting was performed stepwise. Starting with scale and background fits, followed by specimen displacement. Afterwards, a rough estimation of FWHM was inserted manually. The amorphous phase FWHM was fixed to a resulting value for the crystallite size to be smaller than 25 Å. As next step cell refinement by updating FWHM was performed. At this point the preferred orientation was included in the refinement. Finally, all parameters were fitted together if possible.

Problems in the fit of 2θ regions above 30º made a correction in the background setup necessary. Sharp peaks in the 2θ range are not part of the Rietveld refinement and were inserted and refined manually to exclude intensities from the Rietveld refinement.

Remarks:
The refined cellulose cells deviate from the initial starting point. We cannot guarantee that the resulting cells are a correct representation of our cellulose. We found three phase models (cellulose Iβ, cellulose II and amorphous cellulose) based on input parameters that fit the diffractograms. The changing cellulose Iβ to cellulose II ratio ended in a realistic scenario.

Cellulose Iβ ends in two cell scenarios depending on concentration of the NaOH solution used and mercerization time. The Rietveld fitting of the diffractograms of the original, unmercerised cellulose, the cellulose mercerised for 2 min in 40 wt.% NaOH solution, and for 10 min in 40 wt.% NaOH solution resulted in a smaller cell size than that of all samples mercerised in 20 wt.% NaOH and the sample mercerised in 40 wt.% NaOH for 60 min.

Cellulose II seemed to be more stable.

Amorphous Cellulose was refined almost without any restrictions other than the one on crystallite size mentioned above.

Table SI 1-1 Overview of cell refinement results including weight fraction and preferred orientation as well as global parameters

Condition	No NaOH	20% NAOH				40% NaOH			Input cell for Rietveld
Sample	F10_control	F1_20_2	F4_20_10	F6_20_60	F8_20_1440	F11_40_2	F13_40_10	F15_40_60	
Cellulose parameters	cellulose Ib Rietveld Fit								
a [Å]	7.872873	11.53903	11.56523	11.56523	11.53903	7.964858	7.872873	11.67608	8.201
b [Å]	7.792356	7.598397	7.616997	7.616997	7.598397	8.021345	7.792356	7.89165	10.38
c [Å]	7.671636	7.62531	7.645278	7.645278	7.62531	7.797221	7.671636	7.642094	7.784
β [°]	94.99576	85.41122	84.97593	84.97593	85.41122	96.05142	94.99576	86.79299	96.55
Weight fraction [%]	69.12796	18.16103	13.71876	11.70025	9.80685	59.20098	41.47868	11.52418	
Preferred orientation direction [hkl]	1.00 0.00 0.00	1.00 1.00 1.00	1.00 1.00 1.00	1.00 0.00 0.00	1.00 1.00 1.00	1.00 0.00 0.00	1.00 0.00 0.00	1.00 1.00 1.00	
Preferred orientation parameter	0.772391	0.296992	0.308932	0.798418	0.311987	0.882983	0.85167	0.294707	
		cellulose II Rietveld Fit							
a [Å]		7.986681	8.149814	8.149814	7.973149	7.869589	8.004791	8.004791	9.03
b [Å]		8.729842	8.641862	8.641862	8.992444	9.528741	9.218024	9.218024	10.31
c [Å]		8.860025	8.901057	8.901057	8.910447	9.210245	8.975991	8.975991	8.1
β [°]		114.2333	113.9873	113.9873	114.1931	118.7433	114.8596	114.8596	117.1
Weight fraction [%]		51.11383	55.26769	58.92248	60.985	14.60041	26.72649	55.40606	
Preferred orientation direction [hkl]		1.00 0.00 0.00	1.00 0.00 0.00	1.00 0.00 0.00	1.00 0.00 0.00	1.00 0.00 4.00	1.00 0.00 4.00	1.00 0.00 0.00	
Preferred orientation parameter		0.96241	0.888756	1.8	0.757877	0.532111	0.714958	0.836064	
	amorph Rietveld Fit								
a [Å]	9.0532	9.743844	10.23104	10.81496	9.893483	9.173808	9.265846	9.177899	
b [Å]	9.02308	6.285435	6.200345	5.95343	5.412708	8.240123	8.594618	6.964471	
c [Å]	6.729575	9.752365	9.583224	9.866462	9.732595	10.32271	10.94233	9.831288	
β [°]	100.3395	113.5025	117.2071	120.0209	113.2344	117.2022	121.3919	114.9255	
Weight fraction [%]	30.87204	30.73514	31.01855	29.37724	29.20845	26.19061	31.70455	33.06976	
Preferred orientation direction [hkl]	1.00 0.00 0.00	1.00 0.00 0.00	1.00 0.00 0.00	1.00 0.00 0.00	1.00 0.00 0.00	1.00 0.00 0.00	1.00 0.00 0.00	1.00 0.00 0.00	
Preferred orientation parameter	1.067838	1.259303	1.780754	1.8	1.371089	1.239115	1.043326	1.002816	
Global parameters									
Number of used phases	2	3	3	3	3	3	3	3	
Profile function	Pseudo Voigt	Pseudo Voigt	Pseudo Voigt	Pseudo Voigt	Pseudo Voigt	Pseudo Voigt	Pseudo Voigt	Pseudo Voigt	
Instrumental FWHM Curve Type	Caglioti	Caglioti	Caglioti	Caglioti	Caglioti	Caglioti	Caglioti	Caglioti	
R (weighted profile) [%]	3.48264	5.95727	6.00992	7.1548	5.57435	5.68161	5.65503	3.11648	
GOF	1.44957	1.90637	2.13327	2.74883	1.85908	2.00621	1.84203	0.93257	

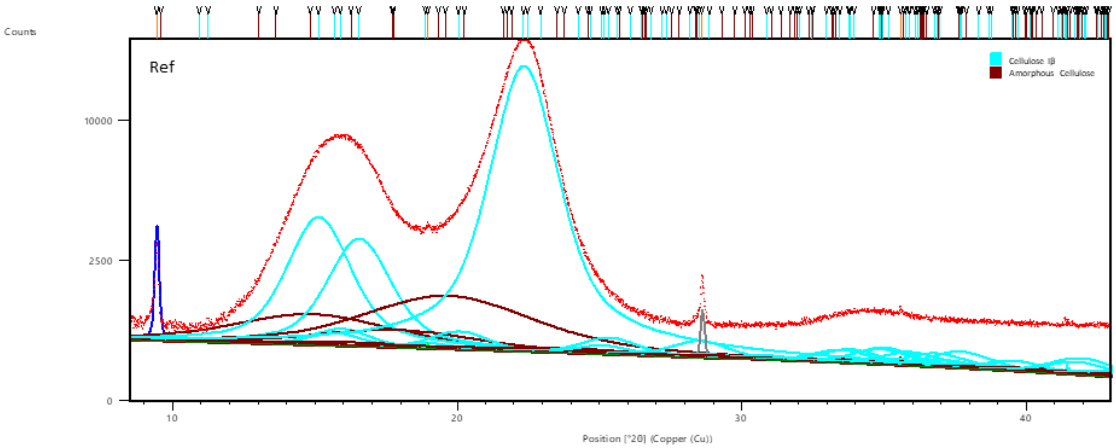

Fig. SI 1-1 Wide Angle PXRD Diffractogram of an unmercerised reference nanopaper

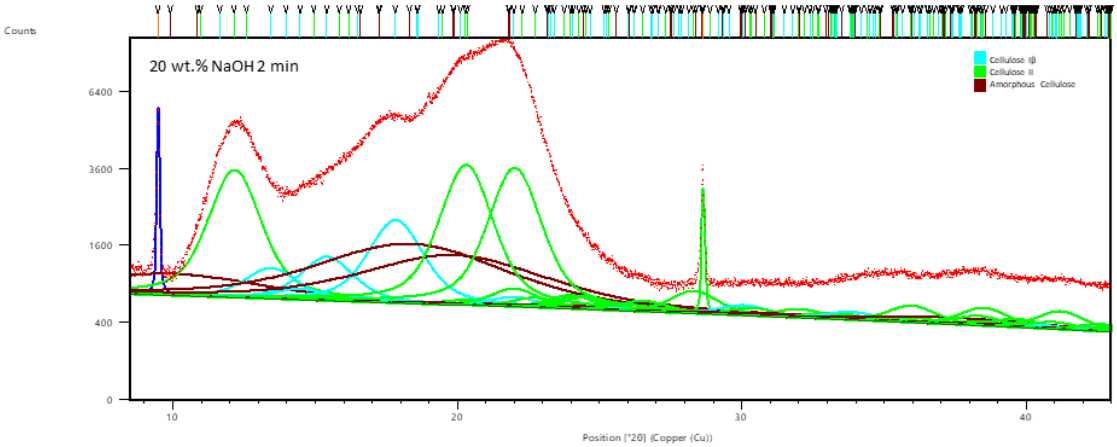

Fig. SI 1-2 Wide Angle PXRD Diffractogram of a nanopaper mercerised for 2 min in 20 wt.% NaOH solution

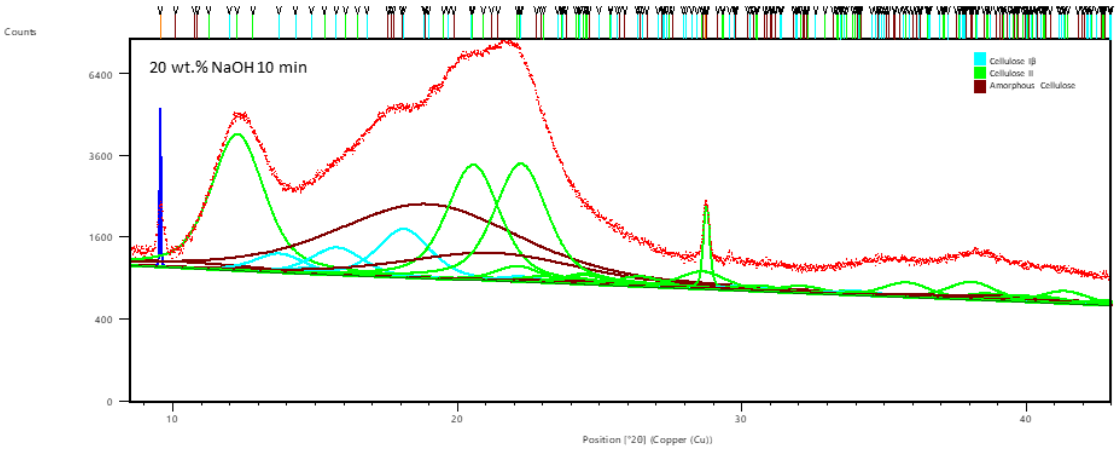

Fig. SI 1-3 Wide Angle PXRD Diffractogram of a nanopaper mercerised for 10 min in 20 wt.% NaOH solution

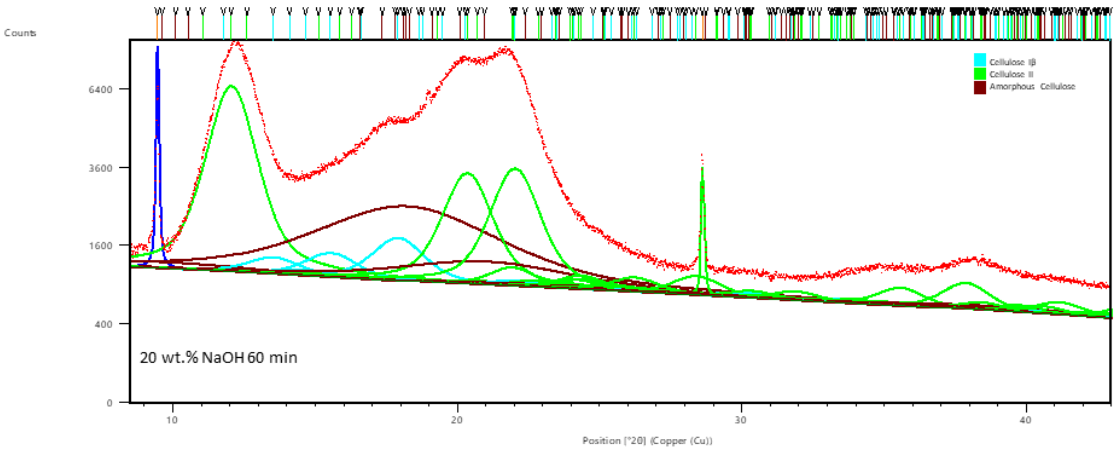

Fig. SI 1-4 Wide Angle PXRD Diffractogram of a nanopaper mercerised for 60 min in 20 wt.% NaOH solution

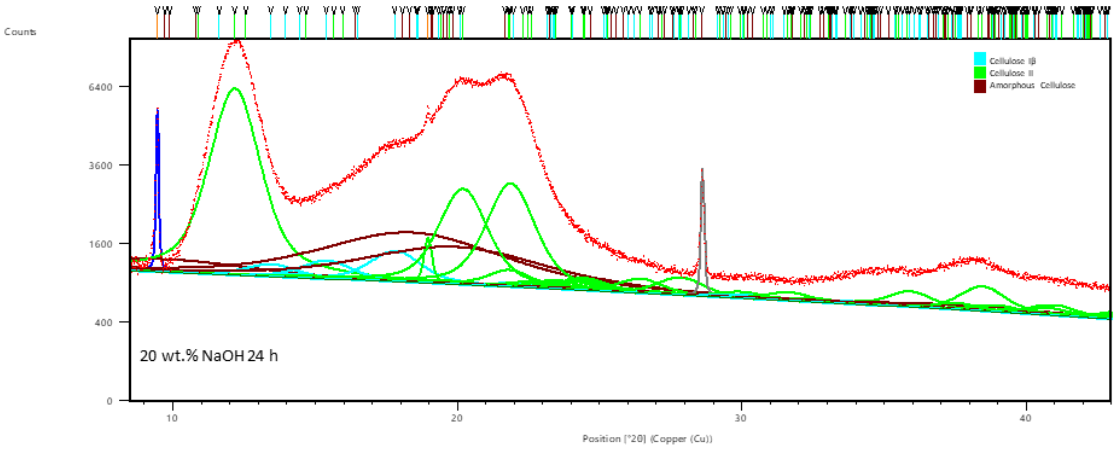

Fig. SI 1-5 Wide Angle PXRD Diffractogram of a nanopaper mercerised for 1440 min in 20 wt.% NaOH solution

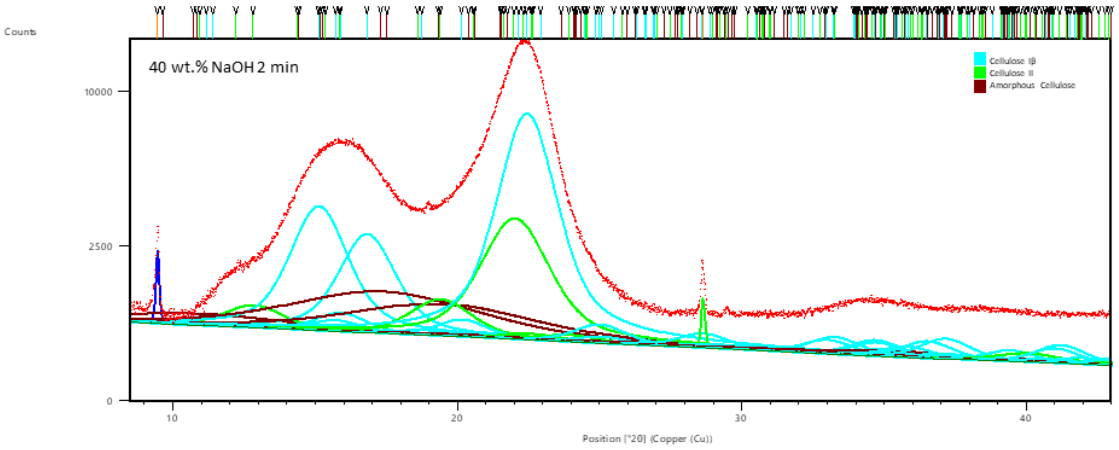

Fig. SI 1-6 Wide Angle PXRD Diffractogram of a nanopaper mercerised for 2 min in 40 wt.% NaOH solution

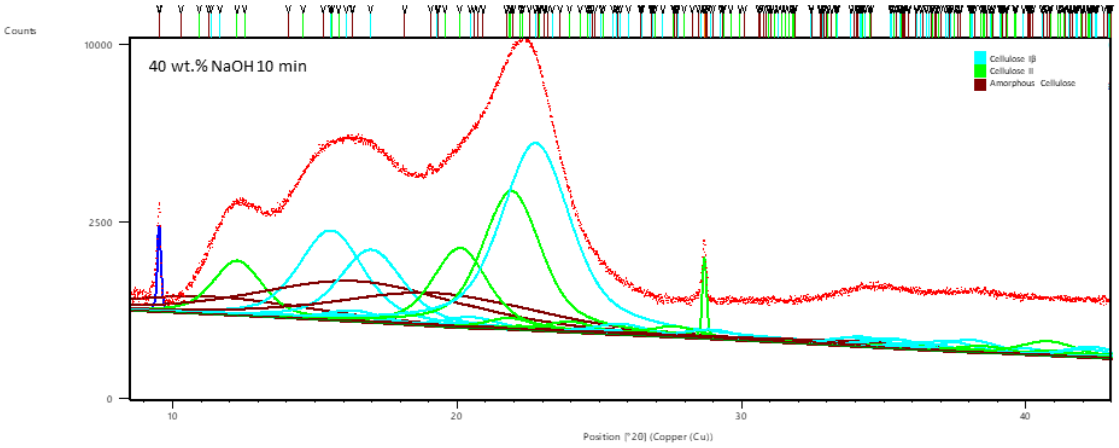

Fig. SI 1-7 Wide Angle PXRD Diffractogram of a nanopaper mercerised for 10 min in 40 wt.% NaOH solution

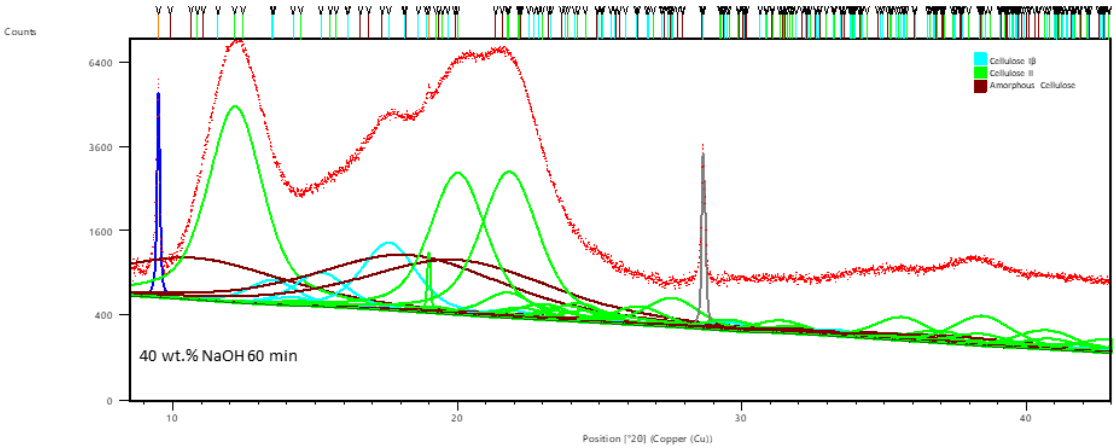

Fig. SI 1-8 Wide Angle PXRD Diffractogram of a nanopaper mercerised for 60 min in 40 wt.% NaOH solution

SI Section 2 Tensile specimen procurement pattern

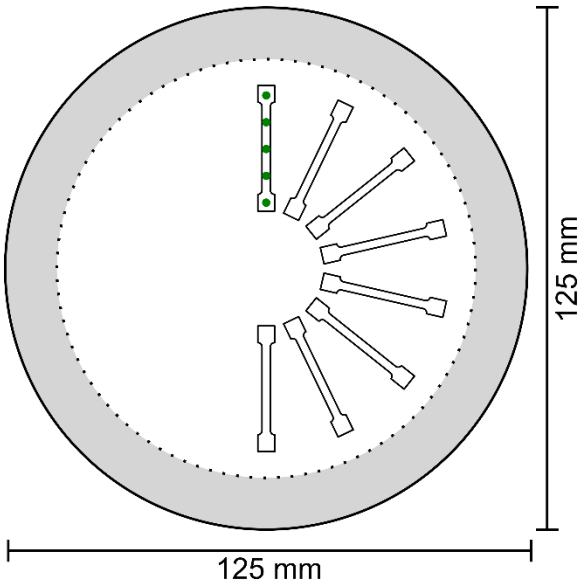

Fig. SI 2-1 Schematic distribution of the punching pattern for the tensile test specimen. The second half was used for XPS, XRD, SEM and optical images and the outer grey ring excluded as to not use sample parts that were covered by the PMMA frame.

SI Section 3. Morphological differences of nanopapers before and after mercerisation

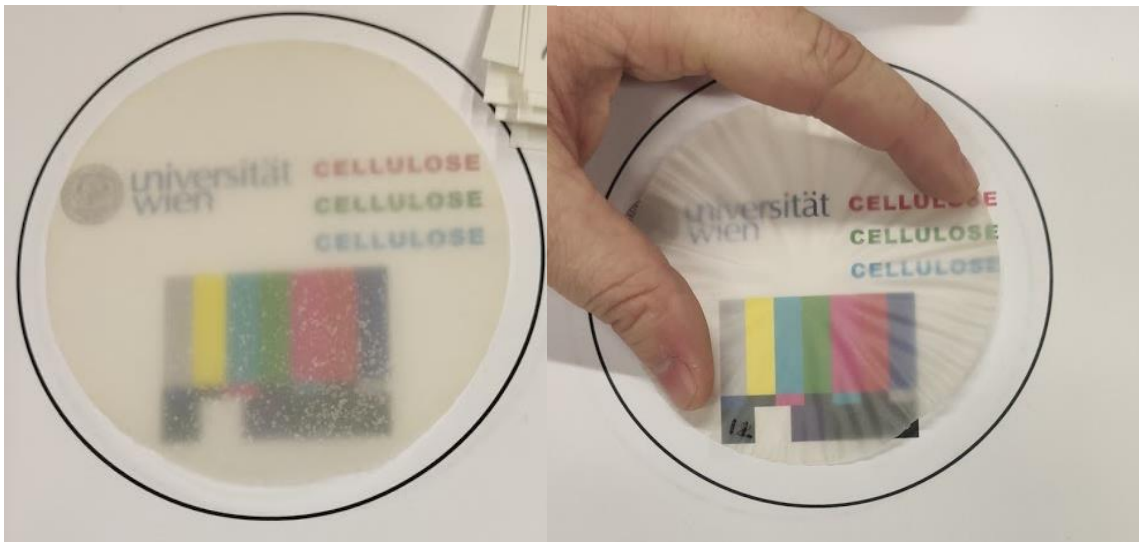

Fig. SI 3-1 comparison of a nanopaper before (left) and after (right) mercerisation in 40 wt.% NaOH solution without clamping for 1h exhibiting shrinkage and cockling.

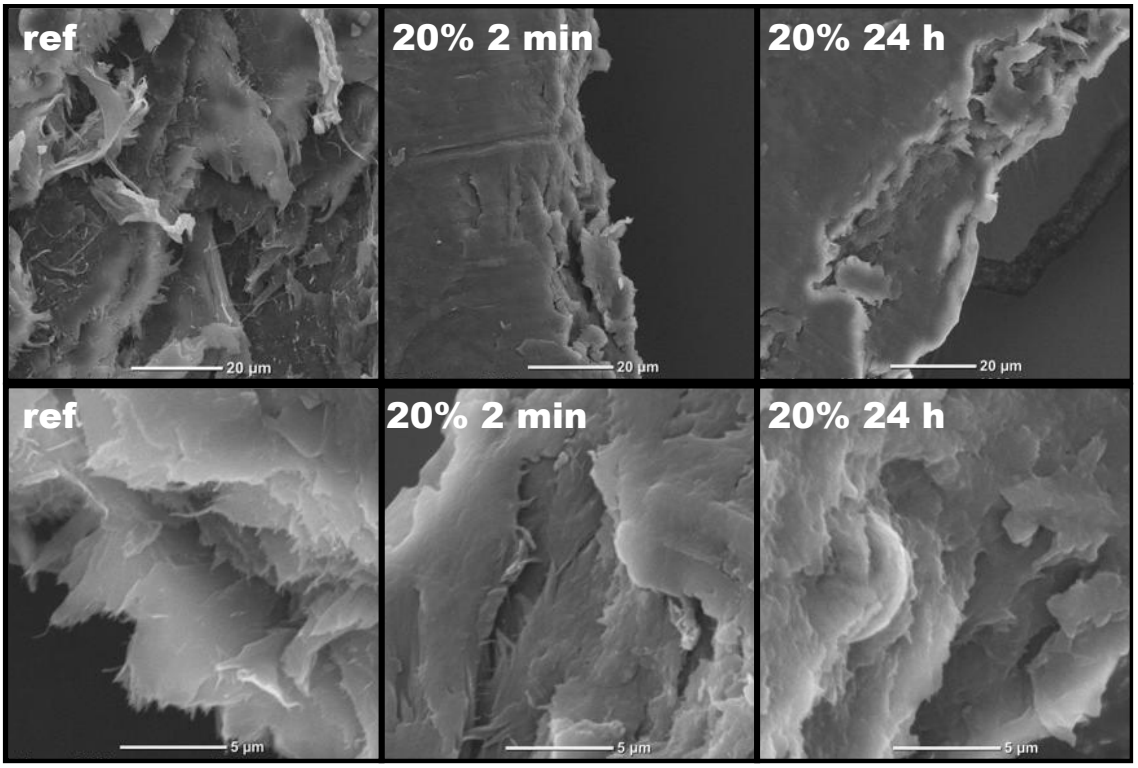

Fig. SI 3-2 Fracture surfaces of un/mercerized cellulose nanopapers

Table SI 3-1 Thickness, Density and porosity of nanopapers before and after mercerisation

Sample Name	Thickness			
	before mercerisation [µm]	after mercerisation [µm]	Δ	
			abs. [µm]	rel. [%]
20% 2min 1	52.0 ± 2.4	55.8 ± 2.4	3.8	7.3
20% 2min 2	59.2 ± 2.6	56.9 ± 3.1	-2.3	-3.9
20% 10min 1	59.3 ± 2.7	59.5 ± 4.0	0.2	0.3
20% 10min 2	52.6 ± 2.3	54.5 ± 2.8	1.9	3.6
20% 60min 1	53.9 ± 1.8	51.9 ± 1.5	-2.0	-3.7
20% 60min 2	54.9 ± 2.5	56.0 ± 2.6	1.1	2.0
20% 24h 1	53.0 ± 2.1	47.9 ± 1.6	-5.1	-9.5
20% 24h 2	53.6 ± 2.0	49.0 ± 2.0	-4.6	-8.6
40% 2min 1	52.6 ± 1.2	53.8 ± 4.1	1.2	2.3
40% 2min 2	53.9 ± 1.9	51.5 ± 2.1	-2.4	-4.4
40% 10min 1	55.3 ± 3.3	54.6 ± 5.1	-0.7	-1.3
40% 10min 2	53.5 ± 1.8	52.3 ± 2.0	-1.2	-2.2
40% 60min 1	53.7 ± 1.3	53.3 ± 1.6	-0.4	-0.7
40% 60min 2	57.9 ± 3.8	57.6 ± 3.0	-0.3	-0.5
20% 10min unrestrained	54.3 ± 2.6	65.5 ± 2.5	11.2	20.6
Ref	51.3 ± 2.3			

Sample Name	Density			
	before mercerisation [kg/m³]	after mercerisation [kg/m³]	Δ density	
			abs. [kg/m³]	rel. [%]
20% 2min 1	998 ± 45	1083 ± 33	85	9
20% 2min 2	959 ± 43	1073 ± 35	114	12
20% 10min 1	1018 ± 47	1110 ± 32	92	9
20% 10min 2	1010 ± 43	1091 ± 17	81	8
20% 60min 1	975 ± 32	1076 ± 27	101	10
20% 60min 2	974 ± 44	1101 ± 25	127	13
20% 24h 1	986 ± 40	1060 ± 22	73	7
20% 24h 2	1005 ± 38	1097 ± 19	91	9
40% 2min 1	1052 ± 24	1067 ± 36	14	1
40% 2min 2	1027 ± 37	1097 ± 20	69	7
40% 10min 1	998 ± 60	1062 ± 51	65	7
40% 10min 2	1065 ± 36	1120 ± 25	55	5
40% 60min 1	1053 ± 27	1105 ± 28	52	5
40% 60min 2	1010 ± 66	1127 ± 20	117	12
20% 10min unrestrained	1034 ± 50	1135 ± 28	101	10
Ref	998 ± 49.0			

Sample Name	Porosity					
	before mercerisation [%]		after mercerisation [%]		Δ	
					abs. [%]	rel. [%]
20% 2min 1	37.9	± 1.7	32.6	± 1.0	-5.3	-14.0
20% 2min 2	40.3	± 1.8	33.2	± 1.1	-7.1	-17.6
20% 10min 1	36.6	± 1.7	30.9	± 0.9	-5.7	-15.6
20% 10min 2	37.1	± 1.6	32.1	± 0.5	-5.0	-13.5
20% 60min 1	39.3	± 1.3	33.0	± 0.8	-6.3	-16.0
20% 60min 2	39.3	± 1.8	31.4	± 0.7	-7.9	-20.1
20% 24h 1	38.6	± 1.6	34.0	± 0.7	-4.6	-11.8
20% 24h 2	37.4	± 1.4	31.7	± 0.6	-5.7	-15.2
40% 2min 1	34.5	± 0.8	33.6	± 1.1	-0.9	-2.6
40% 2min 2	36.0	± 1.3	31.7	± 0.6	-4.3	-12.0
40% 10min 1	38.0	± 2.3	33.9	± 1.6	-4.1	-10.7
40% 10min 2	33.7	± 1.1	30.2	± 0.7	-3.4	-10.2
40% 60min 1	34.4	± 0.9	31.2	± 0.8	-3.2	-9.4
40% 60min 2	37.1	± 2.4	29.8	± 0.5	-7.3	-19.7
20% 10min unrestrained	35.6	± 1.7	29.3	± 0.7	-6.3	-17.7
Ref	36.5	± 1.3	NA		NA	NA

SI Section 4. XPS analysis and elemental composition of nanopapers before and after mercerisation.

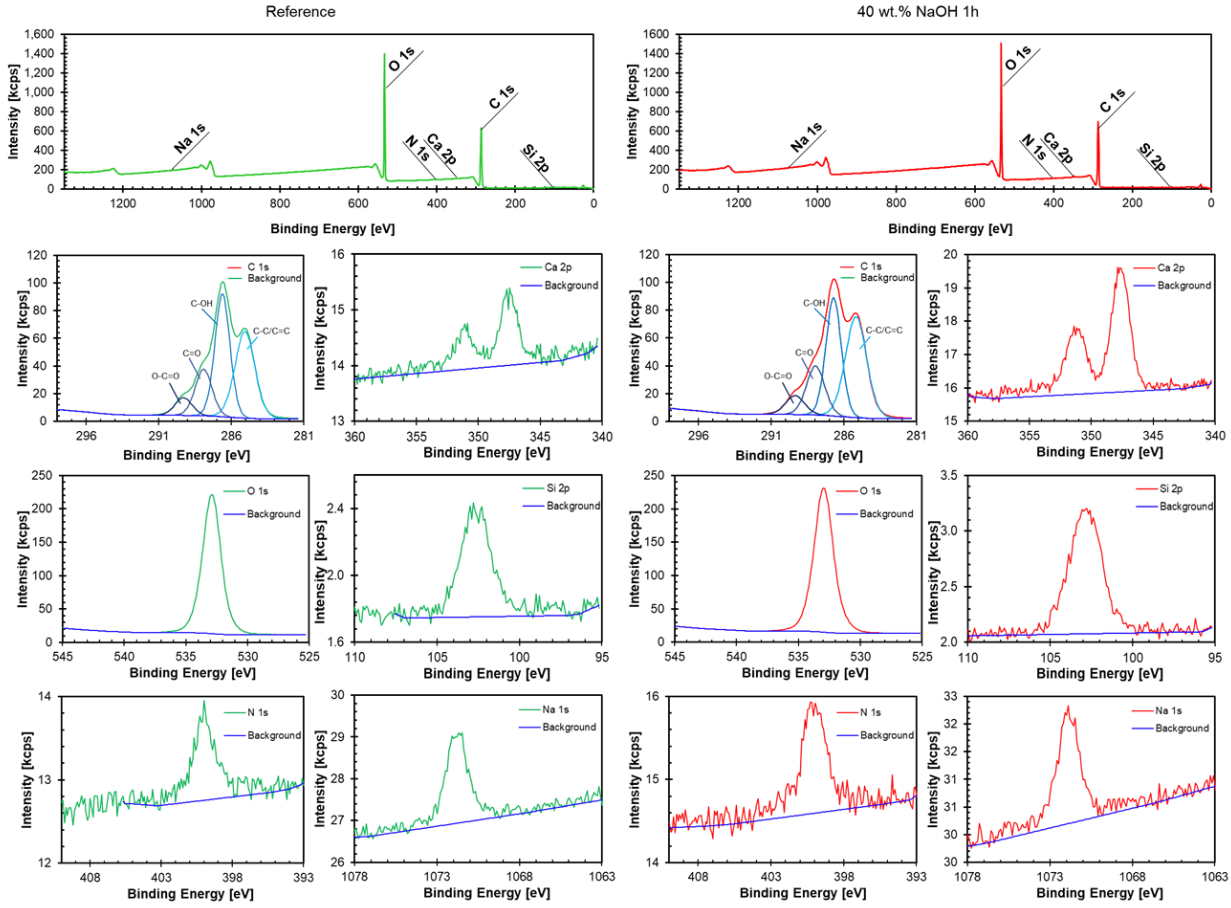

Fig. SI 4-1 XP survey Top) and element specific high-resolution XP spectra (below the respective Survey) after 1 min ablation with 1k atom Ar clusters with an energy of 6 keV to remove adventitious carbon. The elemental composition of original and nanopapers mercerised in 40 wt.% NaOH for 1 h shown in Figure SI 3-2 were determined from the peak areas of the high resolution spectra

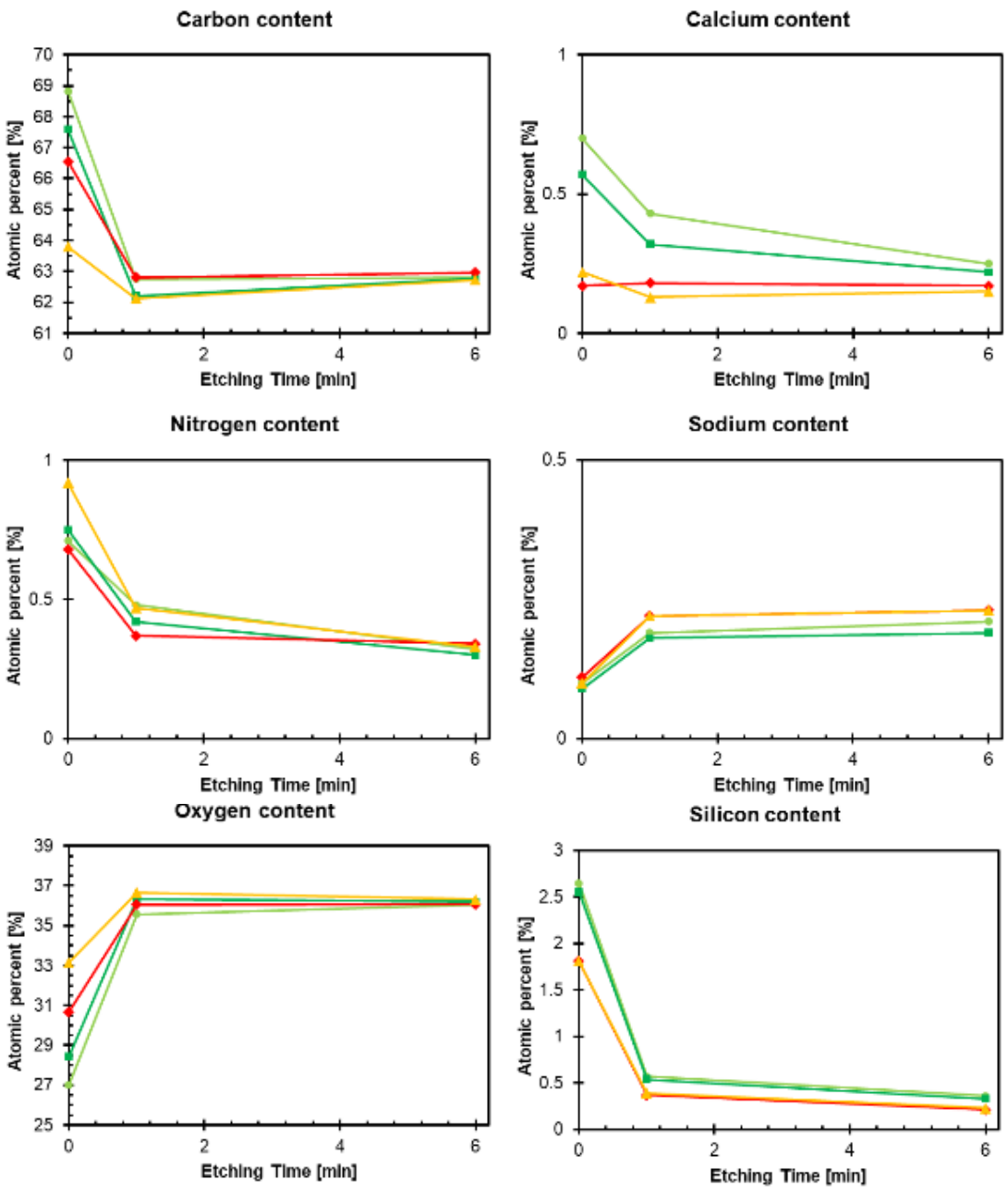

Fig. SI 4-2 Elemental composition of original and mercerised (40 wt.% NaOH for 1h) nanopapers. Two different spots with a diameter of 400 µm were analysed on original (red and orange) and mercerized samples (green colours), respectively

To exclude the possibility of the bulbs formed on the surface of the nanopapers after mercerisation being caused by the precipitation of inorganic salts stemming from (tap) water during the rinsing step. XPS spectra were recorded and the elemental compositions of all samples determined for the original surface as well as after 1 min and 6 min of etching,

respectively. Small amounts of silicon were found on all samples, which can be attributed to the grindstones used for nanocellulose preparation. Also, minor amounts of Ca and Na were found, but too little for the rather high number of bulbs being present. After etching, which removes adventitious carbon species from the surface of the samples, also the Si content had decreased indicating that Si was only present on the surface of the papers, but the elemental composition of samples before and after mercerisation was in essence identical.

SI Section 5. Molecular weight distribution of cellulose of nanopapers mercerised at different NaOH concentrations for various times.

All samples were activated prior to dissolution according to (Potthast et al. 2015, https://doi.org/10.1007/s10570-015-0586-2) by blending 20 mg of nanopaper sample in 800 ml of deionised water three times for 10 s, filtration in a Büchner funnel and subsequent solvent exchange for three times with 250 mL acetone followed by three exchange steps with 10 ml N,N-dimethyl acetamide (DMAc), before storing the still DMAc wet samples in 4 mL DMAc overnight. On the following day, the samples were again filtered and dissolved in 2 mL of a 9 % (wt./vol.) solution of LiCl/DMAc. Prior to injection into the gel permeation chromatograph, the samples were diluted with DMAc and filtered through a 0.45 µm syringe filter. Samples were analysed by GPC/MALS/RI according to (Röhrling et al. 2002, https://doi.org/10.1021/bm020029q).

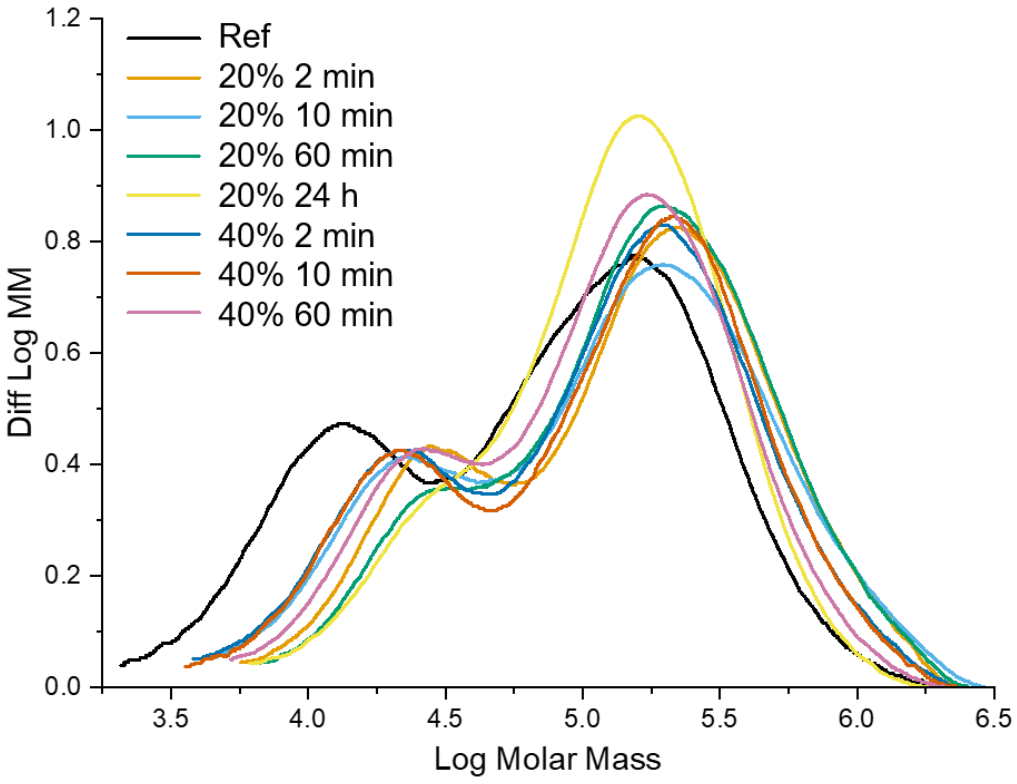

Fig. SI 5-1 Molecular mass distribution of cellulose from (mercerised) nanopapers

SI Section 6. Hypothesised mechanism of processes occurring during mercerisation.

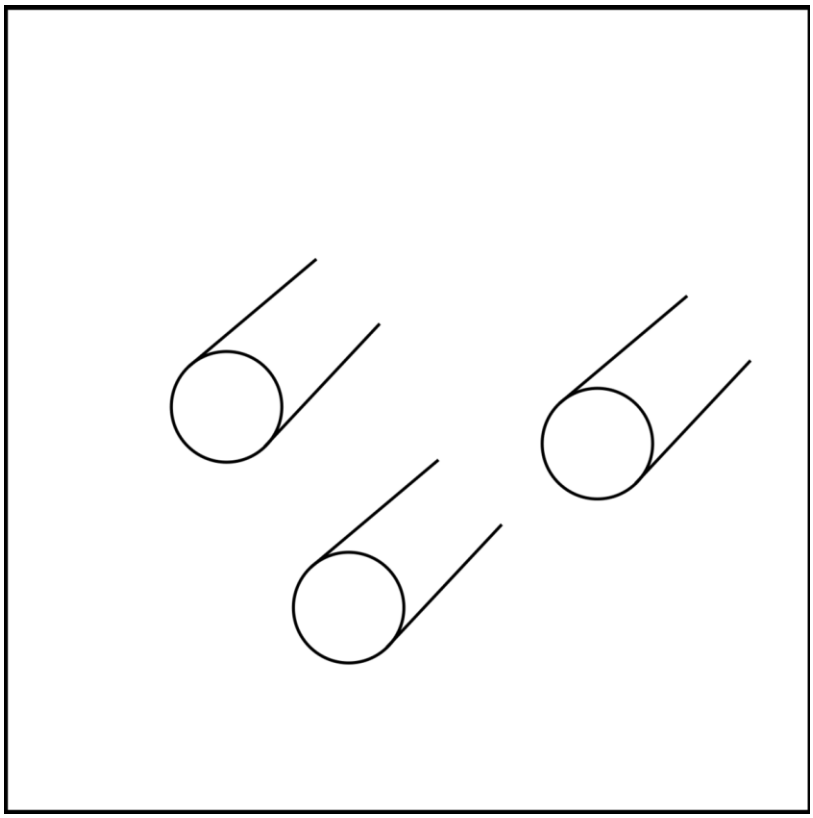

Fig. SI 6-1 Animation of the speculative mechanism of cellulose swelling in caustic soda solutions resulting in formation cellulose I in II core-shell structure and of bulb on the surfaces of mercerised cellulose nanopapers

Publication II

Mayer, F., Sampson, W. W., Wloch, D., Mautner, A., & Bismarck, A. (in Submission as of July 2025) Towards the Efficient Preparation of Tough Cellulose Nanopapers.

Towards the Efficient Preparation of Tough Cellulose Nanopapers

Florian Mayer[a,b], William W. Sampson[c], Daniela Wloch[d], Andreas Mautner[a,e,¤], Alexander Bismarck[a,f,g,*]

[a] Institute of Materials Chemistry and Research, Faculty of Chemistry, University of Vienna, Währinger Straße 42, 1090, Vienna, Austria.

[b] Department of Bioproducts and Biosystems, Aalto University, Vuorimiehentie 1, 02150 Espoo, Finland

[c] Department of Materials, University of Manchester, Manchester, M13 9PL, UK

[d] Department of Aeronautics, Imperial College London, South Kensington Campus, London SW7 2AZ, United Kingdom

[e] Institute of Environmental Biotechnology, IFA-Tulln, University of Natural Resources and Life Sciences, Vienna, Konrad-Lorenz-Straße 20, 3430, Tulln an der Donau, Austria

[f] Division of Materials Science, Department of Engineering Sciences and Mathematics, Luleå University of Technology, Luleå, 971 87, Sweden

[g] Department of Chemical Engineering, Imperial College London, South Kensington Campus, London SW7 2AZ, United Kingdom

[¤] e-mail: andreas.mautner@boku.ac.at

[*] e-mail: alexander.bismarck@univie.ac.at

Keywords
Nanocellulose; Nanopaper preparation; Toughness

ABSTRACT

Cellulose nanopapers (CNPs) are attractive materials with outstanding mechanical and optical properties, yet their production is slow. The use of non-aqueous suspension media, in particular ethanol, for nanopaper production reduced filtration times by 73%. Nanopapers prepared from ethanolic suspensions possessed higher porosities than those prepared from aqueous suspensions, reducing their transparency and tensile properties. Rewetting nanopapers prepared from ethanolic suspensions with water and subsequent drying yielded nanopapers with densities essentially the same as those prepared from aqueous

suspensions, which in turn greatly increased mechanical properties and transparency. The strain to failure of rewetted and dried nanopapers prepared from ethanolic suspensions increased from 2.8% to 7.5%. The strain to failure of rewetted and dried nanopapers prepared from ethanolic suspensions was also greater than that of nanopapers prepared from aqueous suspensions (3.3%) albeit at the expense of a 20% decrease in tensile strength and modulus, which was shown to be attributable to a lower bonding contribution between fibrils in the network. The increased strain to failure results in significantly increased work of fracture. The rewetting and drying treatment also yielded nanopapers with high total luminous transmittance and haze.

1. INTRODUCTION

Cellulose, and in particular nanocellulose, is among the most promising research topics in the quest for sustainable, renewable, and green engineering materials with attractive mechanical and barrier properties. Cellulose is naturally produced by green plants, bacteria and even some animals. [1] Cellulose fibres are a structural component of plants and can be either mechanically or chemically defibrillated to yield cellulose nanofibrils (CNFs). [2-5] The widths of CNFs usually range from 5-60 nm whereas their length can be up to 6 μm,[6] thus constituting a nanomaterial with a high aspect ratio and exceptional physical and mechanical properties.[1, 7] Films and membranes prepared from CNF are often termed cellulose nanopapers (CNP) and have been widely investigated showing favourable physical and chemical properties such as good chemical stability, low thermal expansion, tuneable optical properties, and high tensile strength and modulus.[8-10] The possibility to utilise the abundant surface hydroxyl groups of CNF for a variety of chemical modifications such as click-type reactions or the introduction of charged moieties[5, 11, 12] and hence tune the properties of the resulting CNPs, has made them promising candidates for a variety of applications, e.g. separators in, e.g. supercapacitors and fuel cells. [13-15] Owing to their excellent oxygen barrier performance and tuneable

optical properties CNPs have been explored as alternative packaging materials.[16-18]

The three main CNP manufacturing routes currently discussed in literature are casting, coating and filtration[19, 20]: casting nanocellulose suspensions and evaporating the suspension medium as reported for cellulose nanocrystals by Revol et al.[21] was adapted by Dufresne et al.[22] for CNFs. This was the first method used to produce CNPs and is still widely utilised at laboratory scale to tune the properties and microstructure of the resulting CNPs by controlling the evaporation parameters and addition of solutes[23]. The coating method usually involves the permanent deposition of a CNF suspension on a porous carrier material to create a hybrid material with CNP[23] with the drawback, that usually no freestanding CNPs are obtained. Filtration followed by hot pressing allows production of CNPs in analogy to traditional papermaking techniques relatively easily The main obstacles for the efficient preparation of CNPs however can be found both in the high viscosity of concentrated CNF suspensions and the high water-retention of CNFs, as these facilitate a need to use highly dilute suspensions as feedstock, which require substantial amounts of time and energy to dewater by both filtration or evaporation alike.[20, 24-28] The dewatering time of CNPs also increases dramatically with increasing paper grammage and density, further affecting productivity[29] when producing denser or thicker CNPs. Indeed, industrial processes for the high-volume manufacture of tracing paper utilise hot process water to reduce its viscosity and hence increase drainage speed. The dewatering of nanocellulose suspensions is an intensely studied topic and a wide variety of methods have been reported ranging from the use of electro-assisted filtration, surface modification or the addition of salts, to supercritical CO_2 drying; the reader is referred to several extensive reviews on the topic.[26, 30] One pathway to reduce the dewatering time of CNF suspensions which is not as widely reported, is to replace water with other liquids that interact less with the cellulose fibres or have higher vapour pressures,

thus requiring less energy to remove. Although Henriksson et al.[8] and others[31, 32] have used solvent exchange to facilitate efficient drying of filter cakes, these approaches still formed filter cakes from aqueous suspensions. Onyianta et al.[33] used several solvent exchange and conditioning steps with isopropyl alcohol (IPA) to produce redispersible CNF powders and found that filtration times dropped significantly with increasing IPA content. Most studies reporting on the use of non-aqueous suspension media during CNP preparation, do not document the impacts on the filtration speed but found that the use of lower surface tension solvents influences other properties of the resulting nanopapers, such as porosity, transparency, and haze. [31, 34-37] Ferguson et al.[35] reported a correlation between the surface tension of the CNF suspension medium and the resulting CNP porosity, with lower surface tension solvents yielding more porous CNPs. Huang et al.[31] used solvent exchange to ethanol and hexane after filtration of TEMPO oxidised CNF filter cakes and observed that lower surface tension yielded CNPs with significantly increased pore volumes and larger interlayer pore spaces. Hsieh et al.[36] reported, that using ethanol as suspension medium during manufacture yielded CNPs with high transparency and haze. Importantly, as might be expected, the use of organic solvents as suspension medium for CNP preparation reduces the mechanical properties of the CNPs significantly.[37] A reduction in density inherently reduces the extent of inter-fibre contact and, thus the tensile strength of the resulting papers. In a classic and seminal contribution, Campbell[38] postulated that the use of suspension media with different surface tensions could also affect the intrinsic properties of produced papers (and by extension, nanopapers): during removal of the liquid content during drying, capillary forces, which are proportional to the surface tension of the suspension medium, act in interfibril spaces and pull the fibres together. These ‘Campbell forces’ aid compaction of the resulting fibre network resulting in increased density and hence an increased fibre-fibre bonding area, which, alongside the zero span tensile index directly

contributes to the tensile index as elaborated in the theory of Page, [39] which may be stated as:

$$\frac{1}{T} = \frac{9}{8\,Z} + \frac{12\,\delta}{b\,P\,L\,\Phi} \quad (1)$$

where T [kN m kg^{-1}] is the specific strength or 'tensile index' of a (nano)paper, Z [kN m kg^{-1}] the zero span tensile index, δ [kg m^{-1}] the linear density of nanofibrils with perimeter P [m] and mean length L [m]; Φ represents the relative bonded area and b [N m^{-2}] the shear bond strength per unit area.

The tensile strength of (nano)papers is influenced also by hornification between fibrils during water removal at elevated temperatures, first described by Jayme[40] as "Verhornung" and further elucidated by Minor,[41] who coined the term "hornification". The absence of water during hot pressing when using non-aqueous suspension media directly influences the hydrogen bond structure of the formed cellulose network, resulting in a less "crosslinked" CNF network.[42]

The development of strong and tough CNPs has been of great interest in the scientific community, with studies outlining various approaces to achieve this goal. The addition ionic liquids to the suspension medium has recently been reported by Chen et al.[43] who disclosed that the addition of 30 wt.-% of 1-ethyl-3-methylimidazolium acetate to the suspension medium yielded CNPs with exceptionally high tensile strength (up to 233 MPa) and modulus of toughness (up to 38 MJ m^{-3}), as well as Liu et al.[44] who reported the addition of up to 2 wt.-% of various imidazolium based ionic liquids to the suspension medium more than doubled the tensile strength and tensile toughness of produced CNPs. Another promising strategy to increase the ductility and toughness of CNPs is to partially transform the stiff and brittle cellulose I crystal allomorph to the more ductile cellulose II allomorph, either by way of partially dissolving the cellulose fibril[45, 46] or strong alkaline treatment called mercerization[47, 48]. While these methods yield

CNPs with excellent mechanical properties, they also suffer from the aforementioned drawbacks of CNP production in the form of long dewatering and/or drying times, as well as the consumption of expensive and potentially harmful chemicals. Sethi et al.[49] reported the use of a hybridization approach combining CNF with non-delignified wood nanofibres to increase the hydrophobicity of the resulting CNPs as well as the nascent filtercake, leading to a significantly increased (75 %) filtration speed and increased water resistance of the resulting CNPs albeit at the cost of tensile properties and yellowing/browning depending on the CNF to wood nanofibre ratio.

In this study, we investigate the potential of using ethanol, a non-aqueous suspension medium that can be considered green and easily accessible, for the efficient and fast production of cellulose nanopapers via filtration. After filtration we conducted a systematic investigation of a family of post-forming treatments using rewetting by water and drying to consolidate the resulting nanopapers and investigate the influence on their physical and mechanical properties. The objective of these post-treatments was to exploit Campbell's forces to consolidate and hence densify the intrinsically porous nanopapers filtered from non-aqueous solvents, with a view to increasing their strength and transparency; to the best of our knowledge, this has not been explored previously. This approach could offer a route to exploit the faster filtration times offered by forming from non-aqueous solvents, whilst optising network properties.

2. EXPERIMENTAL

2.1. Materials

Cellulose nanofibres (CNF) were produced by mechanical defibrillation (Granomat JP 150, Fuchs, Switzerland) of never dried, chlorine-free bleached softwood pulp (*picea abies and pinus spp.*) with a composition of 81.3 % cellulose, 12.6 %

hemicellulose and 0.3 % ash,[50] provided by Mercer Stendal (Arneburg, Germany) according to a grinding procedure described in a previous publications.[47] The resulting nanofibrils had an average molecular weight M_w of 141.4 kDa, and a crystallinity of ~70 %.[47] Ethanol (93.8 wt.-%) denatured with 1 vol.-% of petroleum ether was purchased from Brenntag Austria. If not stated otherwise, deionised water was used in all experiments.

2.2. Nanopaper preparation

An overview of the processing parameters and all post processing steps of the nanopapers produced in the subsequent sections is provided in Table 1. For clarity, a schematic overview over the order of manufacturing steps is also provided as Figure SI 1-1 in section SI 1 of the ESI.

Table 1: Sample codes, preparation parameters and eventual Post treatment steps of nanopapers prepared in this study.

Sample	Preparation Parameters		Notes	Post treatment
	Suspension Medium	CNF dry mass [g]		
H_2O-CNP	1000 mL Water	1.2	-	-
Et-CNP-Ref	1000 mL 85 wt.-% EtOH	1.2	-	-
reEt-CNP-35	1000 mL 85 wt.-% EtOH	1.2	-	Rewetting and drying at 35 °C
reEt-CNP-70	1000 mL 85 wt.-% EtOH	1.2	-	Rewetting and drying at 70 °C
reEt-CNP-110	1000 mL 85 wt.-% EtOH	1.2	-	Rewetting and drying at 110 °C
Et-CNP-d	1000 mL 85 wt.-% EtOH	1.2	Dipped in H_2O prior pressing	-

Nanopapers with a nominal areal density of 100 g m-2 were prepared following a previously reported method,[47] which was slightly modified by using ethanol as the suspension medium. In brief, nanocellulose stock (1.2 g dry mass at a dry matter content of 3.37 wt.-%) was combined with 270 g ethanol (93.8 wt.-%) to reach an ethanol concentration of 85 wt.-%. This suspension was then further diluted with 85 wt.-% ethanol to adjust the volume to exactly 1000 mL (to allow for comparison

of the filtration times later on) followed by homogenization via blending (BL-4473, Tristar) at 2000 W for 30 s. The ethanol/CNF suspension was subsequently transferred to a Buchner funnel with a 125 mm diameter fritted glass disk, lined with filter paper (VWR 413, VWR, Leuven, Belgium) and filtered at reduced pressure produced by a water jet pump until a solid filter cake with a matte surface had formed and the flow of suspension medium exiting the Büchner funnel had slowed to one drop per 15 seconds, which – according to previous experience – yielded filter cakes with a cellulose content of 70 – 90 %. The resultant dense, yet wet, filter cake was removed from the filter paper, sandwiched between two metal plates, each lined with two layers of blotting paper (3MM Chr VWR, Lutterworth, UK), and pressed at room temperature (23 °C) using a hydraulic press (type 25–12-2H, Carver Inc., Wabash, USA) at 1.6 MPa for 30 s to increase its solids content. The cold-pressed filter cake was then placed between two metal plates lined with one layer of blotting paper as cushioning and one layer of release paper and hot pressed in the hydraulic press at 1.6 MPa at 120 °C for 15 min to dry and consolidate the network. Of the nine nanopapers filtered from ethanolic suspensions, three were used as reference and thus termed 'Et-CNP-ref', while the rest was used for the production of re-compacted CNPs as described further down.

Another set of nanopapers was prepared as described above from suspensions of CNF in 85 wt.-% ethanol, but the ethanol-wet filter cake was submerged for 5 s in 1 L of deionised water prior to cold pressing – to simulate a short dipping bath in a continuous line process, and to prevent disintegration of the unconsolidated filter cake into the water – followed by hot pressing as described above. These water-dipped Et-CNPs were termed 'Et-CNP-d'.

Reference nanopapers filtered from water were prepared following the same procedure but using water as a suspension medium (1.23 g of CNF dry mass in 1000 mL H_2O), but. These samples are termed, 'H_2O-CNP'.

2.3. Re-compaction of Et-CNPs

To further consolidate cellulose nanopapers produced from ethanolic suspensions they were first submersed in water for 5 min, to allow the nanopaper to fully hydrate but not yet start to disintegrate and subsequently sandwiched between two sheets of blotting paper for 30 s to remove excess water. The still water-wet CNPs were then sandwiched between steel plates, each lined with a sheet of blotting paper and release paper and put under 5 kg-force to prevent cockling during drying. Drying of the wet CNPs was performed at 35 °C, 70 °C, and 110 °C for 30 h, 20 h, and 2 h, respectively, to ensure the nanopapers had fully dried. Consolidated CNPs were termed 'reEt-CNP-X' indicating that they were rewetted and with X denoting the drying temperature. All consolidation experiments were carried out in duplicate.

2.4. Moisture content of nanopapers

The moisture content of prepared nanopapers was determined via dynamic vapour sorption (DVS Resolution, Surface Measurement Systems, Wembley, UK). Approximately 20 mg of nanopaper sample were conditioned in the same room as the subsequent mechanical testing was performed (25 °C, 40-45 % RH) for 1 week, before entering the system and being dried with water-free air for 15h until no change in weight was detected. The moisture content was calculated from the mass loss during drying.

2.5. Thickness, density, and porosity of nanopapers

Thickness d and apparent density ρ_e of all CNPs were determined from the specimen cut for tensile testing. From each paper, eight dumbbell-shaped specimens were punched out (Zwick ZCP 020 Manual Cutting Press, Zwick, Ulm, Germany) in a radial pattern evenly distributed across half of each paper to ensure a homogeneous sample composition without bias and to conserve the second half for other tests. The dumbbell-shape (EN ISO 527-2, Type 1BB) had an overall

length of 30 mm with a 20 mm long and 2 mm wide parallel section and an overall area A of 85.8 mm^2. The thickness d was measured at five points evenly distributed along the specimens' length using a digital micrometer (705-12229, RS Components, Corby, UK) with a clamping pressure of 150 kPa as the specimens' width was below that required for testing with a conventional paper thickness meter.

Each specimen's mass m was determined using a microbalance (MSA 225P, Sartorius, Göttingen, Germany) and used to calculate the average paper grammage Γ (eq. 2), apparent density ρ_e (eq. 3), and hence to estimate porosity ϕ (eq. 4) from A and d of the specimens by approximating the skeletal density ρ_s of cellulose I to be 1500 kg m^{-3}.[51]

$$\Gamma = \frac{m}{A} \tag{2}$$

$$\rho_e = \frac{\Gamma}{d} \tag{3}$$

$$\phi = \left(1 - \frac{\rho_e}{\rho_s}\right) \times 100\ \% \tag{4}$$

2.6. Surface morphology of (consolidated) CNPs

The surface morphology of the produced CNPs was characterised by scanning electron microscopy (SEM) (Supra55VP, Zeiss, Austria) operated at an acceleration voltage of 5 kV and a working distance of 7.4 mm. All specimens were mounted onto aluminium sample holders with carbon tape and coated with an 8 nm layer of 80% Au and 20% Pt (Leica SCD 2020/EM QSG 100).

2.7. Determining the optical properties of nanopapers

Total luminous transmittance and haze of CNPs were determined using a UV-Vis spectrophotometer (Lambda 356, PerkinElmer LAS Ltd., UK) fitted with a 50 mm integrating sphere in the range of 400 to 700 nm at a scan speed of 240 nm min^{-1} and a slit width of 5 nm.

2.8. Determination of tensile properties of nanopapers

Tensile tests were performed on a minimum of ten specimens for each nanopaper sample at 25 °C and 40-45% RH using a dual column universal test frame (Instron Model 5969, Darmstadt, Germany) equipped with a 1 kN load cell, specifically calibrated for low loads. The tensile strain ε was recorded using an optical non-contact video extensometer (Gig ProE, iMETRUM, Bristol, UK). The gauge length of the test specimen was set at 15 mm, and a crosshead displacement velocity of 1 mm min^{-1} was used. The tensile strength σ was calculated from the measured load, the width and thickness of the specimen. The paper tensile index (*cf.* specific strength) T was calculated from the load per unit width and the grammage Γ of the specimen and the (grammage corrected) specific modulus M was determined from the linear elastic region of the T vs. ε curves as a secant between strength values separated by a strain of 0.2%. The modulus of toughness K_f, a measure for the tensile toughness of a material – i.e. the energy a material absorbs during elastic and plastic deformation[52] – was determined by integration of the area under the stress-strain curve using the dimensionless strain (eq. 5):

$$K_f = \int_0^{\varepsilon_f} \sigma \mathrm{d}\varepsilon \qquad (5)$$

For comparison we would like to point out, that K_f is in the literature often referred to as work of fracture.[8, 43, 47, 51, 53] However, per definition, the work of fracture is energy per unit area (J m^{-2}) while K_f is energy per unit volume (Pa or J m^{-3}), which is the quantity termed work of fracture reported in those papers. The modulus of toughness is the work of fracture normalised over the gauge length.

3. Results and Discussion

3.1. Influence of the ethanol content in the suspension medium on the CNP porosity

The results of a preliminary study on the impact of ethanol content in the suspension medium can be found in section SI 2. of the ESI. The results (Figure SI

2-1), while qualitative in nature, revealed the importance of the surface tension of the suspension medium, affecting the strength of the capillary/Campbell forces acting on the fibril network during drying pulling neighbouring fibrils closer together, improving interfibrillar contact. Above a certain ethanol content in the suspension medium (60 wt.-% to 80 wt.-%) network densification does no longer occur, yielding CNPs with a significantly increased porosity. The dependency on the surface tension of the liquid in the wet filter cake during drying inspired the rewetting and redrying procedure used for the re-consolidation of CNPs described in this study.

Based on the preliminary results (section SI 2 in the ESI), we selected 85 wt.-% ethanol in water mixtures as suspension medium for CNP production, as it represented an ethanol content sufficiently above the observed threshold for high porosity CNPs (Figure SI 2-1) while facilitating the reuse of the suspension medium by adding only small amounts of 93 wt.-% ethanol to offset the water introduced by the CNF stock.

3.2. Filtration times during nanopaper preparation

We compared the filtration times of CNPs prepared from 85 wt.-% ethanol-water suspensions with those of CNPs prepared from pure water suspensions. As baseline, we determined the filtration times of pure water and 85 wt.-% ethanol in water using the same Büchner funnel; within error we observed no difference in the 'filtration' speed for both media (Table SI 3-1 section SI 3 of the ESI). However, once nanocellulose was suspended in either water or 85 wt.-% ethanol, we observed a reduction in average filtration time from 71 ± 3 min to 19 ± 1 min, which can be attributed to a variety of factors simultaneously which all affect the flow of the solvent through the nascent filter cake: the pressure drop acting across the filter cake is the sum of the hydraulic pressure of the suspension medium acting from above and the applied vacuum from below, which was constant over all experiments. However, the hydrostatic pressure ($P = \Delta p + \rho \cdot g \cdot h$) acting from

above on the filter cake for water is 20 % greater than for the water-ethanol mixture resulting in a faster compaction of the filter cake in the aqueous suspension resulting in the formation of the initial layers, with high filtration resistance, similar to the findings of Mattsson et al. [54] at neutral pH and when using a cellulose based filtration membrane. Furthermore, the lower dipole of ethanol compared to water, 1.69 D and 1.86 D, respectively,[55] would result in a significantly reduced interaction between the liquid and the hydroxyl groups on the CNFs surface, thus further reducing the filtration resistance and would further reduce the thickness of the hydration shell around the individual cellulose fibrils, thus virtually increasing the porosity of the nascent filter cake. The higher porosity of the ethanolic filter cake leads to a further reduction of the resistance to flow, as described for granular beds by the Kozeny-Carman equation.[56] Another factor contributing to the reduced filtration times could be the reduced polarity of the ethanolic suspension medium, reducing the interaction between the fibril surface and the liquid, in analogy to literature utilising different ionic solutions to improve the filtration procedures of (carboxylated) CNFs.[57-59] These results also suggest that the higher viscosity of ethanol-water mixtures compared to pure water – 1.7 mPa s for 85 wt.-% ethanol/water mixture compared with 1.0 mPa s for pure water[60] – are compensated and even outweighed by the reduced filtration resistance of the forming, more porous filter cake.

3.3. Influence of re-consolidation on the physical properties of CNPs

We investigated the impact of paper re-consolidation after forming from ethanolic suspensions as well as dipping of the ethanol wet filter cake in water prior to hot pressing (reEt-CNP-35, 70 & 110 as well as Et-CNP-d, respectively) on the physical properties, such as thickness and density of these CNPs and compared them to those of reference CNPs produced from aqueous suspensions (H_2O-CNP), and from ethanolic suspensions without post treatment (Et-CNP-ref) (Table 2).

Table 2: Grammage Γ, thickness d, density ρ, and porosity ϕ with standard deviation of the different types of CNPs. Note: the grammage was determined by weighing at ambient conditions, thus including sorbed moisture (~4.5-5.9 %)

Sample	Γ [g m^{-2}]	d [µm]	ρ [kg m^{-3}]	ϕ [%]
Et-CNP-ref	103.7 ± 2.0	98.9 ± 2.3	1049 ± 25	30.1 ± 1.7
reEt-CNP-35	113.7 ± 2.2	91.2 ± 2.1	1247 ± 25	16.8 ± 1.7
reEt-CNP-70	111.9 ± 1.4	89.1 ± 1.8	1256 ± 32	16.3 ± 2.1
reEt-CNP-110	113.2 ± 2.0	90.8 ± 2.3	1247 ± 33	16.9 ± 2.2
Et-CNP-d	108.2 ± 2.0	90.4 ± 2.6	1198 ± 32	20.1 ± 2.1
H_2O-CNP	106.0 ± 3.1	84.9 ± 2.5	1248 ± 29	16.8 ± 1.9

The porosity of the untreated Et-CNP-ref sample is almost double that of H_2O-CNPs. t-Tests revealed that density and porosity of re-consolidated CNPs are not significantly different from those of H_2O-CNPs, indicating significant network compaction during secondary drying steps driven by surface tension/Campbell forces leading to a densification of the rewetted fibril network of CNPs formed from ethanolic suspensions. The compaction during the secondary drying appears to be insensitive to the drying temperature and can be attributed to the comparatively higher surface tension of water compared with that of 85 wt.-% ethanol – 72.8 mN m^{-1} vs. ~24 mN m^{-1} for pure water and 85 wt.-% ethanol in water, respectively[61] – leading to higher Campbell forces during drying; the larger Campbell forces acting on nanofibres in the network exerted by water can overcome the intrinsic fibril network tension, thus pulling neighbouring fibrils closer together and compacting the network. This compaction overwhelmingly occurs in the thickness direction of the papers, as the CNFs are deposited in-plane during filtration. Dipping wet filter cakes produced from ethanolic suspension into water prior to hot pressing resulted in CNPs with higher porosities than those produced from aqueous suspensions indicating that the short dipping time was insufficient to increase the water content of the filter cake sufficiently to produce comparable Campbell forces to those achieved with water alone.

The mechanism of network compaction primarily in the thickness direction of the nanopaper, as reflected by increased density, is apparent in CNP cross-sections (Figure 1). SE micrographs show a lamellar structure of the prepared CNPs, with Et-CNP-Ref (Figure 1A) exhibiting numerous significant interlayer pores. These interlayer pores were less pronounced in re-compacted (i.e. reEt-CNP-70, Figure 1B) CNPs and reference CNPs prepared from aqueous suspensions (i.e. H_2O-CNP, Figure 1C) similar to the findings of Huang et al.[31] indicating that re-compaction yields nanopapers as dense and compact as if produced directly from aqueous suspensions. SE micrographs of Et-CNP-ref's surface (Figure 1D) reveal a more porous and open structure than observed in the surfaces of nanopapers produced from aqueous suspensions or re-compacted CNPs formed from ethanolic suspensions (H_2O-CNP and reEt-CNP-70 in Figure 1E & F, respectively). The micrographs also showed a network structure with separated individual fibres being visible in the case of Et-CNP-ref, while all other nanopapers are composed of a tight fibrillar network, consistent with the incidence of inter-layer pores observed in the cross-sections. The differences in the fibril networks clearly illustrate that the presence of water during drying, either in the initial hot-pressing step or during the re-consolidation treatment, resulted in a denser network.

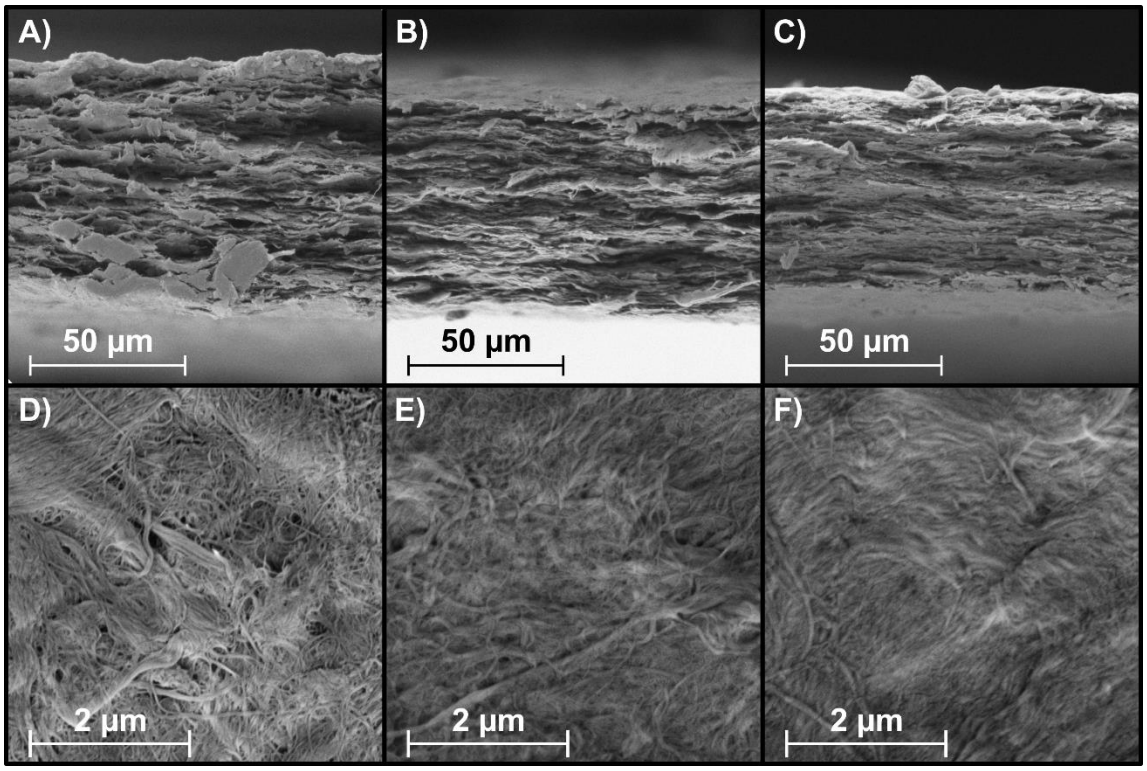

Figure 1: Representative SE micrographs of the nanopaper break edges after tensile testing (top row) and the nanopapers surface of Et-CNP-ref (A & D), reEt-CNP-70 (B & E) and H_2O-CNP (C & F)

3.4. Optical properties of nanopapers before and after re-consolidation

The total luminous transmission of all nanopapers at 572 nm (the wavelength used in the TAPPI T425 standard for the determination of paper opacity) is presented in Figure 2. Both total luminous transmittance and haze over the full visible light range are shown in section SI 4 of the ESI. All three types of nanopapers, which exposed to re-wetting and drying after hot pressing (i.e. Et-CNP-ref, Et-CNP-d and H_2O-CNP) exhibited significantly lower total luminous transmittance (Figure 2) than those nanopapers that were post-treated (reEt-CNP-35/70/110). It is important to note that these nanopapers have lower grammage than those that have been re-wetted and hot-pressed, confirming that their lower transmittance is not caused by more material present in the beam path and can rather be attributable to their greater porosity and hence greater degree of light scattering. Over the full tested spectrum (Figure SI 4-1A), reference nanopapers produced by

filtration from ethanolic suspensions have the lowest light transmittance (Et-CNP-ref, 10-18 %) followed by nanopapers dipped before hot-pressing (Et-CNP-d, 16-27 %) and those produced from an aqueous CNF suspension (H2O-CNP, 21-32 %).

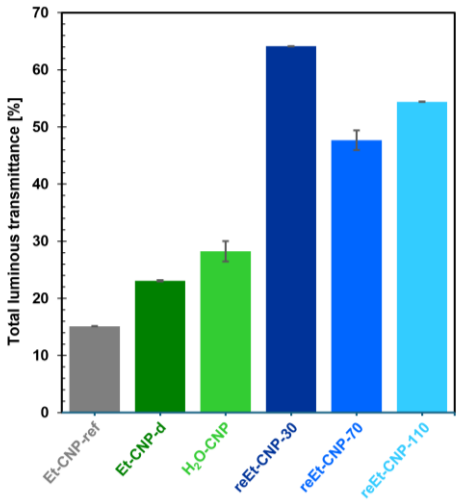

Figure 2: Total luminous transmittance of nanopapers. Error bars represent 95 % confidence intervals.

Re-compacted nanopapers possessed a minimum luminous transmittance of 38 % with reEt-CNP-35 (55-69 %) exceeding those of all other nanopapers. To a lesser extent, optical haze (Figure SI 4-1B) followed the inverse trend of the luminous transmittance and ranged from 84-89 % for all nanopapers. Transmittance is determined by light absorption and scattering whereas haze is determined primarily by refraction of incident light. Since the post-treatment process does not change the CNP's composition, we expect absorption differences among our samples to be negligible, so only scattering (i.e. reflection and refraction) is responsible for changes in transmittance and haze. Scattering occurs at interfaces within the network, and the number of interfaces decreased with increasing density. The trends for haze and transmittance found can be attributed to a higher fraction of pores and voids and hence a larger number of interfaces in Et-CNP-ref, which led to more light scattering. The luminous transmittance of all re-wetted and dried nanopapers compared to all other nanopapers (Figure 2) exceeded that of other nanopapers with similar porosity, consistent with the reduction of scattering

sites within the paper caused by network compaction and a "relaxation" of network tensions.

Figure SI 5-1 in section SI 5 of the ESI shows a qualitative comparison of the coloration all produced CNPs placed on white office paper, showing that the recompaction procedure did not lead to yellowing or other discolorations.

3.5. Tensile properties of nanopapers

Figure 3A shows representative stress-strain curves for all nanopapers and the mechanical properties are summarised in Table 3.

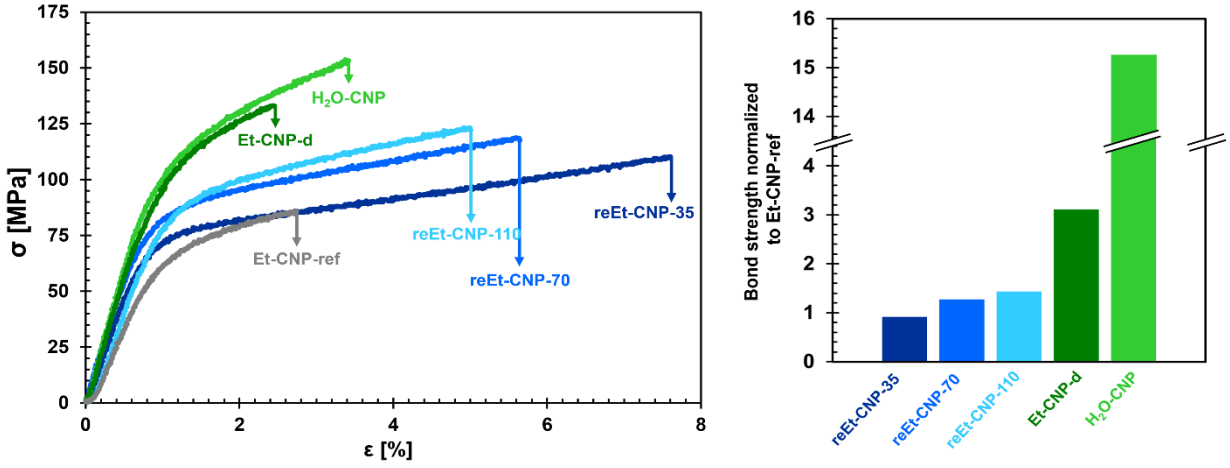

Figure 3: Representative stress-strain curves of all (recompacted) CNPs (A) and the relative bonding contributions to the tensile index normalized to that of Et-CNP-ref (B)

The moisture content of all samples after conditioning for 1 week next to the tensile testing setup was found to be 4.5-5.9 %. All CNPs which were not subjected to re-wetting and drying (i.e. Et-CNP-ref, Et-CNP-d and H_2O-CNP) exhibited low strains to failure, ε_f of 2.5 – 3.4 % whereas the re-consolidation treatment had a significant impact on the ductility of the resulting nanopapers, more than doubling ε_f to values up to 7.5%. The tensile strength of CNPs prepared from aqueous suspensions was significantly higher than that of (re-consolidated) CNPs prepared from ethanolic suspensions. The stress-strain curve of water-dipped Et-CNP-d followed that of

CNPs produced from aqueous suspensions (H_2O-CNP) yet resulted in premature failure in the plastic deformation region.

Table 3: Tensile index *T*, ultimate tensile strain ε_f, (grammage corrected) specific modulus *M*, and modulus of toughness K_f of nanopapers.

Sample Name	T [kN m kg^{-1}]	ε_f [%]	M [MN m kg^{-1}]	K_f [MJ m^{-3}]
Et-CNP-ref	82.5 ± 3.4	2.8 ± 0.4	8.4 ± 0.6	1.7 ± 0.4
reEt-CNP-35	85.5 ± 3.0	7.5 ± 0.4	8.0 ± 0.4	6.4 ± 0.6
reEt-CNP-70	93.8 ± 3.4	5.6 ± 0.4	9.0 ± 0.4	5.2 ± 0.6
reEt-CNP-110	96.4 ± 4.0	5.1 ± 0.6	8.4 ± 0.6	4.7 ± 0.6
Et-CNP-d	104.1 ± 4.7	2.5 ± 0.3	9.8 ± 0.7	2.2 ± 0.3
H_2O-CNP	121.1 ± 7.1	3.3 ± 0.5	10.4 ± 0.6	3.6 ± 0.8

In the electronic supplementary information (section SI 6), we provide the manipulation of eq. 1 to show that the relative difference in the shear bond strength between a pair of nanopapers with different tensile index T and porosity ϕ can be estimated:

$$\frac{b_1}{b_2} = \frac{T_1}{T_2}\frac{(Z_c - T_2)}{(Z_c - T_1)}\frac{RBA_1}{RBA_2}, \tag{6}$$

when assuming that $Z_c = {}^{8Z}/_{9}$ is unaffected by the use of solvents to form the nanopapers. The relative bonded area RBA can be calculated from the porosity ϕ of the respective nanopapers as follows[62]:

$$RBA = 1 - \frac{\phi(1-\phi)(2-\phi)}{\ln({}^{1}/_{\phi})}. \tag{7}$$

The change in shear bond strength per unit area was calculated relative to that of the untreated reference CNPs formed from ethanolic suspensions (i.e. Et-CNP-ref) assuming Z = 140 kN m kg^{-1} and is plotted in Figure 3B. We note that the reported values and trends are very insensitive to the assumed value of Z in the expect range 120 < Z < 150 kN m kg^{-1}. On this basis, we can attribute the increased tensile index

of nanopapers re-consolidated at higher drying temperatures (i.e. reEt-CNP-70 and reEt-CNP-110) to an increase in the shear bond strength per unit area.

The significantly higher strain to failure accompanied by relatively small decreases in strength and modulus (Figure 3A) of CNPs after water rewetting and drying was attributed to network densification (Table 2), which was only associated by marginal increase in interfibrillar bond strength (Figure 3B) normalised to Et-CNP-ref allowing fibrils to slide over each other until final failure resulting in an increased modulus of toughness. Initial hot pressing of CNF films from ethanolic suspension resulted in poorly consolidated, highly porous nanopapers with fewer connection points between fibrils due to the much-reduced Campbell forces acting on the fibrils during removal of the ethanolic suspension medium. This is consistent with the findings of Hashemezehi et al.[63] who analysed the degree of hornification of macroscopic cellulose fibres dried from different solvents. Comparing the mechanical properties of CNPs formed from ethanolic suspensions which were rewetted and dried at different temperatures revealed that higher drying temperatures resulted in slightly stronger yet less ductile nanopapers (Table 3). The influence of the drying temperature on the tensile properties was analogous to the temperature dependency of cellulose hornification;[64] higher drying temperatures resulted in more hornified samples and thus in higher bonding contribution (Figure 3B). The higher strain to failure of rewetted and dried CNPs produced from ethanolic suspensions also resulted in a significantly increased (up to 178% compared to Et-CNP-ref) modulus of toughness K_f – the area under the stress-strain curve – and thus increased tensile toughness albeit at a slight (~22 %) loss of tensile strength and modulus.

A comparison of the mechanical and optical properties of our CNPs with CNPs manufactured by others can only be made with caution, as both the source of the cellulosic material, as well as other pre-treatment and refinement steps can significantly influence the properties of the resulting nanopapers. With this

disclaimer, Figure 4 juxtaposes the tensile strength σ, and the Young's modulus *E*, of a wide variety of lignocellulosic based CNPs from literature[65-71] and our CNPs.

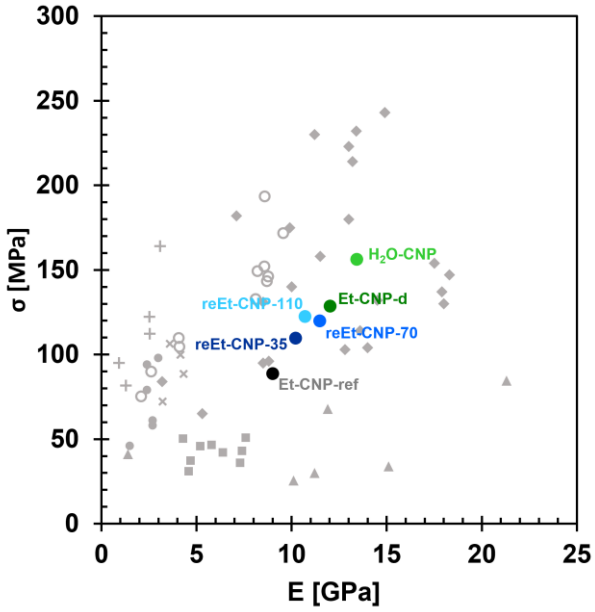

Figure 4: Comparison of the mechanical properties of the CNPs prepared in this study (black, green and blue datapoints) with those of CNPs prepared from lignocellulosic materials using a variety of treatments and preparation methods (grey) reported by Fein et al. (•),[65] Du et al. (×),[66] Rol et al. (▲),[67] Mokhena et al. (◆),[68] Jaiswal et al. (■),[69] Liu et al. (+)[70] and Kontturi et al. (○).[71]

4. CONCLUSIONS

Production of cellulose nanopapers from aqueous suspensions is a time-consuming process. Using ethanol-water mixtures as a suspension medium for CNF allowed for a drastic reduction of filtration times due to the formation of a more porous filter cake reducing the overall filtration resistance. Nanopapers produced from ethanolic filter cakes had much higher porosities and thus significantly lower mechanical properties than papers produced from water-wet filter cakes, because of much lower Campbell forces acting on the drying fibril network. We showed that rewetting with water and drying of CNPs produced from ethanolic suspensions led to significant network compaction, increasing the paper density but only slightly the bonding contribution, resulted in CNPs with increased tensile strength and strain to failure. While having an overall lower tensile strength

and modulus compared to papers produced from aqueous suspensions, CNPs produced from ethanol-water mixtures exhibited a significant increase in their strain to failure and modulus of toughness, and thus, tensile toughness. The compaction of the fibril network during rewetting and drying yielded high haze nanopapers with a much higher optical transmittance than CNPs produced from aqueous suspensions.

5. Acknowledgements

We are grateful to Mag. Dr. Stefan Puchegger of the Faculty Center for Nanostructure Research at the University of Vienna for his help and guidance in using the SEM, Klaus Ritter for the preliminary experiments, which motivated us to further investigate the effect of rewetting of nanopapers, and Fabian Edinger for assistance in determining the CNF-free filtration speed. F.M. is grateful to the University of Vienna and the Institute of Materials Chemistry for funding (#371300).

6. References

[1] Moon, R. J.; Martini, A.; Nairn, J.; Simonsen, J.; Youngblood, J., *Chem. Soc. Rev.* **2011,** *40* (7), 3941-94. DOI 10.1039/c0cs00108b.
[2] Klemm, D.; Heublein, B.; Fink, H. P.; Bohn, A., *Angew. Chem. Int. Ed. Engl.* **2005,** *44* (22), 3358-93. DOI 10.1002/anie.200460587.
[3] Herrick, F. W.; Casebier, R. L.; Hamilton, J. K.; Sandberg, K. R. In *Microfibrillated cellulose: morphology and accessibility*, J. Appl. Polym. Sci.: Appl. Polym. Symp., United States, 1983-01-01; United States, **1983**.
[4] Turbak, A. F.; Snyder, F. W.; Sandberg, K. R. In *Microfibrillated cellulose, a new cellulose product: properties, uses, and commercial potential*, 9. cellulose conference, Syracuse, NY, USA, 1983-01-01; Syracuse, NY, USA, **1982**.
[5] Saito, T.; Kimura, S.; Nishiyama, Y.; Isogai, A., *Biomacromolecules* **2007,** *8* (8), 2485-91. DOI 10.1021/bm0703970.
[6] Klemm, D.; Cranston, E. D.; Fischer, D.; Gama, M.; Kedzior, S. A.; Kralisch, D.; Kramer, F.; Kondo, T.; Lindström, T.; Nietzsche, S.; Petzold-Welcke, K.; Rauchfuß, F., *Mater. Today* **2018,** *21* (7), 720-748. DOI 10.1016/j.mattod.2018.02.001.
[7] Saito, T.; Kuramae, R.; Wohlert, J.; Berglund, L. A.; Isogai, A., *Biomacromolecules* **2013,** *14* (1), 248-53. DOI 10.1021/bm301674e.
[8] Henriksson, M.; Berglund, L. A.; Isaksson, P.; Lindstrom, T.; Nishino, T., *Biomacromolecules* **2008,** *9* (6), 1579-85. DOI 10.1021/bm800038n.
[9] Miao, C.; Du, H.; Parit, M.; Jiang, Z.; Tippur, H. V.; Zhang, X.; Liu, Z.; Li, J.; Wang, R., *Cellulose* **2020,** *27* (6), 3181-3195. DOI 10.1007/s10570-020-03015-x.
[10] Syverud, K.; Stenius, P., *Cellulose* **2008,** *16* (1), 75-85. DOI 10.1007/s10570-008-9244-2.

[11] Liu, P.; Borrell, P. F.; Bozic, M.; Kokol, V.; Oksman, K.; Mathew, A. P., *J. Hazard. Mater.* **2015,** *294*, 177-85. DOI 10.1016/j.jhazmat.2015.04.001.
[12] Thomas, B.; Raj, M. C.; B, A. K.; H, R. M.; Joy, J.; Moores, A.; Drisko, G. L.; Sanchez, C., *Chem. Rev.* **2018,** *118* (24), 11575-11625. DOI 10.1021/acs.chemrev.7b00627.
[13] Mashkour, M.; Rahimnejad, M.; Mashkour, M.; Soavi, F., *Appl. Energy* **2021,** *282*. DOI 10.1016/j.apenergy.2020.116150.
[14] Tafete, G. A.; Abera, M. K.; Thothadri, G., *J. Energy Storage* **2022,** *48*. DOI 10.1016/j.est.2021.103938.
[15] Zhang, Y.; Zhang, L.; Cui, K.; Ge, S.; Cheng, X.; Yan, M.; Yu, J.; Liu, H., *Adv. Mater.* **2018,** *30* (51), e1801588. DOI 10.1002/adma.201801588.
[16] Ahankari, S. S.; Subhedar, A. R.; Bhadauria, S. S.; Dufresne, A., *Carbohydr. Polym.* **2021,** *255*, 117479. DOI 10.1016/j.carbpol.2020.117479.
[17] Kargarzadeh, H.; Huang, J.; Lin, N.; Ahmad, I.; Mariano, M.; Dufresne, A.; Thomas, S.; Gałęski, A., *Prog. Polym. Sci.* **2018,** *87*, 197-227. DOI 10.1016/j.progpolymsci.2018.07.008.
[18] Wang, J.; Gardner, D. J.; Stark, N. M.; Bousfield, D. W.; Tajvidi, M.; Cai, Z., *ACS Sustainable Chem. Eng.* **2017,** *6* (1), 49-70. DOI 10.1021/acssuschemeng.7b03523.
[19] Liu, W.; Liu, K.; Du, H.; Zheng, T.; Zhang, N.; Xu, T.; Pang, B.; Zhang, X.; Si, C.; Zhang, K., *Nano-Micro Lett.* **2022,** *14* (1), 104. DOI 10.1007/s40820-022-00849-x.
[20] Österberg, M.; Vartiainen, J.; Lucenius, J.; Hippi, U.; Seppala, J.; Serimaa, R.; Laine, J., *ACS Appl. Mater. Interfaces* **2013,** *5* (11), 4640-7. DOI 10.1021/am401046x.
[21] Revol, J. F.; Bradford, H.; Giasson, J.; Marchessault, R. H.; Gray, D. G., *Int. J. Biol. Macromol.* **1992,** *14* (3), 170-2. DOI 10.1016/s0141-8130(05)80008-x.
[22] Dufresne, A.; Cavaillé, J.-Y.; Vignon, M. R., *J. Appl. Polym. Sci.* **1997,** *64* (6), 1185-1194. DOI 10.1002/(sici)1097-4628(19970509)64:6<1185::Aid-app19>3.0.Co;2-v.
[23] Hubbe, M. A.; Ferrer, A.; Tyagi, P.; Yin, Y.; Salas, C.; Pal, L.; Rojas, O. J., *BioResources* **2017,** *12* (1), 2143-2233. DOI 10.15376/biores.12.1.2143-2233.
[24] Sehaqui, H.; Liu, A.; Zhou, Q.; Berglund, L. A., *Biomacromolecules* **2010,** *11* (9), 2195-8. DOI 10.1021/bm100490s.
[25] Sethi, J.; Liimatainen, H.; Sirvio, J. A., *ACS Omega* **2021,** *6* (29), 19038-19044. DOI 10.1021/acsomega.1c02328.
[26] Sinquefield, S.; Ciesielski, P. N.; Li, K.; Gardner, D. J.; Ozcan, S., *ACS Sustainable Chem. Eng.* **2020,** *8* (26), 9601-9615. DOI 10.1021/acssuschemeng.0c01797.
[27] Nadeem, H.; Dehghani, M.; Garnier, G.; Batchelor, W., *J. Cleaner Prod.* **2022,** *342*. DOI 10.1016/j.jclepro.2022.130890.
[28] Lindström, T.; Aulin, C., *Scand. J. For. Res.* **2014,** *29* (4), 345-351. DOI 10.1080/02827581.2014.928365.
[29] Hervy, M.; Bock, F.; Lee, K.-Y., *Composites Science and Technology* **2018,** *167*, 126-133. DOI 10.1016/j.compscitech.2018.07.027.
[30] Solhi, L.; Guccini, V.; Heise, K.; Solala, I.; Niinivaara, E.; Xu, W.; Mihhels, K.; Kroger, M.; Meng, Z.; Wohlert, J.; Tao, H.; Cranston, E. D.; Kontturi, E., *Chem. Rev.* **2023,** *123* (5), 1925-2015. DOI 10.1021/acs.chemrev.2c00611.
[31] Huang, Y.; Kasuga, T.; Nogi, M.; Koga, H., *RSC Adv.* **2023,** *13* (31), 21494-21501. DOI 10.1039/d3ra03840h.
[32] Sim, K.; Ryu, J.; Youn, H. J., *Fibers and Polymers* **2015,** *16* (2), 294-301. DOI 10.1007/s12221-015-0294-4.
[33] Onyianta, A. J.; Xu, G.; Etale, A.; Eloi, J. C.; Eichhorn, S. J., *Carbohydr. Polym.* **2023,** *314*, 120943. DOI 10.1016/j.carbpol.2023.120943.
[34] Mautner, A.; Nawawi, W. M. F. W.; Lee, K.-Y.; Bismarck, A., *Composites Part A* **2020,** *131*. DOI 10.1016/j.compositesa.2020.105779.

[35] Ferguson, A.; Khan, U.; Walsh, M.; Lee, K. Y.; Bismarck, A.; Shaffer, M. S.; Coleman, J. N.; Bergin, S. D., *Biomacromolecules* **2016,** *17* (5), 1845-53. DOI 10.1021/acs.biomac.6b00278.
[36] Hsieh, M. C.; Koga, H.; Suganuma, K.; Nogi, M., *Sci. Rep.* **2017,** *7*, 41590. DOI 10.1038/srep41590.
[37] Mautner, A.; Bismarck, A., *Carbohydr. Polym.* **2021,** *251*, 117130. DOI 10.1016/j.carbpol.2020.117130.
[38] Campbell, W. B., *Tappi* **1959,** *42* (12). DOI 10.32964/tj42.12.999.
[39] Page, D., *Tappi* **1969,** *52*, 674-681.
[40] Jayme, G., *Wochenbl. Papierfabr.* **1944,** *6*, 187-194.
[41] Minor, J. L., *Prog. Pap. Recycl.* **1994,** *3* (2), 93-95.
[42] Fernandes Diniz, J. M. B.; Gil, M. H.; Castro, J. A. A. M., *Wood Sci. Technol.* **2004,** *37* (6), 489-494. DOI 10.1007/s00226-003-0216-2.
[43] Chen, F.; Xiang, W.; Sawada, D.; Bai, L.; Hummel, M.; Sixta, H.; Budtova, T., *ACS Nano* **2020,** *14* (9), 11150-11159. DOI 10.1021/acsnano.0c02302.
[44] Liu, Y.; Feng, S.; Zhang, Z.; Meng, Q.; Shi, X., *Cellulose* **2025,** *32* (12), 7067-7081. DOI 10.1007/s10570-025-06678-6.
[45] Abbott, A.; Bismarck, A., *Cellulose* **2010,** *17* (4), 779-791. DOI 10.1007/s10570-010-9427-5.
[46] Gindl, W.; Keckes, J., *Polymer* **2005,** *46* (23), 10221-10225. DOI 10.1016/j.polymer.2005.08.040.
[47] Mayer, F.; Prado-Roller, A.; Mautner, A.; Bismarck, A., *Cellulose* **2024,** *31* (3), 1533-1544. DOI 10.1007/s10570-023-05714-7.
[48] Wloch, D.; Herrera, N.; Lee, K.-Y., *Composites Part A* **2023,** *172*. DOI 10.1016/j.compositesa.2023.107583.
[49] Sethi, J.; Visanko, M.; Osterberg, M.; Sirvio, J. A., *Carbohydr. Polym.* **2019,** *203*, 148-156. DOI 10.1016/j.carbpol.2018.09.037.
[50] Josset, S.; Orsolini, P.; Siqueira, G.; Tejado, A.; Tingaut, P.; Zimmermann, T., *Nord. Pulp Pap. Res. J.* **2014,** *29* (1), 167-175. DOI 10.3183/npprj-2014-29-01-p167-175.
[51] Sehaqui, H.; Zhou, Q.; Ikkala, O.; Berglund, L. A., *Biomacromolecules* **2011,** *12* (10), 3638-44. DOI 10.1021/bm2008907.
[52] Oh, G., *Int. J. Pressure Vessels Piping* **2022,** *199*. DOI 10.1016/j.ijpvp.2022.104733.
[53] Svagan, A. J.; Samir, M. A.; Berglund, L. A., *Biomacromolecules* **2007,** *8* (8), 2556-63. DOI 10.1021/bm0703160.
[54] Mattsson, T.; Sedin, M.; Theliander, H., *Separation and Purification Technology* **2012,** *96*, 139-146. DOI 10.1016/j.seppur.2012.05.029.
[55] Lide, D. R., *CRC Handbook of Chemistry and Physics*. 84 ed.; CRC Press: **2003**.
[56] Carman, P. C., *Chem. Eng. Res. Des.* **1997,** *75*, S32-S48. DOI 10.1016/s0263-8762(97)80003-2.
[57] Fall, A.; Henriksson, M.; Karppinen, A.; Opstad, A.; Heggset, E. B.; Syverud, K., *Cellulose* **2022,** *29* (14), 7649-7662. DOI 10.1007/s10570-022-04719-y.
[58] Sim, K.; Lee, J.; Lee, H.; Youn, H. J., *Cellulose* **2015,** *22* (6), 3689-3700. DOI 10.1007/s10570-015-0784-y.
[59] Mautner, A.; Lee, K.-Y.; Tammelin, T.; Mathew, A. P.; Nedoma, A. J.; Li, K.; Bismarck, A., *React. Funct. Polym.* **2015,** *86*, 209-214. DOI 10.1016/j.reactfunctpolym.2014.09.014.
[60] González, B.; Calvar, N.; Gómez, E.; Domínguez, Á., *J. Chem. Thermodyn.* **2007,** *39* (12), 1578-1588. DOI 10.1016/j.jct.2007.05.004.
[61] Vazquez, G.; Alvarez, E.; Navaza, J. M., *Journal of Chemical & Engineering Data* **1995,** *40* (3), 611-614. DOI 10.1021/je00019a016.
[62] Sampson, W., *J. Pulp Pap. Sci.* **2008,** *34* (2), 91.
[63] Hashemzehi, M.; Sjöstrand, B.; Håkansson, H.; Henriksson, G., *Cellulose* **2024,** *31* (3), 1813-1825. DOI 10.1007/s10570-023-05657-z.

[64] Sellman, F. A.; Benselfelt, T.; Larsson, P. T.; Wagberg, L., *Carbohydr. Polym.* **2023,** *318*, 121132. DOI 10.1016/j.carbpol.2023.121132.
[65] Fein, K.; Bousfield, D. W.; Gramlich, W. M., *ACS Applied Polymer Materials* **2021,** *3* (7), 3666-3678. DOI 10.1021/acsapm.1c00620.
[66] Du, H.; Parit, M.; Wu, M.; Che, X.; Wang, Y.; Zhang, M.; Wang, R.; Zhang, X.; Jiang, Z.; Li, B., *J. Hazard. Mater.* **2020,** *400*, 123106. DOI 10.1016/j.jhazmat.2020.123106.
[67] Rol, F.; Karakashov, B.; Nechyporchuk, O.; Terrien, M.; Meyer, V.; Dufresne, A.; Belgacem, M. N.; Bras, J., *ACS Sustainable Chem. Eng.* **2017,** *5* (8), 6524-6531. DOI 10.1021/acssuschemeng.7b00630.
[68] Mokhena, T. C.; Sadiku, E. R.; Mochane, M. J.; Ray, S. S.; John, M. J.; Mtibe, A., *Carbohydr. Polym.* **2021,** *273*, 118507. DOI 10.1016/j.carbpol.2021.118507.
[69] Jaiswal, A. K.; Kumar, V.; Khakalo, A.; Lahtinen, P.; Solin, K.; Pere, J.; Toivakka, M., *Cellulose* **2021,** *28* (4), 2087-2104. DOI 10.1007/s10570-021-03688-y.
[70] Liu, W.; Zhang, S.; Liu, K.; Yang, H.; Lin, Q.; Xu, T.; Song, X.; Du, H.; Bai, L.; Yao, S.; Si, C., *J. Cleaner Prod.* **2023,** *384*. DOI 10.1016/j.jclepro.2022.135582.
[71] Kontturi, K. S.; Lee, K.-Y.; Jones, M. P.; Sampson, W. W.; Bismarck, A.; Kontturi, E., *Cellulose* **2021,** *28* (10), 6619-6628. DOI 10.1007/s10570-021-03935-2.

SUPPLEMENTARY INFORMATION

Towards the Efficient Preparation of Tough Cellulose Nanopapers

Florian Mayer[a,b], William W. Sampson[c], Daniela Wloch[d], Andreas Mautner[a,e,¤], Alexander Bismarck[a,f,g,*]

[a] Institute of Materials Chemistry and Research, Faculty of Chemistry, University of Vienna, Waehringer Straße 42, 1090, Vienna, Austria.

[b] Department of Bioproducts and Biosystems, Aalto University, Vuorimiehentie 1, 02150 Espoo, Finland

[c] Department of Materials, University of Manchester, Manchester, M13 9PL, UK

[d] Department of Aeronautics, Imperial College London, South Kensington Campus, London SW7 2AZ, United Kingdom

[e] Institute of Environmental Biotechnology, IFA-Tulln, University of Natural Resources and Life Sciences, Vienna, Konrad-Lorenz-Straße 20, 3430, Tulln an der Donau, Austria

[f] Division of Materials Science, Department of Engineering Sciences and Mathematics, Luleå University of Technology, Luleå, 971 87, Sweden

[g] Department of Chemical Engineering, Imperial College London, South Kensington Campus, London SW7 2AZ, United Kingdom

¤ e-mail: andreas.mautner@boku.ac.at

* e-mail: alexander.bismarck@univie.ac.at

SI 1. Process flow of CNP preparation

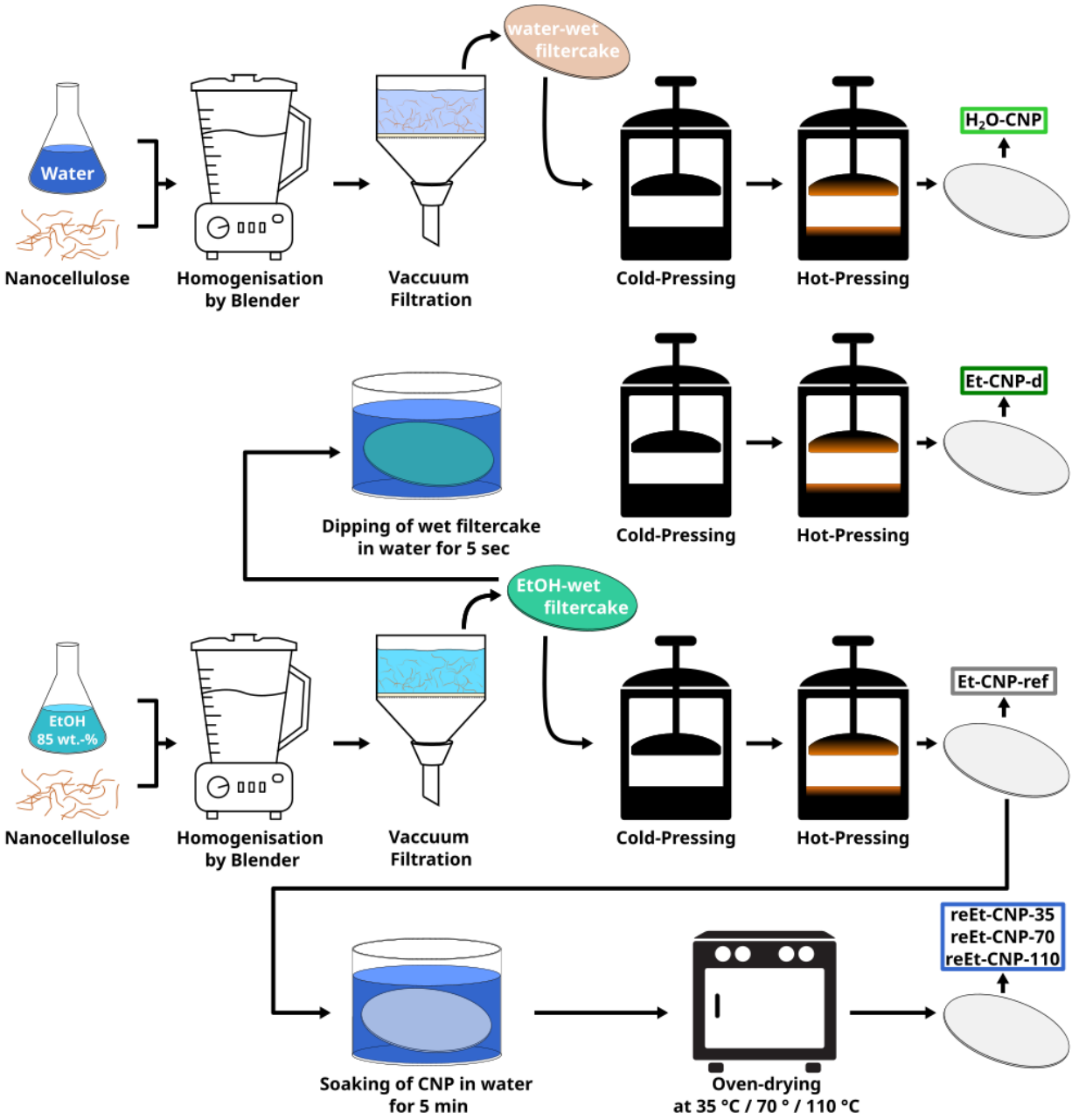

Figure SI 1-1: Schematic depiction of the process flow and order during preparation of the different CNP samples used in this study.

SI 2. Preliminary experiments to determine the influence of suspension medium ethanol content on CNP porosity

To determine the influence of ethanol content in the suspension medium, a set of 10 reference nanopapers was prepared in duplicate (total of 20 CNPs) following the same procedure outlined for the production of Et-CNP-ref and H_2O-CNP. In brief: 1.2 g dry mass CNF stock (aqueous suspension with a CNF content of 3.5 wt.-%) were suspended in 600 mL of suspension medium with varying water/ethanol ratios (Table SI 2-1), and homogenised by blending for 30 seconds, before filtration, followed by cold and hot pressing (see figure SI 1-1) as described in section 2.2 of the main manuscript.

The porosity of each CNP was determined as described in section 2.5 of the main manuscript, by cutting test specimen of precisely known area, measuring their thickness at 5 points along their length, and determining their weight. A minimum of 16 specimen was measured for each datapoint.

Table SI 2-1: preparation parameters and suspension medium composition of CNPs prepared to investigate the influence of suspension medium composition on CNP porosity

Sample	Preparation Parameters	
	Suspension Medium	CNF dry mass [g]
Por-0	Water	1.2
Por-10	10 wt.-% EtOH	1.2
Por-20	20 wt.-% EtOH	1.2
Por-30	30 wt.-% EtOH	1.2
Por-40	40 wt.-% EtOH	1.2
Por-50	50 wt.-% EtOH	1.2
Por-60	60 wt.-% EtOH	1.2
Por-70	70 wt.-% EtOH	1.2
Por-80	80 wt.-% EtOH	1.2
Por-90	90 wt.-% EtOH	1.2

Figure SI 2-1 shows the results of the preliminary investigation into the influence of the water/ethanol ratio of the suspension medium on the porosity of the resulting nanopapers.

We found little to no change in porosity for ethanol contents of up to 60 wt.-%. Increasing the ethanol content of the suspension medium from 60 to 80 wt.-%

resulted in a rapid increase of the porosity, which plateaued when the suspension medium contained more than 80 wt.-% ethanol.

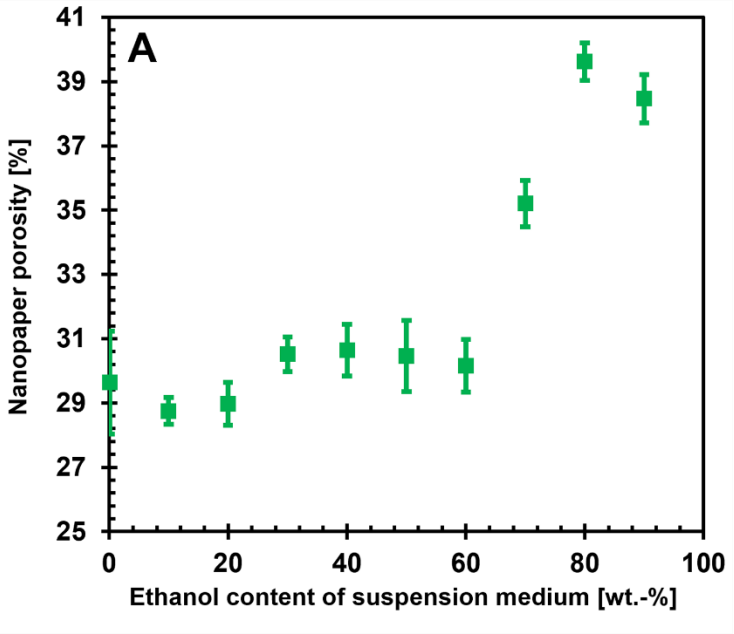

Figure SI 2-1: Dependence of nanopaper porosity on the suspension medium composition. Error bars represent 95 % confidence intervals.

The rapid change in the CNPs porosity can be attributed to the Campbell forces enacted on the fibril network depending on the ethanol content. At a certain point (between 60 and 80 wt.-% ethanol) the capillary forces exerted on the fibril network by the evaporating suspension medium are insufficient to overcome the tension forces of the network and pull them into close enough proximity for hydrogen bonding to occur. Thus, significantly less network compaction by Campbell forces takes place during hot pressing at higher ethanol contents, leading to a more porous fibril network.

SI 3. Determination of the water and ethanol filtration speed without nanocellulose present

The filtration setup was prepared in the same way as described for nanopaper preparation, but instead of a suspension of CNF in ethanol or water, 700 mL of either DI water or 85 wt.-% ethanol, respectively, were filtered through a Büchner funnel lined with filter paper (VWR 413, VWR, Leuven, Belgium). The filtration time was measured, and the experiment was repeated a minimum of 5 times for each solvent. The filtration speeds for both solvents are presented in Table SI 3-1 and show no significant difference between the two.

Table SI 3-1: Filtration rates for solvents without CNF added.

Solvent	Flowrate [L min^{-1}]
H2O	4.4 ± 0.3
EtOH 85 wt.-%	4.4 ± 0.2

SI 4. Total luminous transmittance and haze of nanopapers

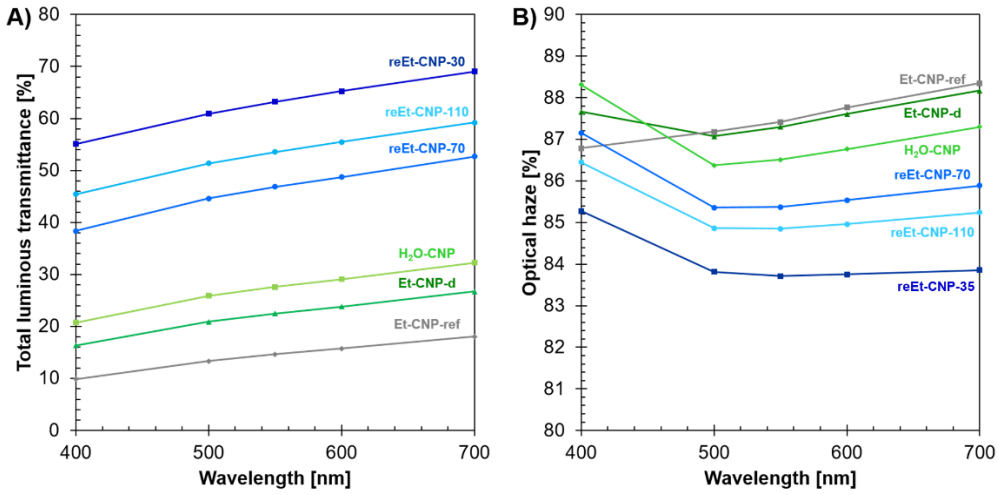

Figure SI 4-1: Total luminous transmittance (A) and optical haze of (recompacted) nanopapers.

SI 5. Impact of the recompaction process on the optical appearance of CNPs

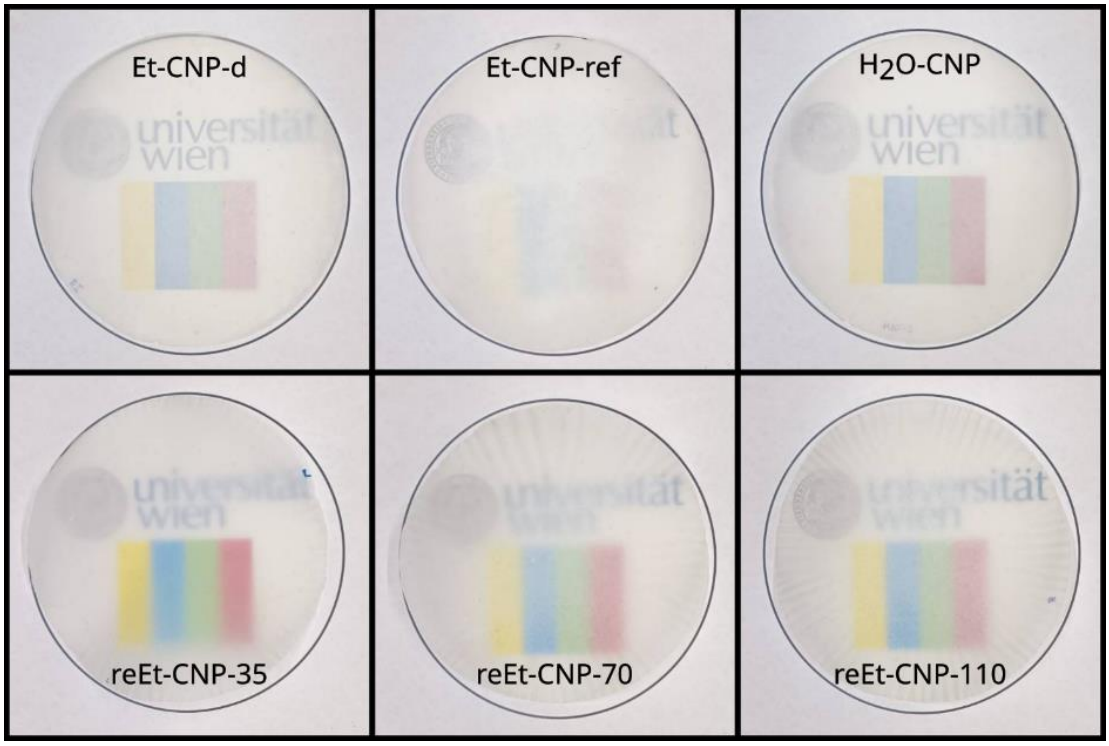

Figure SI 5-1: Qualitative photographs of the CNPs produced in this study on top of white office paper.

SI 6 Determination of changes in shear bond strength per unit area

The Page equation was derived to describe the tensile index of paper but is applicable to the broader family of self-bonded stochastic planar fibrous materials. It is given by

$$\frac{1}{T} = \frac{9}{8\,Z} + \frac{12\,\delta}{b\,P\,L\,RBA} \qquad \text{(S1)}$$

where T (kN m kg^{-1}) is the specific strength or 'Tensile Index' of a nanopaper, Z (kN m kg^{-1}) is its Zero Span Tensile Index, δ (kg m-1) is the linear density of nanofibrils with perimeter P (m) and mean length L (m); RBA represents the relative bonded area and b (N m^{-2}) is the shear bond strength per unit area

Equation (S1) is often used in a simplified form such that

$$\frac{1}{T} = \frac{1}{Z_c} + \frac{1}{B} \tag{S2}$$

where

$$Z_c = \frac{8\,Z}{9} \tag{S3}$$

and

$$B = \frac{b\,P\,L\,RBA}{12\,\delta} \tag{S4}$$

Simple manipulation of Equation (S4) gives

$$B = \frac{Z_c\,T}{(Z_c - T)} \tag{S5}$$

Assuming that our treatments have no effect on the morphology of intrinsic strength of fibres such that d, P, L and Zc are constant, then we can compare the contribution of bonding to the tensile strength of two nanopapers, denoted by subscripts 1 and 2, via Equation (S4) and (S5) such that

$$\frac{B_1}{B_2} = \frac{b_1 RBA_1}{b_2 RBA_2} \tag{S6}$$

$$\frac{B_1}{B_2} = \frac{\frac{Z_c T_1}{(Z_c - T_1)}}{\frac{Z_c T_2}{(Z_c - T_2)}} = \frac{T_1}{T_2}\,\frac{(Z_c - T_2)}{(Z_c - T_1)} \tag{S7}$$

Combining Equations (S6) and (S7) yields

$$\frac{b_1}{b_2} = \frac{TI_1}{TI_2}\,\frac{(Z_c - TI_2)}{(Z_c - TI_1)}\,\frac{RBA_1}{RBA_2} \tag{S8}$$

The relative bonded area can be estimated (S9) from the porosity of the respective nanopaper

$$RBA = 1 - \frac{\varepsilon\,(1-\varepsilon\,)(2-\varepsilon\,)}{\ln(1/\varepsilon\,)} \tag{S9}$$

Publication III

Mayer, F., Schweng, P., Braeuer, S., Hummer, S., Koellensperger, G., Mautner, A., Woodward, R., & Bismarck, A. (2024). Best of Both Worlds: Adsorptive Ultrafiltration Nanocellulose-Hypercrosslinked Polymer Hybrid Membranes for Metal Ion Removal. *Small Science*, 4(10) e2400182

DOI: 10.1002/smsc.202400182

small science
www.small-science-journal.com

Best of Both Worlds: Adsorptive Ultrafiltration Nanocellulose-Hypercrosslinked Polymer Hybrid Membranes for Metal Ion Removal

*Florian Mayer, Paul Schweng, Simone Braeuer, Sebastian Hummer, Gunda Koellensperger, Andreas Mautner, Robert Woodward, and Alexander Bismarck**

Efficient water treatment ideally combines ion exchange for the removal of hardness elements and toxic trace metals as well as ultrafiltration for the removal of particulate matter. Although promising for adsorption, many high-surface-area polymer materials cannot be easily processed into freestanding membranes or packed bed columns, due to poor solution processability and high back pressures, respectively. The preparation of hybrid membranes comprising sulfonated hypercrosslinked polymers entrapped in nanocellulose papers is described. The hybrid membranes are effective for simultaneous ultrafiltration and ion exchange. Increasing the polymer loading of the hybrid membrane produces synergy by increasing the permeance of the membranes while enhancing the ion adsorption capacity to values exceeding those of bulk hypercrosslinked polymers. The maximum ion adsorption capacity for copper is determined to be ≈100 mg g^{-1} outperforming that of pure polymer (71 mg g^{-1}) and commercially available ion exchange resins. Competitive adsorption is tested in samples containing water hardness elements and trace toxic metal ions showing high ion-exchange capacities. Even when fully loaded with water hardness elements, Ba^{2+} and Sr^{2+} are still removed from solution.

1. Introduction

Progressing industrialization and the accompanying increase of heavy metal and microplastic contaminated wastewaters significantly contribute to water scarcity by polluting ground and drinking water.[1–3] Significant attention is being paid to the remediation of heavy metal ions which are toxic at high concentrations. Copper, for example, can cause damage to the immune system, the liver, the central nervous system, and has been identified to contribute to Alzheimer's and other neurodegenerative diseases.[4,5] Removal of heavy metal contaminants is performed in a variety of ways such as precipitation, coagulation, flocculation or flotation, electrochemical processes, membrane separation, and adsorption based methods.[6–11] Each method has advantages and disadvantages, especially with regard to their cost effectiveness, their environmental impact, and their ease of implementation.[7,11] Most water purification methods currently employed suffer from drawbacks such as high energy consumption, especially in the case of distillation technologies.[12] For reverse osmosis and membrane distillation, a combination of significant water waste, membrane fouling, and/or low flux renders them cost ineffective for various scenarios.[13,14] Cost-effective heavy metal removal methods

F. Mayer, P. Schweng, S. Hummer, A. Mautner, R. Woodward, A. Bismarck
Institute of Materials Chemistry and Research
Faculty of Chemistry
University of Vienna
Waehringer Straße 42, 1090 Vienna, Austria
E-mail: alexander.bismarck@univie.ac.at

S. Braeuer, G. Koellensperger
Institute of Analytical Chemistry
Faculty of Chemistry
University of Vienna
Waehrigner Straße 38, 1090 Vienna, Austria

The ORCID identification number(s) for the author(s) of this article can be found under https://doi.org/10.1002/smsc.202400182.

DOI: 10.1002/smsc.202400182

A. Mautner
Institute of Environmental Biotechnology
IFA-Tulln
University of Natural Resources and Life Sciences
ViennaKonrad-Lorenz-Straße 20, 3430, Tulln an der Donau, Austria

A. Bismarck
Division of Materials Science
Department of Engineering Sciences and Mathematics
Luleå University of Technology
971 87 Luleå, Sweden

A. Bismarck
Department of Chemical Engineering
Imperial College London
South Kensington Campus
London SW7 2AZ, UK

are required and should preferably be based on sustainable materials and/or processes.[15–17]

Filtration is a size exclusion method widely used as a low-cost approach for removing nonsoluble and even some soluble water pollutants. The main drawbacks of filtration are its inability to remove dissolved contaminants, for example, heavy metal ions, and its correlation between pore size and permeability. Adsorption is another widely used water treatment method in which contaminant materials are selectively extracted onto the surface of an adsorbent, such as ion exchange resins (IERs) or activated carbons.[18] Although adsorption is effective for the removal of dissolved contaminants, drawbacks such as diffusion limitations and high backpressure have been reported, if implemented in packed beds.[19] Hybrid solutions combining adsorption sites with (ultra)filtration, that is, filtration of particles <100 nm in diameter,[20] offer effective (heavy metal) ion removal combined with high flux.[21–23]

Cellulose is a commonly used filter material, historically used in paper or cloth form for water or air purification.[24–26] Cellulose nanofibers (CNF) are obtained by mechanical or chemical defibrillation of pulp fibers[27] and are typically 5-60 nm in diameter and several micrometers long.[28] Papers made from CNF, called nanopapers (CNP), are considered next-generation filter materials, as the dimensions of CNFs in CNPs enable ultrafiltration.[25,29] Surface modification of CNFs can enable heavy metal adsorption via the introduction of selective chemical moieties, which introduce desired surface charges.[30,31] However, such CNF functionalization's are often cost-intensive and lead to increased filtration times required for paper formation. Hybridization of CNPs with state-of-the-art adsorbent materials could offer a solution to this conundrum.

Potential candidate materials for hybridization are hypercrosslinked polymers (HCPs), amorphous, densely crosslinked porous organic polymers, produced using Friedel–Crafts chemistry.[32] HCPs are a promising class of adsorbents for water purification, as their high surface areas provide abundant sorption sites and their hierarchical pore structures benefit mass transfer of adsorbates.[33] We reported the synthesis of sulfonated HCPs (SHCPs) in a one-pot approach, utilizing chlorosulfonic acid as a dual polymerization catalyst and sulfonating agent,[34] resulting in SHCPs with higher sulfonation density and surface area as compared to conventional approaches.[35,36] SHCPs are useful for application as high-capacity IERs.[36] IERs have broad applications, including water softening, removal of heavy metals from wastewater, and separation of molecules by charge.[37] However, porous organic polymers including HCPs have poor mechanical properties and are typically not solution processable, limiting their application as membrane materials. Nevertheless, studies have reported HCP-based membranes accessible via hypercrosslinking of pre-existing polymer membranes[38,39] and nanocomposite membranes for gas separation, comprising HCPs embedded in matrices of polydimethylsiloxane,[40] poly[1-(trimethylsilyl)-1-propyne],[41] or even polymers of intrinsic microporosity.[42]

Here, we report hybrid membranes of SHCPs and CNFs for water treatment applications. We hypothesize that the use of CNF matrices will facilitate the homogeneous dispersion of embedded SHCP particles to produce membranes combining the ultrafiltration performance of CNP with the ion exchange capability of SHCPs. We manufacture multilayered CNF/SHCP hybrid structures using conventional filter paper carriers. By applying CNF top layers of varying thicknesses, membrane permeances are tailored to control the residence time of the permeate in the SHCP particle layer. The resulting hybrid membranes are tested for their ultrafiltration capabilities, heavy metal ion adsorption, and selectivity.

2. Experimental Section

2.1. Materials

4,4′-Bis(chloromethyl)-1,1′-biphenyl (BCMBP, 95%), chlorosulfonic acid (99%), 1,2-dichloroethane (DCE, ACS reagent, 99%), methanol (HPLC grade, ≥99.9%), ethylenediaminetetraacetic acid disodium salt dehydrate (EDTA), the indicator murexide, anhydrous calcium chloride, anhydrous copper chloride, and 10 nm-diameter gold nanoparticles in citrate buffer were purchased from Sigma-Aldrich. Magnesium chloride 6-hydrate was purchased from BDH Laboratory supplies. Never-dried elemental chlorine-free bleached softwood pulp (*Picea abies* and *Pinus spp.*) was kindly provided by Stendal (Berlin, Germany) and comprised 81.3% cellulose, 12.6% hemicellulose, and 0.3% ash.[43] Aqueous ammonia solution (25% p.a.) and hydrochloric acid (37%, p.a.) were purchased from Th.Geyer (Renningen, Germany). Nitric acid (≥69%, Rotipuran Supra) was obtained from Carl Roth. Mineral water (Longlife, Bad Radkersburg, Austria) was purchased in a local supermarket and ethanol (96% denatured with 1% petrolether) from Brenntag (Austria). Ultrapure water (18.2 MΩ cm, ELGA Water purification system, Purelab Ultra MK 2) was used for dilutions and calibration standards. Element standards were purchased from Labkings. If not stated otherwise, all materials were used as received

2.2. Synthesis of Sulfonated Hypercrosslinked Polymers

We synthesized SHCPs according to a modified procedure previously reported by us.[34] Briefly, 4,4′-bis(chloromethyl)-1,1′-biphenyl (10 mmol, 2.510 g) was dissolved in 1,2-dichloroethane (DCE, 25 mL) at room temperature, before adding a solution of chlorosulfonic acid (40 mmol, 4.661 g) in DCE (5 mL). The reaction mixture was heated to 80 °C for 22 h. The resulting polymer was washed with methanol (≈100 mL) followed by a 24 h Soxhlet extraction using methanol followed by drying under vacuum at 80 °C overnight. We referred to the polymer as SHCP-10 in accordance with our previous publication.[34] The polymer was characterized as in the referenced publication. The full characterization procedure and data of SHCP-10 are provided in the Supporting Information (Section S1).

2.3. Preparation of Cellulose Nanofibrils

Cellulose nanofibrils were prepared according to a procedure previously utilized by our group.[44] In short, never-dried cellulose pulp sheets were cut into $1 \times 1\,cm^2$ pieces and soaked in distilled water for at least 24 h before dispersing them using a mechanical blender (BL-4473, Tristar) at 1500 W for 1 min.

The cellulose suspension was subsequently passed ten times through a disc mill (MKCA6–23, Fuchs disc mill Granomat JP 150, Fuchs Maschinen AG) to refine the pulp to CNF. During the refinement process, the gap size of the disc mill was constantly reduced, and water was added as needed to ensure a consistency suitable for grinding. The resulting nanocellulose suspension was upconcentrated using gravity filtration to a dry mass content of 3.4 wt% before storage in an airtight container.

2.4. Hybrid Membrane Preparation

We developed a preparation technique for three-layer hybrid membranes analogous to a traditional paper-making procedure (**Figure 1**). Hybrid membranes with varying amounts of CNF and SHCP were prepared in duplicate. Ethanol dispersions containing a 1:1 weight ratio of CNF and SHCP-10 (0.2 wt% total) were filtered using a Büchner funnel (125 mm diameter) lined with a cellulose filter paper (5–13 µm pore size, VWR 413), which served as the bottom layer, to form a hybridized middle layer. A suspension of pure CNF in ethanol (0.2 wt%) was then filtered through the filter cake to form a top layer.

The resulting sandwich structure was placed between two steel plates, each lined with two layers of blotting paper (3MM Chr VWR) and pressed under 2 ton-force for 10 s using a hydraulic press (type 25–12-2H, Carver Inc.) at room temperature to remove excess ethanol. The hybrid membranes were then sandwiched between the same two steel plates lined with fresh blotting paper and release paper and pressed under 2 ton-force at 120 °C for 15 min, to dry and consolidate the network. The composition of each hybrid, as well as their sample names, are shown in **Table 1**.

2.5. SHCP-10 Recovery from Spent Hybrid Membranes

An SHCP/CNF-100-10 hybrid membrane was submerged in 75 wt% sulfuric acid at room temperature for 1 h. The reaction was then quenched with 600 mL of ice cold water and centrifuged. After the supernatant was discarded, the polymer was resuspended in water, filtered, and washed until a neutral pH was reached.

2.6. Water Permeance Studies

The water permeance of hybrid membranes was determined using a dead-end cell (HP4750, Sterlitech) with an active filtration area of 1460 mm^2. Distilled water was passed through the membranes under a head pressure of 2 bar at room temperature. The permeate was collected in fractions and the water permeance P was calculated by measuring the volume V forced through the filter using

$$P = \frac{V}{A \cdot t \cdot p} \tag{1}$$

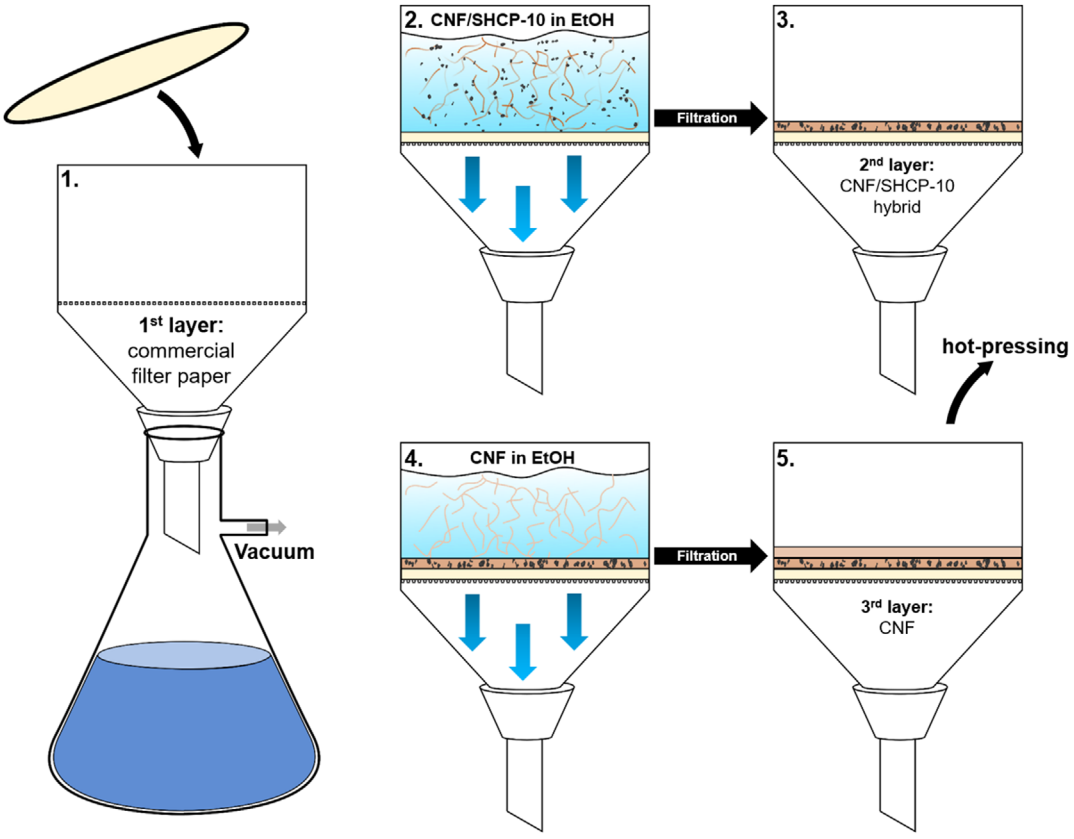

Figure 1. Schematic depiction of the hybrids manufacturing process utilizing a Büchner funnel in analogy to traditional papermaking techniques.

Table 1. Sample code and layer grammages. Note that the middle layer grammage is the combined grammage of both constituents.

Sample Name	CNF/SHCP-10 middle layer [g m^{-1}]	Pure CNF top layer [g m^{-1}]
SHCP/CNF 20-5	20	5
SHCP/CNF 20-10	20	10
SHCP/CNF 20-25	20	25
SHCP/CNF 50-5	50	5
SHCP/CNF 50-10	50	10
SHCP/CNF 50-25	50	25
SHCP/CNF 100-5	100	5
SHCP/CNF 100-10	100	10
SHCP/CNF 100-25	100	25

where A is the active membrane area, t the collection time, and p the driving pressure. To ensure equilibrium was reached, the permeance was measured until a change of $\leq$2% occurred within 1 h.

2.7. Kinetic Studies of Cu^{2+} Adsorption on SHCP-10

The adsorption kinetics of Cu^{2+} on SHCP-10 was tested by suspending 100 mg of polymer in 25 mL of a 10 mmol L^{-1} $CuCl_2$ solution. Samples of 100 µL were taken after 0.5, 1, 1.5, 2, 3, 5, 10, 60, and 1440 min and filtered through a syringe filter to remove any residual polymer. The fractions were analyzed using inductively coupled plasma-mass spectrometry (ICP-MS, Agilent 7800, Agilent Technologies) as this allowed for large numbers of samples to be measured efficiently. The instrument was operated in helium collision mode, to remove possible spectral interferences. Rhodium was added online via a T-piece and used as an internal standard. Quantification was achieved via external calibration with pure element standards. The standard reference material 1643f (Trace elements in water, NIST) was used for quality control. All standards and samples contained 3% nitric acid for stabilization. Adsorption studies were carried out in triplicate at 30, 40, and 50 °C. The measured adsorption capacities at each point in time were fitted using pseudo-first-order and pseudo-second-order kinetic models (Equation (2) and (3), respectively):

$$q_t = q_e\,(1 - e^{-k_1 t}) \tag{2}$$

$$q_t = \frac{k_2 {q_e}^2 t}{1 + k_2 q_e t} \tag{3}$$

where q_t is the uptake of Cu^{2+} [mg g^{-1}] at any given time t [min], q_e the equilibrium adsorption capacity [mg g^{-1}], and k_1 and k_2 the first- and second-order rate constant, respectively. The experimental data was fit with these models using an iterative nonlinear regression fit to reduce potential biases introduced by the uneven temporal spacing of sample collection. The fitting range was adjusted from $t = 0$ to the plateau region, indicating equilibrium (t = 1440 min for 30 °C, t = 60 min for 40 °C and t = 10 min for 50 °C), and the adsorption capacity at 24 h (1440 min) of all samples was reported as the experimental equilibrium adsorption capacity $q_{e,\mathrm{exp}}$. The initial sorption rate h_0 was calculated using the pseudo-second-order model according to Equation (4).

$$h_0 = k_2 {q_e}^2 \tag{4}$$

and the activation energy E_a of the reaction was calculated from the slope of the Arrhenius plot ($\ln(k_2)$ vs. T^{-1}) according to Equation (5).

$$\ln(k_2) = \frac{-E_a}{RT} + \ln(A) \tag{5}$$

2.8. Dynamic Heavy Metal Adsorption Tests of Hybrid Membranes

The dynamic metal adsorption capacity of CNF-SHCP-10 hybrid membranes was tested using a dead-end flow cell with a filtration area of 1460 mm^2. Circular discs were cut from the prepared hybrids and affixed in the cell, which was subsequently filled with 200 mL of $CuCl_2$ solution (2.5 mmol L^{-1}) and pressurized to achieve a flow rate of ≈1 drop s^{-1}. A total of 35 fractions of 5 mL were collected and their concentrations determined by titration, following a procedure previously reported by our group.[45] Briefly, 10 mL of supernatant was diluted in 50 mL water and the pH was adjusted to 10 by addition of an ammonium chloride/ammonia buffer. An aqueous solution of murexide indicator was added to the buffered supernatant until the solution turned yellow. This mixture was subsequently titrated against 0.1 mmol L^{-1} EDTA solution. The solution turned from yellow to red (equilibrium point) to a bright magenta. From the concentration of the supernatant before and after the adsorption experiment, the Cu^{2+} adsorption capacity q of SHCP-10 was calculated according to Equation (6) and (7) by first calculating the mass of adsorbed Cu^{2+} m_{ads} using the Cu^{2+} stock concentration c_S and volume V_S, the titrant concentration c_{EDTA} and volume V_{EDTA}, the molar mass of Cu M_{Cu} (63.5 g mol^{-1}), and the mass of SHCP-10 m_{pol}.

$$m_{\mathrm{ads}} = ((c_S \cdot V_S) - (c_{\mathrm{EDTA}} \cdot V_{\mathrm{EDTA}})) \cdot M_{\mathrm{Cu}} \tag{6}$$

$$q = \frac{m_{\mathrm{ads}}}{m_{\mathrm{pol}}} \tag{7}$$

The concentration of the remaining supernatant in the dead-end cell was also measured. The relative adsorption capacity q was determined from the amount of removed copper in all fractions analogous to the static adsorption tests and normalized to the SHCP-10 content in the respective hybrid. The adsorption capacity per unit area q_A of each hybrid membrane was calculated according to Equation (8) using the filtration area A (1460 mm^2) of the dead-end flow cell.

$$q_A = \frac{m_{\mathrm{ads}}}{A} \tag{8}$$

To evaluate membrane regeneration, 10 mL fractions of HCl solution (0.1 M, 120 mL total) were passed through sample SHCP/CNF 50-10 to desorb Cu^{2+}. The Cu^{2+} concentration in the washback fluid was analyzed as described above. Three adsorption cycles were performed.

2.9. Competitive Adsorption Studies

The capability of SHCP/CNF hybrids to remove common water hardness elements, such as Mg and Ca, and traces of toxic elements such as Sr and Ba were investigated, as well as selectivity. Commercial mineral water (LongLife, Bad Radkersburg, Austria) was diluted in a 1:1 ratio with ultrapure water (170 mL total) and filtered through SHCP/CNF 100-5 at a pressure suitable to reach a permeance of ≈1 drop s^{-1} (0.5–0.8 bar). The eluent was collected in 5–10 mL fractions and analyzed using ICP-MS as this method allowed for the simultaneous analysis of multiple elements. To test the ability of the SHCP/CNF hybrids to remove copper in the presence of the common water hardness elements Mg and Ca, a solution containing 1 mmol L^{-1} of Mg^{2+}, Ca^{2+}, and Cu^{2+} was prepared by diluting 101.7 mg of $MgCl_2{\cdot}6H_2O$, 55.5 mg of $CaCl_2$, and 67.2 mg of anhydrous $CuCl_2$ in 500 mL of deionized water. This solution was treated in the same manner as the previously described mineral water and analyzed via ICP-MS.

2.10. Particle Rejection Tests

To test the ultrafiltration capability of the manufactured membranes, 10 mL of a Au nanoparticle suspension (10 nm, 6×10^{11} particles per mL) were pushed through a 25 mm-diameter SHCP/CNF-20-5 membrane at 2 bar of pressure using a dead-end flow cell. The concentration of the eluent was determined by UV–vis spectroscopy (Agilent 8543 UV–vis Spectroscopy System, Agilent Technologies) using the absorption peak at 524 nm.

3. Results and Discussion

3.1. Sulfonated Hypercrosslinked Polymer Characterization

The full chemical and physical characterization of SHCP-10 is provided in ESI Section S1. The chemical composition and physical properties agree with our previous findings.[46]

3.2. Copper Adsorption Kinetics on SHCP-10

The results of the adsorption kinetic studies (**Table 2** and **Figure 2**) suggest that the pseudo-second-order model gives an accurate representation of the uptake mechanism of Cu^{2+} on SHCP-10, in agreement with James et al.[36] who found similar results for the adsorption of Sr and Cs. Analyzing the temperature dependency of k_2 via an Arrhenius plot yielded an activation energy of 128 kJ mol^{-1} which, along with the pseudo-second-order nature of the uptake curves, suggests that the process is chemisorption based.[47] The adsorbate interacts with specific binding sites—in this case the sulfonate groups—on the adsorbent's surface.

The experimental and fitted q_e values put SHCP-10 in the same order of magnitude as a commercial IER AmberSep M4195 UPS (50 mg g^{-1}) (Product data sheet AmberSepTM M4195 and AmberSepTM M4195 UPS Chelating Resins. Link in: https://www.dupont.com/content/dam/dupont/amer/us/en/water-solutions/public/documents/en/IER-AmberSep-M4195-and-M4195-UPS-PDS-45-D00810-en.pdf accessed on 18.01.2024) or adsorptive ultrafiltration membranes derived from polyvinyltetrazole-co-polyacrylonitrile (45 mg g^{-1})[21] and significantly outperform phosphorylated nanocellulose fibers (20 mg g^{-1}).[48] The molar adsorption capacity of copper for SHCP-10 is comparable to those for other SHCPs reported elsewhere when adsorbing Sr^{2+} and Cs^{1+} ions and considering the ionic charge.[36]

3.3. Manufacture of Three-Layered SHCP/CNF Hybrid Membranes

The membrane preparation procedure was heuristically optimized over several preliminary tests, and issues, such as membrane cracking, low mechanical robustness, poor filtration performance, and heterogeneity of the polymer dispersion (Figure S2-1, Supporting Information) had to be overcome. Eventually, ethanol was chosen as suspension medium as it produced CNF membranes with high porosity and flux[49] and resulted in a uniform SHCP-10 dispersion, which after filtration produced a homogenous distribution of SHCP-10 throughout the adsorption layer.

The general structure and scanning electron microscopy (SEM) images of an SHCP/CNF hybrid membrane are depicted in **Figure 3**, showing a uniform, tight network of CNFs forming the top layer, small SHCP-10 particles embedded within a CNF matrix for the middle layer, and large fibers constituting the commercial filter paper. An increasing middle layer grammage of the hybrids led to a darker color of the resulting filter cake (Figure 3), as a thicker layer of the brownish-black SHCP-10 was deposited.

3.4. Water Permeance of SHCP/CNF Hybrid Membranes

The equilibrium water permeance of the manufactured hybrid membranes is shown in **Figure 4**A and was tested using a dead-end flow cell (Figure 4B). The permeance of a typical measurement is depicted in Figure S3-1 (Supporting Information), showing the gradual decrease of the permeance with filtration time

Table 2. Parameters obtained by fitting the experimental data of the adsorption of Cu^{2+} on SHCP-10 to pseudo-first- and second-order models.

		Pseudo-first-order-kinetic model			Pseudo-second-order-kinetic model			
T [°C]	$q_{e,exp}$ [mg g^{-1}]	$q_{e,cal}$ [mg g^{-1}]	k_1 [min^{-1}]	R^2	$q_{e,cal}$ [mg g^{-1}]	k_2 [g mg^{-1} min^{-1}]	h_0 [mg g^{-1} min^{-1}]	R^2
30	55 ± 5	54	0.34	0.9459	57	0.0090	29	0.9724
40	55 ± 4	47	2.5	0.8845	49	0.094	230	0.9720
50	59 ± 9	60	4.4	0.9276	62	0.20	770	0.9634

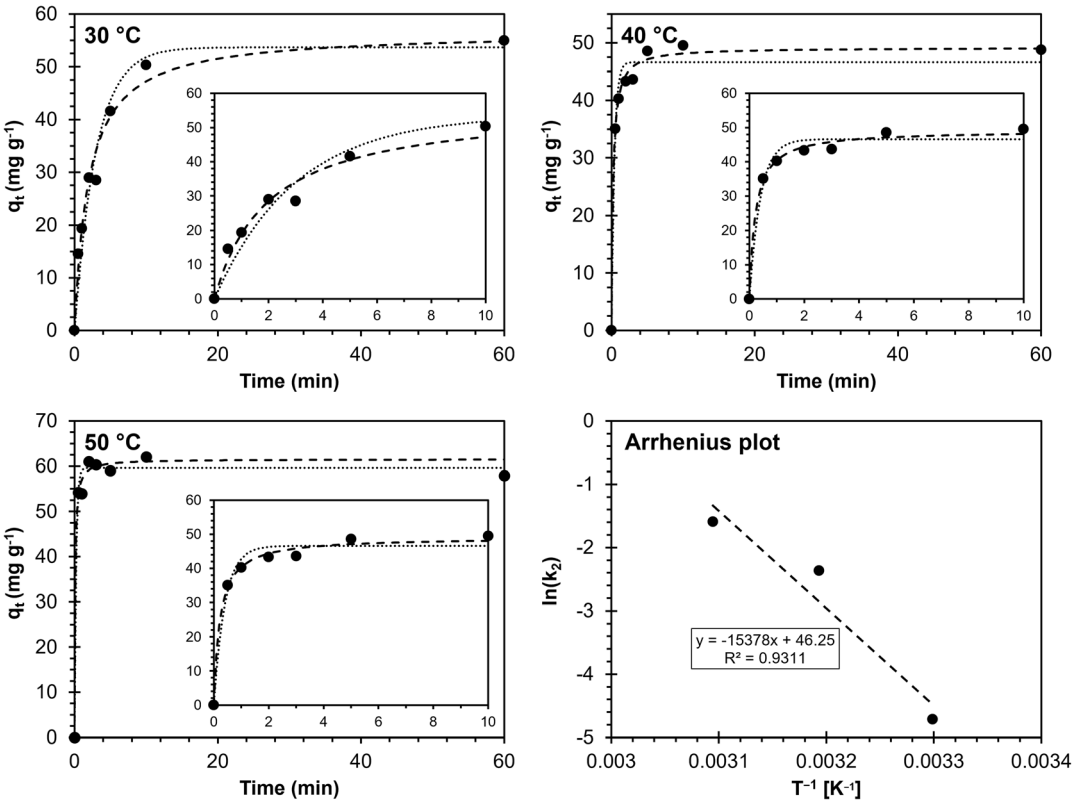

Figure 2. Adsorption studies at different temperatures T. The experimental data is depicted as solid dots, the pseudo-first-order and the pseudo-second-order model are represented by dotted and dashed lines, respectively. The bottom-right graph presents the Arrhenius plot including the fitting function.

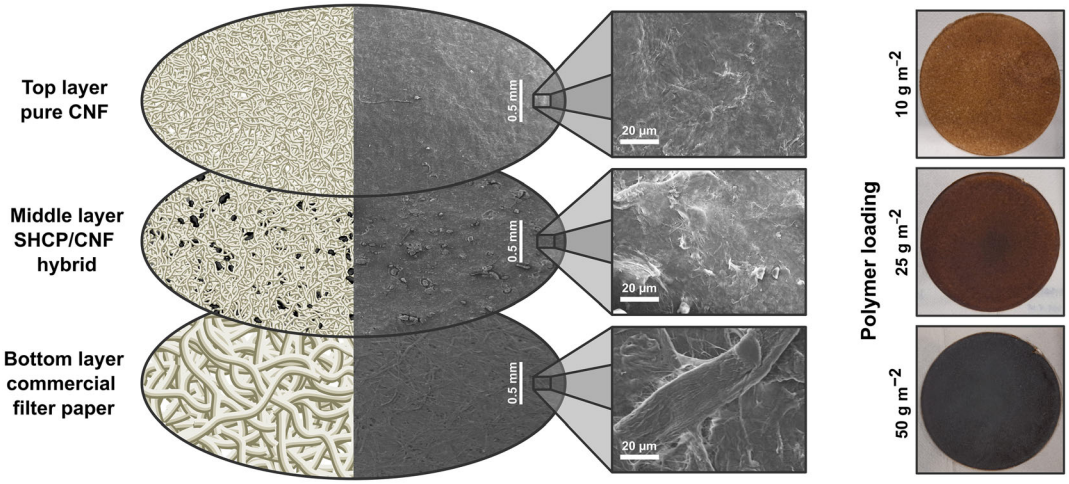

Figure 3. Composition of three-layer SHCP/CNF hybrid membranes with accompanying scanning electron micrographs (left) and photographs of wet hybrid membrane filter cake precursors (membrane diameters are 125 mm) with varying middle layer polymer loading (right).

until a stable plateau was reached. The drop in permeance was caused by compaction of the network under pressure, reducing the thickness and thus pore volume of the membrane. Membrane compaction led to a reduction in the amount of water able to pass the membrane per unit time.[29,50] Hybrid membranes with higher grammage reached equilibrium permeance faster, with SHCP/CNF 100-25 equilibrating almost immediately. Reducing the thickness of the top layer increased the permeance of the hybrid membranes, indicating that the permeance is primarily controlled by the top layer thickness.[29,50]

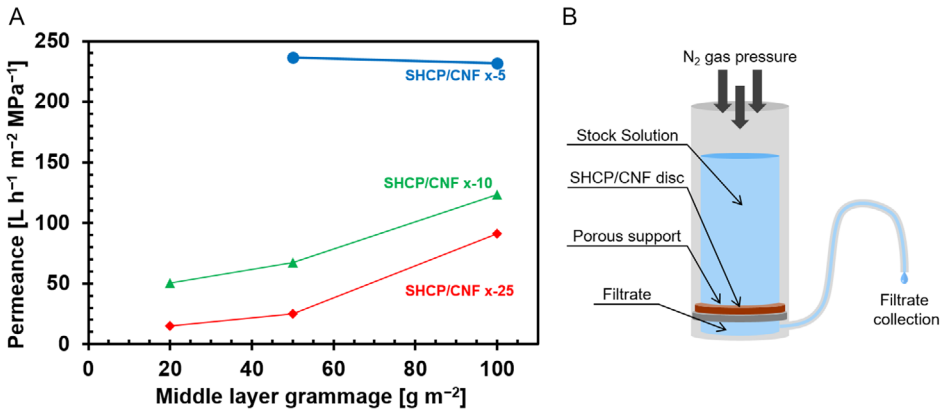

Figure 4. A) Equilibrium permeance of SHCP/CNF hybrid membranes as a function of middle and top layer grammage and B) a schematic depiction of the dead-end cell test setup. Note: the errors are too small to be shown. Lines are provided to guide the eye and do not represent additional data points.

Thicker middle layers, that is, higher SHCP-10 loading within the hybrids, led to an increased permeance for samples with 10 and 25 gsm top layers (SHCP/CNF x-25 and SHCP/CNF x-10, respectively), likely due to the incorporation of SHCP-10 particles into the CNF matrix increasing pore volume and aiding channel formation. Hybrid membranes with 5 gsm top layers did not follow this trend as they already exhibited an overall much higher permeance. The water permeance of SHCP/CNF 20-5 could not be tested as these hybrids were prone to pinhole formation due to the low cellulose content in both the middle and top layers.

To monitor possible SHCP-10 leaching, the sulfur content of eluent fractions was determined using ICP-MS and compared to that of the used DI water (Figure S3-2, Supporting Information). The eluent contained no elevated sulfur content except for a marginal increase in the first fraction. The data suggests no continuous release of SHCP-10 during use.

3.5. Copper Adsorption Capacity and Regeneration of SHCP/CNF Hybrid Membranes

We determined the influence of the middle and top layer grammages of the hybrid membranes on Cu^{2+} adsorption capacity by dynamic adsorption (**Figure 5**). Higher SHCP-10 loading led to a slight decrease in the relative adsorption capacity per gram of SHCP-10 (Figure 5A) yet increased the absolute Cu^{2+} adsorption capacity per membrane area (Figure 5B). The reduced relative capacity was attributed to the increased concentration of inaccessible SHCP-10 particles or the formation of agglomerates. The relative adsorption capacity of SHCP-10 in all hybrid membranes exceeded that of bulk SHCP-10 in static adsorption tests, which was attributed to enhanced surface availability and the continuous replacement of depleted Cu^{2+} solution.

We regenerated SHCP/CNF 50-10 by flushing with 120 mL of 0.1 M HCl solution (Figure 5A inset). SHCP/CNF 50-10 was chosen as it was the median for both the investigated top and

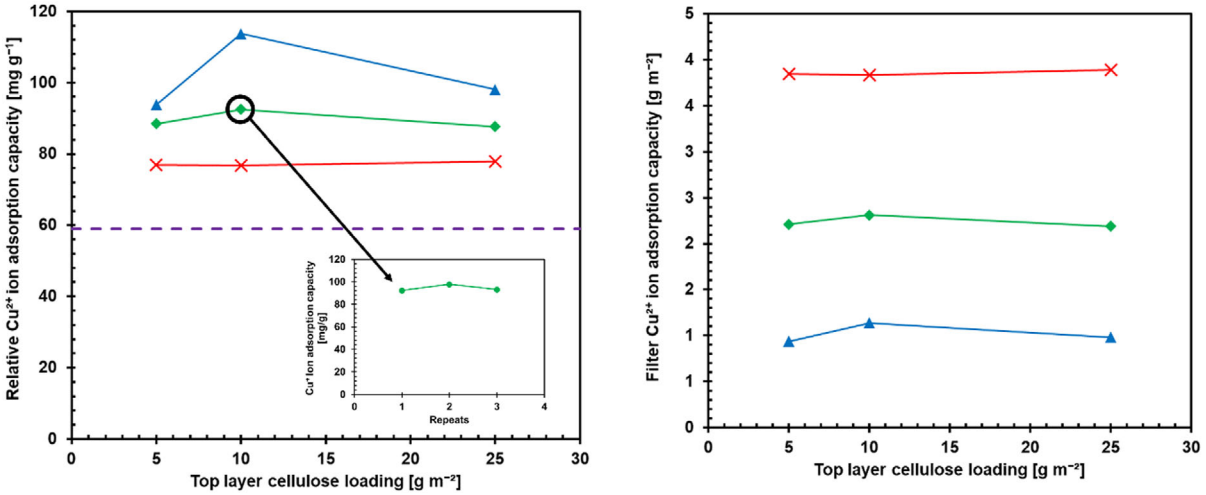

Figure 5. A) Relative Cu^{2+} adsorption capacity per gram of SHCP-10 as a function of middle and top layer grammages of SHCP/CNF hybrid membranes and its performance after two regeneration cycles (inset). The purple dashed line corresponds to the highest batch sorption capacity of SHCP-10. B) The absolute copper adsorption capacity per m^2 of hybrid membrane. Note: Lines are provided as a guide to the eye and do not represent additional data points.

middle layer loading. We found that the relative Cu^{2+} adsorption capacity of the reused membrane did not decrease, demonstrating recyclability. Titration of the eluent fractions during regeneration showed that most of the copper was desorbed by the first 20–40 mL of HCl (Figure S4-1, Supporting Information), demonstrating rapid regeneration and reusability of the hybrid membranes.

A comparison of the copper ion adsorption capacities of SHCP-10 and SHCP/CNF hybrids with other materials for which regeneration is also reported is shown in Table S4-1, Supporting Information. SHCP-10 and its hybrids show an above average maximum Cu^{2+} adsorption capacity, ranging from 55 mg g^{-1} to 113.9 mg g^{-1}. While SHCP/CNF hybrids do not possess the outstanding uptake capacities of, for example, glycine-based magnetic nanoparticles[51] or oxidized multiwalled carbon nanotubes,[52] the ease of manufacture and ability to regenerate them without loss of material or function sets SHCP/CNF hybrids apart from a wide range of adsorbents.

3.6. Competitive Adsorption of Metal Ions on SHCP/CNF Hybrids

We performed a competitive adsorption study on commercially available mineral water using SHCP/CNF 100-5, as this hybrid combined high permeance with high absorption capacity per unit area. Commercial mineral water was chosen as a complex feed containing the most important water hardness elements, Ca and Mg, as well as traces of other problematic alkaline Earth metals including Sr and Ba. The radioactive isotopes of strontium are used as radiopharmaceuticals (^{89}Sr)[53] and are present in nuclear waste and fallout (^{90}Sr).[54] Barium is commonly used as a weighing agent in drilling fluids of oil and gas wells[55] and is considered neurotoxic. The relative breakthrough curves (i.e., the percentage of each ion compared to its feed concentration) are presented in **Figure 6**.

The relative breakthrough curves (Figure 6) show the capability of SHCP/CNF hybrids to exchange ions effectively and, thus, remove, for example, alkaline Earth metals from solutions. The tested concentrations simulate naturally occurring conditions, in which Mg and Ca are present in significant excess of Ba^{2+}, present in trace amounts. In the first fraction, 60–70% of all investigated ions were removed. In subsequent fractions, the removal of Ca^{2+} and Mg^{2+} ions decreased due to saturation of sulfonate sites. In contrast, the removal of Ba^{2+} and Sr^{2+} from the stream continued for the entirety of the experiment. The removal efficiency of each alkaline Earth metal appeared to follow that of the solubility of the sulfate salts of the individual ions: $MgSO_4$ ($pK_{sp} = -0.981$) > $CaSO_4$ ($pK_{sp} = 3.64$) > $SrSO_4$ ($pK_{sp} = 6.46$) > $BaSO_4$ ($pK_{sp} = 9.97$).[55] The state of chemical equilibrium of Ca^{2+} and Mg^{2+} ions with SHCP-10's sulfate moieties implies that there are always a number of free sulfonate sites, which could also be repopulated with the much less soluble Sr^{2+} and Ba^{2+} counterions, leading to an increased relative concentration of Mg and Ca in the permeate of later fractions.

The ability of SHCP/CNF hybrids to adsorb Cu^{2+} ions in the presence of Mg^{2+} and Ca^{2+} was tested on an aqueous solution containing 1 mmol L^{-1} of each ion (**Figure 7**). The solution was formulated to simulate water with copper-contaminated wastewater with high-to-medium hardness, as can be found for example in the effluent wastewater of mirror-making industries.[48]

The breakthrough curves of water containing Cu^{2+}, Mg^{2+}, and Ca^{2+} ions follow the same trend as those of commercial mineral water and show that the membranes are able to adsorb copper ions in the presence of common water hardness elements, albeit without any specificity toward copper. The marginal selectivity toward individual ions once more follows the solubility of the

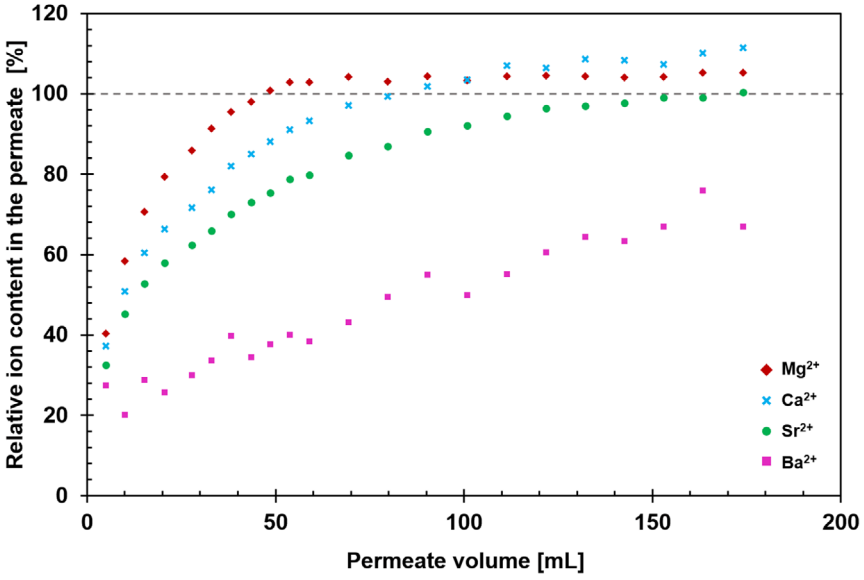

Figure 6. Relative breakthrough curves of various ions found in commercial mineral water upon treatment with hybrid membrane SHCP/CNF 100-5. Typical relative standard deviations of the measurement are 2–3% and are not shown in the graph for legibility. The absolute concentrations of the relevant metal ions in the stock solution before passing through SHCP/CNF 100–5 were: $Mg^{2+} = 82$ mg L^{-1}, $Ca^{2+} = 109$ mg L^{-1}, $Sr^{2+} = 3.2$ mg L^{-1}, and $Ba^{2+} = 0.42$ mg L^{-1}.

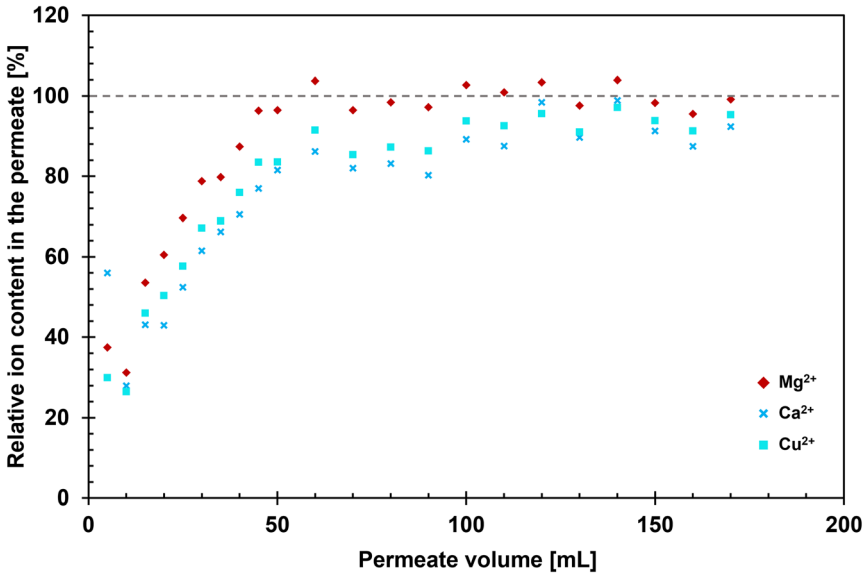

Figure 7. Relative breakthrough curves of an artificial wastewater sample containing Mg^{2+}, Ca^{2+}, and Cu^{2+} ions upon treatment with hybrid membrane SHCP/CNF 100-5. Typical relative standard deviations of the measurement are 2–3% and are not shown in the graph for legibility. The absolute concentrations of the metal ions in the solution before passing through SHCP/CNF 100-5 were 1 mmol L^{-1}, corresponding to $Ca^{2+} = 40$ mg L^{-1}, $Mg^{2+} = 24$ mg L^{-1}, and $Cu^{2+} = 63.5$ mg L^{-1}.

respective ions' sulfate salts ($MgSO_4$ ($pK_{sp} = -0.981$) > $CuSO_4$ ($pK_{sp} = 1.72$) > $CaSO_4$ ($pK_{sp} = 4.31$)).[55]

3.7. Ultrafiltration Ability of SHCP/CNF Hybrid Membranes

We assessed the ultrafiltration capability of our hybrid membranes via size exclusion of 10 nm Au nanoparticles. SHCP/CNF 20-5 was chosen as the substrate as it was the thinnest sample produced in our study, and it is assumed that thicker samples (i.e., hybrids with higher top and/or middle layer grammage) will display at least equivalent or rather improved particle rejection. The UV–vis spectra (Figure S5-1, Supporting Information) of the Au nanoparticle suspension feed and permeate indicated full rejection of the nanoparticles. The full rejection of 10 nm particles confirms that SHCP/CNF hybrid membranes are able to remove, for example, microplastics (smallest reported sizes of ≈1 µm)[56] and/or even the smallest existing viruses, which are ≈20 nm in size.[57,58]

During permeance, adsorption, and particle rejection testing, the samples mounted in dead-end flow cells were subjected to hydraulic pressures of up to 2 bar, without failure occurring. The commercial filter paper used as support constitutes a major portion of the hybrid membranes; thus, its mechanical properties determine that of the hybrids. The filter paper used has a wet and dry burst pressure of 0.6 and 1.9 bar, respectively (VWR product catalogue "VWR for filtration" Link in: https://media.vwr.com/ecatalog/index.html?catalog=EU_AIO_Filtration_2015/EN&shop=uk accessed 10.04.2024), suitable for a myriad of common filtration and ion exchange applications.

3.8. Recovery of SHCP-10 from SHCP/CNF Hybrids

The recovery of SHCP-10 from a used hybrid membrane was investigated by controlled acid digestion of the surrounding CNF matrix. Full polymer characterization was performed and showed no significant change compared to as-synthesized SHCP-10 apart from a slight increase in carbon content and a miniscule decrease in surface area. These changes were due to the presence of undigested carbonization products from the degradation of cellulose during acid digestion (ESI Section 1).

4. Conclusion

We introduced HCP–cellulose nanofibril layered hybrid membranes to utilize the advantageous features of both materials. CNF constitutes the carrier material, lending structural stability to the otherwise powderous SHCP-10 while functioning as a tight ultrafiltration network facilitating rejection of nanoparticles down to 10 nm. The incorporation of SHCP-10 into the hybrid membrane increased water permeance. SHCP-10 adsorbed high concentrations of Cu^{2+} from aqueous solutions in both static and dynamic experiments (up to 114 mg g^{-1}). The most promising membrane, SHCP/CNF 100-5, was used in the treatment of a commercial mineral water containing not only standard water hardness metal ions (Mg^{2+} and Ca^{2+}) but also trace amounts of toxic heavy metals (Sr^{2+}, and Ba^{2+}). In addition to water softening, hybrid membranes also removed trace toxic Sr^{2+} and Ba^{2+} even after saturation of sulfonate groups in the presence of excess concentrations of Ca^{2+} and Mg^{2+}.

Supporting Information

Supporting Information is available from the Wiley Online Library or from the author.

Acknowledgements

The authors thank Sebastian Leclerc, Lena Palm, and Julia Zolles for their assistance in laboratory experiments and Johannes Theiner for performing elemental analysis measurements. F.M. and P.S. greatly acknowledge the financial support provided by the University of Vienna through the Institute of Materials Chemistry and Research (317000) and DoSChem, respectively.

Conflict of Interest

The authors declare no conflict of interest.

Author Contributions

Florian Mayer and **Robert Woodward** conceived the idea. **Florian Mayer** performed ultrafiltration and metal adsorption experiments. **Florian Mayer** and **Paul Schweng** prepared hybrid membranes, performed flux tests, and conducted recovery experiments. **Paul Schweng** prepared and characterized SHCP-10. **Sebastian Hummer** conducted kinetics experiments. **Simone Braeuer** and **Gunda Koellensperger** analyzed metal ion content of solutions. **Alexander Bismarck** made **Florian Mayer** perform competitive adsorption measurements, statistics, and ensure reproducibility. **Alexander Bismarck**, **Andreas Mautner**, and **Robert Woodward** supervised this work. **Florian Mayer**, **Robert Woodward**, and **Alexander Bismarck** prepared the draft manuscript and all authors discussed, edited, and commented on the manuscript. **Alexander Bismarck** secured funding.

Data Availability Statement

The data that support the findings of this study are available from the corresponding author upon reasonable request.

Keywords

hybrid membranes, hypercrosslinked polymers, ion exchange, nanocellulose, ultrafiltration

Received: April 23, 2024
Revised: July 19, 2024
Published online: August 11, 2024

[1] L. Joseph, B. M. Jun, J. R. V. Flora, C. M. Park, Y. Yoon, *Chemosphere* **2019**, *229*, 142.
[2] C. Zamora-Ledezma, D. Negrete-Bolagay, F. Figueroa, E. Zamora-Ledezma, M. Ni, F. Alexis, V. H. Guerrero, *Environ. Technol. Innovation* **2021**, *22*, 101504.
[3] A. A. Koelmans, P. E. Redondo-Hasselerharm, N. H. M. Nor, V. N. de Ruijter, S. M. Mintenig, M. Kooi, *Nat. Rev. Mater.* **2022**, *7*, 138.
[4] B. R. Stern, M. Solioz, D. Krewski, P. Aggett, T. C. Aw, S. Baker, K. Crump, M. Dourson, L. Haber, R. Hertzberg, C. Keen, B. Meek, L. Rudenko, R. Schoeny, W. Slob, T. Starr, *J. Toxicol. Environ. Health, Part B* **2007**, *10*, 157.
[5] G. J. Brewer, *Chem. Res. Toxicol.* **2010**, *23*, 319.
[6] A. K. Badawi, R. S. Salama, M. M. M. Mostafa, *RSC Adv.* **2023**, *13*, 19335.
[7] N. A. A. Qasem, R. H. Mohammed, D. U. Lawal, *npj Clean Water* **2021**, *4*, 36.
[8] J. S. D. Jeremias, J.-Y. Lin, M. L. P. Dalida, M.-C. Lu, *J. Environ. Chem. Eng.* **2023**, *11*, 109336.
[9] E. C. Emenike, A. G. Adeniyi, P. E. Omuku, K. C. Okwu, K. O. Iwuozor, *J. Water Process Eng.* **2022**, *47*, 102715.
[10] P. S. Goh, K. C. Wong, A. F. Ismail, *Desalination* **2022**, *521*, 115377.
[11] F. Y. AlJaberi, S. A. Ahmed, H. F. Makki, A. S. Naje, H. M. Zwain, A. D. Salman, T. Juzsakova, S. Viktor, B. Van, P. C. Le, D. D. La, S. W. Chang, M. J. Um, H. H. Ngo, D. D. Nguyen, *Sci. Total Environ.* **2023**, *867*, 161361.
[12] H. Nassrullah, S. F. Anis, R. Hashaikeh, N. Hilal, *Desalination* **2020**, *491*, 114569.
[13] I. G. Wenten, Khoiruddin, *Desalination* **2016**, *391*, 112.
[14] Z. S. Tai, M. H. D. Othman, K. N. Koo, J. Jaafar, *Desalination* **2023**, *553*, 116484.
[15] I. Gehrke, A. Geiser, A. Somborn-Schulz, *Nanotechnol. Sci. Appl.* **2015**, *8*, 1.
[16] L. Lin, H. Yang, X. Xu, *Front. Environ. Sci.* **2022**, *10*, https://doi.org/10.3389/fenvs.2022.880246.
[17] A. Mautner, *Polym. Int.* **2020**, *69*, 741.
[18] L. Dong, L. Hou, Z. Wang, P. Gu, G. Chen, R. Jiang, *J. Hazard. Mater.* **2018**, *359*, 76.
[19] M. Hua, S. Zhang, B. Pan, W. Zhang, L. Lv, Q. Zhang, *J. Hazard. Mater.* **2012**, *211–212*, 317.
[20] W. J. Koros, Y. H. Ma, T. Shimidzu, *Pure Appl. Chem.* **1996**, *68*, 1479.
[21] M. Kumar, R. Shevate, R. Hilke, K.-V. Peinemann, *Chem. Eng. J.* **2016**, *301*, 306.
[22] J. L. Weidman, R. A. Mulvenna, B. W. Boudouris, W. A. Phillip, *Langmuir* **2015**, *31*, 11113.
[23] F. Farjadian, S. Schwark, M. Ulbricht, *Polym. Chem.* **2015**, *6*, 1584.
[24] A. Etale, A. J. Onyianta, S. R. Turner, S. J. Eichhorn, *Chem. Rev.* **2023**, *123*, 2016.
[25] A. Barhoum, K. Deshmukh, M. L. Garcia-Betancourt, S. Alibakhshi, S. M. Mousavi, A. Meftahi, M. S. K. Sabery, P. Samyn, *Carbohydr. Polym.* **2023**, *317*, 121057.
[26] A. K. Rana, E. Mostafavi, W. F. Alsanie, S. S. Siwal, V. K. Thakur, *Ind. Crops Prod.* **2023**, *194*, 116331.
[27] A. Mautner, F. Mayer, M. Hervy, K. Y. Lee, A. Bismarck, *Philos. Trans. R. Soc., A* **2018**, *376*, https://doi.org/10.1098/rsta.2017.0043.
[28] D. Klemm, E. D. Cranston, D. Fischer, M. Gama, S. A. Kedzior, D. Kralisch, F. Kramer, T. Kondo, T. Lindström, S. Nietzsche, K. Petzold-Welcke, F. Rauchfuß, *Mater. Today* **2018**, *21*, 720.
[29] A. Mautner, K.-Y. Lee, T. Tammelin, A. P. Mathew, A. J. Nedoma, K. Li, A. Bismarck, *React. Funct. Polym.* **2015**, *86*, 209.
[30] R. Das, T. Lindstrom, P. R. Sharma, K. Chi, B. S. Hsiao, *Chem. Rev.* **2022**, *122*, 8936.
[31] Z. Karim, S. Claudpierre, M. Grahn, K. Oksman, A. P. Mathew, *J. Membr. Sci.* **2016**, *514*, 418.
[32] L. Tan, B. Tan, *Chem. Soc. Rev.* **2017**, *46*, 3322.
[33] M. Gomez-Suarez, Y. Chen, J. Zhang, *Polym. Chem.* **2023**, *14*, 4000.
[34] A. Blocher, F. Mayer, P. Schweng, T. M. Tikovits, N. Yousefi, R. T. Woodward, *Mater. Adv.* **2022**, *3*, 6335.
[35] S. Bhunia, B. Banerjee, A. Bhaumik, *ChemComm* **2015**, *51*, 5020.
[36] A. M. James, S. Harding, T. Robshaw, N. Bramall, M. D. Ogden, R. Dawson, *ACS Appl. Mater. Interfaces* **2019**, *11*, 22464.
[37] C. E. Harland, *Ion Exchange: Theory And Practice*, The Royal Society of Chemistry, London **1994**.
[38] Z. A. Qiao, S. H. Chai, K. Nelson, Z. Bi, J. Chen, S. M. Mahurin, X. Zhu, S. Dai, *Nat. Commun.* **2014**, *5*, 3705.
[39] A. Chinnappan, W.-J. Chung, H. Kim, *J. Mater. Chem. A* **2015**, *3*, 22960.
[40] H. Zhou, A. Akram, A. J. C. Semiao, R. Malpass-Evans, C. H. Lau, N. B. McKeown, W. Zhang, *J. Membr. Sci.* **2022**, *644*, 120172.
[41] C. H. Lau, X. Mulet, K. Konstas, C. M. Doherty, M. A. Sani, F. Separovic, M. R. Hill, C. D. Wood, *Angew. Chem. Int., Ed. Engl.* **2016**, *55*, 1998.
[42] R. S. Bhavsar, T. Mitra, D. J. Adams, A. I. Cooper, P. M. Budd, *J. Membr. Sci.* **2018**, *564*, 878.

[43] S. Josset, P. Orsolini, G. Siqueira, A. Tejado, P. Tingaut, T. Zimmermann, *Nord. Pulp Pap. Res. J.* **2014**, *29*, 167.
[44] F. Mayer, A. Prado-Roller, A. Mautner, A. Bismarck, *Cellulose* **2024**, *31*, 1533.
[45] J. Janesch, M. Jones, M. Bacher, E. Kontturi, A. Bismarck, A. Mautner, *React. Funct. Polym.* **2020**, *146*, 104428.
[46] P. Schweng, F. Mayer, D. Galehdari, K. Weiland, R. T. Woodward, *Small* **2023**, *19*, e2304562.
[47] V. J. Inglezakis, A. A. Zorpas, *Desalin. Water Treat.* **2012**, *39*, 149.
[48] P. Liu, P. F. Borrell, M. Bozic, V. Kokol, K. Oksman, A. P. Mathew, *J. Hazard. Mater.* **2015**, *294*, 177.
[49] A. Mautner, A. Bismarck, *Carbohydr. Polym.* **2021**, *251*, 117130.
[50] A. Mautner, K. Y. Lee, P. Lahtinen, M. Hakalahti, T. Tammelin, K. Li, A. Bismarck, *ChemComm* **2014**, *50*, 5778.
[51] N. C. Feitoza, T. D. Goncalves, J. J. Mesquita, J. S. Menegucci, M. K. Santos, J. A. Chaker, R. B. Cunha, A. M. Medeiros, J. C. Rubim, M. H. Sousa, *J. Hazard. Mater.* **2014**, *264*, 153.
[52] T. C. Egbosiuba, A. S. Abdulkareem, *J. Mater. Res. Technol.* **2021**, *15*, 2848.
[53] R. G. Robinson, *JAMA, J. Am. Med. Assoc.* **1995**, *274*, 420.
[54] J. G. Reynolds, G. A. Cooke, D. L. Herting, *J. Radioanal. Nucl. Chem.* **2020**, *326*, 435.
[55] D. R. Lide, *CRC Handbook of Chemistry and Physics*, 84th ed., CRC Press, Boca Raton, FL **2003**.
[56] M. Kooi, A. A. Koelmans, *Environ. Sci. Technol. Lett.* **2019**, *6*, 551.
[57] T. S. Baker, N. H. Olson, S. D. Fuller, *Microbiol. Mol. Biol. Rev.* **1999**, *63*, 862.
[58] J. Louten, *Essential Human Virology*, Elsevier, Amsterdam **2016**, pp. 19–29.

Supporting Information

Best of both worlds: Adsorptive ultrafiltration nanocellulose-hypercrosslinked polymer hybrid membranes for metal ion removal

Florian Mayer[a], Paul Schweng[a], Simone Braeuer[b], Gunda Koellensperger[b], Andreas Mautner[a,c], Robert Woodward[a], Alexander Bismarck[a,d,e]

[a] Institute of Materials Chemistry and Research, Faculty of Chemistry, University of Vienna, Waehringer Straße 42, 1090, Vienna, Austria.

[b] Institute of Analytical Chemistry, Faculty of Chemistry, University of Vienna, Waehrigner Straße 38, 1090, Vienna, Austria

[c] Institute of Environmental Biotechnology, IFA-Tulln, University of Natural Resources and Life Sciences, Vienna, Konrad-Lorenz-Straße 20, 3430, Tulln an der Donau, Austria

d Division of Materials Science, Department of Engineering Sciences and Mathematics, Luleå University of Technology, Luleå, 971 87, Sweden

e Department of Chemical Engineering, Imperial College London, South Kensington Campus, London SW7 2AZ, United Kingdom

SI 1. Sulfonated hypercrosslinked polymer characterisation

Finely ground samples were analysed using Fourier-transform infrared (FTIR) spectroscopy using a Bruker Tensor II FTIR spectrometer equipped with a Platinum ATR module (Bruker) and constantly flushed with dry air. Spectra were acquired in double-sided forward backward acquisition mode with a resolution of 4 cm−1 in the range of 400-4000 cm^{-1} and the obtained spectra were averaged over a total of 32 scans using Blackman–Harris 3-term apodisation function and a zero-filling factor of 4.

Thermogravimetric analyses were performed using a TA instruments Discovery TGA. Platinum sample pans were loaded with approximately 20 mg of sample and ramped at a rate of 10 °C·min^{-1} under either air or N_2 gas flow (100 mL·min^{-1}) from room temperature to 800 °C.

Elemental analysis was performed using a Eurovector EA 3000 CHNS-O Elemental Analyser. 0.75-3.0 mg of each sample was weighed into tin vials (4×6 mm) using a microbalance (Sartorius, ME 5 OCE). Samples were run in triplicate. The operating temperatures for the combustion and reduction were 1000 °C (1480 °C for O analysis) and 750 °C, respectively. He (99.999+) was used as carrier gas.

Porous properties of SHCP were determined at –196 °C using N_2 gas sorption (TriStar II, Micromeritics). Samples were degassed (FlowPrep 060, Micromeritics) for at least ten hours at 120 °C under constant N_2 flow. For surface area calculations the Brunauer-Emmett-Teller (BET) model was applied to the adsorption branch in the range of 0.05-0.2 P/P_0. The total pore volume was calculated from the amount of N2 adsorbed at P/P_0 = 0.97. For the determination of the micropore volume the t-plot method was applied to the adsorption branch in the range of 0.15-0.4 P/P_0.

The elemental composition of SHCP-10 was determined by X-ray photoelectron spectroscopy (Nexsa, Thermo Fischer) using Al K_α X-rays at 72 W using a spot size with 400 µm diameter. Survey spectra with resolutions of 1 eV, a pass energy of 200 eV and a dwell time of 10 ms were recorded and averaged over 50 scans. High resolution spectra for carbon (C1s 279-298 eV), oxygen (O1s 525-545 eV), nitrogen (N1s 392-410 eV), chlorine (Cl2p 190-210 eV) and sulfur (S2p 157-175 eV) were recorded with a resolution of 0.1 eV, a pass energy of 50 eV, a dwell time of 50 ms, and were averaged over 30 scans. The spectra were analysed using the software package Avantage (ver. 5.9931, Thermo Scientific, East Grinstead, UK) and the elemental composition calculated from the respective peak areas using the included ALTHERMO1 scaling factor database.

The size distribution of SHCP-10 particles was determined via LASER-diffraction testing using a HELOS KR (Sympatec GmbH, Clausthal-Zellerfed, Germany) fitted

with a RODOS dry dispersion unit and utilising the incorporated SUBMICRON Fourier-lens system with a focal length of 50 nm. The experiment was carried out in duplicate.

The successful synthesis of SHCP-10 was confirmed by ATR-FTIR (Fig. SI 1-1). Bands assigned to S=O and C-S stretching vibrations were found at 1140 cm^{-1} and 600 cm^{-1}, respectively.

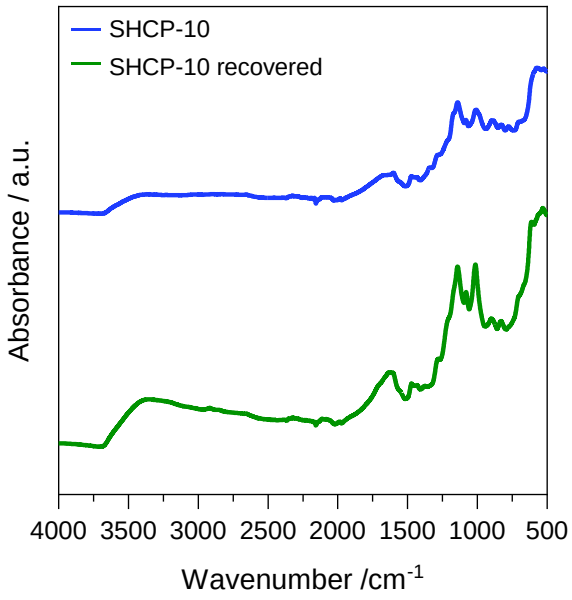

Figure SI 1-1. ATR-FTIR spectra of pristine and recovered SHCP-10

The elemental composition of SHCP-10 was determined via X-ray photoelectron spectroscopy (Table SI 1-1) and showed a sulfur content of 6.4 at.-%, in good agreement with our previous work. Elemental analysis (Table SI 1-2) gave sulfur values of ~3.8 at.-%, lower than that measured by XPS. The difference in sulfur content between the two methods is attributed to water adsorption due to the strongly hydrophilic nature of SHCP-10 prior to EA, [1] as well as the inability of XPS to consider

hydrogen. The actual sulfur content likely lies somewhere between the results of XPS and EA. [2] ,

Table SI 1-1 Atomic composition of SHCP 10 after synthesis and after reclaim via acid digestion as determined by XPS

	C (at.%)	O (at.%)	S (at.%)
SHCP-10	70.6	20.8	6.4
SHCP-10_recycled	72.2	19.9	6.0

Table SI 1-2. Atomic composition of SHCP 10 after synthesis and after reclaim via acid digestion as determined by elemental analysis

	C (wt.%)	H (wt.%)	N (wt.%)	O (wt.%)	S (wt.%)
SHCP-10	42.07 ± 0.39	4.73 ± 0.13	0.05 ± 0.00	36.70 ± 0.16	13.41 ± 0.09
SHCP-10 recovered	50.65 ± 0.33	4.32 ± 0.09	0.20 ± 0.01	31.58 ± 1.01	10.83 ± 0.14

The N_2 gas sorption isotherms (Figure SI 1-2) showed characteristics of both type I and type IV(a), as described by IUPAC. [3] A steep slope in the low-pressure region ($P/P_0 < 0.1$) confirmed microporosity and the hysteresis stemming from capillary condensation in the high relative pressure region ($P/P_0 > 0.9$), is indicative of mesopores.

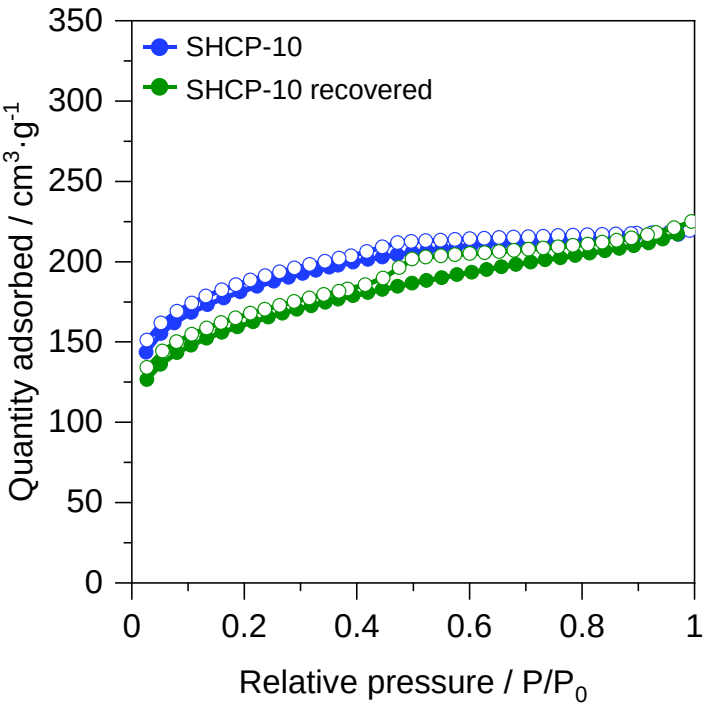

Figure SI 1-2. BET plots of virgin and recovered SHCP-10

The BET specific surface area was determined to be 697 ± 35 $m^2 \cdot g^{-1}$ $m^2 \cdot g^{-1}$ and the micropore and total pore volume was 0.17 ± 0.01 $cm^3 \cdot g^{-1}$ and 0.38 ± 0.04 $cm^3 \cdot g^{-1}$, respectively.

Thermogravimetric analysis in air atmosphere (Figure SI 1-3) showed an initial weight loss of 23 wt.-% up to 120°C, which was attributed to the desorption of water, after which the weight was stable until ~200 °C, at which point the decomposition of the sulfonategroups takes place.

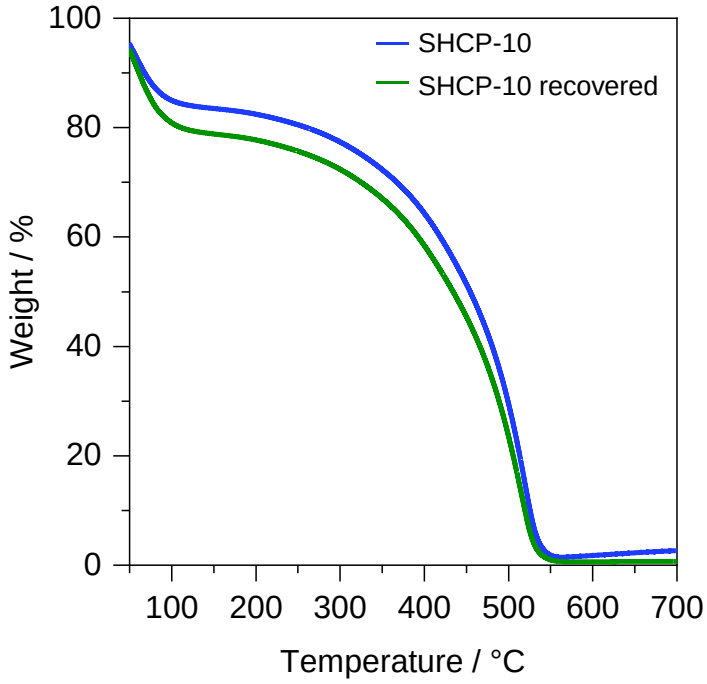

Figure SI 1-3. TGA graphs in air of virgin and recovered SHCP-10

We explored the possibility to recover SHCP at the end of a membranes use cycle via controlled digestion of the surrounding CNF in 75 wt.-% sulfuric acid at room temperature. Post-treatment, the N_2 sorption isotherms (Figure SI 1-2) of recovered SHCP indicate a slight decrease in sorption at the meso/macropore region, resulting in a decrease in BET specific surface area from 697 ± 35 $m^2 \cdot g^{-1}$ to 504 ± 60 $m^2 \cdot g^{-1}$, paired with a decrease in total and micro pore volume . Upon re-analysis, the network displayed some reduction in sulfonic acid group density, apparent through a decrease in sulfur content from 3.84 ± 0.03 to 3.12 ± 0.04 at.-%, according to EA and 6.4 to 6.0 at.-%, as determined by XPS. The decrease in sulfur content was accompanied by an increase in carbon content, which we hypothesise is due to some residual carbon from CNF acid degradation. Additional physical and chemical characterisations, including FTIR (Figure SI 1-1) and TGA (Figure SI 1-3) revealed no measurable change.

The particle size distribution of hand-ground SHCP-10 (Figure SI 1-4 left) shows that the majority of the particles are in the 20 to 40 µm range. It should be noted that small quantities of larger particles (120 µm and above) were observed in SEM (Figure SI 1-4 right), which are outside of the measuring range for LASER-diffraction experiments.

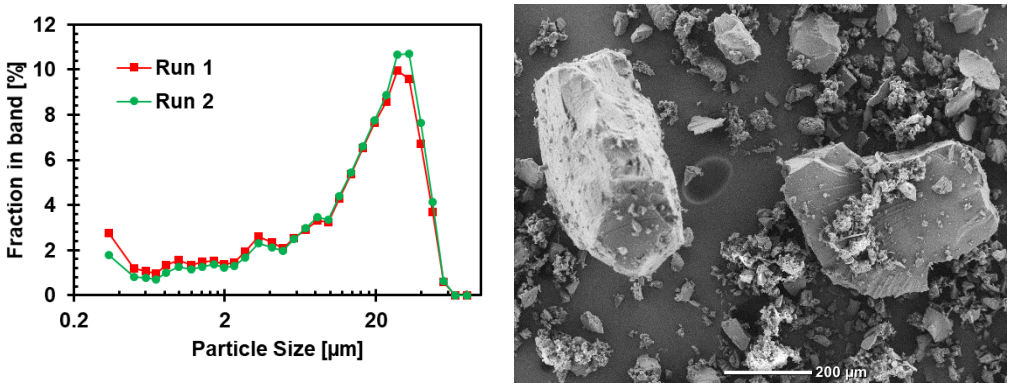

Figure SI 1-4: Particle size distribution of SHCP-10 used for the manufacturing of hybrids (left) and an SEM image showing the larger particles found.

SI 2. Results of preliminary hybrid manufacturing tests

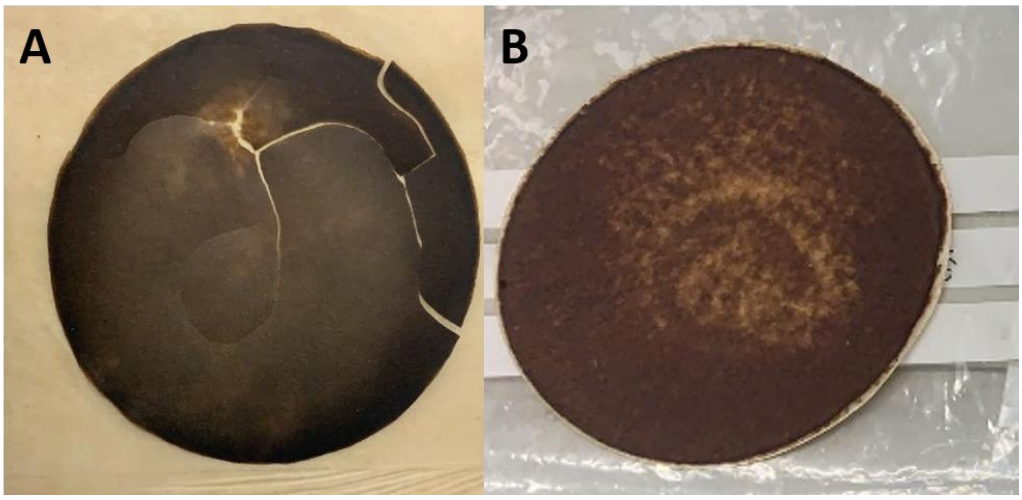

Figure SI 2-1: Photographs of defective SHCP/CNF hybrids. Increasing the polymer content of the middle layer above 50 wt.-% led to cracking during hot pressing (A) and using water as suspension medium led to uneven deposition and agglomeration of SHCP-10.

SI 3. Water permeance measurements

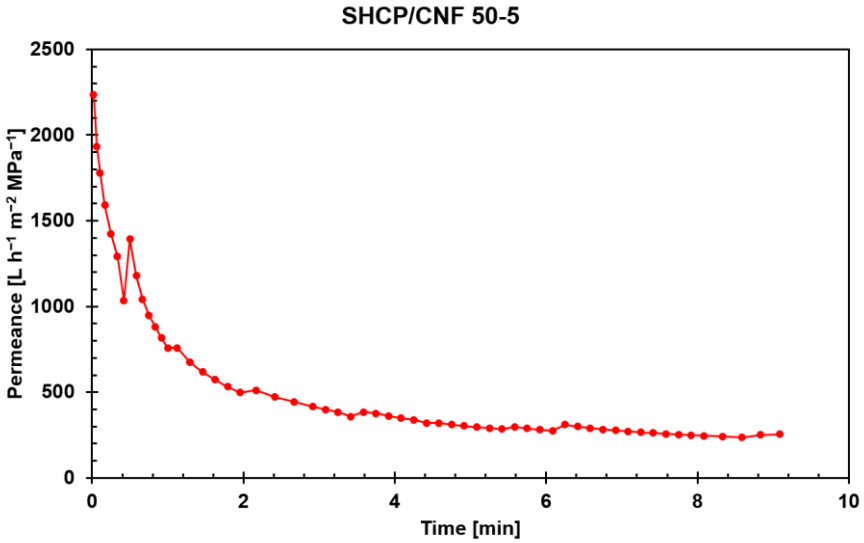

Figure SI 3-1: Representative permeance over time curve as recorded during water permeance tests. The sudden increase in permeance for some points is caused by the water changes necessary to refill the setup which in turn depressurise the system,

allowing for the compressed hybrid paper to relax to a certain extent, increasing the flow rate briefly.

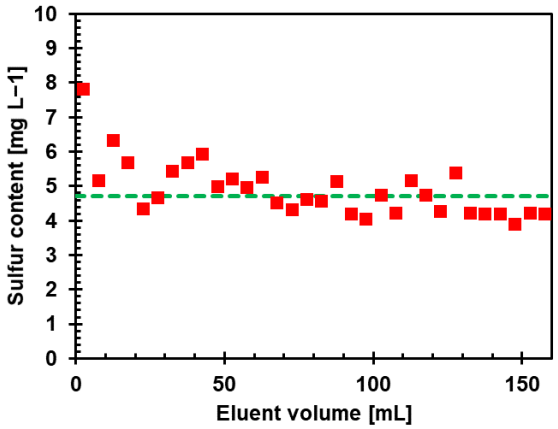

Figure SI 3-2: Sulfur content of the eluent fraction of pure water after passing through a hybrid (red dots) vs the sulfur content of the used stock solution (green dashed line). Note: these values were obtained via single measurements.

SI 4. Cu^{2+} desorption during regeneration

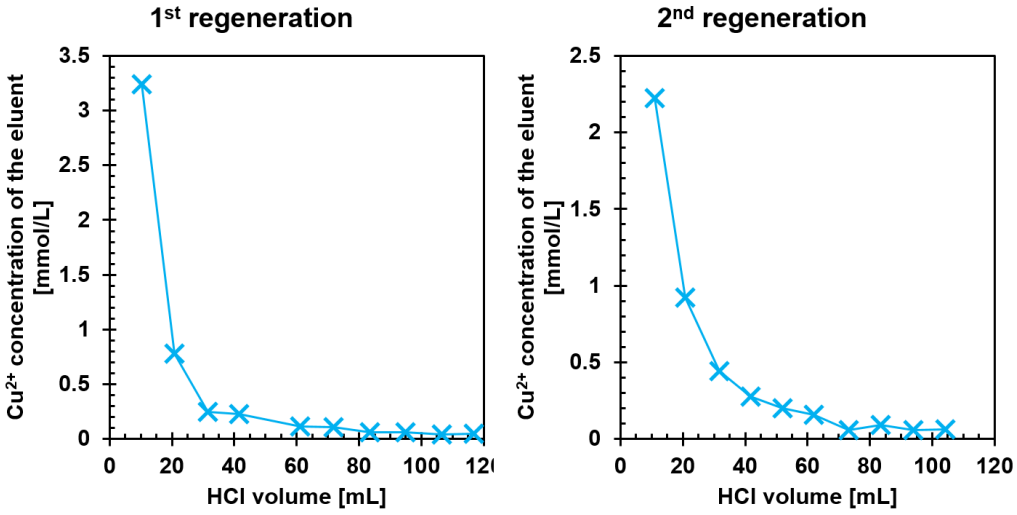

Figure SI 4-1 Concentrations of the eluent fractions during Regeneration of SHCP/CNF 50-10

Table SI 4-1 Comparison of copper adsorption capacity and regeneration performance of a variety of materials with SHCP-10 and SHCP/CNF hybrids.

Adsorbent	q_{max} (mg/g)	Regeneration		Ref.
		Number of Cycles	% q_e retained	
Glycine functionalized magnetic nanoparticles	625	4	89	[4]
Oxidised multiwall carbon nanotubes	416.5	6	87	[5]
Carboxylated graphene oxide	357.1	5	96	[6]
Schiff base ligand nanocomposites	173.6	7	92	[7]
Graphene nanosheet/MnO_2	103	4	–	[8]
2D $Ti_3C_2T_x$ MXene Nanosheets	78.45	3	30	[9]
Chitosan/Ag nanoparticle/Cu nanoparticle/carbon nanotube composites	70.4	5	approx. 60	[10]
Pectin functionalised Fe_3O_4 nanoparticles	48.99	5	58.66	[11]
Bovine manure compost	29.9	3	>99	[12]
Poly(methacrylamide-co-acrylic acid)/montmorillonite nanocomposites	29	5	90	[13]
diethylenetriamine functionalized SiO_2/Fe_3O_4 nanoparticles	13.46	3	75	[14]
SHCP-10	55-59			this study
SHCP-10 in SHCP/CNF membranes	77.9-113.7	3	>99	this study

SI 5. Au nanoparticle rejection tests

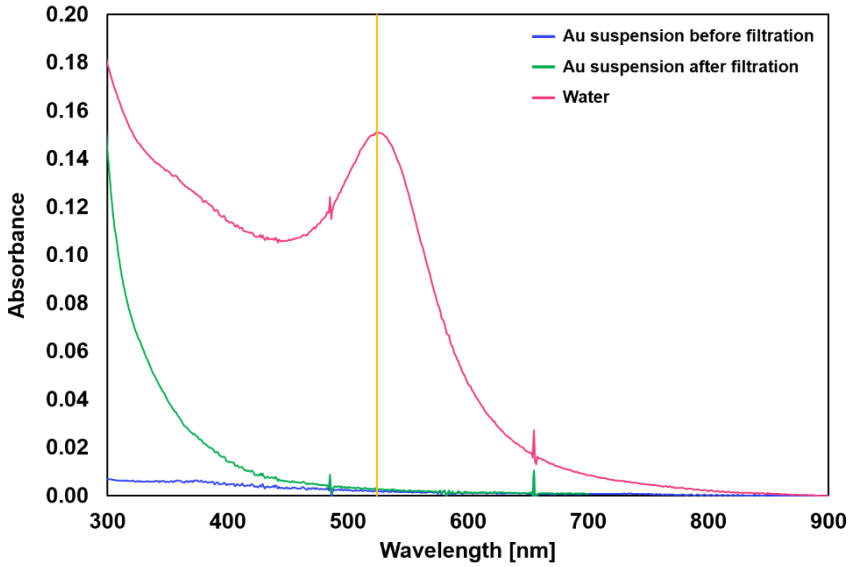

Figure SI 5-1 UV-Vis spectra comparing Au NP stock solution before (red) and after (green) passing through SHCP/CNF 20-5. The spectrum of water is included as reference. The yellow line denotes the peak maximum at 524 nm.

The absorbance peak at 524 nm, attributed to the Au nanoparticles, was reduced to the equivalent of pure water after filtration. Only the adsorption peak of the citric acid stabilizer exhibiting its maximum below the tested wavelength range remained.

References

[1] Schweng, P.; Mayer, F.; Galehdari, D.; Weiland, K.; Woodward, R. T., *Small* **2023,** *19* (50), e2304562. DOI 10.1002/smll.202304562.

[2] Blocher, A.; Mayer, F.; Schweng, P.; Tikovits, T. M.; Yousefi, N.; Woodward, R. T., *Mater. Adv.* **2022,** *3* (15), 6335-6342. DOI 10.1039/d2ma00379a.

[3] Thommes, M.; Kaneko, K.; Neimark, A. V.; Olivier, J. P.; Rodriguez-Reinoso, F.; Rouquerol, J.; Sing, K. S. W., *Pure Appl. Chem.* **2015,** *87* (9-10), 1051-1069. DOI 10.1515/pac-2014-1117.

[4] Feitoza, N. C.; Goncalves, T. D.; Mesquita, J. J.; Menegucci, J. S.; Santos, M. K.; Chaker, J. A.; Cunha, R. B.; Medeiros, A. M.; Rubim, J. C.; Sousa, M. H., *J. Hazard. Mater.* **2014,** *264*, 153-60. DOI 10.1016/j.jhazmat.2013.11.022.

[5] Egbosiuba, T. C.; Abdulkareem, A. S., *J. Mater. Res. Technol.* **2021,** *15*, 2848-2872. DOI 10.1016/j.jmrt.2021.09.094.

[6] White, R. L.; White, C. M.; Turgut, H.; Massoud, A.; Tian, Z. R., *J. Taiwan Inst. Chem. Eng.* **2018,** *85*, 18-28. DOI 10.1016/j.jtice.2018.01.036.

[7] Awual, M. R.; Eldesoky, G. E.; Yaita, T.; Naushad, M.; Shiwaku, H.; AlOthman, Z. A.; Suzuki, S., *Chem. Eng. J.* **2015,** *279*, 639-647. DOI 10.1016/j.cej.2015.05.049.

[8] Ren, Y.; Yan, N.; Feng, J.; Ma, J.; Wen, Q.; Li, N.; Dong, Q., *Mater. Chem. Phys.* **2012,** *136* (2-3), 538-544. DOI 10.1016/j.matchemphys.2012.07.023.

[9] Shahzad, A.; Rasool, K.; Miran, W.; Nawaz, M.; Jang, J.; Mahmoud, K. A.; Lee, D. S., *ACS Sustainable Chem. Eng.* **2017,** *5* (12), 11481-11488. DOI 10.1021/acssuschemeng.7b02695.
[10] Alsabagh, A. M.; Fathy, M.; Morsi, R. E., *RSC Adv.* **2015,** *5* (69), 55774-55783. DOI 10.1039/c5ra07477k.
[11] Gong, J.-L.; Wang, X.-Y.; Zeng, G.-M.; Chen, L.; Deng, J.-H.; Zhang, X.-R.; Niu, Q.-Y., *Chem. Eng. J.* **2012,** *185-186*, 100-107. DOI 10.1016/j.cej.2012.01.050.
[12] Zhang, M., *Chem. Eng. J.* **2011,** *172* (1), 361-368. DOI 10.1016/j.cej.2011.06.017.
[13] Barati, A.; Asgari, M.; Miri, T.; Eskandari, Z., *Environ. Sci. Pollut. Res.* **2013,** *20* (9), 6242-55. DOI 10.1007/s11356-013-1672-3.
[14] Chen, H. W.; Chang, S. H., *Environ. Technol.* **2022,** *43* (6), 805-814. DOI 10.1080/09593330.2020.1805027.